SYNTHESIS, PHOTO-PHYSICAL AND LASER CHARACTERIZATION OF FLUORESCENT DYES

By

Monika Gupta

(CHEM01200904019)

BHABHA ATOMIC RESEARCH CENTRE, MUMBAI

A thesis submitted to the

Board of Studies in Chemical Sciences

In partial fulfillment of requirements

For the Degree of

DOCTOR OF PHILOSOPHY

of

HOMI BHABHA NATIONAL INSTITUTE

November, 2014

HOMI BHABHA NATIONAL INSTITUTE

Recommendations of the Viva Voce Board

As members of the Viva Voce Board, we certify that we have read the dissertation prepared by **Monika Gupta** entitled **"SYNTHESIS, PHOTO-PHYSICAL AND LASER CHARACTERIZATION OF FLUORESCENT DYES"** and recommend that it may be accepted as fulfilling the dissertation requirement for the Degree of Doctor of Philosophy.

Date: 29/05/2015

Chairman: Dr. Sisir K. Sarkar

Date: 29/05/2015

Guide: Dr. Alok K. Ray

Date: 29/05/2015

Member 1: Dr. Sandip K. Nayak

Date: 29/05/2015

Member 2: Dr. H. Pal

Final approval and acceptance of this dissertation is contingent upon the candidate's submission of the final copies of the dissertation to HBNI.

I hereby certify that I have read this dissertation prepared under my direction and recommend that it may be accepted as fulfilling the dissertation requirement.

Date: 29/05/2015

Place: HBNI, Mumbai, India

Guide: Dr. Alok K. Ray

STATEMENT BY AUTHOR

This dissertation has been submitted in partial fulfillment of requirements for an advanced degree at Homi Bhabha National Institute (HBNI) and is deposited in the Library to be made available to borrowers under rules of the HBNI.

Brief quotations from this dissertation are allowable without special permission, provided that accurate acknowledgement of source is made. Requests for permission for extended quotation from or reproduction of this manuscript in whole or in part may be granted by the Competent Authority of HBNI when in his or her judgment the proposed use of the material is in the interests of scholarship. In all other instances, however, permission must be obtained from the author.

Monika Gupta

DECLARATION

I, hereby declare that the investigation presented in the thesis has been carried out by me. The work is original and has not been submitted earlier as a whole or in part for a degree / diploma at this or any other Institution / University.

Monika Gupta

LIST OF PUBLICATIONS

Journal papers

1. **Gupta Monika,** Maity D. K., Singh M. K., Nayak S. K. and Ray Alok K. Supramolecular Interaction of Coumarin 1 Dye with Cucurbit[7]uril as Host: Combined Experimental and Theoretical Study *Journal of Physical Chemistry B* **2012**, *116,* 5551-5558.
2. **Gupta Monika**,[#] Mula Soumyaditya,[#] Tyagi Mrityunjay, Ghanty Tapan K., Murudkar Sushant, Ray Alok K. and Chattopadhyay Subrata Rational Design of Some Bodipy-based Functional Molecule *Chemistry A Europeon Journal* **2013**, *19*, 17766–17772. Equal contribution[#]
3. **Gupta Monika**, Jagtap Krishna K., Sudersan V. and Ray Alok K. Taming Fluorescence Yield of Dye Insensitive to Temperature By Non-Covalent Complex with Host CB[7] for Aqueous Dye Laser *Pramana Journal of Physics* **2014**, *82*, 277-281.
4. Boraste Deepak, **Gupta Monika**, Shankarling Ganpati, Ray Alok K. and Nayak Sandip K. Spectroscopy and Laser Characterization of Synthesized Supramolecular Host Cucurbit[7]uril using Aqueous Rhodamine B Dye *Pramana Journal of Physics* **2014**, *82*, 271-275.
5. **Gupta Monika,** Maity D. K., Nayak S. K. and Ray Alok K. Modulation of Photophysics and Photostability of Cationic Coumarin 1 dye upon Inclusion with Macrocyclic Host Cucurbit[7]uril *J. Photochem. Photobiol. A* **2015**, 300, 15-21.

6. **Gupta Monika**, Kamble Priyadarshani, Rath M. C., Naik D. B. and Ray Alok K. High laser efficiency and photostability of Pyrromethene Dyes mediated by non-polar solvent *J. Applied Optics*, **2015**, (under review)
7. **Gupta Monika**,[#] Mula Soumyaditya,[#] Ray Alok K., Ghanty Tapan K., Naik D. B. and Chattopadhyay Subrata Laser Properties and Photostability of New Boradiazaindacene (BODIPY) Dye: Effect of Solvent Polarity *Chemistry A Europeon Journal* **2015**, (communicated). Equal contribution[#]
8. **Gupta Monika,** Mula Soumyaditya, K. Parvathi, Maity D. K. and Ray Alok K. Supramolecular interaction of novel water soluble BODIPY dyes with host cucurbit[7]uril (manuscript under preparation)

Conference Papers:

International:

1. **Gupta Monika**, Maity D. K., Nayak S. K. and Ray Alok K. Interactions of Neutral and Cationic Coumarin1 dye with Cucurbit[7]uril Third International Conference on Cucurbiturils (**ICCB-2013**), Canberra, Australia November 17-20, 2013, (oral presentation).

National:

1. **Gupta Monika** and Alok K. Ray Synthesis, Photophysics and Laser Characterization of Fluorescent Dyes National Laser Symposium (**NLS-23**) Shree Venkateswara University, Tirupati, A. P., Dec. 3-6, 2014, (oral presentation)
2. **Gupta Monika** and Alok K. Ray Synthesis of water soluble Bodipy Fluorophore with a large Stokes' shift 4th National Symposium on Functional Applications of Colorants (**NSFAC-2014**), ICT, Matunga, Mumbai, Oct. 16-17, 2014, (oral presentation).

3. **Gupta Monika** and Ray Alok K. Synthesis Photo-physics and Laser Characterizition of New Fluorescent Dyes Research Scholar Meet (**RSM-2014**), Changu Kana Thakur College, New Panvel, Mumbai, Feb. 21-21, 2014, (oral presentation).
4. **Gupta Monika**, Rath M. C., Naik D. B. and Ray Alok K. Studies on Triplet State of PM567 and New B-centre Dye by Pulse Radiolysis Technique Trombay Symposium on Radiation and Photochemistry (**TSRP-2014**), BARC, Mumbai, Jan. 6-9, 2014, (abstract no. PC-111)
5. **Gupta Monika**, Mula Soumyaditya, Ray Alok K. and Chattopadhyay Subrata Effect of Solvent Polarity in Lasing Efficiency and Photo-stability of New BODIPY Laser Dyes National Laser Symposium (**NLS-22**), Manipal University, Karnataka, Jan. 7-10, 2014, (abstract no. CP-02-04).
6. **Gupta Monika**, Nayak S. K., Ray A. K. and Maity D. K. Structure and Stability of Host-Guest Complexes of Neutral and Cationic Coumarin1 dyes with Cucurbit[7]uril: A Theoretical Rationalization Current Trends in Theoretical Chemistry (**CTTC-2013**), BARC, Mumbai, Sep. 26-29, 2013, (abstract no. CP-91)
7. **Gupta Monika**, Mula Soumyaditya, Ray Alok K. and Chattopadhyay S. Highly Efficient B-substituted Bodipy Laser Dye with Increased Photo-stability National Laser Symposium (**NLS-21**), BARC, Mumbai, Feb. 6-9, 2013, (abstract no. CP-03-25).
8. **Gupta Monika**, Jagtap Krishna K., Sudersan V. and Ray Alok K. Study of Temperature Dependence of Fluorescence of Rhodamine B by Non-covalent Complexation for Laser Applications National Laser Symposium (**NLS-21**), BARC, Mumbai, Feb. 6-9, 2013, (abstract no. CP-03-29).

9. Jagtap Krishna K., **Gupta Monika**, Kombrabail Mamata and Ray Alok K. Rotational Relaxation rate of Dye Molecule and Laser Efficiency National Laser Symposium (**NLS-21**), BARC, Mumbai, Feb. 6-9, 2013, (abstract no. CP-01-35).
10. Kamble Priyadarshani, **Gupta Monika**, Jagtap Krishna K., Sasikumar S. and Ray Alok K. Solvent Mediated Improvement in Laser Performances of Pyrromethene Dyes National Laser Symposium (**NLS-21**), BARC, Mumbai, Feb. 6-9, 2013, (abstract no. CP-11-11)
11. **Gupta Monika**, Mula Soumyaditya, Ray Alok K. and Chattopadhyay Subrata Design and Development of Bodipy Based Proton Sensor Interdisciplinary Symposium on Material Chemistry (**ISMC-2012**) BARC, Mumbai, Dec. 11-15, 2012, (abstract no. J-12)
12. **Gupta Monika**, Nayak S. K., Maity D. K. and Ray Alok K. Inclusion Behaviour of Coumarin 1 Dye with Cucurbit[7]uril Host Trombay Symposium on Radiation and Photochemistry (**TSRP-2012**), BARC, Mumbai, Jan. 4-7, 2012, (abstract no. PC-131)
13. **Gupta Monika**, Nayak S. K., Maity D. K. and Ray Alok K. Inclusion Behavior of Cationic Coumarin1 Dye with Host Cucurbit[7]uril and Photo-physics National Symposium on Functional Application of Colorants (**NSFAC-2011**), ICT, Matunga, Mumbai, Oct. 14-15, 2011, (oral presentation)
14. Jagtap K. K., Ray Alok K., **Gupta Monika**, Sarkar S. K. and Dasgupta K. Dynamics of Spontaneous and Stimulated Emission on the Photochemical Stability of Pyrromethene Laser dyes 3rd Asia Pacific Symposium on Radiation Chemistry and Trombay Symposium on Radiation and Photochemistry (**APSRC and TSRP-2010**), Lonavala, Mumbai, Sep. 14-17, 2010, (abstract no. PC-86)

Dedicated to . . .

. . .My Beloved Parents

ACKNOWLEDGEMENT

A major research work like this is never the work of anyone alone. The contributions of many different people, in their different ways, have made this possible. I would like to extend my appreciation especially to the following.

I would like to express my gratitude to my supervisor, ***Prof. Alok K. Ray, Scientific officer H+ Laser & Plasma Technology Division, BARC,*** *whose expertise, understanding, and patience, added considerably to my graduate experience. I appreciate his vast knowledge and skill in many areas and his assistance in writing reports which have on occasion made me "GREEN" with envy.*

I would like to thank the other members of my doctoral committee, ***Prof. Sisir K. Sarkar, Prof. Sandip K. Nayak*** *and* ***Prof. H. Pal*** *BARC, for their encouragement, insightful comments, and valuable questions provided at all levels of the research project. Finally, I would like to thank* ***Dr. B. S. Tomar*** *from Radio-Analytical Division for taking time out from his busy schedule to come and discuss of my research work.*

I express my deep sense of gratitude to ***Dr. S. Chattopadhyay****, Head of Bio-Organic Division, for his valuable suggestion, innovative ideas and constructive discussion throughout my research work. I also thanks to* ***Dr. K. Dasgupta, Dr. A. K. Das,*** *and* ***Dr. L. M. Gantayet,*** *Beam Technology Development Group for supporting my research work.*

A very special thanks goes out to ***Dr. Soumyaditya Mula****, Bio-Organic Division, BARC, without whose motivation and encouragement, I would not have considered an actual path of my career in Synthetic research work.* ***Dr. Mula*** *is the one teacher/ guide/supporter who always encourage me in every difficulty during my research work. It was under his tutelage that I developed a focus and became interested in research work specially synthesis. He provided me with direction, technical support and became more of a mentor and friend. It was though his, persistence, understanding and kindness that I completed my Ph. D. degree. I doubt that I will ever be able to convey my appreciation fully, but I owe him my eternal gratitude.*

I am indebted to ***Dr. Dilip K. Maity,*** *and* ***Dr. Tapan K. Ghanty*** *of Theoretical Chemistry Section, BARC for his help in doing the DFT/TDDFT calculation. I also take an opportunity to thank* ***Dr. D. B. Naik****, and* ***Dr. M. C. Rath*** *Radiation and Photochemistry Division, BARC, for helping me in carrying out the LINAC experiments of Laser Dyes. My sincere thanks also goes to* ***Dr. V. K. Jain, Mr. Kamal Chaudhari, Mr. Manoj pal*** *from Chemistry Division for their help in NMR characterization. Special thanks to* ***Mrityunjay Tyagi*** *for carrying out biological experiments. Also, Of course, this thesis would not have been possible without the participation of IIT, and TIFR, Mumbai, Who provided instrumental help for sample analysis.*

I cannot find words to express my gratitude to my best friend ***Ms. Shikha Sharma*** *who always provided me with statistical advice at times of critical needs, exchanges of knowledge, skills, and venting of*

frustration during my research work, which helped enrich the experience.

I thank my fellow labmates in Bio-organic Group: ***Dr. A. K. Bauri, Dr. Anubha Sharma, Mrs. Abha N. Kumar, Mrs. Kshama Kundu, Mr. Mrunesh Koli, Dr. Neelam Shivran*** *and all BOD members for the stimulating discussions, their cooperation, unconditional help, and whole hearted support in the lab and for all the fun we have had in the last five years. Also I thank my friends in Laser and Plasma Technology Group:* ***Dr. Krishna Jagtap, Mr. Vindhyesh Singh, Dr. Sunita Kedia, Ms. Priyadarshini Kamble, Ms. Harshada Jadhav*** *and all other people of Tunable laser section. They have been there all the times to encourage and motivate me to work cheerfully. Their constant support and presence have been an emotional support for me to overcome all the obstacles on my path.*

Apart from the intellectual support, an emotional support is always needed to conquer the hardships. For this, I would like to thank, from the bottom of my heart, my friends ***Arun, Shailesh, Sushant, Dilip, Neelanjal, Juby, Neha, Veer, Priyanka, Nidhi, Sneh Toprani, Shree Shalke, Venkateshwararao, Lalita, Vasundhara, Jerina, Suman, Shagufta, Sumit Chillar, Sunil B, Ramamohan, Ahmed, Yusuf, Avishek, Ganga and Anand*** *for their warm friendship and feel extremely fortunate to them as my friends who, be it a scientific or personal matter, were always be with me in any situation. Thank you so much for laughing with me, sharing my pains and caring for me.*

Finally, my deepest gratitude is to my family. The phrase "Thank you" can never capture the gratitude. I want to express to my ***Mummy*** *and* ***Papa*** *who always supported me to pursue my dreams, stood by me during all ups and downs of my life and took the pain of separation. Their faith in me, encouragement and good wishes made me to achieve this goal of my life. Also, Immense love and affection of my sweet sisters* ***Uma*** *and* ***Anju****, lovely jiju* ***Akshay*** *and* ***Vivek*** *and dearest bhiya-bhabhi* ***Shambhu*** *and* ***Alka*** *who have been invaluable in the journey towards my goal. I am very much thankful to my all family members for their moral support during my study and to achieve this stage of my life.*

Last, but not the least special thanks to ***God*** *for the wisdom and perseverance that he has been bestowed upon me during this research project, and indeed, throughout my life: "I can do everything through him who gives me strength." (Philippians 4: 13)*

In conclusion, I recognize that this research would not have been possible without the financial assistance of Homi Bhabha National Institute, Department of Atomic Energy, BARC during the five years of my research. Without this, I could not survive in Mumbai.

*……****Monika***

CONTENTS

CHAPTER 4: IMPROVED PHOTO-PHYSICS OF COUMARIN USING THE HOST CUCURBIT[7]URIL

CHAPTER 5: HOST-GUEST INTERACTION STUDY OF WATER SOLUBLE BODIPY DYES

SYNOPSIS

The growing demand for tailored functional organic chromophores, has been continuing as these molecules attract the attention of chemists, physicists, biologists and material scientists from an ever expanding multidisciplinary arena. Their practical applications as active molecule in diverse areas, such as tunable lasers, fluorescent biosensors, chemical sensors, sensitizer for solar cells, artificial light harvesters, molecular photonics, among others, have been increasing. Among numerous commercially available classes of fluorescent molecules, coumarin in UV region, rhodamine and lately pyrromethene (PM, also known as BODIPY) in visible spectral region have been used widely till now in dye lasers, sensors, biolebels etc.

In parallel there has been considerable interest on design, synthesis and evaluation of photo-physical and photochemical characteristics of new dye molecules belonging to these groups and their correlations to functional properties and use in devices are important. Many coumarin dyes, a few are also extracted from plants, are moderately fluorescent and have been found useful as optical brighteners, fluorescent indicators and even as sunburn preventive materials. On the other hand, among fluorescent dyes in visible region, BODIPY dyes have gained recognition as being one of the more versatile fluorophore and steadily increased in popularity and functional use over the past two decades. The use of BODIPYs as effective biological label has been complemented by their propensity to function as a tunable laser dye. BODIPY molecules have attracted interest for dye laser applications since they have small intersystem crossing rate (k_{ISC}) and low loss of fluorescent photons due to triplet state absorption, about one-fifth that of the rhodamine dyes. However, the two major inherent deficiencies of PM molecules are their small Stokes shift and fast photo-chemical degradation rate due to reaction with *in situ* generated singlet O_2 ($^1O_2$) in air equilibrated solvents. The poor

photochemical stability of commercially available PM dyes, in commonly used alcohol solvents, continues to be major hurdle in the long term operation of its use as active media in liquid dye lasers especially for high average power and high repetition rate (tens of kHz) operations.

However, liquid dye lasers usually contain very small concentration of dye, typically in the range of 10^{-3} to 10^{-4} molar. Hence, the solvent in which the dye is dissolved also play an important role to modulate physical properties, photostability and safety. In comparison to organic solvents, water is an ideal solvent for making dye laser safer in terms of fire hazards, easy treatment and disposal. Also, water is particularly useful in high repetition rate dye lasers, arising primarily from its weaker dependence of refractive index on temperature (dn/dT), due to its considerable higher photo-thermal figure of merit. In spite of these advantages, water solution of dye is not generally used in dye lasers, because in pure water dye molecules form non-radiative TICT (twisted intramolecular charge transfer) state as well as aggregate to dimers that drastically reduce the fluorescence and lasing efficiency. Although many de-aggregating or dispersing additives to incorporate the aqueous dye molecules have been proposed, a scientifically as well as technologically viable combination fulfilling comparable or superior laser performance in terms of efficiency, photostability and photo-thermal characteristics of dye solutions is not clearly established.

Considering these drawbacks of presently used organic dyes and solvents, this thesis have explored work with design and synthesis of new fluorescent BODIPY and coumarin1 dyes along with study of their comparative photo-physics, photostability and laser characteristics using water and organic solvents, which are briefly summarized in the following.

Chapter -1 Introduction to Fluorescent Dyes:

This chapter concerns with important photo-physical and chemical characteristics of fluorescent dyes, followed by general requirements for design and development of new dye molecules for tunable laser and sensor applications. Further describe the different category of laser dyes from UV to far IR region with their chemical structures, discussion on reported synthetic strategies, important features and diverse applications. Next, the role of polar and non-polar solvents in modulating the optical properties of laser dyes, especially eco-friendly water, are briefly described with its importance, major limitations and rising above this limitation. Further study is extended towards important characteristics of improving photo-physical properties of aqueous dye molecules by interaction with relatively recent macrocyclic host cucurbit[7]uril (CB[7]).

Chapter-2 Experimental Techniques:

The various experimental techniques used in this work are briefly described in this chapter. It includes different spectroscopy techniques such as UV-vis absorption, steady state and time resolved fluorescence, cyclic voltammetry, pulse radiolysis, FTIR and NMR for evaluating photo-physical and chemical properties of fluorescent dyes. Also discussed laser characterization of potential dyes using a constructed pulsed dye laser, pumped by the second harmonic (532 nm) of a Q-switched Nd:YAG (10 Hz) laser, which include principle, experimental set up and application in spectroscopy and present study.

Chapter-3 Effect of Solvent in Lasing Efficiency and Photostability of BODIPY Dyes:

BODIPY (Boradiazaindacene) dyes are extensively used as efficient active media in solid and liquid dye lasers during past decade, but these molecules offer low photostability in alcohol

solvents by reacting with *in situ* generated singlet oxygen ($^1O_2$). With this problem in mind, this chapter of thesis deals with laser characterization of BODIPY dyes using polar (ethanol) and non-polar (1,4-dioxane and heptane) solvents, initially starts with comparative study of known dyes named as PM567 (**1**) and PM597 (**2**). These two molecules differ from structural modification at 2 and 6 positions of BODIPY core (Figure 1) resulting different photo-physics, photostability and lasing properties. This allowed better understanding of important molecular features required for synthesis of new **(3)** BODIPY dyes, which was investigated.

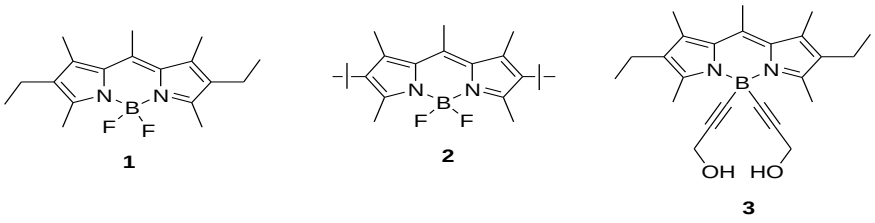

Figure 1: Molecular structures of PM567 (dye **1**), PM597 (dye **2**) and new dye (dye **3**)

The second harmonic (532 nm) of Nd:YAG laser pumped pulsed dye laser set up was used to determine the relative utility of new dye-solvent combinations for high average power dye lasers. Lasing efficiencies of both known and new PM dyes in non-polar solvents are increased by 3.5% and 5.2 % for dye **1** and dye **2 (**in heptane**),** respectively. But, interestingly, both dyes showed a large enhancement (90-100 times) in their photostability in non-polar heptane and 1,4-dioxane as compared to commonly used ethanol. For mechanistic rationalization to the observations of high photostability of PM dyes in non-polar solvents, complimentary photochemical methods have been used to determine relative capability of generation of reactive $^1O_2$ through triplet state of dye and reactivity of $^1O_2$ with dye molecules. The rates of $^1O_2$ generation from the PM dyes in different solvents have been evaluated by irradiating it with a visible light source, along with efficient $^1O_2$ quencher diphenylisobenzofuran (DPBF) or DABCO as an additive. Further, we have studied rate of reactivity of $^1O_2$ with each PM dye in presence of methylene blue (MB), a

known singlet oxygen generator. Pulse radiolysis experiment of dyes was also performed using binary solvents comprising of a mixture of non-polar solvent and benzene, and observed that energy transfer from triplet dye to dissolved oxygen is less for dye **2** than **1** in both non-polar solvents. Thus, we have established that the generation of $^1O_2$ and reactivity with $^1O_2$ for both the PM dyes (**1** and **2**) are very low in heptane and 1,4-dioxane than that in ethanol. These results are in excellent agreement with laser photostability experiments that both the PM dyes are extraordinary photostable in heptane and 1,4-dioxane as compared to ethanol. Also, in comparison between two, dye **2** is more photostable than **1**. Thus, we have compared the lasing and photostability properties of two known PM dyes which have different optical properties

Further, a new congener of BODIPY, by substitution at B-centre from its precursor PM567 (**1**), was designed and synthesized with aim to explore new PM dye molecule. This new dye showed absorption and fluorescence spectra in similar spectral region to PM567 but with better lasing characteristics. Narrow band lasing efficiency profiles and photostability data of new dye (**3**) using ethanol and 1,4–dioxane solvents were shown in Figure 2 and Table 1, respectively. Dye **3** was found to be highly fluorescent and gave slightly lower lasing efficiency (2%) than **1** but showed better photostability in absence and presence of $^1O_2$ inhibitor DABCO, in both ethanol (2.1 fold) and 1,4-dioxane (3.3 fold) than known dye **1**. The observations of smaller improvement in photostability of dye **3**, in presence of DABCO, indicated that singlet oxygen generation capability is lower for dye **3**. This was also corroborated by photochemical experiments using additive DPBF and MB.

Taken together the above results revealed that despite being more prone to oxidation (cyclic voltammeter result), new dye **3** are more photo-stable with higher fluorescence quantum yield

than its precursor dye **1** due to their lower reaction rates with $^1O_2$ and lower $^1O_2$ generation capacity but less than dye **2**. Also both dyes were more photostable in 1,4-dioxane than ethanol.

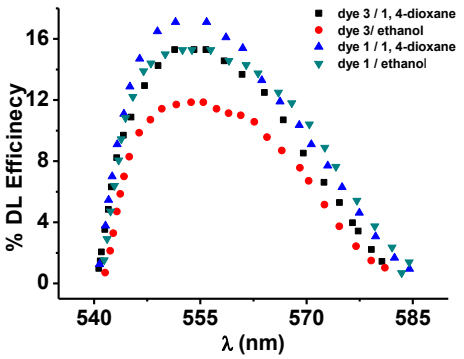

Figure 2: Narrow band lasing efficiency of dye **1** and **3** in ethanol and 1,4-dioxane

Dyes	Solvent	Φ_{pd}	$\Phi_{pd}^{-1}{}_{dye\ 3}$ / $\Phi_{pd}^{-1}{}_{dye\ 1}$	$\Phi_{pd}^{-1}{}_{dioxane}$ / $\Phi_{pd}^{-1}{}_{ethanol}$	$\Phi_{pdDABCO}$	$\Phi_{pd}^{-1}{}_{DABCO}$ / Φ_{pd}^{-1}
1	ethanol	6.7×10^{-4}	-	-	1.5×10^{-4}	4.5
	1,4-dioxane	3.1×10^{-5}	-	21.5	1.5×10^{-5}	2.1
3	ethanol	3.2×10^{-4}	2.1	-	1.4×10^{-4}	2.3
	1,4-dioxane	9.4×10^{-6}	3.3	34.2	8.1×10^{-6}	1.2

Table 1: Photostability (Φ_{pd}^{-1}) of the BODIPY dyes **1** and **3** in ethanol and 1,4-dioxane

Chapter-4 Improved Photo-physics of Coumarin using the Host Cucurbit[7]uril:

This chapter deals with improvement of photo-physical properties of coumarin dye in water, which otherwise reduces its fluorescence properties drastically due to formation of non-radiative dimer and TICT state of dye molecules, employing host-guest strategy. The supramolecular host-guest interaction is a dynamic phenomenon and usually occurs in aqueous solution. On the other hand coumarin class of hydrophobic dyes, highly soluble in organic solvents, are used in fluorescence microscopy, dye sensitized solar cells, dye lasers as UV dyes etc. As representative study of aqueous based coumarin dyes for investigating its interaction with the recent macrocyclic host Cucurbit[7]uril (CB[7]) in water, we have chosen widely used fluorescent molecule coumarin 1, in which 7-diethylamino moiety plays an important role in modulating its photo-physics in solutions. Further a proton salt of this dye molecule, allowing improved solubility in water, was investigated for possible stronger interaction with electron rich portals of the host CB[7], which were monitored using various spectroscopy techniques and laser irradiation.

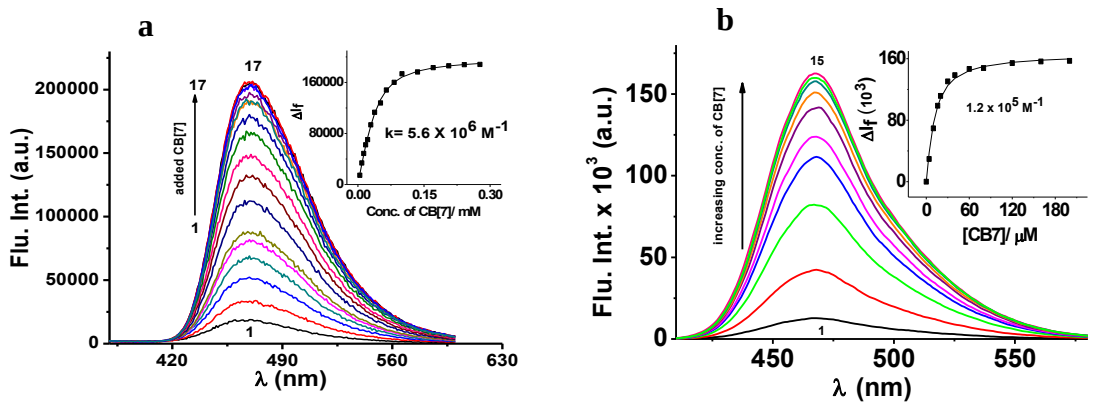

Figure 3: Fluorescence spectra of (a) cationic (15.4 μM) and (b) neutral (9.7 μM) coumarin 1 dye in aqueous solution with increasing concentration of CB[7]. INSET: Fluorescence titration curve in the presence of CB[7] showing 1:1 complex with binding constant for cationic and neutral dyes (a) 5.6 x 10^6 M^{-1} and (b) 1.2 x 10^5 M^{-1}, respectively.

Both neutral and cationic forms of dye showed characteristic longest wavelength absorption maxima in water at 380 nm and 306 nm, respectively. Interestingly, fluorescence measurements indicated a large enhancement (24 fold) in the fluorescence intensity of cationic form of coumarin 1 dye as well as neutral dye (13 fold) in presence of the host CB[7] (Figure 3). Various spectroscopic techniques viz UV-vis absorption, steady state and time resolved fluorescence,^{1}H NMR, Job's plot revealed the formation of 1:1 dye:CB[7] inclusion complex for both the cases. Non-linear fitting of increase in fluorescence intensity of dye in presence of CB[7] gave binding constant of dye with CB[7], k= (5.6 ± 0.2) x 10^6 M^{-1} and (1.2 ± 0.2) x 10^5 M^{-1} for cationic and neutral dye molecules, respectively. The geometries of both the dye complexes were determined by applying quantum chemical calculation based on B97D/cc-pVDZ level of theory (DFT calculation). The total interaction energy of cationic dye:CB[7] complex was found to be -91.1kcal/M, which is more than two times higher than that in case of neutral dye complex as -44.7kcal/M. These results also supported by ^{1}H NMR study which suggested that cationic dye penetrates deeper within CB[7] cavity than the neutral dye. Comparative laser photostability study of cationic and neutral form of dyes in presence of CB[7], using third

harmonic (355 nm) of a pulsed Nd:YAG laser, showed better photostability of cationic dye complex, almost 2 times higher than normally used ethanol solution of dye.

Chapter-5 Host-Guest Interaction Study of Water Soluble BODIPY Dyes:

In continuation of study with water based fluorescent dyes, host-guest interaction strategy of new BODIPY (PM) dyes in visible region, which are hardly reported, was carried out and discussed in this chapter. With an attempt to make water soluble PM, we hypotheses that an aza analogue of PM597 containing Me_3N^+ group in place of Me_3C moiety might offer good Stokes shift because of steric crowding and also improves its solubility in water. The synthesis started with controlled nitration of starting reactant PM546 (**1'**) (Scheme 1) using dilute nitric acid (45%) to obtain 2-nitro Bodipy (**2'**) followed by catalytic hydrogenation transfer of dye **2'** afford amino dye **3'**. From there two different reactions, one by passing HCl gas to make quaternary ammonium HCl salt, dye **4** and in another reaction dye **5** was synthesized by N-alkylation of dye **3'** with methyl iodide. Purity was characterized by NMR, mass and elemental analysis.

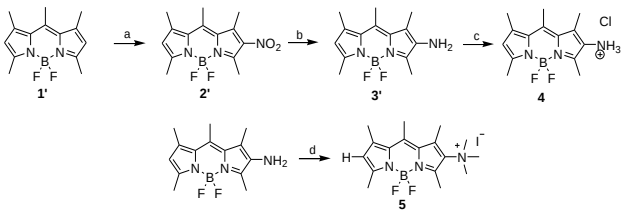

Scheme 1: Synthesis of dye **4** and **5**

Dye (dye:CB[7])	λ^a_{max} (nm)	λ^f_{max} (nm)	Φ_f	τ_f (ns)	$k_r(s^{-1})$ (10^9)	k_{nr} (10^9)
4 (1:0)	476	505	0.02	0.30	0.07	3.27
4 (1:50)	485	508	0.1	0.39	0.26	2.31
5 (1:0)	482	520	0.4	2.52	0.16	0.24
5 (1:50)	482	520	0.45	2.96	0.15	0.18

Table 2: Photophysical data of dye **4** and **5** in water with and without CB[7].

To avoid formation of non-radiative aggregates and improve its solubility in water, host-guest interaction of these PM dye molecules was studied with the host CB[7]. Absorption spectra were red shifted by 9 nm and a large enhancement in fluorescence intensity (~7 fold) in presence

of CB[7] for dye **4** was observed (Table 2). The binding constant of dye **4** was found to be k =4.4 x $10^3 M^{-1}$ which was two times stronger than that of dye **5,** k = 2.1 x 10^3 M^{-1}. ^1H NMR study suggested that aromatic part of both dyes make hydrophobic interaction with inner cavity and cationic amino moiety makes ion dipole interaction with portals of CB[7].

In addition to interaction of these dyes with CB[7], a different type of host-guest interaction of water soluble dye **5** was also studied with calf thymus DNA as host and found dye **5** binds with DNA strongly with a binding constant of 3.6 x 10^4 M^{-1}. The increase in its life time (τ) 2.22 ns in water to 3.27 ns in presence of DNA and subsequently reduction to 2.69 ns by addition of NaCl confirmed electrostatic nature of binding. Dye **5** also showed photo-nuclease activity via singlet oxygen generation as revealed by DNA gel electrophoresis in absence or presence of singlet oxygen inhibitor (NaN_3) and activator (D_2O). Fluorescence microscopy also showed good uptake of dye **5** by human lung cancer A549 cells. However it was not cytotoxic to the A549 cells even up to 50 mM concentrations both under dark or photo irradiation condition. Taken together the good fluorescence quantum yield (0.4) and a large Stokes shift (38 nm) of dye **5** suggests that it may be potentially good water soluble laser dye.

Chapter-6 Red Shifted BODIPY Schiff Bases with High Stokes Shift:

To improve another inherent limitation of BODIPY dyes i.e. small Stokes shift is the major concern of this chapter. A small Stokes shift reduces the fluorescence as well as laser emission intensity by self absorption. In the present study we rationally designed two different colored red shifted BODIPY schiff bases with a large Stokes shift. These new dyes were synthesized in order to further extend the conjugation of amino BODIPY as described in earlier chapter starting from 2,6-unsubstituted PM546. Then schiff bases **6** and **7** were synthesized by

condensation of **3'** and **3"** with p-methoxybenzaldehyde (Scheme 2). Photo-physical results showed that absorption (33 and 69 nm) and emission maxima (76 and 106 nm) of dye **6** and **7** respectively, were red shifted with respect to dye **1'** (PM546) making Stokes shift ~5 fold more of dye **6** and **7** than dye 1'(11nm). Large Stokes shift of both dyes were rationalized by the optimized geometry of molecules at ground (S_0) and excited states (S_1) by DFT method and it reveals that in compare to ground state (S_0) geometry of both dyes, the dihedral angle become more coplanar in excited state (S_1). Moreover the presence of C=N bonds of both dyes are very sensitive towards acidic environment and would be useful tool for pH sensing.

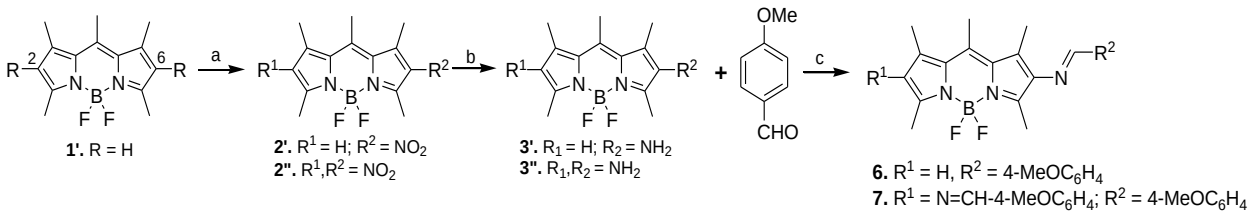

(a) HNO_3, 0°C, 1.5 h; (b) HCO_2NH_4, Zn-dust, MeOH, 25°C, 10 min; (c) Na_2SO_4, CH_2Cl_2, 25°C, 30 min.

Scheme 2: Synthesis of dye **6** and **7**

Photo-physical study showed that with addition of H^+ both dyes first converted to the corresponding amine then to the chloride salt (Figure 4). This was clearly understood from change in spectra. This wide change in spectra could be easily identified from its change in color from orange of dye **6** and red of dye **7** to green would be very helpful to measure the H^+ concentration.

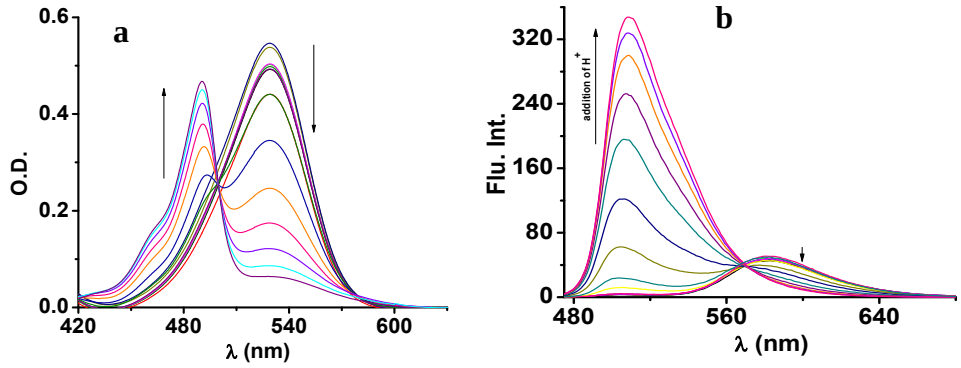

Figure 4: Proton sensing by dye **6** illustrated by (a) absorption and (b) fluorescence plot with addition of acid.

Summary:

Different types of new fluorescent dyes were planned and synthesized starting from UV to visible (red) region and characterized using different non-polar and polar solvents including water by host-guest strategy with objectives to make highly efficient and photo-stable laser dyes. Photo-physical, photochemical and laser properties of these dye molecules were carried out by using different spectroscopy techniques and constructed dye laser set up. Most of the synthesized dyes were well suited for laser application. While red dyes would be useful for pH sensing.

LIST OF FIGURES

LIST OF TABLES

LIST OF SCHEMES

LIST OF ABBREVIATION

Å	Angstrom(s)
Ar	Aryl
BODIPY	Borondipyrromethene, 4,4-difluoro-4-bora-3a,4a-diaza-*s*-indacene
CB[7]	Cucurbit[7]uril
δ	Chemical shift
DABCO	1,4-Diazabicyclo[2.2.2]octane
DCM	Dichloromethane
DDQ	2,3-Dichloro-5,6-Dicyano-1,4-benzoquinone
ESA	Excited state Absorption
Et	Ethyl
EtOAc	Ethyl acetate
EtOH	Ethanol
eq	equivalents
g	gram(s)
FRET	Fluorescent-Resonance-Energy-Transfer
GSA	Ground State Absorption
Hz	Hertz
IC	Internal Conversion
ISC	Inter System Crossing
J	Coupling constant (in NMR spectroscopy)

MeOH	Methanol
NMR	Nuclear Magnetic Resonance
ns	Nanosecond
PBS	Phosphate buffered saline
PD	Photodiode
PDT	Photodynamic therapy
PM	Pyrromethene
ppm	Parts per million
ps	Picosecond
RH	Rhodamine
τ	Lifetime
SNAr	Nucleophilic aromatic substitution
tBu	*tert*-Butyl
TBAP	Tertrabutylammoniumperchlorate
TFA	Trifluoroacetic acid
THF	Tetrahydrofuran
TMS	Trimethylsilyl
TS	Transition state
TCSPC	Time correlated single photon counting

CHAPTER 1

INTRODUCTION TO FLUORESCENT DYES

Chapter 1: Table of Contents

1.1 Introduction:

Originally a dye was defined as an organic compound with conjugation of double bonds that appeared as a brilliant color when exposed to visible light called fluorescent dyes. Fluorescent dyes have been studied in multidisciplinary area and have diverse applications such as active media of tunable lasers, in the development of photoelectric devices, sensitizer for solar cell, as a fluorescent probes and chemical as well as biological sensors.[1-4] Study of the photophysical and photochemical properties of fluorescent dyes, is very important in design and development of new dyes with tailored properties. Indeed a satisfactory correlation between the photophysical properties and lasing characteristics of several dyes has been established[5, 6] by changing the molecular structure of the chromospheres (substituent effect) and the environmental conditions (solvent effect, incorporation of rigid solid materials etc.)

1.2 Important feature of laser dyes:

Ever since its discovery in 1966 by Sorokin, Lankard and Schäfer *et al*, dye lasers have become important tool for spectroscopy and photochemistry. In order to select potential laser dye from a large number of available organic compounds and thousands of new compounds that can be synthesized, several research groups have made attempts to define empirical and theoretical criteria for correlating molecular structure with lasing properties of organic dyes.[7-9] It is in theory possible to incorporate the desired spectral properties into the laser dyes. The extensive studies of laser dyes by Schäfer[10] and many other workers illustrate the extent of which modification of the molecular structure of laser dyes can produce predictable improvements in lasing performance. However, incorporation of all the desired properties into a single laser dye molecule such as: a) high solubility in common solvents, b) high absorption cross sections at

pump wavelengths, c) near unity fluorescence quantum yield, d) low singlet-triplet intersystem crossing rate, e) short triplet state life time, f) stimulated emission cross section greater than induced absorption cross section, g) minimum self absorption of lasing emission due to ground state and triplet state absorptions, h) heat photochemical stability and i) negligible molecular aggregation in water at working temperature, presents a great challenge in molecular structure design and synthesis.

1.3 Principle of dye laser:

The term LASER is an acronym for Light Amplification by Stimulated Emission of Radiation. A laser is a device used for the amplification or generation of coherent light waves using an active medium in the UV, VIS, and near IR region. In dye lasers, a liquid solution of fluorescent dye is generally the active medium. A condition for stimulated emission to occur is that the number of molecules in the excited state S_1 is higher than that in the ground state S_0 at the moment of flash. The situation in which a large number of dye molecules exist predominantly in an excited state rather than ground state is known as population inversion and is brought about by pumping the system with a source of energy.

1.4 Classification of dye laser:

There are several ways in which we can classify the different types of laser.

(a) Depending on their mode of operation: (i) Continuous wave (CW) dye laser and (ii) Pulsed dye laser.

(b) On the basis of material used as an active medium: (i) Solid state dye lasers and (ii) Liquid dye lasers.

Among these, the family of liquid dye laser finds more suitable and more frequently used laser media than others due to several advantages such as inherent optical homogeneity and cooling by circulation, homogeneous spectral broadening by collision with solvent molecules and low cost. Moreover liquid is self repairing in comparison to solid-state active media where damage is usually permanent. In spite of several advantages, the major concern of liquid dye laser operation is its efficiency and photochemical stability. The approximate working ranges of various laser dyes are shown (Figure 1.4.1)

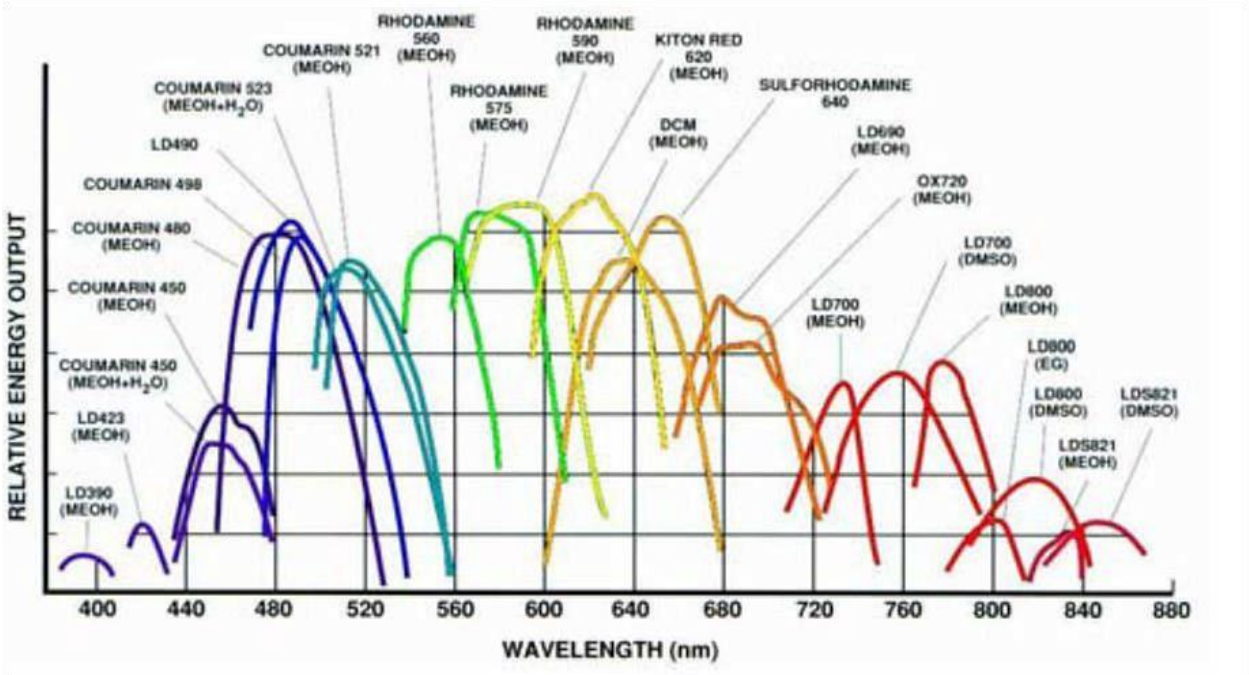

Figure1.4.1: Dye spectral emission characteristic

1.5 Dyes for laser application:

For effective performance, dye molecules should have following characteristics-

i. Strong absorption at excitation wavelength and minimal absorption at lasing wavelengths, i.e., minimum overlap between absorption and emission spectra.

ii. High quantum yield of fluorescence (Φ_f)

iii. Good photochemical stability

iv. A short fluorescence life time (τ_f)

v. Low absorption in the first excited state at the pumping and lasing wavelengths

vi. Low probability of intersystem crossing to the triplet state

vii. High purity of synthesized laser dyes since impurities frequently quench the laser output

1.6 Different class of laser dyes:

Generally, laser dyes are complex organic molecules containing a number of ring structures with polarized π electrons, which lead to strong absorption and emission in UV-vis-IR spectral region. The structure and composition of the molecule has an important influence on spectral emission.

1.6.1 Coumarin laser dyes:

Coumarin dyes are well known laser dyes for the blue green region.[11] Chemically these molecules are the derivatives of 1,2-benzopyrone. A group of widely used laser dyes derived from coumarins by substituting 7-position with oxochromes such as -OH, -OCH_3, -$NHCH_3$, -$N(CH_3)_2$, -NH_2, and other electron donating substituents. The amino analogue, 7-amino-4-methylcoumarin (coumarin 120) (**1**) shows laser action at 440 nm. In some coumarin dyes the basic chromophore is replaced with its heterocyclic analogues like aza-coumarin, quinolone or aza-quinoline in order to enhance the fluorescence properties. AC3F dye (**2**) is an example of these classes of dyes (Figure 1.6.1.1).

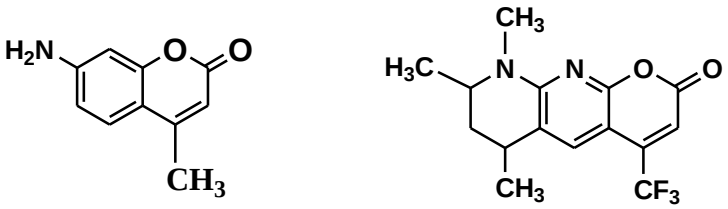

Figure 1.6.1.1: Molecular structures of coumarin 120 (**1**) and AC3F (**2**)

Coumarin molecules as such are non-fluorescent, but it exhibits intense fluorescence on substitution of various functional groups at different positions. In general, electron-donating substituent tends to enhance emission intensity while electron-withdrawing substituent tends to diminish it. Some of the important coumarin laser dyes are listed in Figure 1.6.1.2

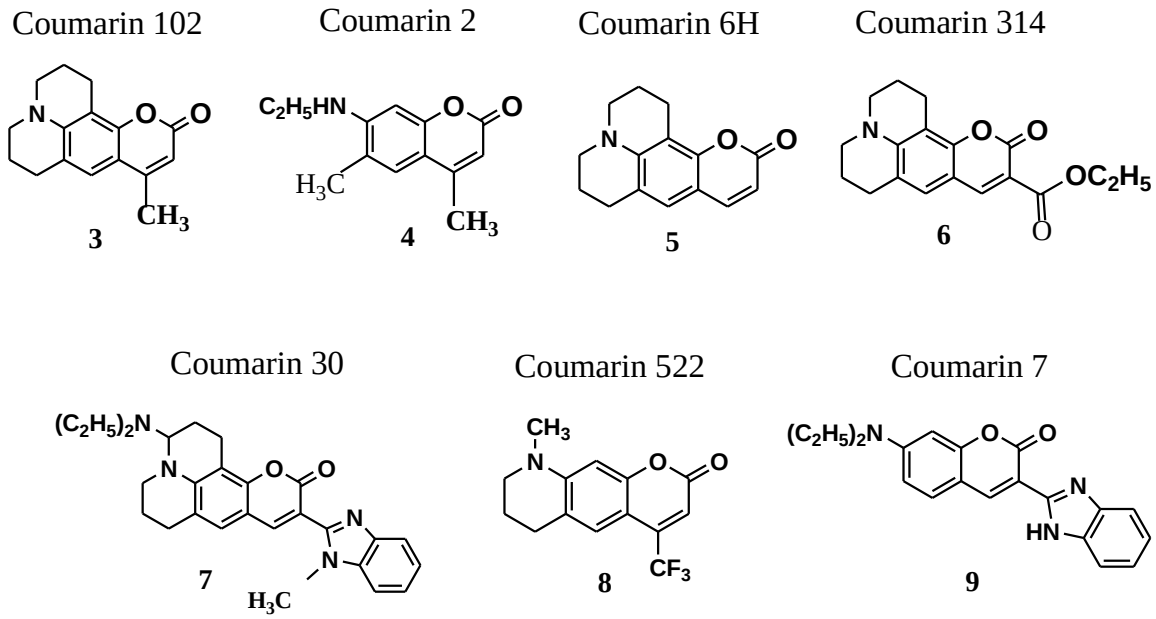

Figure 1.6.1.2: Examples of Coumarin laser dyes

1.6.2 Xanthene laser dyes:

Xanthenes or Rhodamine family of dyes cover wavelength region from 500 to 700 nm and are generally very efficient. The electronic distribution in the chromospheres of xanthenes

dyes can be described by the following two identical mesomeric structures, (**10**) and (**11**) shown in Figure 1.6.2.1

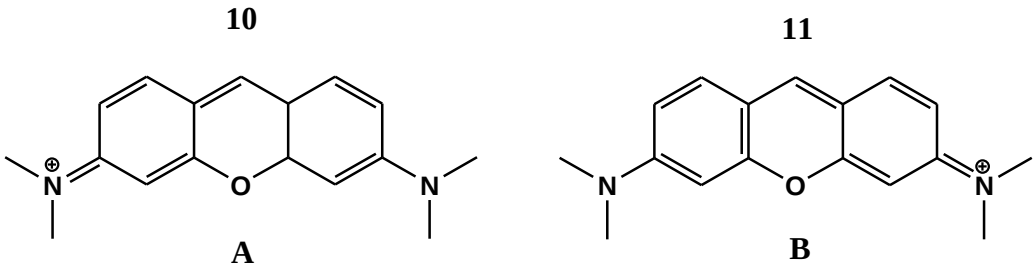

Figure 1.6.2.1: π electron distribution in the chromophore of xanthenes dyes

Rhodamine 6G (**12**) shows efficient laser action in the 590 nm region. It is used as a reference dye to measure the efficiency and photochemical stability of other dyes. This laser dye is one of the most often used and studied. Most of the xanthenes dyes show efficient laser action in the 560 to 800 nm region. Some xanthenes class of laser dyes were shown in Figure 1.6.2.2

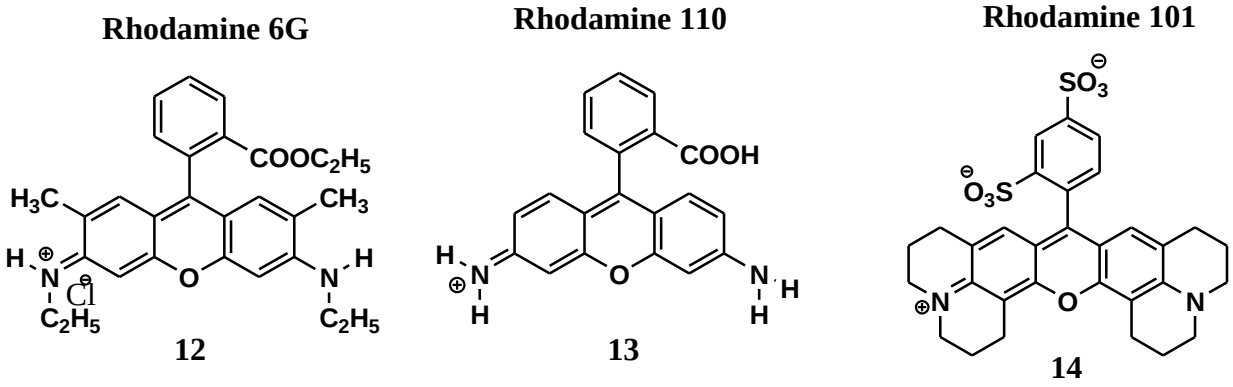

Figure 1.6.2.2: Examples of Rhodamine laser dyes

1.6.3 Pyrromethene laser dyes:

Boron-dipyrromethene (PM) dyes, also known as BODIPY, are composed of dipyrromethene complexes with a distributed boron atom, generally a BF_2 moiety. Due to the

complexation with BF_2, the bodipy fluorophore considered as an example of a "rigidified" monomethine cyanine dye with fixed planarity of the chromophoric π-electron system.[12] BODIPYs or Pyrromethenes are an important class of laser dyes. They are tunable in the green-yellow visible region of the electromagnetic spectrum. They have a low intersystem crossing (ISC) rate[13,14] and often possess a triplet-triplet absorption coefficient about one-fifth that of the rhodamine dyes.[15] Some of the Pyrromethene (PM) dyes outperform the widely used laser dye, rhodamine 6G (**12**), considered as the benchmark in lasing efficiency and photochemical stability. The photophysical properties of these dyes can be modulated to some extent by incorporating the adequate substitution in the molecular structure of the parent BODIPY chromophore (**15**). These dyes have excellent thermal stability both in solution and in solid state. BODIPY framework favors both nucleophilic and electrophilic substitution reaction on the chromophore core. The molecular structure of BODIPY chromophores are shown in Figure 1.6.3.

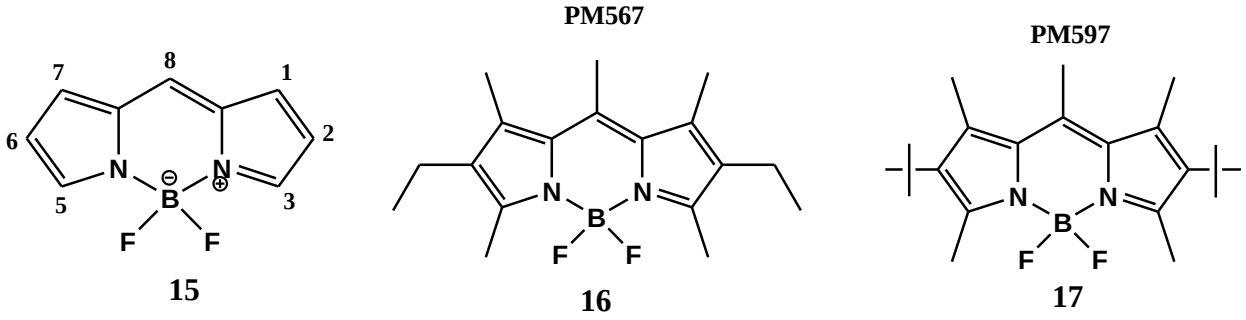

Figure 1.6.3.1: Chemical structures of common BODIPY dyes

1.6.3.1 Modification in BODIPY core:

Various analogues of PM dyes were synthesized by changing the substituent in pyrrol ring and boron centre of the BODIPY core. Some of the commonly used PM dyes are commercially available. Among these, 1,3,5,7,8-pentamethyl 2,6-diethyl pyrromethene-BF_2 (**16**) complex, known as **PM567,** and 1,3,5,7,8-pentamethyl 2,6-di-t-butyl pyrromethene-BF_2 (**17**) complex, known as **PM597,** are the most efficient and popular dyes (Figure 1.6.3.1). From structure modification point of view it can be classified into two categories-

(i) Electrophilic substitution:

BODIPY molecules at the 2 and 6 positions readily undergo electrophilic substitution reactions. This high level of reactivity was exploited by Boyer and coworkers. After this water soluble analogue was also synthesized.[13c] Other electrophiles can be introduced by providing the facile route to the isolation of BODIPY dyes. It should be noted that this approach leaves the B-F bonds unscathed, the substitution reaction occur exclusively at 2,6-positions, and is therefore a valuable route for selective substitution. A BODIPY core bearing a methyl group at 3,5-position can be subjected to chemical modifications on the methyl carbon atoms due to its strong nucleophilic character. Several synthetic procedures have been used to extend the π- electron conjugation and have effect of introducing a bathochromic shift to both absorption and fluorescence spectral maxima[16] (Scheme 1.6.3.1.1).

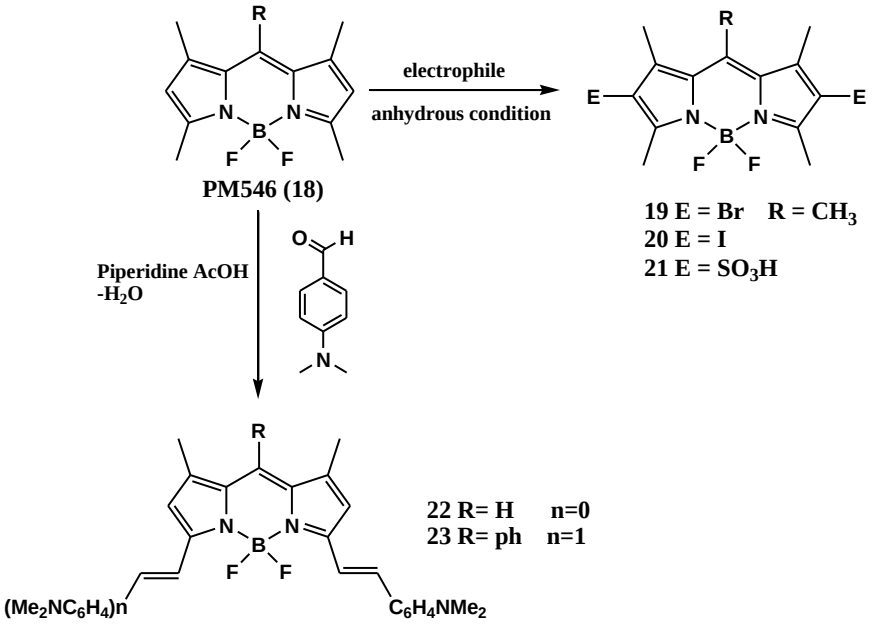

Scheme 1.6.3.1.1: Electrophilic substitution reaction and introduction of styryl group

(ii) Nucleophilic substitution:

The presence of good leaving group (Cl, I) in the BODIPY core facilitate the introduction of amino or alkoxy group at the sites by nucleophilic substitution reaction and also facilitate further extension of the conjugation length.[17] A thiophenyl group at the 8-position is also an effective leaving group in the presence of an amine.[18] (Scheme 1.6.3.1.2).

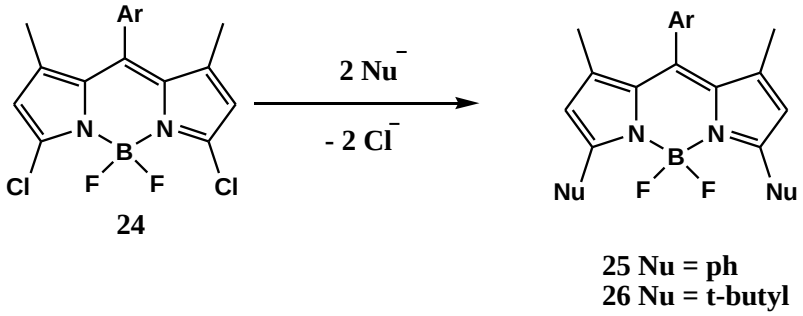

Scheme 1.6.3.1.2: General method of nucleophilic substitution

(iii) Modification at boron centre:

B-centre offers another option for substitution with no electronic effect on the BODIPY core because the changes in the π–electron density on the fluorine atom in the S_0 and S_1 states are very low.[19] Substitution at B-centre has recently been used[20] in particular to increase their Stokes shift,[20a, 21a] solubility,[21b] and chemical stability.[21b] Depending on the nature of the substrate, organolethium or Grignard reagent were used to efficiently substitute the fluorine atom Figure 1.6.3.1.1.

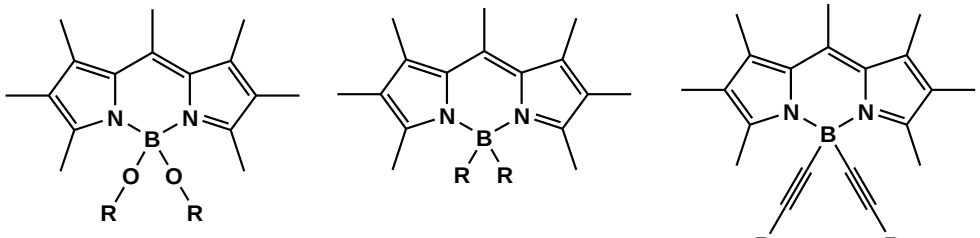

Figure 1.6.3.1.1: Examples of B-centre substituted BODIPY dyes

1.6.3.2 Application of BODIPY dyes:

BODIPY dyes have diverse applications in several fields in addition to tunable laser media via different substitution at molecular framework. A well known laser dyes PM567 (**16**), PM597 (**17**) and PM546 (**18**) has been used with chemical modification for desired applications as follows-

(i) Biological applications:

BODIPY dyes are the most promising candidate as a fluorescent biolabeling probe due to their small molecular size and they do not significantly influence the biological function. Several BODIPY based fluorescent probes are widely used to target important biological makers such as DNA, RNA, proteins etc.[22]

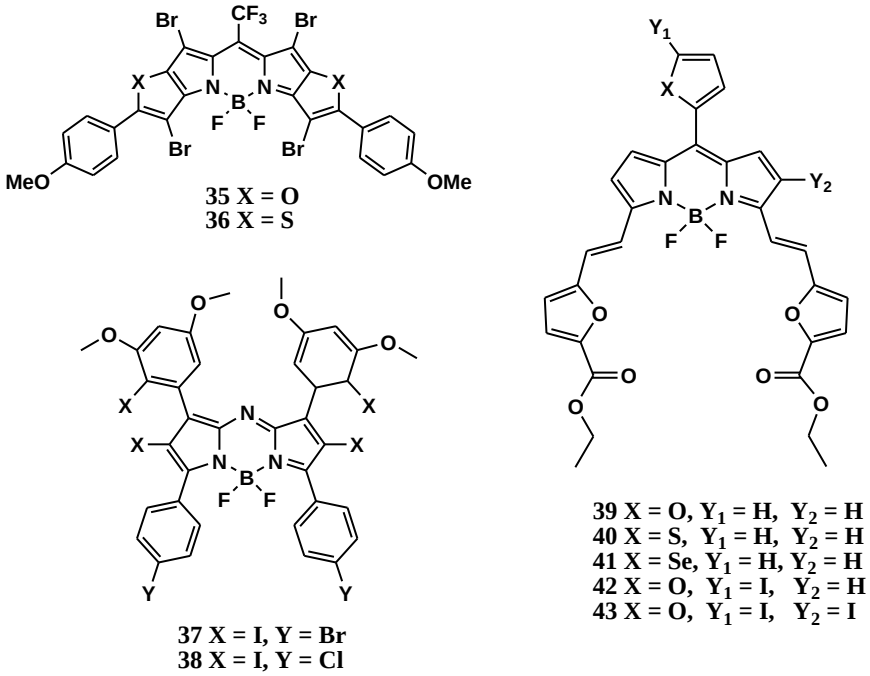

Figure 1.6.3.2.1: Examples of BODIPY photosensitizers

Apart of these, BODIPY dyes also have important application in photo dynamic therapy (PDT). The intense absorption of these dyes in the near-IR region makes them suitable for PDT application. In 2002 O' Shea and coworkers were first prepared the series of aza-BODIPY as a photosensitizer to give the resulting dyes have high singlet oxygen ($^1O_2$) quantum yield and potent photodynamic activity (Figure 1.6.3.2.1).[23] After this structural modification of these dyes displayed varying degrees of singlet oxygen generation based on heavy atom substitution. The

position and number of heavy atom substitution modulated the generation of singlet oxygen due to spin-orbit perturbation.[24] Latter on introduction of functionalized styryl and distyryl groups with water soluble moieties enhanced biocompatibility, hydrophobicity and cellular uptake.[25]

(ii) Chemical sensor:

The development of efficient sensor that operates by fluorescence modulation is of great interest in chemistry for the clinical, medical and environmental science.[1b] The key feature of such applications is that the trapping of an analyte at some predesigned site causes a pronounced change in the fluorescence properties of the sensor. BODIPY dyes have several attributes that make them good candidates as a fluorescent sensor in biological system. Their spectroscopic and photophysical properties can be finely tuned by substitution on the dipyrromethene core. Dehaen and coworkers originally performed systematic work on the reactivity of the 3,5-dichlorinated BODIPY with carbon, nitrogen, oxygen and sulphur directed towards nucleophilic aromatic substitution and palladium catalyzed cross coupling.[26] Mono and disubstituted products were prepared selectively by careful tuning of the reaction conditions. In many cases improved selectivity can be obtained when the sensing events perturb a charge transfer excited state or interrupts intramolecular electron transfer.[27] Daub and Rurack,[2b,28] were the first to show high potential for these dyes in this field and their original research has been followed by number of BODIPY based fluorescent molecular sensor. Some of the examples are shown in Figure 1.6.3.2.2

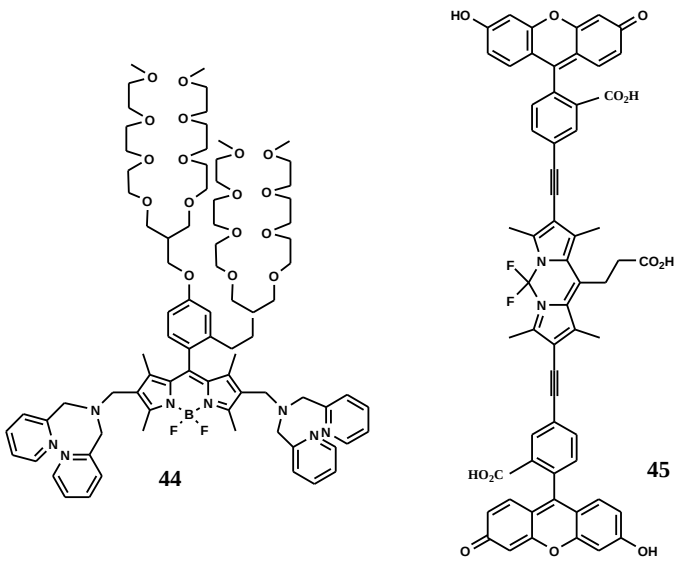

Figure 1.6.3.2.2: Chemical structures of Bodipy based sensors

In addition to above BODIPY molecules also have attractive interest in solar cell, as luminescent devices, energy transfer cassettes etc.

1.7 Role of solvent in laser dye:

Dye molecules in liquid dye laser were surrounded by electrostatic environment of solvent. Nature of solvent play an important role deciding the photophysical, photochemical and laser properties of dye molecules.[4,29] Many application of organic dye laser require achievement of high average power. This limit is very much dependent upon the properties of the solvent used for the lasing dyes. The solvent of choice are water (H_2O) and heavy water (D_2O) because of their large heat capacity, small variation of refractive index with temperature (dn/dT), photostability, non-flammability, non toxic and easy treatment and disposal properties. But the water as a solvent for dye laser has some limitation. Generally organic dyes in aqueous solution have very poor solubility and tendency to form dimmers. In most of the cases the fluorescence of the dimmer is completely quenched. Although low solubility and aggregation in aqueous

solution is very common with most of the dyes, it usually does not occur in organic solvents, even at very high concentration and low temperature.[30] It is possible to suppress the aggregation of dyes in aqueous solution by addition of organic compounds or some additives forming cage around the dye molecules and shed from water. These compounds are known as host molecules and also used to solubilize guest dye molecules that are insoluble in water.

1.8 Host-Guest interaction:

The host-guest interaction in solution have been the subject of much interest in recent years.[31] The interaction of dye molecules with macrocyclic host often leads to increased photostability of the guest dyes along with significant changes in their photophysical and other properties.[32] Studies on such system have gathered tremendous interest for the long time aiming to explore their potential applications in different areas.[33] Macrocyclic hosts are unique cage-like molecule and guest molecules can be encapsulated partially or fully.[34] Although in most host-guest system, the hydrophobic interaction plays a major role,[35] in some of the system depending upon the nature of the host and guest molecules, H-bonding,[32a, 33d, 36] ion-dipole[32,33a,35] or charge dipole[32b, 36a] interaction can also render additional binding strengths to the host-guest complexes.

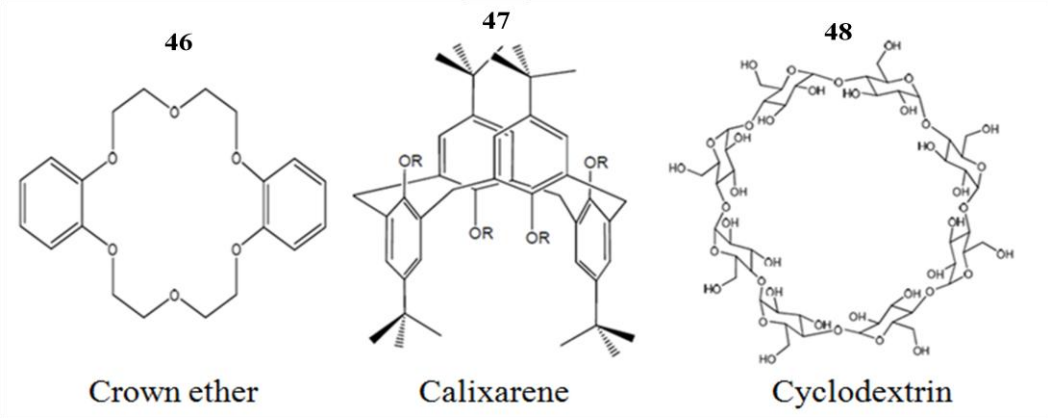

Figure 1.8.1: Examples of macrocyclic host molecules

There are a number of families of organic host molecules which have been used (Figure 1.8.1) to encapsulate guest molecules including cyclodextrin,[37] calixarenes,[38] dendrimers,[39] cavitands[40] and cucurbit[n]urils. Among them, the cucurbit family of host has received immense attention in study of host-guest interaction due to their rigid structure, enhanced thermal stability, broad range of size and high selectivity for guest binding as compared to the other host molecules.

1.8.1 Cucurbituril as a host molecule:

Cucurbituril (CBn) are the family of macrocyclic host composed of n glycoluril units. The name of these pumpkin shaped host is derived from Latin word *Cucurbitaceae,* taken from name of the plant family that includes pumpkins.[41] The cucurbituril was characterized initially by Mock and synthesized earlier by Bhrend.[42] More recently, Kimmom Kim[43] and Anthony Day[44] have independently developed method to separate the different homologous of cucurbit[n]uril from the reaction mixture. The isolation of these homologous has dramatically increased the popularity of cucurbituril as host. Different size of known CBs are shown in Figure 1.8.1.1.

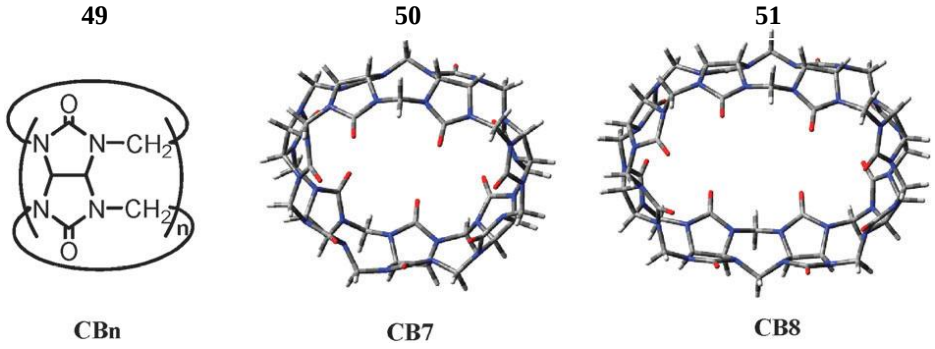

Figure 1.8.1.1: Chemical formula and energy optimized structures of Cucurbituril

1.8.2 Synthesis and classification of cucurbiturils:

Cucurbituril are an interesting class of macrocyclic receptor molecules composed of methylene bridge glycoluril monomers with highly symmetrical hydrophobic cavities accessible

through two identical carbonyl laced portals. Depending upon the number of monomer units, different homologous of cucurbiturils (CB[n] n= 5-10) with varying cavity and portal dimensions are known.[41,45] Properties of different types of cucurbiturils were shown in Table 1.8.2.1.

Table 1.8.2.1: Cavity dimensions and aqueous solubility of CB[n] host

Host	Portal Diameter (Å)	Interior Cavity Dia (Å)	Hight (Å)	Cavity Volume ($Å^3$)	Solubility in Water (mM)
CB[5]	2.4	4.4	9.1	82	20-30
CB[6]	3.9	5.8	9.1	164	0.018
CB[7]	**5.4**	**7.3**	**9.1**	**279**	**20-30**
CB[8]	6.9	8.8	9.1	479	< 0.01
CB[10]	9.5-10.6	11.3-12.4	9.1	870	-

The synthetic approach involves the acidic condensation of glycoluril with formaldehyde at 75-90^0C for 72 h to yield a mixture of CB[n] homologous[43,44,46] (Scheme 1.8.2.1). From the mixture of different CBs, the individual CBs are separated in pure form using fractional crystallization and dissolution using various solvent system such as acetone-water and methanol-water mixtures and involve multiple solvent based separation cycles.[43,44,46] Among the set of CBs the complexation behavior of cucurbit[7]uril (CB[7]) has been extensively studied due to its substantial solubility in water as well as wider cavity as compared to other homologous like CB[5], CB[6], CB[8] and CB[10].

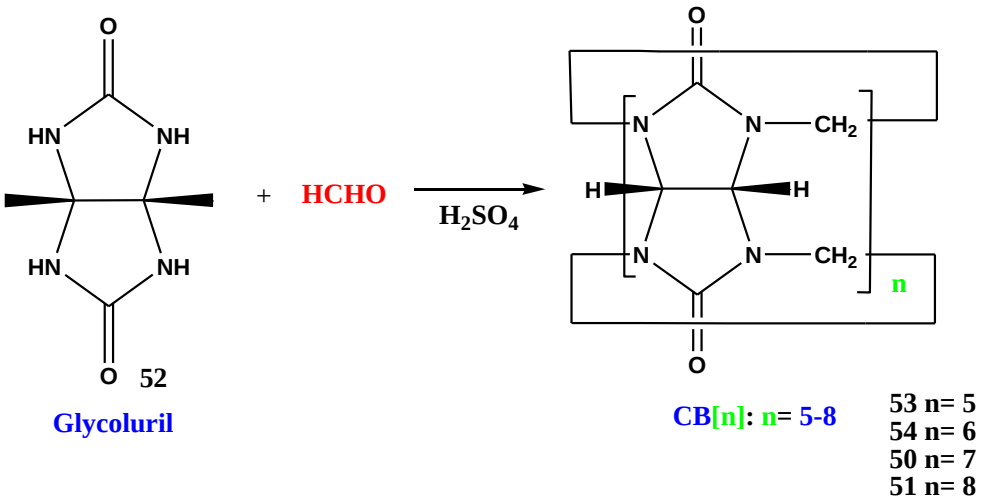

Scheme 1.8.2.1: Synthesis of Cucurbit[n]uril

1.8.3 Probability of binding sites of cucurbiturils:

From the structure point of view, major concern of these CBn has the two specific sites for interaction (i) Non-covalent interaction occur in the interior region of the cage which is hydrophobic in nature and suitable for interaction of nonpolar organic residue. (ii) Ion–dipole interaction or Electrostatic interaction occurs at the carbonyl laced portals of CB[n] which have tendency to form strong inclusion complex with cationic guest molecules due to the participation of cationic charge of the guest and negatively polarized portal of the host. Specific interaction sites of cucurbiturils are shown in Figure 1.8.3.1

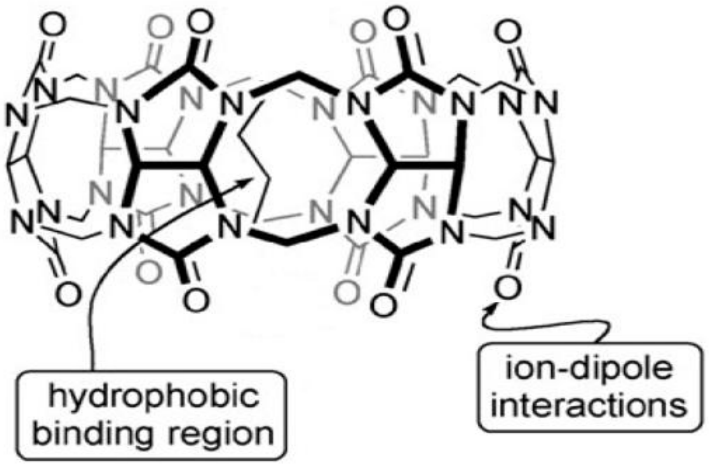

Figure 1.8.3.1: Specific sites of interaction of Cucurbituril hosts

1.8.4 Important properties of cucurbit[n]uril:

Cucurbituril are the proficient host for host-guest study of fluorescent dyes compare to other macrocyclic host to bind a range of guest molecules. Important properties are as follows-

(i) They are capable of forming strong complex with positively charged (or neutral) dye molecules by coordination of cationic sites with their portals and various organic residues in their hydrophobic cavities.[42a, 47]

(ii) CB[n] molecules have the potential to increase the solubility of poor-water soluble or insoluble guest molecules by formation of inclusion complex. Among all CBs, CB[5] and CB[7] has very good solubility (20-30 mM) in aqueous solution. The solubilization effect of CB[7] suppresses also the absorption of fluorescent dyes to material surfaces. In addition, the absorption/fluorescence intensity of aqueous dyes deplete rapidly with time during ongoing experiment which can be entirely prevent by the addition of CB[7]. CB[7] and its complex have only a very low propensity to absorb to glass and polymer materials.

(iii) Large enhancement in their fluorescence intensity frequently observed when host molecules are added to the aqueous solution of fluorescent dyes, which leads to avoid charge transfer in excited state from ICT (intramolecular charge transfer) to TICT (twisted intramolecular charge transfer) and further reduced the non-radiative decay rate.

(iv) Variation in the absorption and fluorescence spectra can be principally employed to estimate the polarity of inner cavity which cannot be assessed by direct spectroscopic technique. Guest molecules encapsulated by CB[n] experienced low polarizability due to its rigid cavity size, close to the gas phase which leads to the novel and unprecedented chemical and photophysical property.

(v) With respect to the chemical reactivity, a low polarizability invariably reduces the rate of chemical reactions which gave a chemically inert reaction environment. The low polarity of CBs cavity and efficient exclusion of water molecules further reduces the rate of ionization reaction[48] and therefore provide a novel approach to achieve photostabilization of dyes in water.

(vi) Host cucurbiturils are transparent in the UV and visible region and do not act as a fluorescence quenchers at typically relevant concentration (mM). On the opposite, encapsulation by cucurbiturils greatly reduces the fluorescence quenching of dyes by external additives because it provides a protective shield.

(vii) The extinction coefficient presents an additional parameter to characterize the goodness of fluorescent dyes and it is good practice to define “brightness” as product of extinction coefficient. Complexation by CBs leads quite universally in an increased brightness of chemically quite different fluorescent dyes.

(viii) The CB[n] hosts are relatively rigid and also thermally stable, resisting decomposition at temperatures below 420^0C for most of the members of CB[n] family.[41]

1.8.5 Application of cucurbiturils:

The encapsulation of dye by cucurbituril is an emerging field with numerous applications. In comparison to cyclodextrin and calixarenes, cucurbiturils appear to be a better water soluble host molecule due to their desirable photophysical and photochemical effect on dye properties.

1.8.5.1 Drug delivery system:

Considerable interest has been devoted to cucurbiturils as drug delivery vehicle. CB[n] was observed to bind a variety of platinum based anticancer drugs by Day[49] and coworkers and Kim's group.[50] This attention has also been extended to metellocene based anticancer drug[51] as well as organic anti-tumor drugs such as albendazole[52] and comptothecin.[53] Day and coworkers observed that encapsulation of dinuclear platinum drugs by CB[7] was able to protect it from decomposition by guanosine while not affecting its cytotoxity or ability to bind to DNA.[49a,54] However, Kim's group noted that the complexation of oxaliplatin reduced it cytotoxicity. They also recently explored the use of nanoparticles based on functionalized CB[6] as a drug delivery vehicle.[55] There are a variety of benefits that may potentially arise from the use of cucurbiturils as host for drug. In addition to delivery of the drug, the host may also be useful for slow or controlled release of a drug. Also, depending upon the situation, they may also improve the solubility of drug,[52] reduced its undesired toxicity,[49a] improves its stability[56] or activate the drug.[56]

1.8.5.2 Biological application:

CB[7] has been observed to complex with biological relevant guests such as histamine H_2-receptor, antagonist ranitidine[57] and also to the nucleotide base that binds to the cobolt(III) centre of the vitamine B_{12} and coenzymes B_{12}. Encapsulation of base by CB[7] has been found to have the capacity to stabilize the base off forms of vitamine B_{12} and coenzymes B_{12}.[58] CB[7] has been shown to discriminate between dipeptide sequences, by binding to one sequence over another with a very high selectivity.[59]

1.8.5.3 Molecular sensor:

Recently Nau and coworkers have developed a method for using CB[7] as a part of a sensor in enzyme essays used to monitor amino acid decarboxylases, which can play important role in tumor growth and inflammation. A fluorescent dye, Dapoxy was used as a competitor with amino acid substrate for binds with CB[7] because dapoxy fluorescence signal differed significantly between its free form and its CB[7] bond species. A change in the dyes fluorescence signal could be used to indicate that it was being displaced by the decarboxylated amino acid.[60] Kim and coworkers has also shown the ability of CB[7] to be used as glucose sensors.[61] Nau and coworkers proposed that enhancement of dyes fluorescence life time by binding with CB[7] could have applications toward fluorescence life time imaging microscopy.

1.8.5.4 Separation:

Karcher and coworkers have explored the use of CB[6] for water treatment, specially the removal of reactive dyes from textile, waste water.[62] Liu and coworkers have found that HILIC chromatography utilizing CB[6] immobilized stationary phase could be successfully used to separate alkaloids. Cucurbituril tend to have higher selectivity compared to other host such as

cyclodextrin and calixarines, which facilitate their potential use in separation as well as self sorting systems.

1.8.5.5 Molecular switches:

Molecular devices are system whose properties can be changed by external stimuli such as pH, electrochemical potential, temperature, solvent polarity. Some examples have the complexation between CB[8] and methyl viologens, where the stiochiometry of the host-guest system is affected electrochemically. The first report by Mock and Pierpont, of a host-guest system with cucurbiturils acting as a molecular switch, was for the complex between CB[6] and $PhNH(CH_2)_6NH(CH_2)_4NH_2$ with the position of CB[6] being controlled by pH.[63] Kaifer and coworkers have reported pseudorotexanes between CB[7] and guest containing central viologen units, with the position of CB[7] being controlled by pH.[64]

More recently Pal and Nau[35b] have proposed that salt addition may be useful method to induce the release of a guest such as a drug from CB[7] cavity. For example with addition of NaCl observed decrease in binding constant between CB[7] and neutral red and also a decrease in the pKa shift that is observed with complexation to CB[7] so that unprotonated species of the dye becomes more favorable when salt is added.

1.8.5.6 Catalysis and stabilization of guest:

The ability of CB[n] to act as a catalyst for a chemical reaction was recognized by Mock. He noted that if reactants were efficiently bulky, the product may not be able to dissociate from the CB[n]. Nau and coworkers have used CB[6] as well as CB[7] to catalyze the acid hydrolysis of guest (Figure 1.8.5.6.1). The larger macrocycles such as CB[7] and specially CB[8] have shown further use for catalyzing and inhibiting reactions as their large cavity size allow them to

form complexes with a greater variety of guests. The stabilization of guest have also been observed by Kim and coworkers as when diprotonated trans isomer was bound to the macrocycle, and subsequently irradiated with UV light, it was converted to cis-isomer. This isomer was relatively stable in the presence of CB[7] due to the better alignment between cationic centers and electron rich portals.

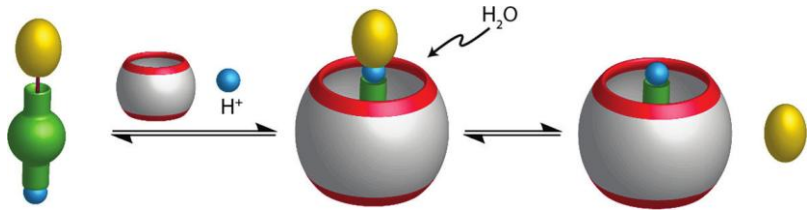

Figure 1.8.5.6.1: Schematic view of the strategy used by Nau and coworkers for the catalysis of hydrolysis with CB[6] and CB[7]

1.9 Conclusion and content of the present work:

Dye laser technology had advanced significantly over the last 50 years. Development of new laser dye is related to the development in terms of easy tunability, wide wavelength coverage, high photostability and synthetic simplicity. Changing the functional group within the classes of laser dyes having good host-guest interaction and laser characteristics has proven to be a useful way of creating new laser dyes and study of modified water soluble dyes molecules in aqueous system.

With this, aim is to design and development of new derivatives of fluorescent dyes ranging from UV to near IR region. The outline of the thesis as follows:

The experimental techniques used in the research work are described in **chapter 2**. The techniques are steady state absorption, fluorescence, NMR, Cyclic voltammetry, LINAC,

Nd:YAG pumped grazing incident grating, narrow band and broad band pulsed dye laser setup. The general overviews of these techniques are discussed, which includes principle, experimental setup and application in spectroscopy and present study.

Chapter 3 describes comparative photo-physical, laser characterization and triplet state reactivity of dyes and $^1O_2$ generation from dyes in polar and non polar solvent system of commercially available known PM dyes PM567 (**16**) and PM597 (**17**). Also, synthetic strategy to development of new bodipy dye (**58**) via substitution at B-centre of **16** with improved photo-physics, photostability and laser efficiency, in polar and non polar solvent compared to its starting substrate PM567 (**16**).

Chapter 4 concerns with study of water soluble UV dyes starting with Coumarin 1 neutral (**59**) and its cationic (**60**) form, its comparative inclusion complex with CB[7] has been studied via photo-physics, NMR and DFT calculation. Also, laser photostability of coumarin dyes (cationic and neutral forms) has been studied in presence and absence of host CB[7].

Then further extended our work (**chapter 5**) moving towards green-yellow region BODIPY dyes for design and development of new water soluble fluorescent dyes (**63** and **64**) via modification at 2 or 6-position of the core known as pyrromethene 546 (**18**) and their study of host-guest interaction with CB[7] was performed to improves its solubility and stability in water via experimental (steady state absorption fluorescence, fluorescence life time, NMR) and theoretical (DFT calculation) study. Also, new water soluble ammonium salt (**64**) of BODIPY dye has been studied for good DNA binding.

In next chapter (**Chapter 6**) extending the studies toward design and development of derivative of red BODIPY dyes (**67** and **68**) with large Stokes shift by introduction of styryl moieties at 2 or 6 or both position of the core which act as a proton sensor.

CHAPTER 2

EXPERIMENTAL TECHNIQUES

Chapter 2: Table of Contents

2.1 Introduction:

This chapter gives an overview of the various experimental techniques, which have been employed to illuminate the objective of the present thesis. Various important components of the instruments used in the current work are also concisely described in the present chapter.

For detail understanding of effect of molecular structure on photo-physical and laser performances of fluorescent dyes, both steady-state and time-resolved photo-physical measurements were carried out using absorption and fluorescence techniques. To understand the effect of anisotropy dynamics of dye molecule on dye laser operation, rotational relaxation times were evaluated using time-resolved fluorescence anisotropy measurements. High resolution ^{1}H-NMR spectroscopy was used to study the sites of interaction of dyes with the supramolecular host as well as identification of structure of synthesized compound. The triplet states decide the extent of $^{1}O_2$ generation by the dyes via energy transfer to dissolved O_2 in dye solution, and also reduction in the lasing efficiency by absorbing the dye laser photons. Hence, the triplet state studies can provide valuable information on the lasing characteristics and the photostabilities of the fluorescent dyes. The triplet states studies of the dyes in various solvent were carried out using the nanosecond pulse radiolysis technique. Electrochemical studies have been performed using cyclic voltammetry which gives an idea about oxidation potential of the molecules in different solvent system.

2.2. Ground-state absorption measurements:

To realize the effect of light on chromophoric molecules, it is vital to know the detailed absorption and fluorescence characteristics of the systems under examination. Optical absorption (UV-vis) spectroscopy is a widely used technique to gain information about the ground-state absorption characteristics of the chemical systems in terms of the wavelengths of the absorption

bands and the extinction coefficients at different wavelengths. UV-vis absorption spectroscopy, being dependent on the electronic structure and the environment of the absorbing chromophore, permit the characterization or the identification of various chromophoric systems and their microenvironments. Any alteration in the solvent polarity, polarizability and hydrogen bonding characteristics often induces a significant shift in the absorption spectra.[4,29,65,66] Hence, this simple photochemical technique can impart much useful information regarding the nature of interactions between the ground-state of a chromophoric molecule and its surrounding environment. Measurements of the optical absorption spectra and thus to get information about the absorbance of the experimental solution in the ground-state are always very essential to adjust the concentration of the absorbing species in the solution for the purpose of their analysis. The absorbance (A) of an absorbing species in a solution is directly proportional to the concentration (C) of the species and its molar extinction coefficient (ε_λ) at the measuring wavelength λ, and is given by the equation 2.1[4,29,65,66]

$$A = \log (I_o / I) = \varepsilon_\lambda \text{ x } c \text{ x } l \qquad (2.1)$$

where I_0 and I are the intensities of the incident and transmitted light, respectively, and l is the path length for the light beam passing through the sample. For absorbance measurements, the sample is usually kept in a quartz cuvette of 1 cm path length. For concentrated solutions, thinner quartz cell with path length of 0.1 cm is used. Ground-state optical absorption spectra for the dye solutions to be investigated in the present study were carried out using double beam UV-vis spectrophotometers (Jasco, Japan (model V530)). The wavelength ranges covered by the spectrophotometer is 200-1100 nm. As the light sources, the spectrophotometer uses W-lamp for the 1100 to 350 nm region and a D_2 lamp for the 350-200 nm region. The minimum wavelength resolution for the spectrophotometer is 0.2 nm and lowest absorbance measurable is ~0.005. The

technique was useful to adjust the O.D. of dye solutions at particular wavelength, in estimating the quantum yield of photo-degradation values of dye molecules by observing change in the optical densities before and after photo irradiation etc.

2.3. Fluorescence spectroscopy:

2.3.1. Steady-state fluorescence measurements:

The technique of fluorescence spectroscopy is extremely powerful. Various photophysical processes that take place in the excited state of the chromophoric molecules are investigated efficiently by this technique. The intensity of the fluorescence emission, the fluorescence peak position (emission maximum), as well as the shape of the fluorescence spectrum of dye molecule are in general very susceptible to the environmental effects.[4,29,65,66]

Principle:

Under normal condition, state molecules are generally excited from the lowest energy (υ=0) vibrational level of ground electronic state (S_0) to higher vibrational level excited electronic state (S_1) after photon absorption. The fluorescence emission generally occurs from molecule in the υ'=0 vibrational level of the first excited state. Consequently, emission maximum is always observed at longer wavelength as compared to the wavelength at which absorption maximum is observed.

The difference between absorption and emission maxima is known as 'Stokes shift'. Generally, detrimental ground state absorption (GSA) of dye molecules at dye laser wavelengths decreases with increase in the Stokes shift. We can also measure another important parameter viz., quantum yield of fluorescence (Φ_f), which is defined as the ratio of the number of fluorescence photons emitted from the sample to the number of light quanta absorbed by the sample. Thus Φ_f is expressed by the following equation.[4,29,66,67]

$$\Phi_f = \frac{\text{Number of Quanta Emitted}}{\text{Number of Quanta Absorbed}} \qquad (2.2)$$

The fluorescence quantum yield of an unknown sample is normally determined by using a comparative method, as the determination of the absolute number of photons absorbed and emitted by the sample is very difficult.[4,29,65,66] In comparative method, the integrated emission intensity of the sample is compared with that of an optically matched (very close absorbance at the excitation wavelength) reference sample whose quantum yield is already known. Thus, keeping the excitation wavelength same for both the sample and the reference, the fluorescence quantum yield of the sample (Φ_s) can be expressed with respect to the quantum yield of the reference (Φ_r) by using the traditional equation 2.3.[4,29,65,66]

$$\Phi_s = \frac{A_r}{F_r} \times \frac{F_s}{A_s} \times \frac{\eta_s^2}{\eta_r^2} \times \Phi_r \qquad (2.3)$$

Where A_r and A_s are the respective absorbance at the excitation wavelength, F_r and F_s are the integrated fluorescence intensities and η_r and η_s are the refractive indices for the reference and the sample solutions, respectively. The measurement of fluorescence quantum yield (Φ_f) of dye solutions were also carried out using the comparative method of Williams *et al.*,[67] which additionally validates the use of standard dye solution and its Φ_f value and is much more reliable in comparison to the above traditional method. In this method, the integrated fluorescence intensity of dyes are recorded by preparing dye solutions in a known range of concentrations (~10^{-6} M), ensuring linearity of fluorescence yield across the concentration range, and acquiring data at a number of different absorbance. The standard samples should be chosen to ensure they absorb at the excitation wavelength of choice for the test sample, and if possible, emit in a similar region to the test sample. The standard samples must be well characterized and suitable

for such use. Refractive indices of solvents were considered for calculations. Standard 10 mm path length quartz cuvette was used for fluorescence measurements. In order to minimize re-absorption effects, absorbance in the 10 mm fluorescence cuvette was kept below 0.1 at the excitation wavelength, which is close to absorption maximum of dye solutions. The gradient for each sample solution is proportional to the fluorescence quantum yield of that sample. Conversion into an absolute Φ_f is achieved using the equation 2.4:

$$\Phi_x = \Phi_{st} [Grad_x/Grad_{st}][\eta_x^2 / \eta_{st}^2] \qquad (2.4)$$

Where the subscripts 'st' and 'x' denote standard and test respectively, 'Grad' the gradient from the plot of integrated fluorescence intensity vs. absorbance, and η the refractive index of the solvent. First, the two standard dye solutions were cross checked by calculating the Φ_f of each standard sample relative to the other using this equation. Our measured values were considered reliable as good linearity with a zero intercept was obtained. For each test dye, two Φ_f values were obtained, relative to both the standard. The average of the two values for each dye solutions are considered for respective Φ_f values.

In the present study, steady-state fluorescence measurements were carried out using a Hitachi model F-4500 fluorescence spectrometer. The instrument uses a 150 watt continuous powered high pressure Xenon lamp as the excitation source and R-928F (Hamamatsu) photomultiplier tube (PMT) as the photo-detector. Sample is excited in a 1 cm x 1 cm suprasil quartz cuvette and the fluorescence is collected and measured in a perpendicular direction with respect to the direction of the excitation beam. The wavelength range covered in the present instrument is 220 to 800 nm.

2.3.2. Time resolved fluorescence measurements:

Time-resolved fluorescence measurements are very crucial to obtain information about the kinetics and dynamics of various photophysical processes involved in the deactivation of the excited molecules. Excitation of a sample containing fluorophoric molecules with a very short pulse of light results in an initial population (n_0) of fluorophores in the excited state. Since emission from the individual excited molecules is a random process, for a given time-window following photoexcitation with an ultrashort light pulse each of the excited fluorophores should have the same probability to emit a fluorescence photon. This condition in effect results the excited state population to decay following a first order rate equation as,[4,29,65,66,68-71]

$$(dn(t) / dt) = - (k_r + k_{nr})\, n(t) \qquad (2.5)$$

where n(t) is the number of excited molecules at time t following the very short pulse excitation of the sample, k_r is the radiative decay rate constant and k_{nr} is the non-radiative decay rate constant of the excited fluorophores. In an actual experiment, it is often difficult to know the exact number of the excited molecules present in the sample. However, knowing the fact that the fluorescence intensity is directly proportional to the number of excited molecules present in the solution, equation 2.5 can be simply expressed in terms of the time-dependent intensity I(t) and the integration of the resulting equation gives us the expression for the fluorescence decay I(t) as,

$$I(t) = I_o \exp(-t / \tau_f) \qquad (2.6)$$

Where I_0 is the intensity at time zero and τ_f is the fluorescence lifetime of the sample and the latter is related to the radiative and non-radiative decay rate constants as,

$$\tau_f = 1 / (k_r + k_{nr}) \qquad (2.7)$$

If the width of the excitation pulse is unusually short (δ-pulse) and the response time of the detection system is very fast compared to the fluorescence lifetime of the sample, the

fluorescence lifetime can be obtained from the observed fluorescence decay by using the following two procedures. In the first method, the τ_f can be obtained merely by recording the time at which the fluorescence intensity decreases to 1/*e* of its initial value. Other method, the lifetime can be determined from the slope of the plot of log I(t) versus t.[4,29,65-69]

Regarding the fluorescence decay, however, since the excited fluorophores emit randomly, different molecules spend different length of times in the excited states. Thus, for an ensemble of excited molecules in the system, some may emit at very short times following the excitation but others may emit at times much longer than the measured fluorescence lifetime of the sample. Accordingly, the time distribution of these emitted photons actually represents the measured fluorescence decay curve of the experimental sample. It is thus manifested that, the estimated lifetime from the observed fluorescence decay is actually the statistical average of the time that the excited molecules spend in the excited state. As already mentioned, the time-dependent fluorescence measurement is very essential to inspect the dynamics and mechanism of the photoinduced processes in the excited singlet (S_1) state of the molecules. The further details regarding basic principle, instrumentation and analysis may be obtained from references.[4,29,65,66, 68-72]

Time-Correlated Single Photon Counting (TCSPC) technique is the most widely used experimental method to measure the time-dependent fluorescence of a sample in the nanosecond to picosecond time scales. In the present study a LED-based time-correlated single-photon-counting (TCSPC) spectrometer (IBH, UK) was used to measure the fluorescence lifetime of the samples under investigation. The fluorescence decays were measured with a 490 nm LED (~100 ps, 1 MHz repetition rate) excitation source and a TBX4 detection module coupled to a special Hamamatsu PMT instrument. The instrument response function was 1.2 ns at full width half

maximum (FWHM). Following deconvolution analysis of the fluorescence decays, the time resolution of the present setup was around 50 ps.

2.3.3. Fluorescence anisotropy measurements:

The ground-state fluorophores are all randomly oriented in a homogeneous solution. When such an isotropic ensemble of chromophores is excited with a polarized light beam, due to the selective excitation of the suitably oriented chromophoric molecules in the solution an anisotropic distribution is generated in the excited state (also in the ground-state which is not considered at present). Thus, observation and measurement of fluorescence anisotropy is based on the photo-selective excitation of fluorophores, which can be better understood in the following manner. With respect to the molecular axis, each fluorophore within its molecular framework has a fixed absorption and fixed emission transition dipoles which have specific orientations. These two transition dipoles in a molecule are usually separated from each other by an angle β. Those fluorophores preferentially absorb the excitation photons that have their absorption transition dipoles parallel to the electric field vector of the polarized excitation light. The probability of absorption for a molecule for which its transition dipole is oriented at an angle θ is with respect to the direction of the electric field vector of the polarized light is proportional to $\cos\theta$. Therefore absorption is maximum when $\theta = 0^0$ and becomes negligible when θ approaches 90^0.[65,68,70,73] Thus, the excited state population obtained following the excitation of the sample by a polarized excitation pulse is not randomly oriented but highly anisotropic in nature. This preferential excitation of molecules creates anisotropy in excited electronic state and this is schematically shown in Figure 2.3.3.1. Similarly, an excited molecule emits a photon preferentially with its electric field vector parallel to the emission transition dipole of the molecule. At any other angleϕ, the probability of emission is again proportional to $\cos\phi$, where ϕ

is the angle between the electric field vector of the emitted light and the emission transition dipole of the molecule. Thus, due to the selective excitation and emission, the fluorescence obtained following excitation with a polarized light is highly anisotropic in nature. In dilute solution, where depolarization of the excited molecules via energy transfer among chromophoric components is very insignificant, the excited-state anisotropy of the system decays mainly due to the rotational relaxation of the excited species. The anisotropy measurements reveal the average angular displacement of the fluorophore that occurs between the absorption and the subsequent emission process. This angular displacement is dependent upon the rate and the extent of the rotational diffusion of the excited species during the lifetime of the excited state. As expected the rotational diffusion of a molecule depends upon its size and shape as well as on the viscosity or the rigidity of its local environment. Thus, studies on the fluorescence anisotropy have been utilized extensively to explore the local environment of the chromophoric dyes as well as to investigate their interactions with various host molecules or supramolecular systems.

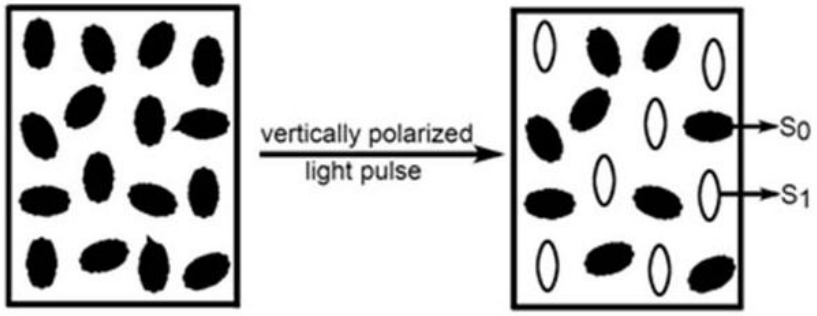

Figure 2.3.3.1: Creation of ground-state and excited state anisotropies from an isotropic distribution of molecules

Fluorescence anisotropy can be measured using both steady-state and time-resolved fluorescence spectrometers. In the steady-state measurement, the sample is illuminated with a continuous beam of plane polarized light, and the intensities of the fluorescence emission are recorded for both parallel and perpendicular polarizations of the emitted light with respect to the

vertically polarized excitation light. In the time-resolved anisotropy measurement, the sample is excited with a vertically polarized pulsed excitation light source and the fluorescence decays are collected for both parallel and perpendicular polarizations of the emitted light with respect to the excitation polarization. The general measurement procedure of the fluorescence anisotropy (both steady-state and time-resolved) is illustrated in Figure 2.3.3.2.[65,68,70,71]

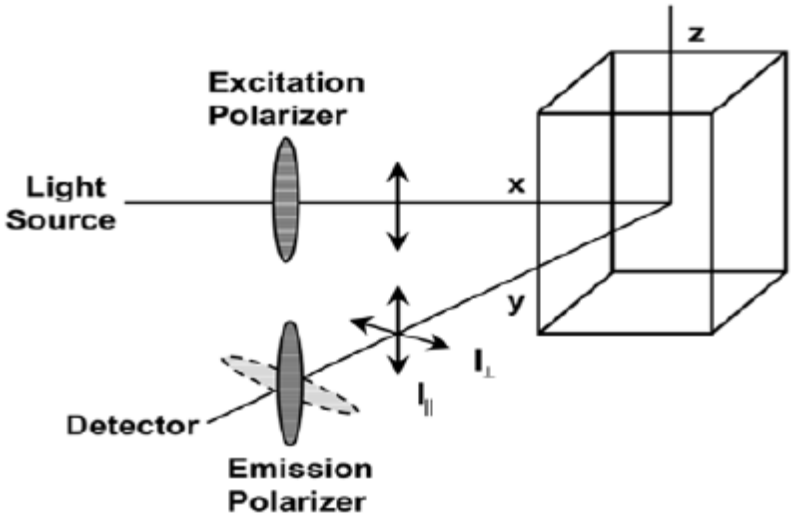

Figure 2.3.3.2: Schematic describing measurement of fluorescence anisotropy

Time-resolved fluorescence anisotropy decays of dyes were determined by time correlated single photon counting (TCSPC) setup coupled to a picosecond laser diode. For the measurement of time-resolved fluorescence anisotropy, the fluorescence intensity decays were collected with the emission polarizer kept at parallel ($I_\parallel$) and perpendicular ($I_\perp$) orientations with respect to the excitation polarizer. These polarized components were then corrected for the grating factor (G-factor). The G-factor of the TCSPC set-up was measured by the area matching method, using dye in a homogeneous solvent such as ethanol.

Using the experimentally obtained G-factor, for the sample whose anisotropy decay was to be experimentally measured, $I_\perp$ was collected for the time $t_\parallel G$ where $t_\parallel$ is the time for which $I_\parallel$ was collected. These two polarized intensity decays were used to compute the fluorescence

anisotropy decay and rotational relaxation time (τ_{rot}). The goodness of the fit of a given set of observed data and the chosen function was evaluated by the reduced $\chi 2$ ratio which ranged between 1.0 and 1.2. Hence, these techniques of fluorescence spectroscopy are very much useful in elucidating the excited state properties of dye molecules in various microenvironments.

2.4 Laser properties of fluorescent dyes:

Laser properties of the dyes were studied by constructing a Grazing Incidence Grating (GIG) configured narrow band pulsed dye laser setup, pumped by second harmonic (at 532 nm) of a Q-switched Nd:YAG laser (EKSPLA, Lithuania).

2.4.1 Grazing incidence grating (GIG) Narrowband dye laser:

Lasing properties of dyes, using aqueous and organic solvents, were studied by the constructed a narrow band dye laser setup, transversely pumped by second harmonic output of a Q-switched pulsed (rep. rate 10 Hz) Nd:YAG laser (at 532nm) with pulse energy (~ 6-7 mJ) of 5-7 ns duration. The dye laser was set up in a grazing-incidence-grating prism pre-expander configuration.[74] In this configuration, the grating is used as a disperser, as well as, an expander. The beam expansion of the grating is given by $\cos\varphi / \cos\theta$, where θ and φ respectively, the angles of incidence and diffraction, are determined by grating equation, $a(\sin\theta + \sin\varphi) = n\lambda$. Where, 'a' and 'n' are groove spacing and order of diffraction, respectively. To keep the cavity loss low and bandwidth of dye laser narrow, the grating was used in the first order diffraction, as well as, higher angle of incidence. Intra-cavity prism pre-expander was used so that the grating could be used at a smaller angle of incidence ($\theta \sim 81^0$). The schematic diagram of the dye laser set up is shown in Figure 2.4.1.1.

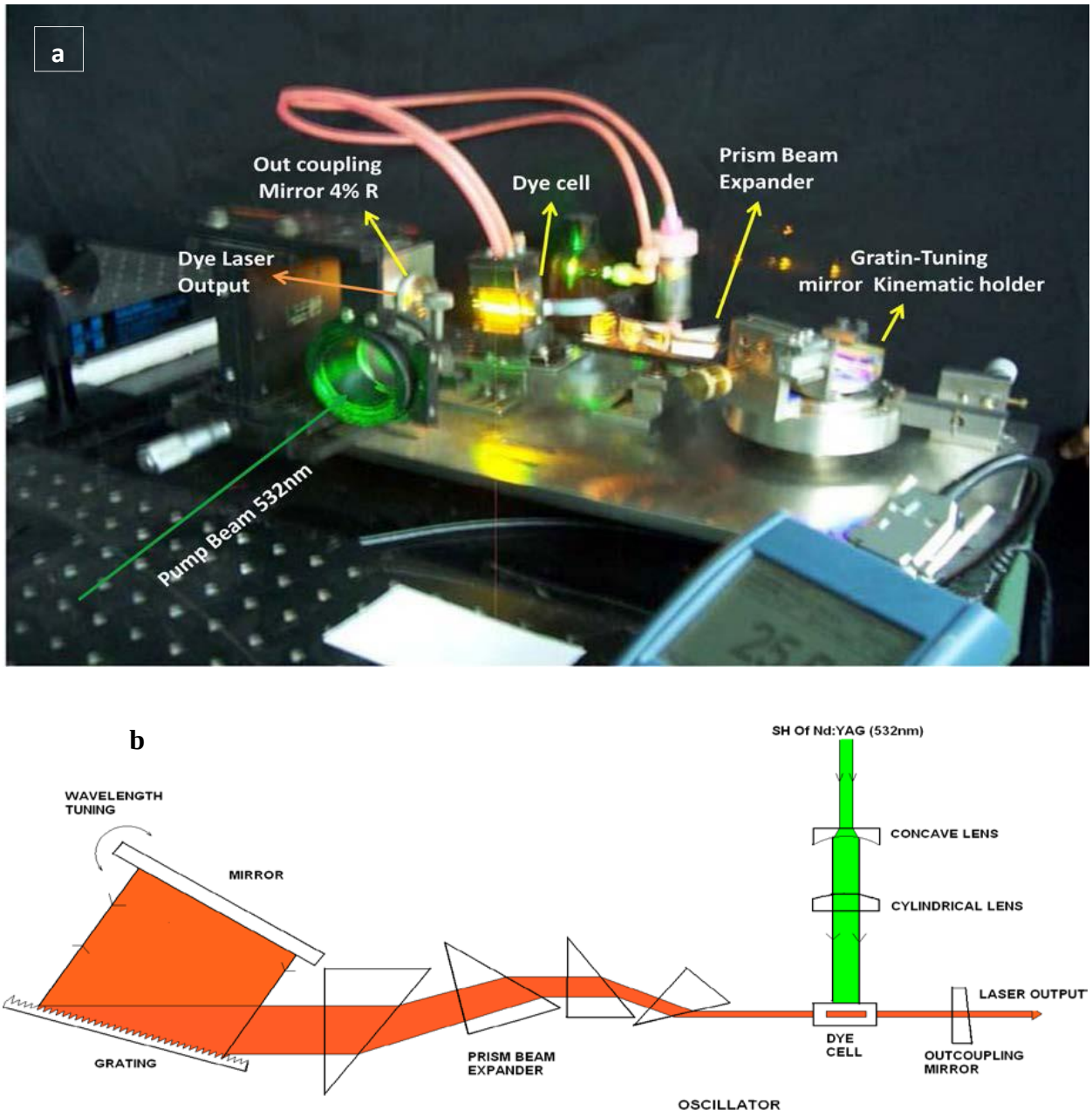

Figure 2.4.1.1: (a) Photographic image and (b) schematic of grazing incidence grating configured narrowband dye laser setup

Oscillator cavity has length 32 cm and dye laser output was derived from a 4% reflectivity wedge flat (wedge angle ~30'') output coupler. A 6 cm long dielectric coated tuning mirror with high reflectivity (flatness of λ/10 at 600 nm) and a diffraction grating with 2400 lines/mm were

used to obtain narrow line width (~0.1 cm^{-1}) dye laser. The green pump beam was expanded by a plano-concave (f = -50 cm) lens and line focused by a cylindrical lens (f =15 cm) onto a flow through dye cell (20 mm gain length, Lambda Physik made). The image of pump beam formed on the dye cell having a spot size of (0.5 x 20 mm^2) and cross sectional area of (0.5 x 0.5 mm^2) so that dye laser output was nearly circular. The flow speed of dye solution through the dye cell was measured by photothermal deflection spectroscopy technique, and was found ~1 m/sec with ethanol solvent, which was sufficient to clear the excited region between two successive pump pulses. This was found adequate to clear excited hot zone in dye cell before next pump pulse arrived (100 ms intra pulse time), even for solvents with higher viscosity. The dye laser was built mainly out of kinemetically designed S.S. optical mounts and assembled on a stainless steel base plate for good thermal and mechanical stability. The tuning curve of each dye solutions was obtained by scanning the wavelength of dye laser through the gain profile of dye and measuring the average pump and dye laser power with same power meter (OPHIR). The plot of dye laser efficiency (%) i.e. [(dye laser (DL) output power / Pump input power) x 100] Vs wavelength described the possible tunable output which was achieved by selection of dye, solvent and pump combination. A small fraction of the dye laser output was routed to a wavelength meter (WS-6, Angstrom) through an optical fiber to measure the wavelengths. The pump threshold energies (E_T) and slope efficiencies (η_s) for each of the laser dyes at their respective peak wavelengths (λ_L) of the tuning curves were obtained by measuring the laser output power as a function of the input pump power used. This data gives important information about the gain achieved during dye laser operation. Higher slope efficiency means higher gain can be achieved in the dye laser media.

2.4.2 Broad band dye laser setup:

For long term service life of dye laser system, the photostability studies of laser dyes are of utmost importance. We have studied the photostability of laser dyes in two different ways. In the first method, the quantum yield of the photo-degradation (Φ_{pd}) of the dyes is calculated and it is defined as the probability of the decomposition of the dye molecules by the absorbed pump photons. The photostability is the inverse of the Φ_{pd} value. In this method a known quantity of dye solution (2 ml) in a dye laser cuvette was exposed to 532 nm pump beam (pulse energy ~4 mJ, rep. rate 10 Hz, FWHM 6 ns, beam dia. 7 mm). The concentration of the dye solution was chosen such that the pump beam was totally absorbed within the dye solution in the cuvette during the excitation for a known duration of time. The solution was constantly stirred with a teflon-coated magnetic stirrer to avoid local heating.

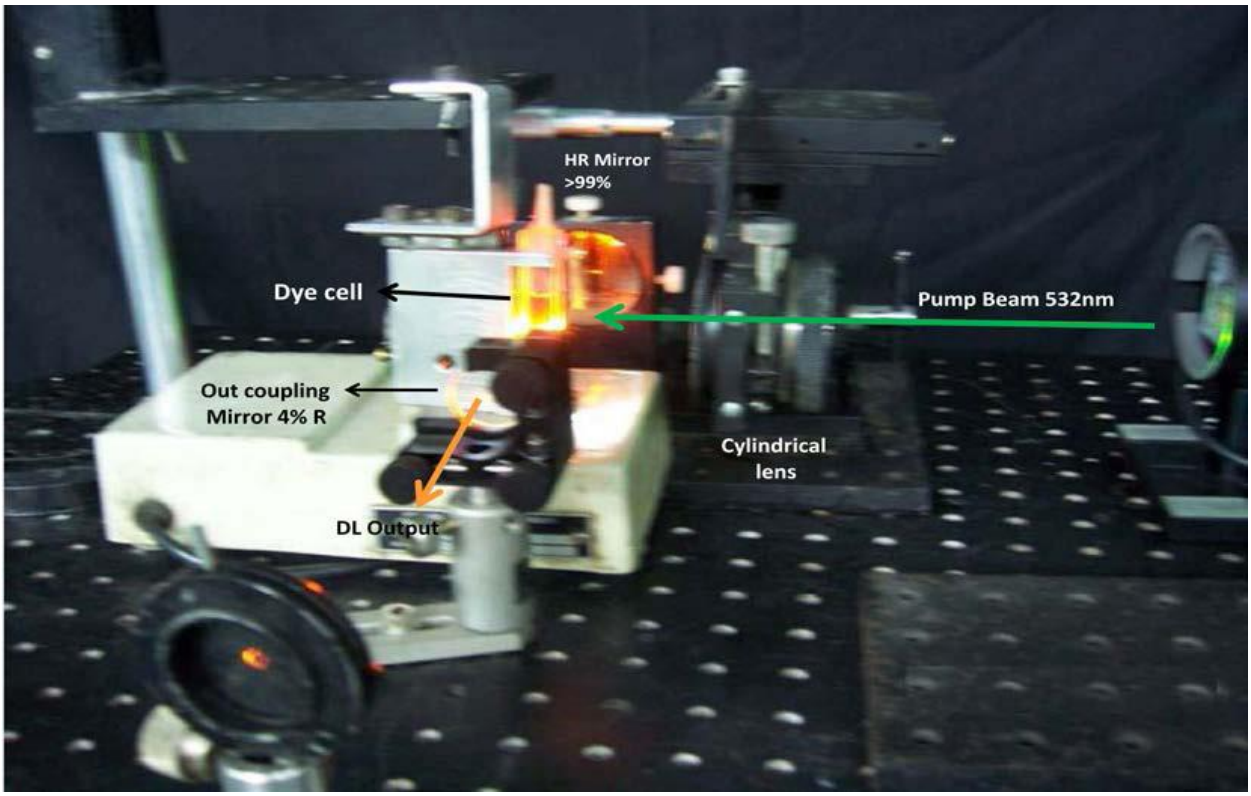

Figure 2.4.2.1: Photographic image of broad band dye laser setup

The number of photo-degraded dye molecules in the exposed volume of the dye solutions was quantitatively estimated from the absorbance at the corresponding λ_{max} before and after photo exposure for a set period of time. The reflection loss of the pump beam on incident surfaces of the dye cell was considered to calculate the absorbed cumulative pump photons.

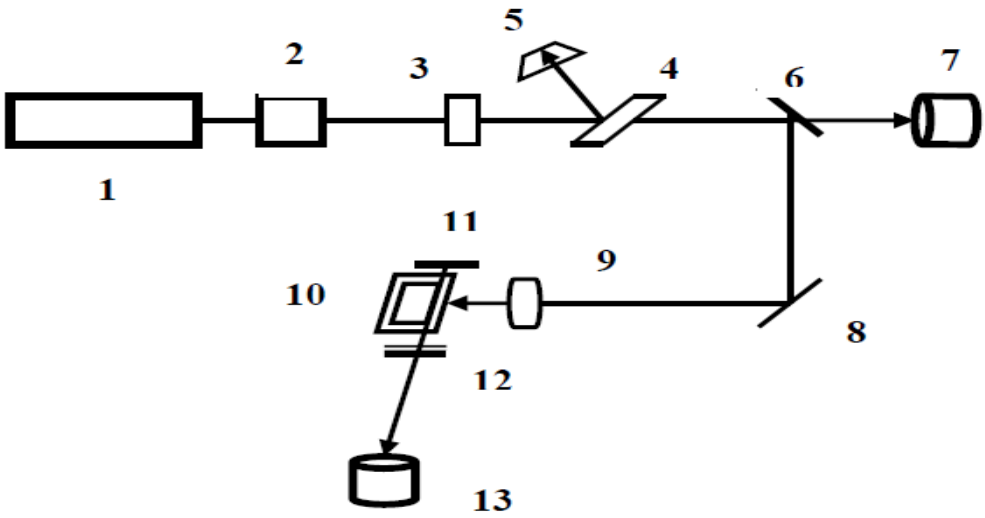

Figure 2.4.2.2: Schematic diagram of the Nd:YAG laser pumped broad band dye laser set up. Different blocks represent 1- Nd:YAG laser, 2- second harmonic Generator, 3- half-wave plate, 4- polarizer plate, 5- Beam dump, 6- beam splitter (50%), 7- power meter, 8- mirror, 9- cylindrical lens, 10- dye cell, 11- high reflectivity mirror, 12- output coupler, 13- power meter

In the second method we measure the drop in dye laser efficiency with time by constructing a broadband dye laser setup, pumped by the second harmonic (532 nm) of the Nd:YAG laser (pulse energy ~4 mJ, rep. rate 10 Hz, FWHM 6 ns, beam dia. 7 mm). This is a comparative method of measurement, in which optically matched dye solutions (~2ml) in sealed quartz cuvette was used. The sealed cuvette containing dye solution was placed between a high reflectivity (>99%) mirror and output coupler (4% reflectivity). The photographic image and schematic diagram of this broad band dye laser setup is shown in Figure 2.4.2.1 and 2.4.2.2. The

beam is focused on dye cuvette after passing through a cylindrical lens (f =10 cm). The image of pump beam formed on the dye cell having a spot size of (0.5 x 7 mm^2) and cross sectional area of (0.5 x 0.5 mm^2) so that dye laser output was nearly circular. The solution was constantly stirred with a teflon-coated magnetic stirrer to avoid local heating due to the pump beam. The pump input and DL output was measured using power meter (OPHIR). The above measured quantities are useful to improve the operational life of dye laser by modifying the solvent environment and to test newly synthesized laser dyes with improved photo-physical and laser properties.

2.5 Quantum chemical calculations:

Search for the minimum energy structures in the ground (S_0) state of all dyes was carried out applying a correlated hybrid density functional, namely, B3LYP[75,76] using a Dunning-type correlation consistent atomic basis set, cc-pVDZ for all the atoms. Quasi Newton-Raphson based algorithm was applied to carry out geometry optimization for each of these dyes with various possible conformers as the initial structures. Electron correlated method, namely, time dependent density functional theory (TDDFT) with B3LYP density functional was applied to study the excited state structure of the dyes in the first excited (S_1) state. Note that Dunning-type correlation consistent atomic basis set, cc-pVDZ was also used for all the excited state calculations. The ground (S_0) state minimum energy structures of dyes, including PCM[77] model with B3LYP functional was searched by testing effect of macroscopic hydration. Excited state calculations are also carried out on these solvent modified geometries to determine the effect of solvent applying TDDFT with B3LYP functional coupled with PCM solvent model. All electronic structure calculations were carried out applying the GAMESS suite of *ab initio* program.[78]

2.6 Nuclear magnetic resonance (NMR):

NMR spectroscopy is one of the most important instrument to identify and check weather synthesized organic molecule is pure or mixture. Also, in host-guest studies, proton NMR spectroscopy is understood to be a very useful technique to explore information regarding the host-guest interaction. The binding activity of two molecules causes to considerably modify their electronic environments, which effectively lead to a shift in the NMR signals in comparison to the signals in the free state of the molecules. This is the basic principle to make use of the NMR spectroscopy in the investigation of the host-guest systems.[35b,47,56,79-84] As expected, NMR spectroscopy can thus be suitably used in the host-guest studies for the elucidation of stoichiometry of the host-guest complexes, the preferential orientation of the guest molecule inside the host cavity, the effect of functionality in the host or guest molecule on their host-guest binding affinity, the binding and relocation of guest from one host to another, and many others.[35b,47,56,79-84] In general, it is observed in the NMR spectra that if the active H (proton) of the functional group of guest is inside the host cavity then its signal shows an upfield shift (i.e. δ shifts to lower values) and if it is outside the host cavity then its signal shows a downfield shift (i.e. δ shifts to higher values). Factors such as hydrogen bonding, electrostatic charge distribution, Van der Waals interaction and π-π interaction also affects the δ values of the active protons.[47,85-87] Thus, by monitoring the changes in the δ values of the guest molecule on addition of host, it is possible to obtain many useful information regarding the binding modes for the concerned host-guest systems. In our investigation we have used Bruker Advance WB 500 MHz spectrometer to elucidate NMR spectra of host-guest systems and for structural characterization of new synthesized molecules.

2.7 Principle of pulse radiolysis:

In Pulse Radiolysis, a highly intense pulse of electrons is given to a system to achieve a non-equilibrium situation in which significant concentration of transient species is produced in a short time interval. These transient species are monitored by following the changes in their characteristic properties such as optical absorption,[88] electrical conductivity,[89] electron spin resonance[90] and diffusion current at a suitably polarized electrode i.e., polarography.[91] Basic requirements of pulse radiolysis are as follows. It should produce very short (i.e., short in relation to the life time of the species under observation) pulses of radiation of sufficiently high energy to produce an adequate concentration of chemical species and of suitable penetration characteristics to ensure homogeneous distribution of the species formed in the irradiated sample. The radiation chemical changes should be observable either optically or by other means.

2.7.1 Pulse radiolysis set up:

The basic arrangement of pulse radiolysis set up is as shown in the following Figure 2.7.1.1. Sample solutions were irradiated with the help of 7 MeV electron pulse from a linear electron accelerator (Forward Industries, formerly and Viritech Ltd. U.K., and Radiation Dynamics). Sample solutions are taken in a suprasil quartz cuvette and are kept at a distance of 12 cm from the titanium electron beam window, where the beam diameter is 1 cm. The transient changes in the absorbance of the solution caused by the electron beam pulse are monitored with the help of collimated light beam from a pulsed 450 W Xenon arc lamp (Kratos Model LH 151). The accelerator, the sample cell and the monitoring light source are housed in a shielded cave with 1.5 m thick concrete wall and roof. The monitoring light beam, after passing through the sample cell, is directed to the detection equipment through a tunnel in the wall by making use of fused silica lenses and mirrors coated with aluminum on the front surface.

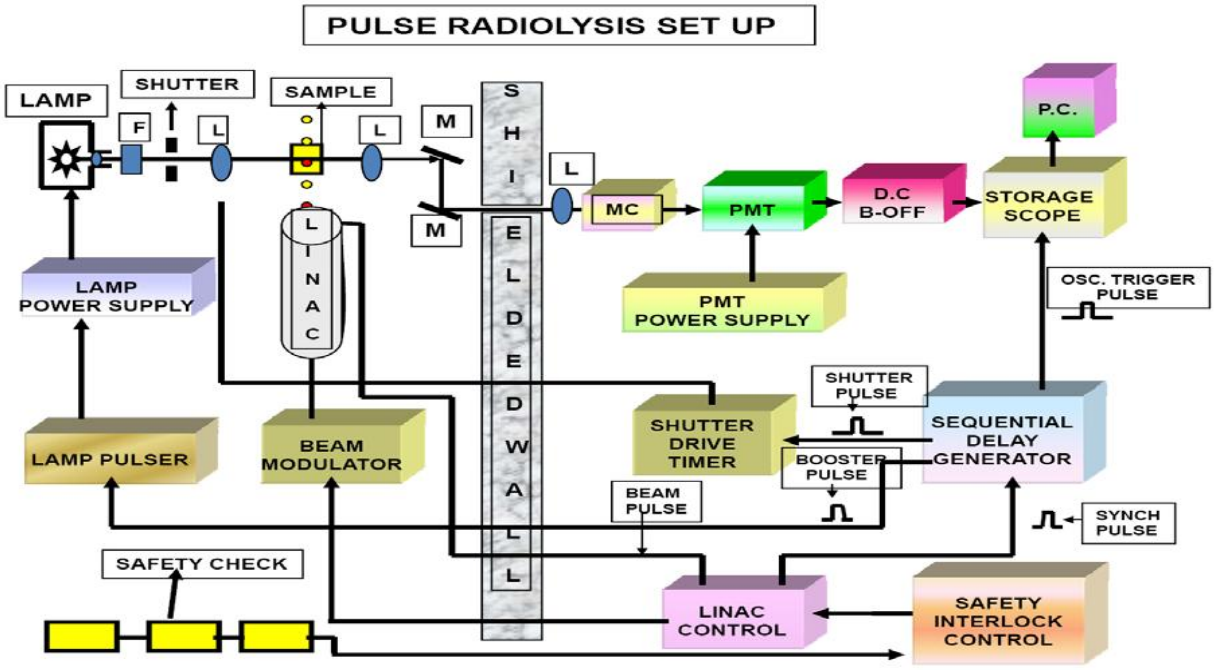

Figure 2.7.1.1: Basic set-up for pulse radiolysis using kinetic spectrophotometric method

The light beam is finally focused on the entrance slit of a monochromator (Kratos GM 252), on the exit slit of which a photomultiplier (model no. Hamamatsu Model-955) is fixed. Photomultiplier signal is fed into a storage oscilloscope from which traces transferred to a computer (Figure 2.7.1.1).

2.7.2 Transient absorption measurements:

The photo multiplier tube (PMT) output voltage (V) developed across a suitable anode resistor is directly proportional to the anode current which in turn, at fixed values of the photocathode potential, is directly proportional to the intensity of the monochromatic light incident on the photocathode. As a result of action of electron pulse on the sample solution in the cell, transient species formed capable of absorbing light at a given wavelength are produced; the intensity of light transmitted through the cell is given as

$$I = I_0\, 10^{(-\epsilon c l)} \qquad (2.8)$$

Where, I_0 is the intensity of light transmitted just prior to the electron pulse, c is the molar concentration of the species formed in the sample, ϵ its molar extinction coefficient and l the length of the light-path through the cell contents. Because of the proportionality between V and I, the PMT output voltage just after and prior to pulsing are related as

$$V = V_0\, 10^{(-\epsilon c l)} \qquad (2.9)$$

As the concentration of the transient species produced by electron pulse would change with time due to various chemical processes, I and hence V will be time-dependent. This time-dependence of V is monitored with an appropriate digital oscilloscope and subsequently processed to get the kinetic information. The quantity ε.c.l called the optical density or absorbance is also time-dependent. From the experimental quantities V and V_0, the absorbance (A) of the transient species at any given time can be calculated using the following equation

$$A = log\ (V_0/V) \qquad (2.10)$$

At any instant of time after pulse, a plot of the absorbance *vs*. wavelength reflects the absorption spectrum of the species present in the system at that instant of time.

2.7.3 Dosimeters for pulse radiolysis:

Dosimetry for pulse radiolysis differs from the dosimetry from conventional steady state radiolysis (γ-ray of ^{60}Co) as pulse radiolysis involve high dose rate. In pulse radiolysis experiment, thiocyanate dosimeter is commonly used to measure the absorbed dose per pulse. It is an aerated aqueous 0.01 mol dm^{-3} potassium thiocyanate solution. Upon irradiation with the electron pulse, e_{aq} and H-atom are scavenged by the dissolved oxygen and $OH^{\bullet}$ radical oxidizes SCN^{-} ions to produce $(SCN)^{2\,\bullet -}$ radical according to the following reaction 2.11 and 2.12.

$$SCN^{-} + OH^{\bullet} \rightarrow SCN^{\bullet} + OH^{-} \qquad (2.11)$$

$$SCN^{\bullet} + SCN^{-} = (SCN)^{2\,\bullet -} \qquad (2.12)$$

Species $(SCN)_2^{\bullet -}$ formed has strong absorption in the visible region. The radiation dose is estimated from the maximum absorbance of the radical $(SCN)_2^{\bullet -}$ at 475 nm. The G value for this species is reported to be 3.3 per 100 eV of absorbed dose and the extinction coefficient (ϵ) of this radical is reported to be 7600 dm^3 mol^{-1} cm^{-1} at 475 nm.[92] The G value remains unchanged when the solution is saturated with O_2 instead of air and is doubled in an N_2O-saturated solution. From the measured absorbance, the absorbed dose per pulse (D) is computed from the following equation:

$$D = \frac{\Delta O.D}{G.\varepsilon.l} \times N \times 1.602 \times 10^{-19}\, Gy \qquad (2.13)$$

where, N is the Avogadro number. Substituting the value of G. ϵ for $(SCN)_2^{\bullet -}$ at 475 nm, the above expression (2.13) can be written in a simplified way as:

$$D = \Delta O.D. \times 385 Gy \qquad (2.14)$$

For estimation of the extinction coefficient of transient species studies, experiments were carried out at lower doses.

2.7.4 Analysis of transient absorption signals:

The absorption signal/traces recorded on the oscilloscope as a result of light absorption by transient species are in mV *vs.* time scale. Measured mV signals are converted into OD values as described in section 2.7.2. Plot of OD values *vs.* wavelength constitutes the transient absorption spectrum. If the OD values recorded at different time intervals and plotted *vs.* wavelength, it gives time-resolved absorption spectra which gives an idea about number of species present and also indicates if there is any product formed as a result of decay of the initially formed transient species.

2.8 Cyclic voltammetry:

Cyclic voltammetry is a method for investigating the electrochemical behaviour of a system. It was first reported in 1938 and described theoretically by Randles.[93] In this technique current flowing between the electrode of interest (whose potential is monitored with respect to a reference electrode) and a counter electrode is measured under the control of a potentiostat. The voltammogram determines the potentials at which different electrochemical processes occur. The working electrode is subjected to a triangular potential sweep, whereby the potential rises from a start value E_i to a final value E_f then returns back to the start potential at a constant potential sweep rate. In this case the voltage is swept between two values at a fixed rate, however when the voltage reaches V_2 the scan is reversed and the voltage is swept back to V_1. The essential elements needed for an electrolysis measurement are as follows:

• **The electrode**: This is usually made of an inert metal (such as Gold or Platinum)

• **The solvent**: This usually has a high dielectric constant (eg. water or acetonitrile) to enable the electrolyte to dissolve and help aid the passage of current.

• **A background electrolyte**: This is an electrochemically inert salt (eg. NaCl or Tetra butylammonium perchlorate, TBAP) and is usually added in high concentration (0.1 M) to allow the current to pass.

• **The reactant**: Typically in low concentration 10^{-3} M.

Thus, Cyclic voltammetry containing three electrodes namely reference, working and counter electrodes. The redox potentials were standardized with ferrocene (Fc) as the internal reference, and converted to SCE assuming that $E_{1/2}$ (Fc/Fc^+) = +0.38 V SCE. The error in half-wave potentials was ±10 mV. All waves were monoelectronic performed at 25^0C in deoxygenated solution containing TBAP as a reference (0.1 M), and a solute concentration of 1-5

$\times 10^{-3}$ M. A typical cyclic voltammogram recorded for a reversible single electrode transfer reaction is shown in Figure 2.8.1.

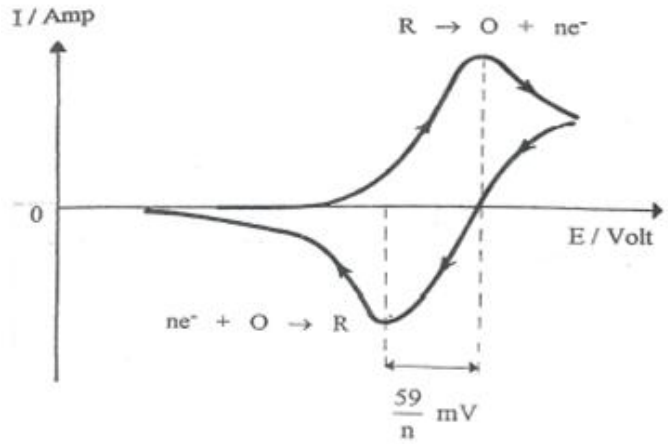

Figure 2.8.1: A schematic cyclic voltammogram of a reversible redox process

CHAPTER 3

EFFECT OF SOLVENT IN LASING EFFICIENCY AND PHOTOSTABILITY OF BODIPY DYES

Chapter 3: Table of Contents

3.1 Introduction:

Dye lasers[94] have been used till now as a spectroscopy tool in basic and applied sciences of chemistry, physics and biology. Hundreds of dyes have been demonstrated[95] to obtain good lasing efficiency and photostability in UV-VIS-IR spectral regions. Among them, relatively recent BODIPY class of dyes[13b,13c,96] also known as pyrromethene (PM), have continued to attract interests to scientists and technologists due to their versatile applications in the areas such as dye sensitized solar cells, photodynamic therapy, chemo sensors, dye lasers etc. PM dyes are extensively used as efficient active media for solid as well as liquid dye lasers due to their high fluorescence yields, intense absorption profiles in the green spectral region and low triplet-triplet extinction coefficients over the entire fluorescence region.[13a,14a,14b,97] However, their applications in high-average-power liquid dye lasers remains limited due to the rapid photochemical degradation of the dyes. For example, alcohol solution of the commercially available BODIPY dyes, PM567 (**16**), PM597 (**17**) and PM580 undergoes extensive degradation on exposure of highly repetitive (6-20 kHz) pump lasers under aerobic conditions. The degradation is primarily mediated by their reaction with *in situ* generated singlet oxygen ($^1O_2$) during photochemical excitation.[19,98] Different strategies known to enhance the laser photostability of these dyes such as use of deoxygenated dye solutions[14a] or the addition of high concentrations of $^1O_2$ quenchers (Tin770, TBP or DABCO),[13a,99,100] are either inconvenient for large-scale dye laser operation or show reduced laser efficiency due to fluorescence quenching. Change of chemical structures of the dyes also has much effect on the photostability of the BODIPY dyes.[98a] Earlier similar approaches have been adopted to synthesize a host of analogues of the most extensively used laser dye (**16**) by incorporating different substituent at C-8 (meso position), the boron centre and/ or both the sites (C-2 or and C-6) position of BODIPY dyes.

However, choice of solvent dramatically affects the photostability of BODIPY dyes even under air saturated conditions.[98c] But lack of photo-physical data such as quantum yield of fluorescence, triplet state properties, rate of generation of $^1O_2$ and its reactivity with dyes in different solvents make it difficult to rationalize the observed photostability changes with the solvent. In addition the photo-physics and photostability of the dyes in different solvents would depend both on the dye structure as well as solvent selection due to its specific solute-solvent interaction.

On the other hand dissolved oxygen concentration in dye solution, rate of generation of reactive singlet oxygen ($^1O_2$) during photo excitation, lifetime of generated $^1O_2$, and its reactivity with dyes in different solvent systems play important roles and affect the overall photostability of the PM dyes, but unfortunately these results were never been studied and discussed thoroughly. A few studies have been directed towards singlet oxygen generation of PM dyes and its reactivity with singlet oxygen as a function of solvent polarity to understand their photo-degradation rate. Generally the lasers study of PM dye has been focus of numerous investigations.[101] However, these tailored approaches have shown a limited practical utility since the photostability of dyes improved by only a few times but concurrently unable to deliver comparable laser efficiency in most cases. Recently, it has been demonstrated that photostability of PM dyes in non-polar solvents is more than that in polar solvents.[102] But very few studies have been directed towards rate of singlet oxygen generation and reactivity with singlet oxygen with solvent polarity to understand their photo-degradation and lasing efficiency.

To this end, for clear understanding of the various influences that can affect the photo-physical properties and lasing action of BODIPY dyes are studied in this chapter and described in two sections. First section carried out comparative study of well known BODIPY dyes PM567

(**16**) and PM597 (**17**) having different optical properties using three different solvent systems such as ethanol, 1,4-dioxane and heptane. Then further proceed in next section towards synthesis and comparative laser study of new derivative of BODIPY via substitution at boron centre having similar optical properties as its precursor **16** in two solvents (ethanol and 1,4-dioxane) and determine the relative utility of these dye-solvent combinations for high average power dye lasers. Molecular structures of PM567 (**16**), PM597 (**17**) and their new derivatives (**58**) were shown in Figure 3.1.

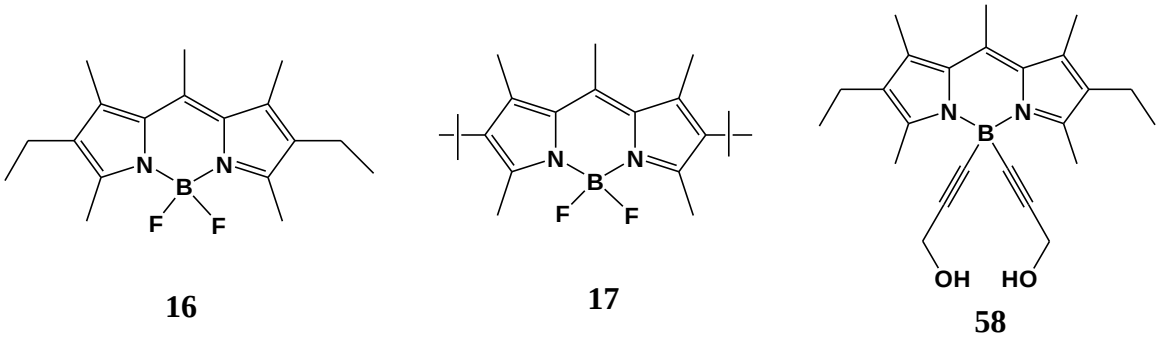

16 **17** **58**

Figure 3.1: Molecular structures of BODIPY dyes

3.2 Experimental:

3.2.1 Materials:

Laser grade dye **16**, **17** was obtained from Lambda Physik, Germany and spectroscopy grade Methylene blue (MB), 4,4-dimethylbiphenyl (DMBP) and 1,3-diphenylisobenzofuran (DPBF) were procured. Their high purity were checked by TLC and used without further purification. Spectroscopy grade ethanol, 1,4-dioxane, n-heptane and benzene were used to prepare the dye solutions.

3.2.2 Synthesis:

Compound 56: A mixture of propergyl alcohol (1.5 g, 26.7 mmol), 2,3-dihydropyran (2.92 g, 34.8 mmol) and PPTS (10 mg) was stirred in dry CH_2Cl_2 (50 ml) for 12 h. The resulting mixture was washed with H_2O (50 ml) and brine (50 ml), and dried. Removal of solvent under *vacuo* followed by column chromatography of the residue (silica gel, hexane-EtOAc) furnished **56.** Yield: 2.6 g (70%); colourless liquid; ^{1}H NMR (300 MHz, $CDCl_3$, 25 ^{o}C, TMS): δ = 1.48-1.80 (m, 6H), 2.39 (t, J = 2.4 Hz, 1H), 3.46-3.52 (m, 1H), 3.75-3.83 (m, 1H), 4.14-4.28 (m, 2H), 4.76-4.79 (m, 1H). ^{13}C NMR (75 MHz, $CDCl_3$, 25 ^{o}C, TMS): δ = 18.9, 25.3, 30.1, 53.8, 61.8, 74.0, 79.7, 96.6 ppm; EI-MS *m/z* (%):140.1 (100) $[M]^+$; elemental analysis calculated (%) for $C_8H_{12}O_2$: C 68.54, H 8.63; found: C 68.22, H 8.31.

Compound 57: To a stirred solution of **56** (350 mg, 2.5 mmol) in THF (30 ml) was added EtMgBr (2.5 ml, 1M in THF, 2.5 mmol). Then the mixture was heated at 60^{o}C for 2 h, brought to room temperature, and then transferred *via* a canula into a solution of PM567 (**16**) (318 mg, 1mmol) in THF (20 ml). The mixture was stirred at 50^{o}C for 24 h, NH_4Cl solution (20 ml) was added into it and the mixture was extracted with EtOAc (30 ml). The organic layer was washed with H_2O (30 ml) and brine (30 ml), dried, and concentrated under *vacuo*. The crude product was purified using flash chromatography (silica gel, hexane/EtOAc) to furnish **57.** Yield: 442 mg (79%); orange needles (CH_2Cl_2/cyclohexane); Mp: 177°C; ^{1}H NMR (200 MHz, $CDCl_3$, 25 ^{o}C, TMS): δ = 1.00 (t, J = 7.6 Hz, 6H), 1.45-1.81 (m, 12H), 2.32 (s, 6H), 2.43 (q, J = 7.6 Hz, 4H), 2.58 (s, 3H), 2.66 (s, 6H), 3.40-3.50 (m, 2H), 3.74-3.86 (m, 2H), 4.21 (s, 4H), 4.80 (t, J = 3.2 Hz, 2H). ^{13}C NMR (50 MHz, $CDCl_3$, 25 ^{o}C, TMS): δ = 13.8, 14.6, 15.0, 17.1, 17.3, 19.3, 25.4, 30.4, 55.3, 62.0, 96.3, 129.9, 132.3, 134.1, 139.5, 151.6 ppm; EI-MS *m/z* (%): 558.1 (35) $[M]^+$, 557.3

(100) [*M* -1]$^+$; elemental analysis calcd (%) for $C_{34}H_{47}BN_2O_4$: C 73.11, H 8.48, N 5.02; found: C 73.32, H 8.19, N 5.31.

Compound 58: A mixture of **59** (0.442 g, 0.8 mmol) and PTS (0.273 g, 1.59 mmol) was stirred in methanol and water mixture (50 ml, 9:1) for 10 h. The resulting mixture was concentrated under *vacuo* and $CHCl_3$ (30 ml) was added into it. The organic layer was washed with H_2O (20 ml) and brine (20 ml), and dried. Removal of solvent under *vacuo* followed by column chromatography of the residue (silica gel, hexane-EtOAc) furnished **58.** Yield: 273 mg (88.0%); orange needles (CH_2Cl_2/cyclohexane); Mp: 208°C; ^{1}H NMR (200 MHz, $CDCl_3$, 25 ^{o}C, TMS): δ = 1.05 (t, *J* = 7.4 Hz, 6H), 2.34 (s, 6H), 2.40 (q, *J* = 7.4 Hz, 4H), 2.61 (s, 3H), 2.67 (s, 6H), 4.20 (s, 4H); ^{13}C NMR (50 MHz, $CDCl_3$, 25 ^{o}C, TMS): δ = 13.9, 14.6, 15.0, 17.2, 17.4, 52.1, 129.9, 132.6, 134.5, 139.6, 151.7 ppm; EI-MS *m/z* (%): 390.3 (36) [*M*]$^+$, 389.2 (100) [*M* -1]$^+$; elemental analysis calcd (%) for $C_{24}H_{31}BN_2O_2$: C 73.85, H 8.01, N 7.18; found: C 73.52, H 8.12, N 7.11.

3.2.3 Photo-physical studies:

The absorption and emission spectra of the dyes (~10^{-6} M) in various solvents were measured using a 1 cm quartz cuvette. The fluorescence quantum yields (Φ_f) of the dyes relative to that of the reference dye **16**[98a] and **17**[19] in ethanol and the molar extinction coefficients (ε_{max}) were determined in heptane and 1,4-dioxane. Detail description was given in chapter 2.

3.2.4 Lasing studies:

Lasing study of the dyes in ethanol, 1,4-dioxane and heptane were carried out using a narrow-band and broad-band dye laser set-up, transversely pumped by the second harmonic (at 532 nm) output of a Q-switched pulsed Nd:YAG laser at a repetition rate of 10 Hz with ~6 mJ pulse energy and 5-7 ns FWHM pulses (described in chapter 2). In narrow band laser study, the

dye solutions (O. D. = 0.7 at 532 nm, 1 mm cell) in ethanol, 1,4-dioxane and heptane were used separately to determine the lasing efficiency. The tuning curve of the dye solutions were obtained by scanning of the wavelength of dye laser through the gain profile of dyes, and measuring the average pump and dye laser powers with a power meter (OPHIR). For broad band studies, the individual dye solutions were kept in a 1cm quartz dye cell (optical path ~ 6 mm along the dye laser axis) that was carefully sealed by a teflon stopcock to avoid solvent evaporation during experiment. The dye cell was suitably tilted along the dye laser axis to avoid dye cell window lasing along the resonator axis. The broad band lasing efficiency of each dye solution was determined as a function of the dye concentrations, keeping other parameters, including alignment of the cavity, unchanged. For this, different concentrations of dyes in ethanol were used keeping the optical density at 1-4 at the pump wavelength (532 nm).

3.2.5 Photostability studies:

The photostability of dye solution is defind as the inverse of the quantum yield of photodegradation (Φ_{pd}) value. A known quantity of dye solution (2 ml) in a dye laser cuvette was exposed to pump energy of ~4 mJ at 532 nm. The concentration of the dye solution was chosen such that the pump beam was totally absorbed within the dye solution in the cuvette during the excitation of about 4 h for dyes **16, 58** and 6 h for dye **17**. The solution was constantly stirred with a teflon-coated magnetic stirrer to avoid local heating. The number of photo-degraded dye molecules in the exposed volume of the dye solutions was quantitatively estimated from the absorbance at the corresponding λ_{abs} before and after photo-exposure for a set period of time. The reflection loss of the pump beam on incident surfaces of the dye cell was determined for calculating the absorbed cumulative pump photons.

3.2.6 Studies on relative capability of $^1O_2$ generation of the dyes:

In this study, PM dye solution generated $^1O_2$ under photoexcitation from a tungustan lamp and these $^1O_2$ sepcies were allowed to react with a $^1O_2$ sensitizer, DPBF. For this, 3 ml of aerated ethanol containing DPBF (50 μM) and each PM dye separately (5 μM) taken in 10 mm quartz cells were irradiated at 20 W/m^2 intensity of filtered light source of >495 nm wavelength at room temperature for 15 min. Change in absorbance of all the solutions were measured at λ_{abs} of DPBF (412 nm) at various fixed exposure intervals (2 min). Relative $^1O_2$ generation capacities of PM dyes in ethanol, 1,4-dioxane and heptane were determined by measuring the reduction in DPBF absorbance at 412 nm over time. Irradiation of DPBF solution in the absence of dyes as a negative control and solution of dyes as positive controls were also carried out.

3.2.7 Pulse radiolysis study:

The triplet state studies of the dyes were carried out using the nanosecond pulse radiolysis technique described in chapter 2.[92,103] The dye solutions (1×10^{-4} mol dm^{-3}) were prepared in spectroscopy grade 1,4-dioxane/benzene (9:1) and heptane/benzene (9:1) and purged with high purity N_2 to remove dissolved oxygen. The pulse radiolysis experiments were carried out using 4,4-dimethylbiphenyl (DMBP) (5×10^{-3} mol dm^{-3}) as the triplet sensitizer. Formation of the dye triplets and their extinction coefficients were determined by energy transfer from the DMBP triplet to the dyes. For studying the reactions of the dyes at triplet state with O_2, the experiments were carried using a high concentration of the dye (3×10^{-3} mol dm^{-3}) without any triplet sensitizer. The decay of the triplet states of the dyes were monitored at their respective λ_{max}. Concentration of oxygen in solutions was adjusted by mixing appropriate volumes of nitrogen purged dye solutions in 1,4-dioxane/benzene (9:1) and heptane/benzene (9:1) with aerated dye solutions in 1,4-dioxane/benzene (9:1) and heptane/benzene (9:1).

3.2.8 Studies on reactivity of $^1O_2$ with dyes:

In this study, a $^1O_2$ sensitizer, MB generated $^1O_2$ under photoexcitation from filtered tungustan lamp and these $^1O_2$ species were allowed to react with PM dyes. For this, 3 ml of aerated ethanol containing MB (10 μM) and each PM dye separately (10 μM) in 10 mm quartz cells were irradiated at 7.5 W/m^2 of filtered light source of >590 nm wavelength using a long path cut off filter at room temperature for 1.5 h for **16**, dye **58** and 50 min for **17**. MB was used as a photo sensitizer and 590 nm cut off filter was used in order to assure that light was absorbed by MB only. Absorbance at λ_{abs} of **16** (518 nm), dye **58** (515) and dye **17** (524 nm) were measured at various fixed intervals (15 min for dye **16** and **58** and 10 min for dye **17**). Relative reactivity of the dyes with $^1O_2$ in ethanol was determined by measuring the reduction in absorbance of the respective dyes at their λ_{abs} over time. Irradiation of MB solution in the absence of dyes as a negative control and solution of dyes as positive controls were also carried out.

Similar experiments were carried out in 1,4-dioxane/ethanol (1:4) and heptane/ethanol (1:4) to measure relative $^1O_2$ generation capacities of dyes in 1,4-dioxane/ethanol (1:4) and heptane/ethanol (1:4). The experiments could not be done in neat 1,4-dioxane and heptane due to poor solubility of MB.

Results and Discussion:

3.3. Section 1: Comparative Laser study of dye 16 vs. dye 17:

3.3.1. Photo-physical characteristics:

The photo-physical properties of the dyes **16** and **17** were evaluated in three different solvents (ethanol, 1,4-dioxane, heptane) at room temperature. The measured photo-physical parameters (longest wavelength absorption maximum (λ_{abs}), emission maximum (λ_{em}),

fluorescence quantum yield (Φ_f), maximum molar absorptivity (ε_{max}), fluorescence lifetime (τ_f) and calculated Stokes shift (ν), radiative (k_r) and nonradiative (k_{nr}) decay rates of the dye **16** and **17** in ethanol 1,4-dioxane and heptane were presented in Figure 3.3.1.1 and Table 3.3.1.1

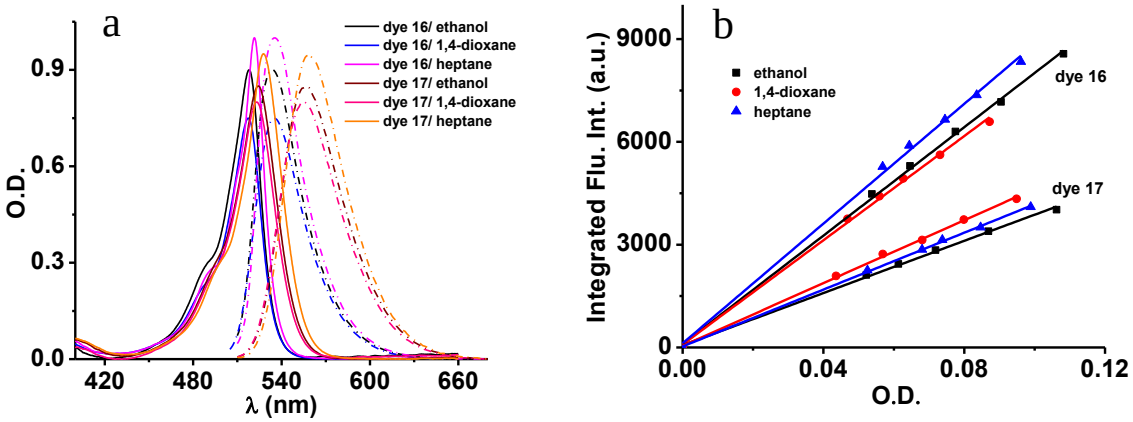

Figure 3.3.1.1: (a) Absorption (bold line) and emission (dotted line) spectra and (b) Comparative fluorescence quantum yield plots of dyes **16** and **17** in three (ethanol, 1,4-dioxane and heptane) solvents at room temperature.

Both the dyes have intense S_0 to S_1 absorption bands at 517-526 nm. The shapes of absorption spectra of dyes were similar in all solvents. The fluorescence spectra were almost mirror images of the respective absorption spectra, with minimum energy loss in each solvent. In non-polar solvents, the absorption band is centered at 521 and 526 nm with high molar absorption coefficient 9.1 and 8.3 x 10^4 M^{-1} cm^{-1}, whereas the fluorescence spectrum is centered at 535 and 557 nm with highest fluorescence quantum yield of 0.97 and 0.48 of dyes **16** and **17,** respectively. Quantum yield of fluorescence (Φ_f) has been increased from 0.84 to 0.97 of **16** and 0.43 to 0.48 of **17** on changing the solvent from polar to non-polar, calculated by comparative method using dye **16** and **17** in ethanol as standard. A typical illustration of observed linear fluorescence intensity plots vs. OD of both dyes in three different solvent are shown in Figure

3.3.1.1b. On comparison of photophysical parameters of **16** and **17**, it has been observed that λ_{abs} and λ_{em} maxima of dye **17** were shifted to lower energies. This might be due to presence of bulky t-butyl groups at 2 and 6 positions of the PM core which attributed to higher inductive electron-donor character than ethyl group of dye **16**. The larger Stokes shift in dye **17** suggested important geometrical rearrangement in S_1 excited state, which was also originated from bulky groups at 2 and 6 positions of the PM core.

Table 3.3.1.1: Photo-physical properties of dye **16** and **17** in ethanol, 1,4-dioxane and heptane

Dye	Solvent	λ_{abs}[a] (nm)	ε_{max}[b] (10^4 M^{-1} cm^{-1})	λ_{em}[c] (nm)	Φ_f[d]	ν (cm^{-1})	τ_f[e] (ns)	k_r[g] (s^{-1}) (10^8)	k_{nr}[g] (s^{-1}) (10^8)
16	ethanol	518.0	7.1	533.0	0.84[f]	543	6.48	1.3	0.25
	1,4-dioxane	518.0	6.2	535.0	0.89	613	6.52	1.4	0.17
	heptane	521.0	9.1	535.0	0.97	502	6.12	1.6	0.05
17	ethanol	524.0	6.8	556.0	0.42[f]	1098	4.04	1.06	1.4
	1,4-dioxane	525.0	6.58	558.0	0.45	1126	4.37	1.03	1.3
	heptane	526.0	8.3	557.0	0.48	1058	4.83	0.99	1.1

[a] Error: ± 0.2 nm. [b] Extinction coefficients at respective λ_{max}. [c] Error: ± 0.3 nm. [d] The fluorescence of the dyes **16** and **17** were measured at the excitation wavelength 505 nm of **16** and 515 nm of **17**. [e] Error: ± 0.05 ns. [f] This data is taken from ref. [19, 103a]. [g]The values of k_r and k_{nr} were calculated using the following equations: $k_r=\Phi_f/\tau_f$, $k_{nr} = (1-\Phi_f)/\tau_f$, assuming that the emitting state is produced with unit quantum efficiency.

The ε_{max} of both dyes were increased in heptane suggesting that lower concentration of dyes will be required for dye laser experiment. Interestingly, it was noticed that radiative decay rate (k_r) of dye **16** is slightly increased and non-radiative decay rate (k_{nr}) decreased more (5 times) in heptane than in ethanol. However, almost negligible change was observed for dye **17** on altering the solvent.

3.3.2 Laser study:

The narrow band lasing characteristics of dyes **16** and **17** dyes using three solvents are illustrated in Table 3.3.2.1 and Figure 3.3.2.1. The laser gain curves of PM dyes showed the maximum efficiency at a particular λ_L, characteristics of dye, and laser tuning range in different solvents were almost similar for each dye. Laser tuning ranges of dyes **16** and **17** using heptane are 540-586 nm and 560-625 nm, respectively.

Table 3.3.2.1: Lasing properties of dyes **16** and **17** using ethanol, 1,4-dioxane and heptane

Dyes	Solvent	Conc. (mM)	λ_L[a] (nm)	Tuning range (nm)	η[b] (%)	GSA[c] (10^{-18} cm^2) at λ_L
16	Ethanol	1.0	553.8	541-583	15.3	1.34
	1,4-dioxane	1.2	555.8	540-584	17.1	1.36
	Heptane	1.3	556	540-586	18.8	1.76
17	Ethanol	0.5	579	560-625	13.4	0.63
	1,4-dioxane	0.6	578	560-625	17.0	0.84
	heptane	0.7	578	560-625	18.6	1.56

[a] Error: ± 0.2 nm. [b] Error: ± 1.0 % [c] Error: ± 0.005

Interestingly, the lasing efficiency of both dyes **16** and **17** in non-polar solvents, especially in heptane, increased by 3.5% and 5.2 %, respectively. The maximum lasing efficiency values (η) of the dye **16** (15.3% in ethanol, 17.1 % in 1,4-dioxane, 18.8% in heptane) and dye **17** (13.4% in ethanol, 17% in 1,4-dioxane, 18.6% in heptane) at respective λ_L. This suggests that solvent polarity also affects the lasing efficiency of PM dyes. This agrees with the superior photophysical properties of both the dyes in heptane (Table 3.3.1.1). Expectedly, the ground state absorption (GSA) cross section of both the dyes in three different solvents at the corresponding λ_L, determined by absorption spectroscopy, is less in case of dye **17** than dye **16**, due to larger Stokes shift of the former dye. Moreover, the present laser study required significantly lower

concentration of dye **17** than **16** in all solvents to maintain similar gain depth of pump beam (at 532 nm). Thus, the net loss of laser photons due to GSA is less in dye **17**, which explained its similar laser maximum efficiency in spite of lower fluorescence quantum yield and higher non-radiative decay rate in three different solvents than **16**. The higher lasing efficiency of **17** in spite of a very low fluorescence quantum yield is beneficial for power scaling in the master oscillator power amplifier (MOPA) design of pulsed dye lasers.

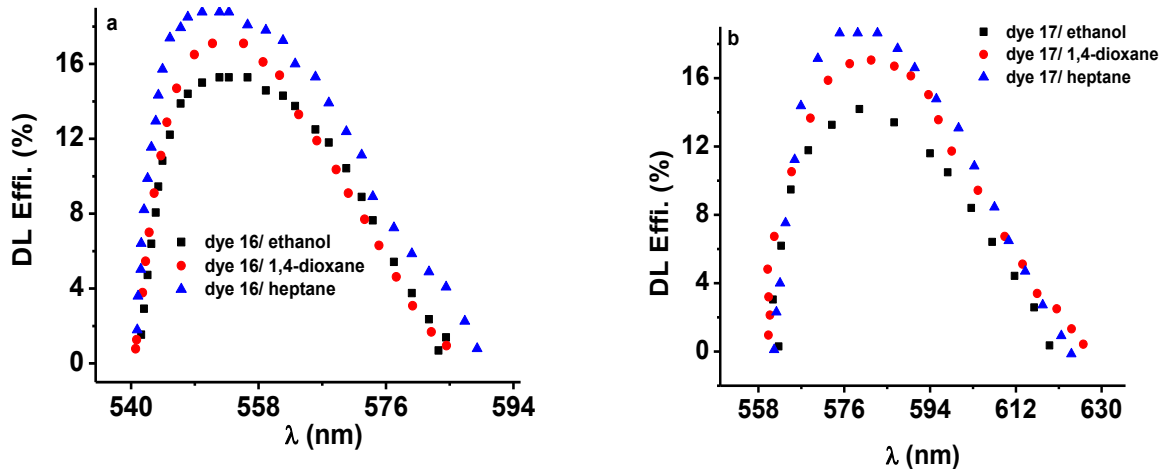

Figure 3.3.2.1: Narrow band lasing efficiency of dye (a) **16** and (b) **17** in ethanol, 1,4-dioxane and heptane, determined by pumping with 532 nm radiation of a Q-switched pulsed Nd:YAG laser.

3.3.3 Laser photostability:

To obtain the quantum yield of photo-degradation (Φ_{pd}), dye **16** and **17** were irradiated by second harmonic of the Nd:YAG laser (at 532 nm) in air equilibrated solution of three separate different solvents, ethanol, 1,4-dioxane, heptane. The extent of photodegradation was measured under non-lasing condition, and is shown in Table 3.3.3.1. The input power was constant for each dye in different solvents. After photo-exposure, there were no change in shape of the

longest wavelength absorption bands (S_0-S_1) of the dyes, but the peak heights were reduced. This is due to the fact that the degradation of dyes at the olifinic site would produce smaller molecules which do not absorb at this visible wavelength.[102a]

Table 3.3.3.1: Photostability of dyes **16** and **17** in ethanol, 1,4-dioxane and heptane

Dyes	Solvent	Φ_{pd}	$\Phi_{pd}^{-1}{}_{17}/\Phi_{pd}^{-1}{}_{16}$	$\Phi_{pd}^{-1}{}_{dioxane}/\Phi_{pd}^{-1}{}_{ethanol}$	$\Phi_{pd}^{-1}{}_{heptane}/\Phi_{pd}^{-1}{}_{ethanol}$
16	Ethanol	6.7×10^{-4}	-		
	1,4-dioxane	3.1×10^{-5}	-	21.3	
	Heptane	7.3×10^{-6}	-		90.7
17	Ethanol	2.8×10^{-4}	2.4		
	1,4-dioxane	2.8×10^{-6}	11.5	100	
	heptane	2.7×10^{-6}	2.7		102.7

The calculated data on the photostability (Φ_{pd}^{-1}) of both dyes in three different solvents, in absence and presence of singlet oxygen quencher DABCO, are tabulated in the Table 3.3.3.2. It is interesting to note that the nature of solvent has a prominent role to control the photo-degradation rate of the PM dyes. One of the most striking observations was that the dye **16** showed a large enhancement in photostability, respectively 91 and 21 fold in heptane and 1,4-dioxane than in ethanol (Table 3.3.3.1, column 5 and 6). The other dye **17** showed much higher photostability enhancement (100-103 fold) in 1,4-dioxane and heptane than in ethanol. Moreover, it was observed that dye **17** is 2.4, 11.5 and 2.7 times more photostable than dye **16** in ethanol 1,4-dioxane and heptane, respectively (Table 3.3.3.1, column 4). Expectedly, photostability enhancement was also observed in presence of singlet oxygen ($^1O_2$) quencher DABCO. The photostability was 10 and 29 times more in 1,4-dioxane and 30 and 58 times more in heptane than ethanol of dye **16** and dye **17,** respectively (Table 3.3.3.2, column 6 and 7). This confirms that generated $^1O_2$ is responsible for degradation of these PM dyes. However, it was

noticed that the photostability enhancement of both the dyes in presence of DABCO is higher in polar ethanol (Table 3.3.3.2, column 5).

Table 3.3.3.2: Photostability of dyes **16** and **17** with additive DABCO in ethanol, 1,4-dioxane and heptane

Dyes	Solvent	$\Phi_{pdDABCO}$	$\Phi_{pd}^{-1}{}_{DABCO}/\Phi_{pd}^{-1}$	$\Phi_{pd}^{-1}{}_{dioxane}/\Phi_{pd}^{-1}{}_{ethanol}$ With DABCO	$\Phi_{pd}^{-1}{}_{heptane}/\Phi_{pd}^{-1}{}_{ethanol}$ With DABCO
16	Ethanol	1.5×10^{-4}	4.4	-	-
	1,4-dioxane	1.5×10^{-5}	2.1	10	-
	Heptane	5.0×10^{-6}	1.5	-	30
17	Ethanol	6.9×10^{-5}	4.0	-	-
	1,4-dioxane	2.4×10^{-6}	1.2	29	-
	heptane	1.2×10^{-6}	2.2	-	58

Thus, the photostability of both the dyes are significantly higher in non-polar solvents although the lifetime of singlet oxygen is ~2.6 and 3 times more in 1,4-dioxane (25.0 μs) and heptane (28.0 μs) than in ethanol (9.7 μs).[104] This may be due to their less capacity of generating $^1O_2$ and/or less reactivity with $^1O_2$ in non-polar 1,4-dioxane and heptane than in polar ethanol. Moreover, the photostability of dye **17** is higher than dye **16** in all three solvents. These data clearly indicate that (i) $^1O_2$ generation and/or reactivity with $^1O_2$ of dye **17** is less than that of dye **16** and (ii) $^1O_2$ generation and/or reactivity with $^1O_2$ of both the dyes is less in non-polar than in polar solvent. These were further investigated by studying comparative capability of generating singlet oxygen, its reactivity and characteristics of triplet state of dyes in three solvents as described below.

3.3.4 Generation of $^1O_2$ by PM dyes:

Relative $^1O_2$ generation capacity of both BODIPY dyes were determined by monitoring the dye-sensitized photo-oxidation of 1,3-diphenylisobenzofuran (DPBF).[105] For this, polar ethanol and non-polar 1,4-dioxane and heptane solvents based DPBF with **16** or **17** dye solutions were irradiated by a visible lamp (driven by voltage stabilized power supply) using a cut off (>495 nm) filter with emission wavelengths higher than 495 nm over a exposure period of 900 s.

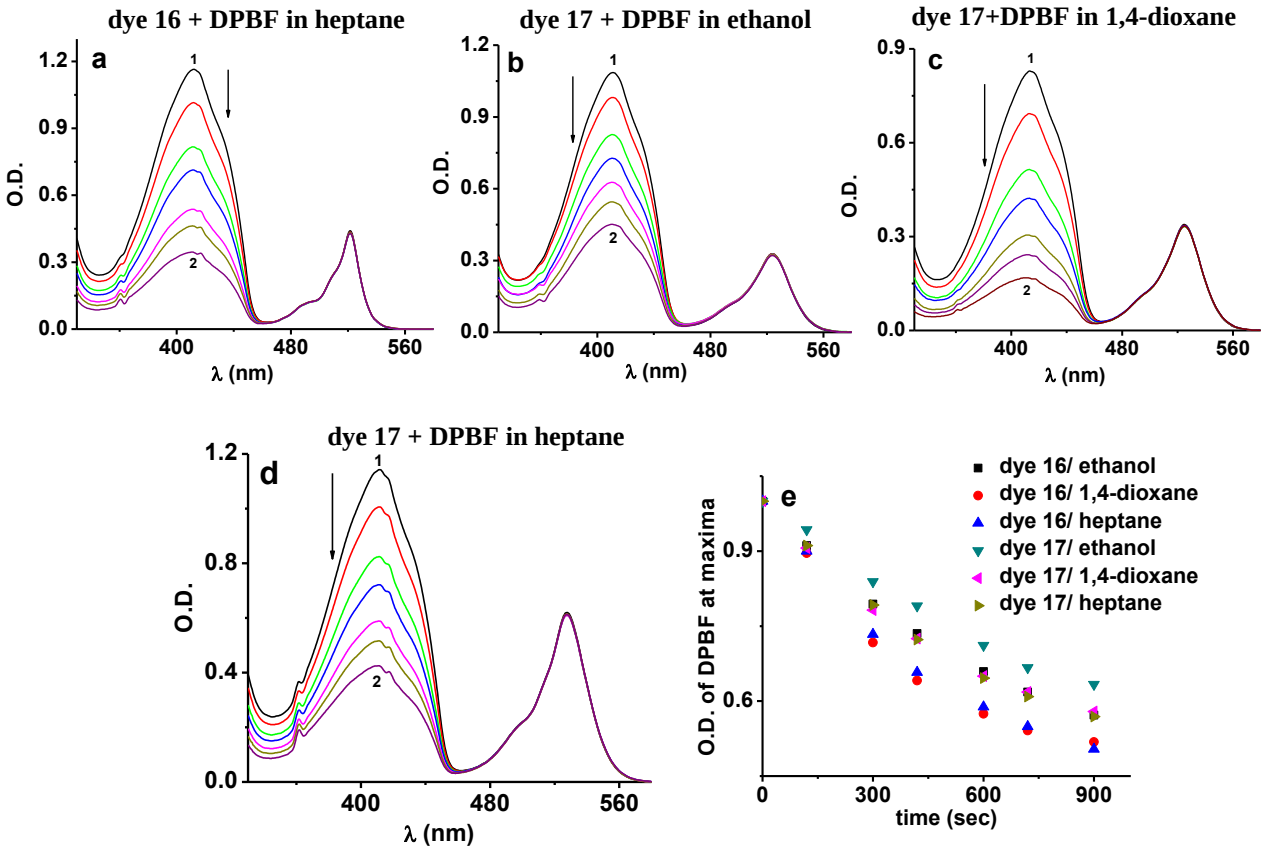

Figure 3.3.4.1: Absorption spectra of DPBF (50µM) during dye sensitized photo-oxidation in presence of **16** (5 µM) in (a) heptane; and in presence of **17** (5 µM) in (b) ethanol (c) 1,4-dioxane and (d) heptane: 1) 0 min. 2) 15 min., (e) Relative rate of $^1O_2$ generation of dyes **16** and **17** in ethanol, 1,4-dioxane and heptane determined by measuring time dependent OD of DPBF at its λ_{max} (412 nm) under dye-sensitized photo-oxidation in presence of dye **16** and **17** separately.

The concentration of DPBF (~ 50 μM) was taken about ten times higher than that of dyes (~ 5 μM). Under these conditions the lamp radiation excited only dye molecules and through reaction of excited dye at triplet (T_1) state with dissolved oxygen in the particular solvent generated $^1O_2$. The generated $^1O_2$ radicals reacted mainly with quencher DPBF, since concentration of dye was very low as well as rate of reaction of $^1O_2$ with DPBF is faster.[106] Under these stipulations the absorption bands of DPBF were observed to reduce gradually due to reaction with dye sensitized $^1O_2$ (Figure 3.3.4.1a-d). The rate of DPBF consumption i.e. the slope corresponds to the relative efficiency of $^1O_2$ generation by the dyes in the particular solvent. It was observed that rate of $^1O_2$ generation of both dyes were lower in ethanol compared to 1,4-dioxane and heptane (Figure 3.3.4.1e). It may be noted that longer lifetime[104,107] of $^1O_2$ in 1,4-dioxane (25 μs) and heptane (28 μs) as compared to in ethanol (9.7 μs) may also influences these observations. However, dye **17** showed smaller rate of generation $^1O_2$ than dye **16** in the respective solvents. To compare further the $^1O_2$ generation probabilities of the dyes, we investigated the triplet states of the dyes by pulse radiolysis.

3.3.5 Pulse radiolysis studies:

Pulse radiolysis is one of the established methods for study of triplet states of the dyes in solvents. The characterization of triplet states gives information about (i) the extent of $^1O_2$ generation by the dyes via energy transfer to dissolved O_2 in solvents, and also (ii) reduction in the lasing efficiency by triplet (T_1)-triplet (T_n) absorption loss of the dye laser photons. Here, the triplet state spectroscopy and the energy transfer processes of the dyes were investigated by pulse radiolysis in binary solvents of 1,4-dioxane/benzene and heptane/benzene separately in the volume ratio of 9:1. Triplet state characterization of dyes in ethanol by pulse radiolysis was not carried out due to the formation of solvated electrons and other reactive radicals on radiolysis of

ethanol, which can react with dye to give transient species. Radiolysis of benzene gives a high yield of the triplet state (G = 4.2 /100 eV) with energy of 82 kcal mol^{-1}, which can generate the dye triplets by energy transfer. However, due to the low lifetime (τ = 3 ns) of benzene triplet, a high concentration of solute is required. This limitation was overcome using a triplet sensitizer 4, 4-dimethylbiphenyl (DMBP) (E_T = 65 kcal mol^{-1}) along with the solute.[108]

Table 3.3.5.1: Triplet-state data of **16** and **17** in 1,4-dioxane/benzene and heptane/benzene (9:1)

Dye	**solvent**	**λ_{ma} [nm]**	**ε_{max}[a] [$M^{-1}cm^{-1}$]**	**k[^{3}Dye $\rightarrow O_2$] [$10^8 M^{-1}S^{-1}$]**
16	1,4-dioxane	710	2440	8.7
	heptane	710	2280	8.5
17	1,4-dioxane	700	2630	5.2
	heptane	700	2340	4.8

[a] Extinction coefficients at respective λ_{max}.

The triplet state of the laser dyes **16** and **17** in 1,4-dioxane/benzene and heptane/benzene (9:1) solution were generated by pulse irradiation in the presence of DMBP. In this condition, DMBP triplets are initially formed, which, in turn, transfer energy to generate the triplet states of the PM dyes. The triplet states absorption spectra (Figure 3.3.5.1) of both the dyes showed absorption at 600-800 nm. The triplet spectra of both the dyes are similar and consist of a single peak with λ_{max} at 700 nm and 710 nm for **17** and **16,** respectively (Table 3.3.5.1).

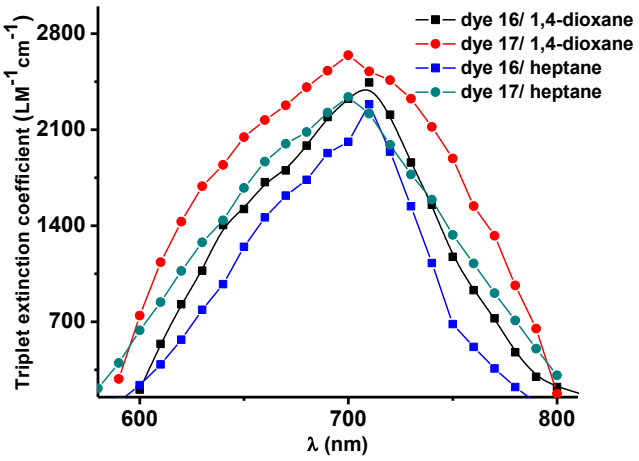

Figure 3.3.5.1: Triplet state absorption spectra of dye **16** and **17** in 1,4-dioxane/benzene and heptane/benzene (9:1) mixture in presence of triplet sensitizer DMBP.

The molar extinction coefficient (ε_{max}) at respective maxima of dyes in heptane was slightly smaller than in 1,4-dioxane, and thus loss of laser photons due to triplet-triplet absorption may be lower in heptane. The triplet state extinction coefficient (ε_{max}) at λ_{max} and, rate constant for energy transfer from the dyes to dissolved O_2 (k (^{3}Dye → O_2)) are calculated from experimental data and given in Table 3.3.5.1. Interestingly, the k (^{3}Dye → O_2) values of dye **17** was smaller than dye **16** in both non-polar solvents (1,4-dioxane and heptane), which was in agreement with our earlier experimental results (section 3.3.4). Also, rate of energy transfer from triplet dyes to dissolved oxygen is slightly less in heptane than 1,4-dioxane of both dyes. This suggests that $^1O_2$ generation probability of both the dyes is less in heptane than 1,4-dioxane. The reactivity of *in situ* generated $^1O_2$ with dyes in solvents was studied separately and discussed in the following section

3.3.6 Reactivity of $^1O_2$ with dyes 16 and 17:

The studies on reactivity of $^1O_2$ with dyes **16** and **17** were carried out experimentally by measuring the gradual decrease of the absorbance of the dyes at respective λ_{max} in presence of

methylene blue (MB), a known efficient $^1O_2$ generator under light illumination,[109] in pure ethanol, and mixture of 1,4-dioxane/ethanol and heptane/ethanol in 1:4 ratio separately. The experiment could not be carried out in pure 1,4-dioxane and heptane because of poor solubility of MB in these solvents. The mixture of dye **16** and MB, and dye **17** and MB were illuminated separately for 90 min and 50 min in three different solvents, respectively.

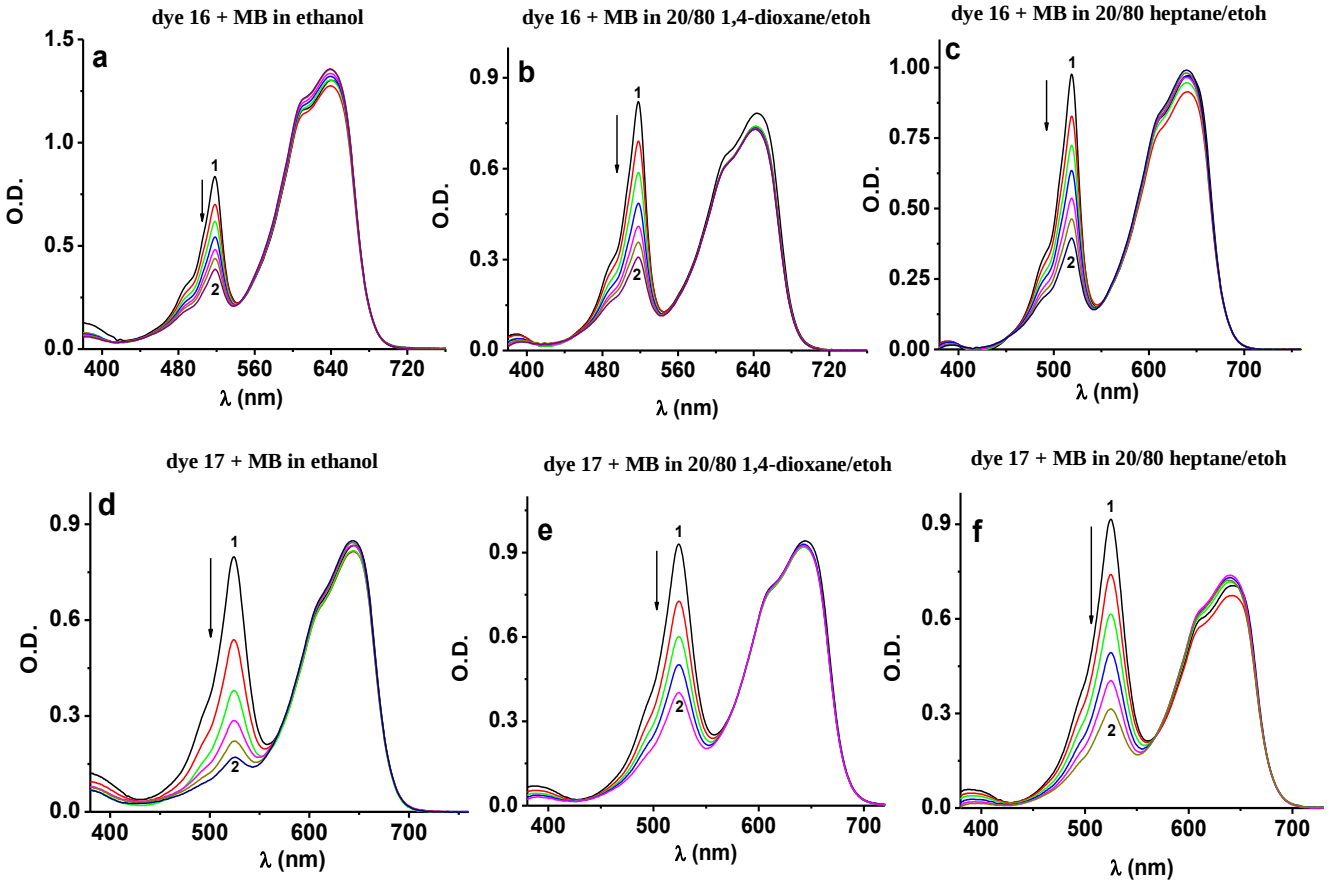

Figure 3.3.6.1: Absorption spectra of dye **16** (10µM) in (a) ethanol (b) mixture of 1,4-dioxane/ethanol (1:4) (c) mixture of heptane/ethanol (1:4) in presence of MB: 1) 0 min. 2) 50 min; and dye **17** (10µM) in (d) ethanol (e) mixture of 1,4-dioxane/ethanol (1:4) (f) mixture of heptane/ethanol (1:4) in presence of MB: 1) 0 min. 2) 50 min.

The absorbance of the dyes **16** and **17** was observed to reduce gradually with time although there was no change in the shape of the absorption bands of the dye (Figures 3.3.6.1 a-f). The rate of degradation of dyes (i.e., the slope) corresponds to the reactivity of $^1O_2$ with the dyes. The maximum degradation on reaction of $^1O_2$ with dye **16** (50% in ethanol, 48% in 1,4-dioxane/ethanol (1:4), 40% in heptane/ethanol (1:4) after irradiation of 90 min and with dye **17** (63% in ethanol, 58% in 1,4-dioxane/ethanol (1:4), 54% in heptane/ethanol (1:4)) after irradiation of 50 min. under similar conditions suggest that the reactivity of $^1O_2$ with dye **16** is lower (13% in ethanol, 10% in 1,4-dioxane/ethanol and 14% in heptane/ethanol at ratio of 1:4) than that of with dye **17** (Figure 3.3.6.2). Also, both the dyes degrade slowly in heptane/ethanol (1:4) than in 1,4-dioxane/ethanol (1:4) and pure ethanol solution.

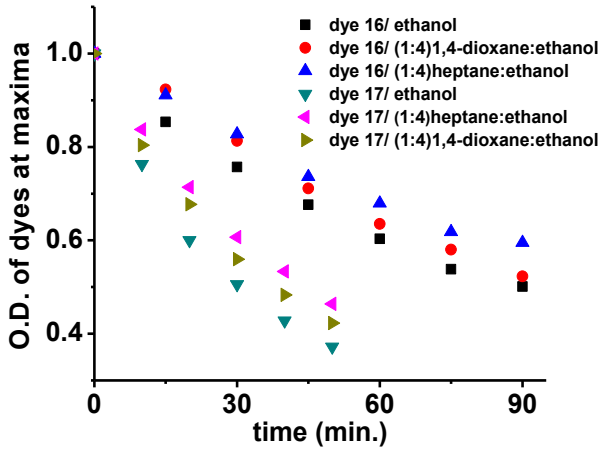

Figure 3.3.6.2: Relative rate of reactivity of $^1O_2$ with dyes **16** and **17** in ethanol, 1,4-dioxane/ethanol (1:4) and heptane/ethanol (1:4) determined by measuring time dependent OD of the dyes at their respective λ_{max} in presence of photo-excited methylene blue (MB).

Thus the degradation profile of dyes **16** and **17** confirmed that the relative reactivity of $^1O_2$ with the dyes would be dye **17** > dye **16.** However, we observed that dye **17** is more photostable that dye **16.** These two opposing results and other probable factor such as smaller singlet to triplet conversion rate (k_{ISC}) of the dye may be favorable for **17** and showed its higher stability in all three solvents (Table 3.3.3.1). Interestingly, the non-polor solvents showed to decrease the reactivity of $^1O_2$ with both the dyes and the pattern would be ethanol > 1,4-dioxane/ethanol > heptane/ethanol. This is matching with our experimental observations that both the dyes are more photostable in heptane/ethanol (1:4) than in ethanol.

3.4 Section 2: Comparative laser study of new PM dye 58:

3.4.1 Design and synthesis:

Previously we showed that the substitutions at B-centre improve the photostability of the BODIPY dyes.[108] Thus we designed the new dye **58** with a small alkynyl alcohol appendage at the B-centre. The appendage, propergyl alcohol (**55**) was chosen to keep a balance between the hydrophobicity and hydrophilicity of the dye **58** so that it can offer good solubility in both polar ethanol and non-polar 1,4-dioxane for the laser studies. At first the hydroxyl group of **55** was protected *via* acid catalyzed reaction with 2,3-dihydropyran furnishing **56** (Scheme 3.4.1.1). Synthesis of protected propergyl alcohol **56** was confirmed by NMR (^1H and ^{13}C) (Figure 3.4.1.1) Then the nucleophilic substitution of the F atoms of **16** was accomplished by reacting with the Grignard reagent, prepared from **56** to get the dye **57** (Scheme 3.4.1.1, Figure 3.4.1.2, and 3.4.1.3).[21b] Subsequently, the acid cleavage of the pyran groups of **57** furnished dye **58**. Presence of new peaks in ^1H and ^{13}C NMR correspond to propergyl alcohol indicate formation of dye **58** (Figure 3.4.1.4 and 3.4.1.5). Purity of the compound was also charecterized by mass spectroscopy and elemental analysis.

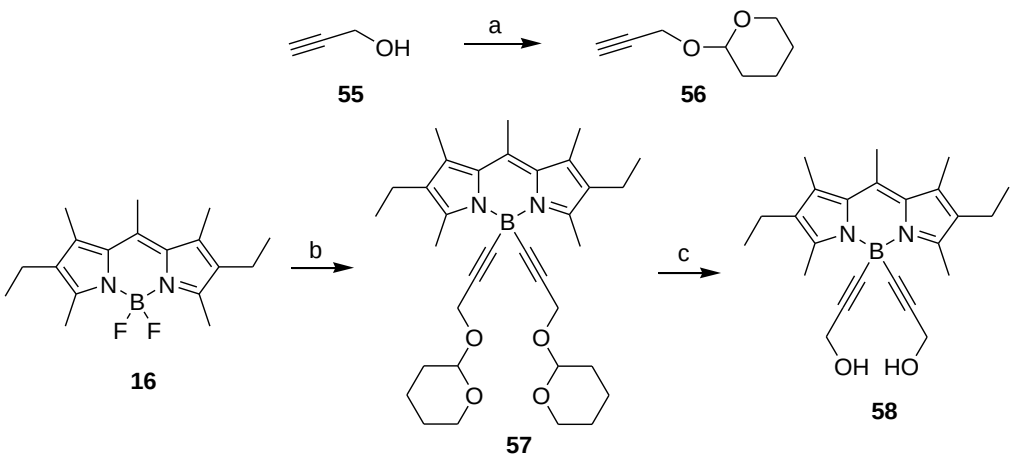

Scheme 3.4.1.1: Synthesis of dye **58** a) 2,3-dihydropyran, PPTS, CH_2Cl_2, 25^oC, 12 h. b) **56**, EtMgBr, THF, 60^oC, 24 h. c) PTS, MeOH/H_2O (9:1), 25^oC, 10 h.

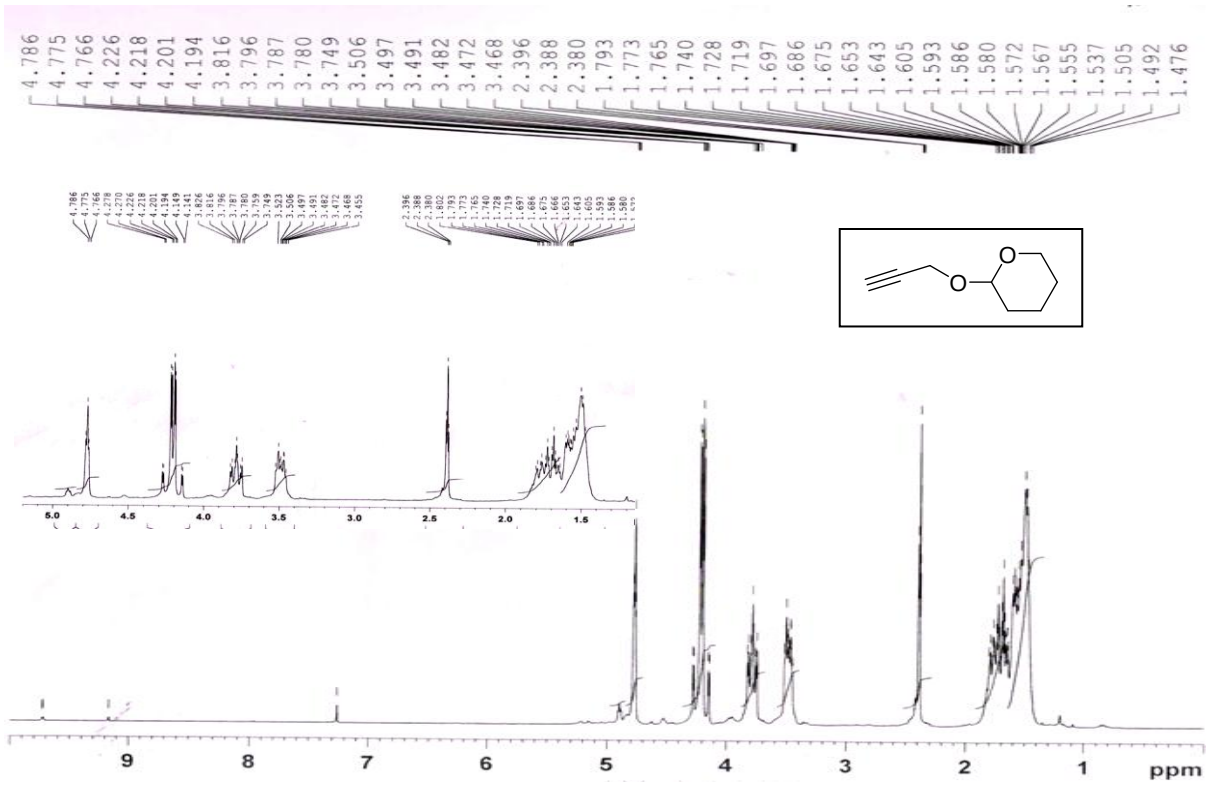

Figure 3.4.1.1a: ^1H NMR spectra of **56** in $CDCl_3$

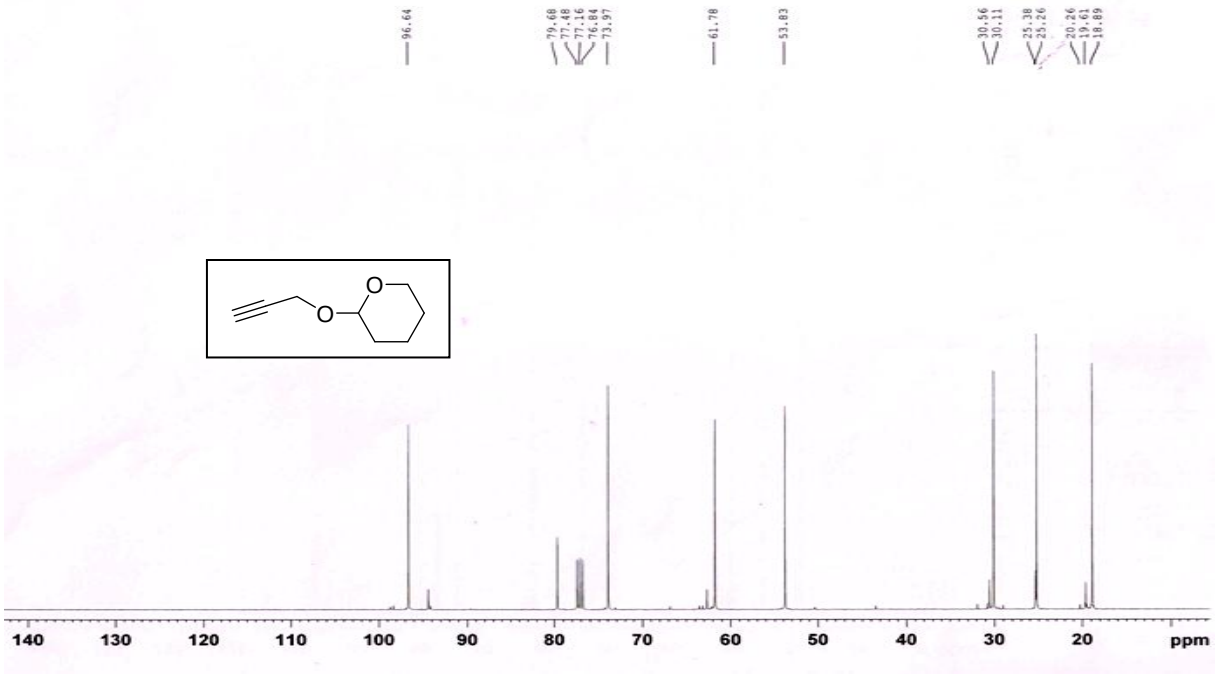

Figure 3.4.1.1b: ^{13}C NMR spectra of **56** in $CDCl_3$

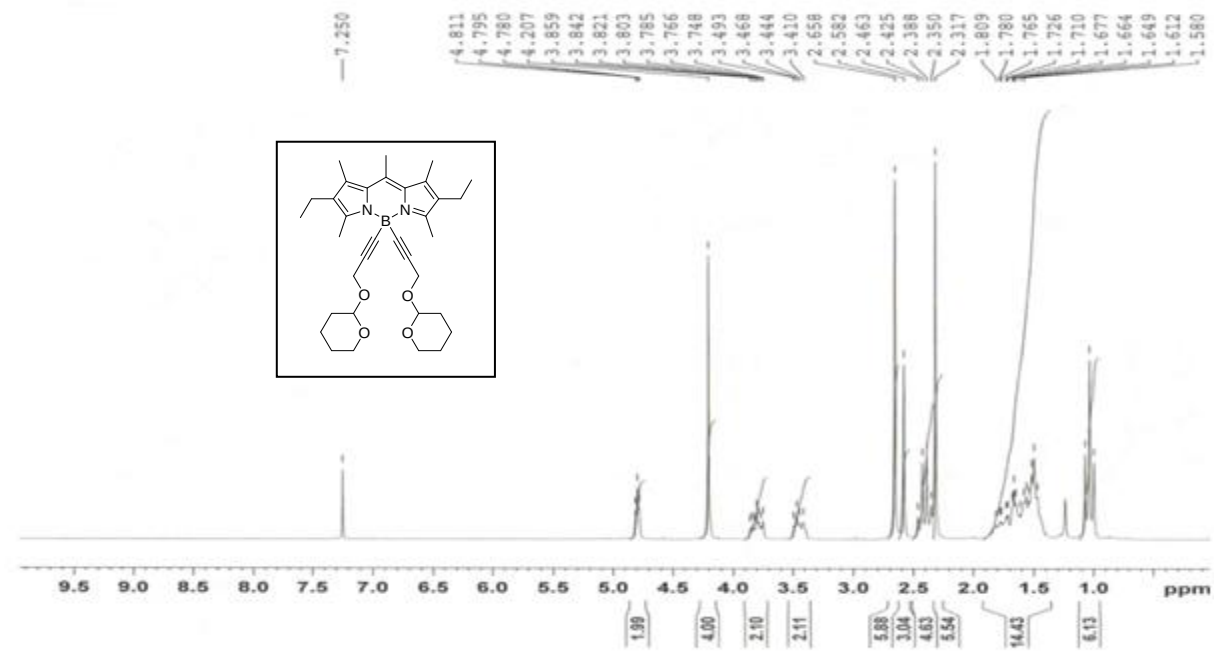

Figure 3.4.1.2: ^{1}H NMR spectra of **57** in $CDCl_3$

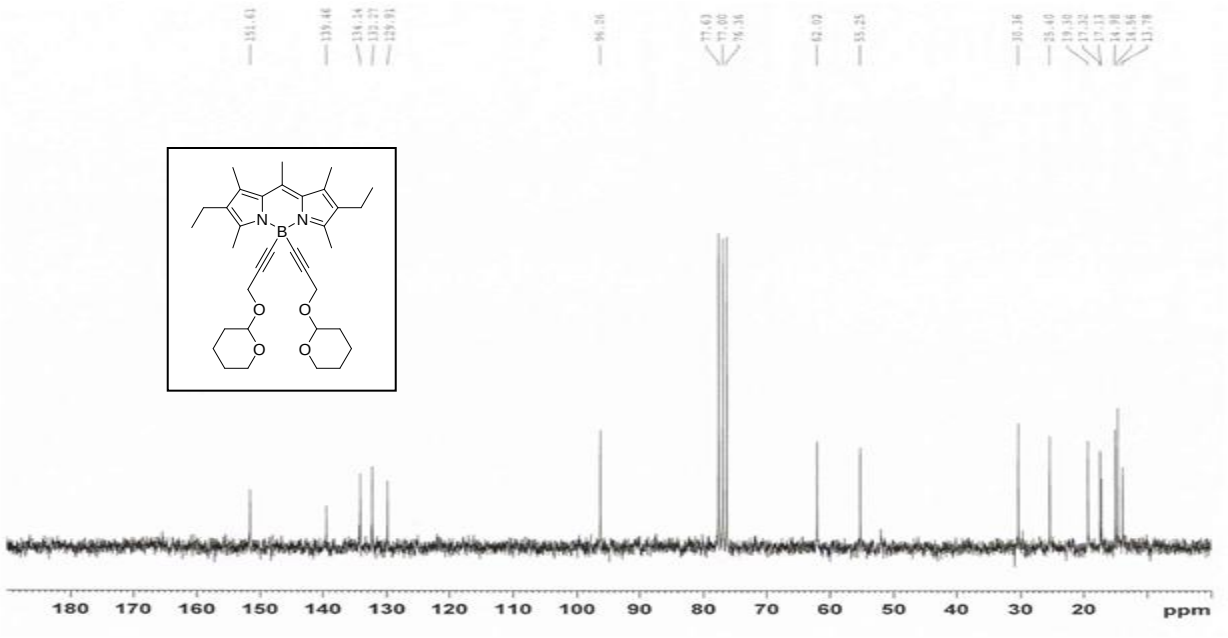

Figure 3.4.1.3: ^{13}C NMR spectra of **57** in $CDCl_3$

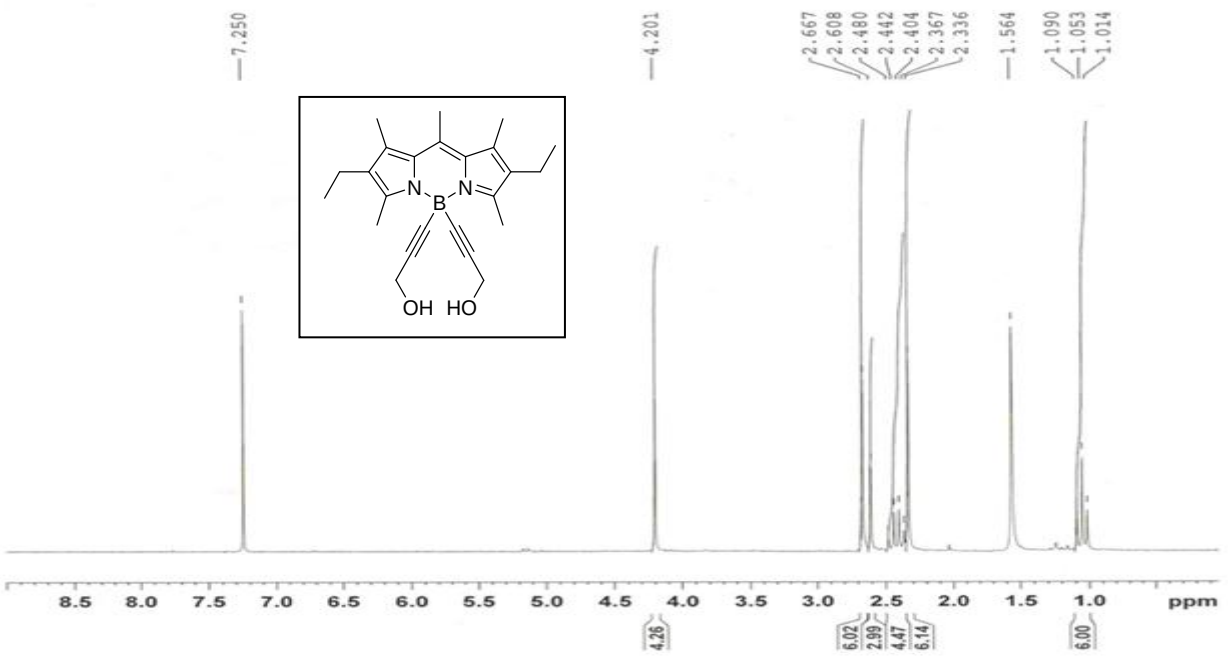

Figure 3.4.1.4: ^{1}H NMR spectra of **58** in CD_3OD

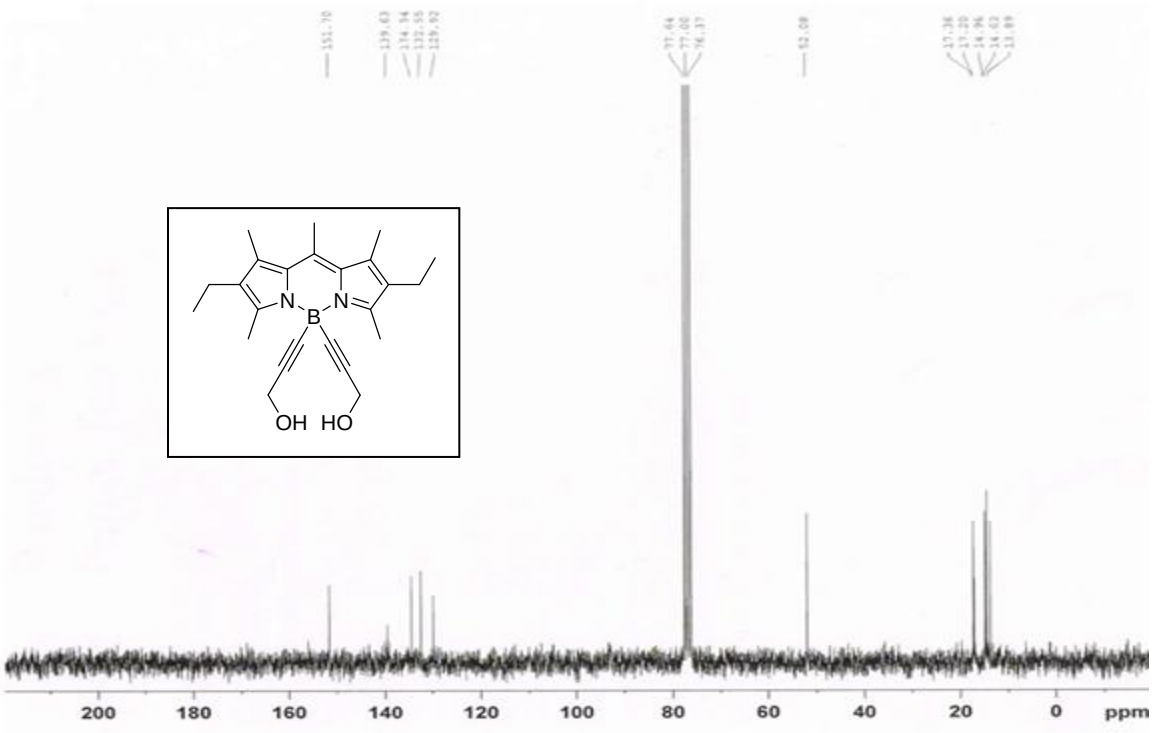

Figure 3.4.1.5: ^{13}C NMR spectra of **58** in CD_3OD

Design and synthesis of new PM dye was also based on considerations that the energy of $^1O_2$ (~27 kcal/mole) is comparable with the energy associated with high frequency vibrations of C-H and O-H bonds. This energy matching may play a role in increasing the quenching rate ($k_{\Delta Q}$) resulting from an electronic-to-vibrational energy transfer occurring from $^1O_2$ to the dyes.[107] Thus, extra C-H bonds and specially the two O-H bonds of the dye **58** would be very helpful to physically quench i.e. reducing the lifetime of $^1O_2$ (τ^{Δ}) in both the solvents. This is important as per photostability of **58** is concerned specially in 1,4-dioxane as τ^{Δ} is almost 3 times in 1,4-dioxane (25.0 μs) than ethanol (9.7 μs) discussed earlier.[104,107]

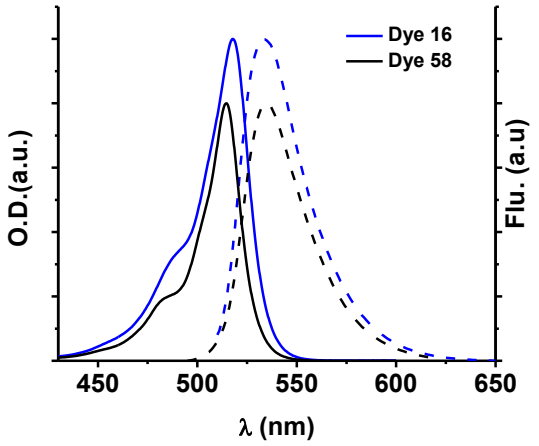

Figure 3.4.2.1: Normalized absorption (bold line) and emission (dotted line) spectra of dye **16** (blue) and **58** (black) in ethanol.

3.4.2 Optical properties:

The measured photo-physical parameters of the dye **58** relative to those of dye **16** in ethanol and 1,4-dioxane is presented in Table 3.4.2.1. Figure 3.4.2.1 show the normalized absorption and emission spectra of dyes **16** (PM567) and **58** in ethanol which are similar to each other. Both the dyes showed typical absorption features of the BODIPY dyes such as a strong $S_0 \rightarrow S_1$ transition at about 520 nm[98a,108,110] which indicate that the energy of the singlet state of both the dyes are similar in both the solvents. Both λ_{abs} and λ_{em} of the dye **58** are blue shifted by 3 nm than that of the dye **16** in both the solvents. Also λ_{em} of **16** and **58** are red shifted by 2 nm in 1,4-dioxane than λ_{em} in ethanol of respective dyes. These make Stokes shift of both the dyes marginally more in 1,4-dioxane than in ethanol. Maximum molar absorptivity (ε_{max} in 10^4 M^{-1} cm^{-1}) of the dyes **16** are 7.1 and 6.2 and of dye **58** are 8.6 and 6.7 in ethanol and 1,4-dioxane, respectively. Thus, ε_{max} of dye **58** is higher than that of dye **16** in respective solvents. Both the dyes were found to be highly fluorescent ($\Phi_f > 0.78$). Interestingly, Φ_f of both the dyes are more

in 1,4-dioxane than in ethanol and Φ_f of **16** and **58** are similar in 1,4-dioxane. The photo-physical data clearly revealed that substitution of the F-group did not affect the optical properties of the BODIPY chromophore.

Table 3.4.2.1: Photo-physical properties of dyes **16** and **58** in ethanol and 1,4-dioxane

Dye	Solvent	λ_{abs} [a] (nm)	ε_{max} [b] ($10^4 M^{-1}cm^{-1}$)	λ_{em} [c] (nm)	ν (cm^{-1})	Φ_f [d]	τ_f [e] (ns)	k_r (10^8 s^{-1})	k_{nr} (10^8 s^{-1})
16	ethanol	518.0	7.1	533.0	543	0.84[f]	6.48	1.3	0.25
	1,4-dioxane	518.0	6.2	535.0	613	0.89	6.52	1.36	0.17
58	ethanol	515.0	8.6	530.0	543	0.78	6.77	1.15	0.32
	1,4-dioxane	515.0	6.7	532.0	613	0.89	7.18	1.24	0.15

[a] Error: ± 0.2 nm. [b] Extinction coefficients at respective λ_{max}. [c] Error: ± 0.3 nm. [d] The fluorescence of the dyes **16** and **58** were measured at the excitation wavelength 505 nm. The fluorescence quantum yield of **58** is relative to that of **16**, reported earlier.[98a] [e] Error: ± 0.05 ns. [f] This data is taken from ref. [98a]

3.4.3 Lasing characteristics:

3.4.3.1 Narrow band lasing:

Narrow band lasing characteristics of the BODIPY dyes **16** and **58** in ethanol and 1,4-dioxane are compared and presented in Table 3.4.3.1.1 and Figure 3.4.3.1.1. The tuning curve follows an expected pattern, with maximum efficiency at a particular wavelength (λ_L), characteristic of the dye. The laser tuning range and λ_L of **16** and **58** are similar in both ethanol and 1,4-dioxane. The maximum lasing efficiency values (η) of the dye **58** are (11.8% in ethanol

and 15.3% in 1,4-dioxane) at the respective λ_L (Table 3.4.3.1.1). These results reveal a marginal reduction in the efficiency of PM dye on substitution at the B-centre.

Table 3.4.3.1.1: Narrow band lasing properties of dyes **16** and **58** in ethanol and 1,4-dioxane

Dye	Solvent	λ_L[a] [nm]	Tuning range [nm]	η[b] [%]	L_T [mJ]	GSA [10^{-18}cm^2] at λ_L
16	ethanol	553.8	541-583	15.3	2.90	1.34
	1,4-dioxane	555.8	540-584	17.1	6.14	1.36
58	ethanol	554.0	541-581	11.8	2.84	1.45
	1,4-dioxane	554.0	540-580	15.3	4.90	1.06

[a] Error: ± 0.5 nm. [b] Error: ± 1.0 %.

Interestingly, the lasing efficiency of both the dyes in 1,4-dioxane is higher than that of in ethanol. This is in accordance with the superior optical properties such as larger radiative and smaller non-radiative decay rates of **16** and **58** (refer Table 3.4.2.1) in 1,4-dioxane. The excited S_1–S_n absorption process (ESA) may also contribute to this, although the excited-state absorption cross-sections for the BODIPY derivatives are very low.[111] The threshold pump energy values (L_T) (Table 3.4.3.1.1, column 6) of the **16** and **58** are larger in 1,4-dioxane than in ethanol. Importantly, L_T of dye **58** in both the solvents are less than L_T of **16** in corresponding solvents. Thus, both the dyes showed higher laser efficiency in spite of higher threshold of pump energy at respective dye laser maxima (λ_L) in 1,4-dioxane. To understand this, the ground state absorption (GSA) cross-sections of dyes in both the solvents at the corresponding λ_L, were determined by absorption spectroscopy. The ground state absorption (GSA) cross-sections of the dye **58** in 1,4-dioxane at the corresponding λ_L, determined is lower than that of dye **16** in ethanol and in 1,4-dioxane, and that of dye **58** in ethanol, which indicates that the loss of laser photons will be less

in case of dye **58** in 1,4-dioxane due to the lower GSA. It may be noted that dye laser efficiency essentially depends on net gain that depends, in turn, on stimulated emission cross-section, absorption losses due to GSA and ESA at the peak wavelength, as well as on cavity losses and dynamic changes caused by time dependent saturation of the gain.

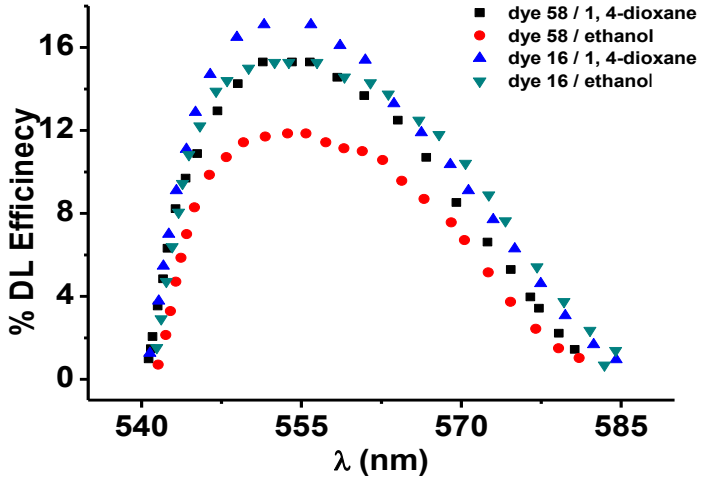

Figure 3.4.3.1.1: Narrow band dye laser (DL) efficiency of **16** and **58** in ethanol and 1,4-dioxane determined by pumping with 532 nm radiation of a Q-switched pulsed Nd:YAG laser

3.4.3.2 Broad band lasing:

The concentration dependent broad band lasing efficiency of the BODIPY dyes in ethanol was studied and followed an expected pattern, initially increasing with the dye concentration and reaching a maximum before decreasing again. Brief description of the dye laser set up is given in chapter 2. Maximum lasing efficiency values (η) of the dyes at their respective optimum dye concentrations are listed in Table 3.4.3.2.1. The dye **58** showed very high lasing efficiency (49.3%) which is slightly better than that of dye **16** (47.4%) (Figure 3.4.3.2.1)

Table 3.4.3.2.1: Broad band lasing properties of dye **16** and **58**

Dyes	solvent	η (%)	Conc. (mM)
16	ethanol	47.7	1.03
58	ethanol	49.3	1.96

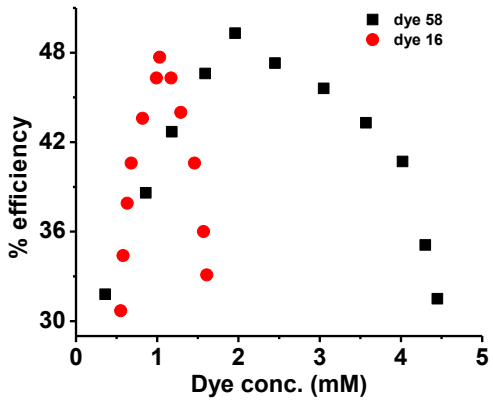

Figure 3.4.3.2.1: Conc. dependent broad band lasing efficiency of dye **16** and **58** in ethanol

3.4.4 Photostability:

The quantum yields of photo-degradation (Φ_{pd}) of the dyes **16** and **58** in air-equilibrated ethanol and 1,4-dioxane, measured under non-lasing conditions are shown in Table 3.4.4.1. It is noticed that the substitutions of the F-atoms increase the photostability (Φ_{pd}^{-1}) of dye **58**, compared to that of dye **16** in both the solvents. The dye **58** is 2.1 and 3.3 times more photostable than **16** in ethanol and 1,4-dioxane, respectively (Table 3.4.4.1, column 4). The stability of the dye **58** in 1,4-dioxane is found to be comparable to that of Rhodamine 6G in ethanol solution, an established benchmark in photostability of laser dyes. The higher photostability of **58** may be due to its less $^1O_2$ generation capacity and/or less reactivity with $^1O_2$ as compared to **16**.[108] The dyes **16** and **58** are respectively 22 and 34 fold more photostable in 1,4-dioxane than in ethanol (Table 3.4.4.1, column 5) although the lifetime of singlet oxygen is higher in 1,4-dioxane than in

ethanol. Also this stability enhancement in lowering the solvent polarity is more in case of dye **58** as compared to dye **16**. In general, higher residence time of $^1O_2$ in solvent helps in more photo-degradation but in present cases the observed results were just opposite. This may be due to the fact that $^1O_2$ generation and/or reactivity with $^1O_2$ of both the dyes are less in non-polar 1,4-dioxane than in polar ethanol.

Table 3.4.4.1: Photostability of dyes **16** and **58** in ethanol and 1,4-dioxane

Dye	Solvent	Φ_{pd}	$\Phi_{pd}^{-1}{}_{dye\ 58}$ / $\Phi_{pd}^{-1}{}_{dye16}$	$\Phi_{pd}^{-1}{}_{dioxane}$ / $\Phi_{pd}^{-1}{}_{ethanol}$	$\Phi_{pdDABCO}$	$\Phi_{pd}^{-1}{}_{DABCO}$ / Φ_{pd}^{-1}
16	ethanol	6.7×10^{-4}	-	-	1.5×10^{-4}	4.5
	1,4-dioxane	3.1×10^{-5}	-	21.5	1.5×10^{-5}	2.1
58	ethanol	3.2×10^{-4}	2.1	-	1.4×10^{-4}	2.3
	1,4-dioxane	9.4×10^{-6}	3.3	34.2	8.1×10^{-6}	1.2

Addition of singlet oxygen ($^1O_2$) quencher DABCO showed photostability enhancement of both the dyes in both the solvents (Table 3.4.4.1, column 6). This confirms that $^1O_2$ is responsible for the dye degradation. It was noticed that the photostability enhancement in presence of DABCO (50 times of dye in molar concentration) was almost half in case of **58** than **16** in both the solvents (Table 3.4.4.1, column 7). Also the photostability enhancement of both the dyes, **16** and **58** in 1,4-dioxane were less than in ethanol. The reason behind these results might be the difference in reactivity with $^1O_2$ or/ and generation of $^1O_2$ by dye solutions. These were investigated by different experimentation as described below.

3.4.5 Cyclic voltammetry:

Cyclic voltammetry analysis of the BODIPY dyes **16** and **58** were carried out in highly polar acetonitrile and less polar dichloromethane. The aim was to check (i) the relative oxidation potentials (E_{ox}) of dyes **16** and **58** and (ii) how the E_{ox} changes with solvent polarity.

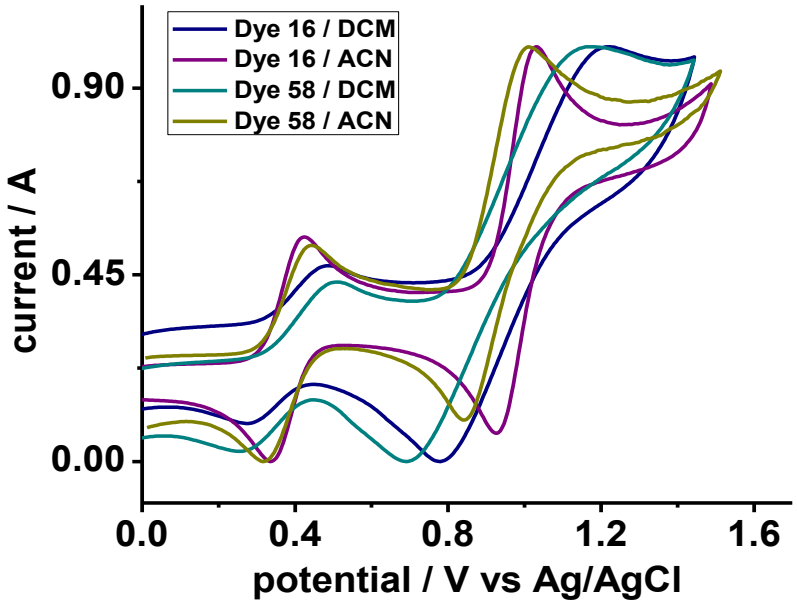

Figure 3.4.5.1: Cyclic voltammograms of dyes **16** and **58** in acetonitrile (ACN) and dichloromethane (DCM) at room temperature.

Both the dyes showed a reversible peak in each case in the anodic portion of the cyclic voltammograms (Figure 3.4.5.1), which was assigned to one electron oxidation of the BODIPY unit.[112] The data revealed that the B-substitution had a negative effect on oxidation potential. The dye **58** was more easily oxidizable by 70 mV and 60 mV in dichloromethane and acetonitrile, respectively. Thus the trend in oxidation probability of dyes in both the solvents was **16** < **58**, which is opposite to that observed rate of photodegradation (Φ_{Pd}). Interestingly, decrease of

solvent polarity has positive effect on E_{ox} of the dyes. The dye **16** and **58** are less oxidizable in dichloromethane than in polar acetonitrile by 20 mV and 10 mV respectively (Table 3.4.5.1).

Table 3.4.5.1: Electrochemical properties of dyes **16** and **58** in dichloromethane and acetonitrile

Dye	Solvent	E_{ox} [V]	$E_{ox,\ dichloromethane} - E_{ox,\ acetonitrile}$ [mV]
16	dichloromethane	1.00	20
	acetonitrile	0.98	
58	dichloromethane	0.93	10
	acetonitrile	0.92	

This indicates that both the dyes will be more stable towards oxidation in non-polar 1,4-dioxane than in polar ethanol which was observed experimentally. But, exceptionally high stability of the dyes in 1,4-dioxane suggests that the rate of reaction with $^1O_2$ and $^1O_2$ generation capacity of the dyes might have a crucial role in the relative photostability of the dyes. To investigate these, we measured the relative $^1O_2$ generation rate and relative reaction rates with $^1O_2$ of both the dyes which were rationalized by pulse radiolysis and theoretical calculations of the ground and excited states of the dyes as well as $^1O_2$.

3.4.6 Relative $^1O_2$ generation of dye 16 and 58:

Relative $^1O_2$ generation capacity of BODIPY dyes **16** and **58** were compared by monitoring the dye-sensitized photo-oxidation of 1,3-diphenylisobenzofuran (DPBF).[105] For this, ethanol and 1,4-dioxane solution of DPBF with dye **16** and **58** separately were irradiated using a stabilized tungsten lamp with wavelengths cut off filter > 495 nm over a time period of 900 s. Under these conditions only BODIPY dye was excited to generate singlet oxygen, which reacted primarily with DPBF. For this DPBF was taken 50 times higher molar concentration in

comparison to that of dye. It may also be noted that reaction rate of $^1O_2$ is significantly higher with DPBF then that with BODIPY dyes. Therefore the absorbance bands of dye **16** and **58** remained unchanged but the absorbance peaks of DPBF were found to decrease gradually due to dye-sensitized photo-oxidation (Figure 3.4.6.1).

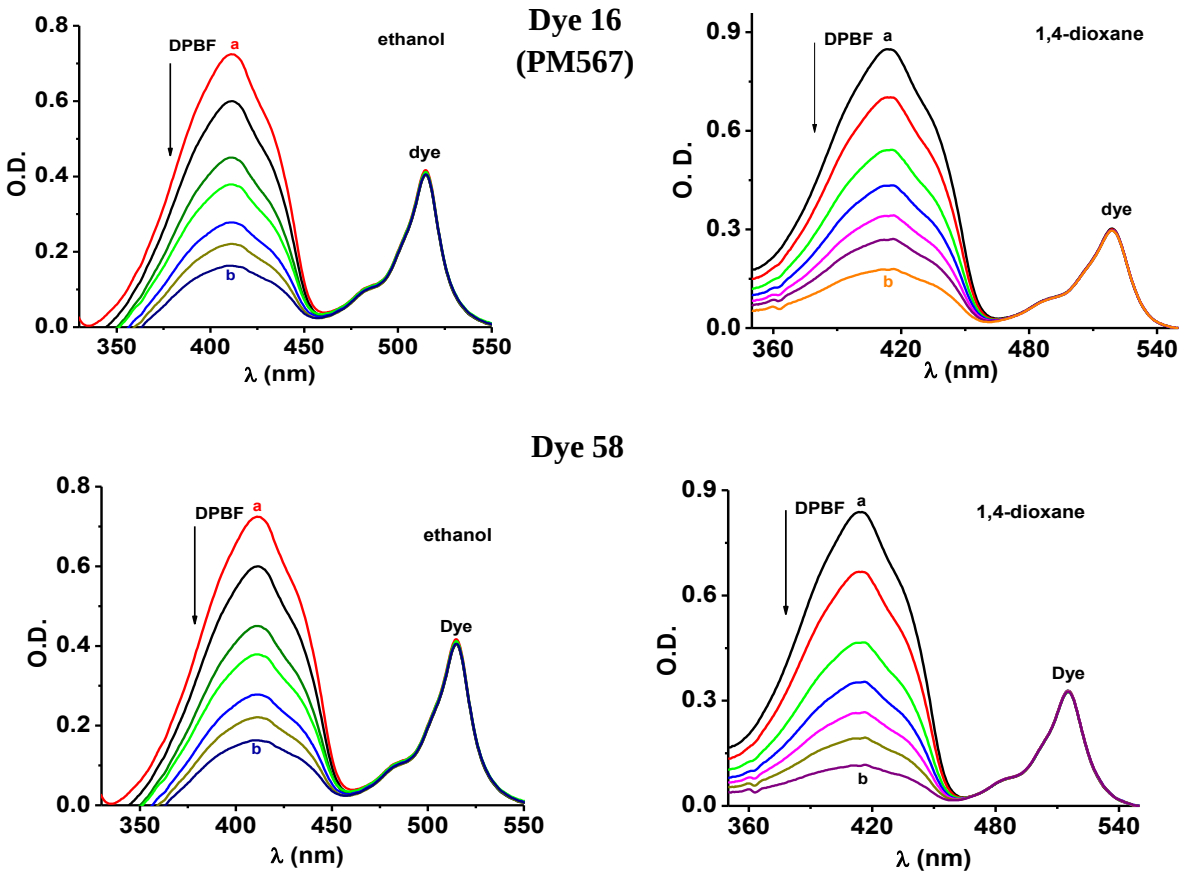

Figure 3.4.6.1: Change in absorption spectra of DPBF (50µM) in ethanol and 1,4-dioxane during dye-sensitized photo-oxidation in presence of dye **16** and **58** (5µM): (a) 0 min. (b) 15 min.

It was seen that both the dyes generated $^1O_2$ in ethanol almost at equal rate (Figure 3.6.6.2). However, in 1,4-dioxane $^1O_2$ generation rate of both the dyes were although similar but higher

than that of in ethanol. To further investigate the $^1O_2$ generation probabilities of the dyes **16** and **58**, we also determined characteristics of the triplet states of the dyes by pulse radiolysis.

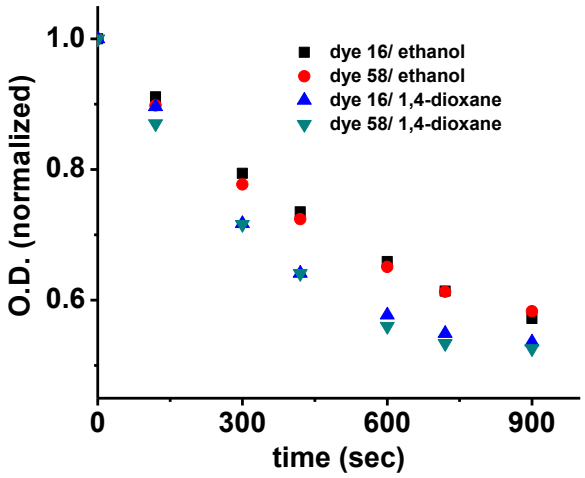

Figure 3.4.6.2: Relative rate of $^1O_2$ generation of dyes **16** and **58** in ethanol and 1,4-dioxane determined by measuring time-dependent OD of DPBF at its λ_{max} (412 nm) under dye-sensitized photo-oxidation in presence of dye **16** and **58** separately.

3.4.7 Pulse radiolysis studies:

The triplet state spectroscopy and the energy transfer processes of the dyes **16** and **58** were investigated by carrying out their pulse radiolysis (same procedure as described in section 1) in 1,4-dioxane/benzene (9:1) solutions. The triplet state of the dyes **16** and **58** in 1,4-dioxane/benzene (9:1) solution were generated by pulse irradiation in the presence of DMBP. The absorption spectra (Figure 3.4.7.1) of the triplet state of both the dyes showed absorption at 600-800 nm. The triplet spectra of the dyes consist of a single peak with λ_{max} at 710 nm and 720 nm for **16** and **58**, respectively (Table 3.4.7.1). Thus triplet state spectra of both the dyes **16** and **58** were found to be similar.

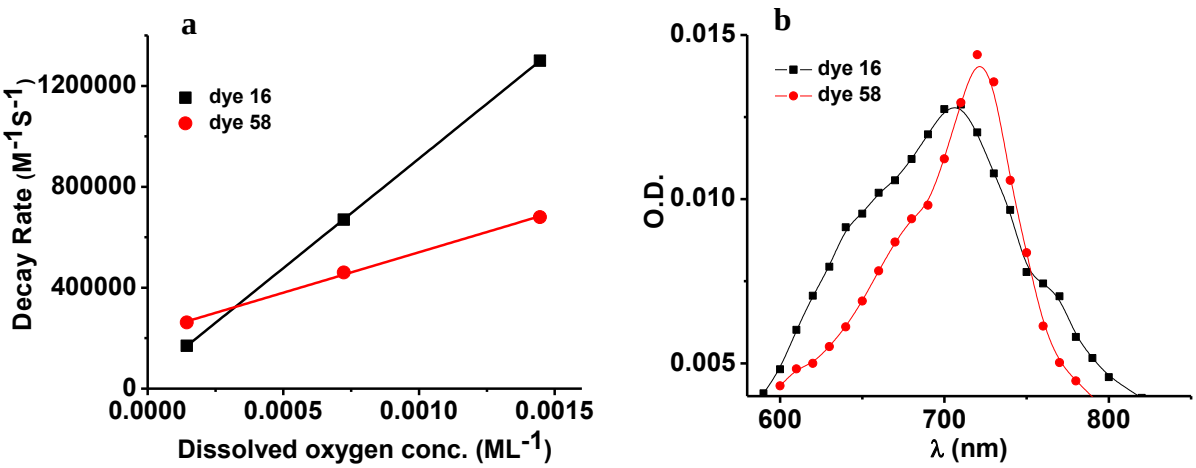

Figure 3.4.7.1: (a) Plot of decay rate vs. dissolved oxygen concentration of dye **16** and **58** in mixture of 1,4-dioxane/Benzene in 9:1 ratio; (b) Triplet state absorption spectra of dye **16** and **58** in 1,4-dioxane/benzene (9:1) mixture in presence of triplet sensitizer DMBP.

The triplet state extinction coefficients (ε^{T}_{max}) at λ_{max} and, rate constants for energy transfer from DMBP triplet to the dyes (k_{et}) and from the dyes (**16** and **58**) to $^1O_2$ (k (^{3}Dye → O_2)) are calculated from experimental data and given in Table 3.4.7.1. Interestingly, the k (^{3}Dye → O_2) value for **58** was 3 fold less than that of **16**. This suggests that $^1O_2$ generation probability of dye **58** is lesser as compared to dye **16,** which was not observed in dye-sensitized photooxidation experiment (section 3.4.6). This indicates that other factors like singlet to triplet intersystem crossing rate (K_{ISC}) of the dye might higher for dye **58** than dye **16**. It may be noted that in dye sensitized photooxidation study, dye molecules are excited to triplet state (T_1) by intersystem crossing (ISC) from excited singlet (S_1) state.

Table 3.4.7.1: Triplet-state data for dyes **16** and **58** in 1,4-dioxane/benzene (9:1)

Dye	λ_{max} [nm]	ε_{max} [a] [$M^{-1}cm^{-1}$]	k_{et} [^{3}DMBP→Dye] [$10^9 M^{-1}S^{-1}$]	k[^{3}Dye →O_2] [$10^8 M^{-1}S^{-1}$]
16	710	2440	2.0	8.7
58	720	2830	3.7	3.2

[a] Extinction coefficients at respective λ_{max}.

3.4.8 Relative reactivity of $^1O_2$ with dye 16 and 58:

The reactivity of *in situ* generated $^1O_2$ with dyes **16** and **58** were examined separately by devising an experiment in which $^1O_2$ was generated by adding methylene blue (MB), under light illumination[109] of the tungustan lamp in ethanol and 1,4-dioxane/ethanol (1:4).

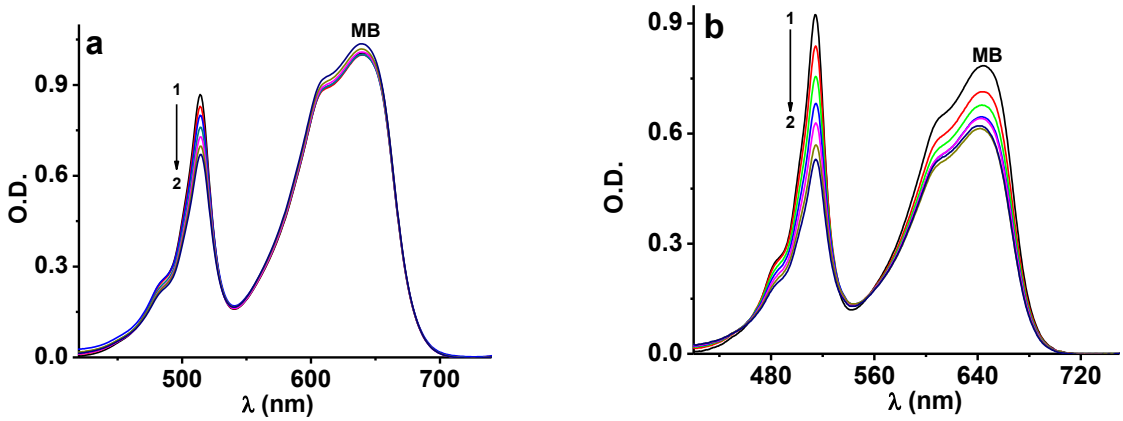

Figure 3.4.8.1: Change in absorption spectra of dye **58** (10μM) in (a) pure ethanol and (b) mixture of ethanol/ 1,4-dioxane in 4:1 ratio via photo-oxidation in presence of methylene blue (MB) as a sensitizer (10μM). (1) 0 min (2) 90 min

The absorbance of the dye **16** and **58** were found to reduce gradually with exposure time although there were no change in the shape of the corresponding absorption bands of the dye (Figure 3.4.8.1 and Figure 3.3.6.1 a-c). After 90 min. of illumination, 50% of the dye **16** was found to degrade whereas only 37% of initial dye **58** was degraded under similar conditions (Figure 3.4.8.2). Therefore, the rate of reactivity of $^1O_2$ with the dye **58** was smaller than that of with dye **16**.

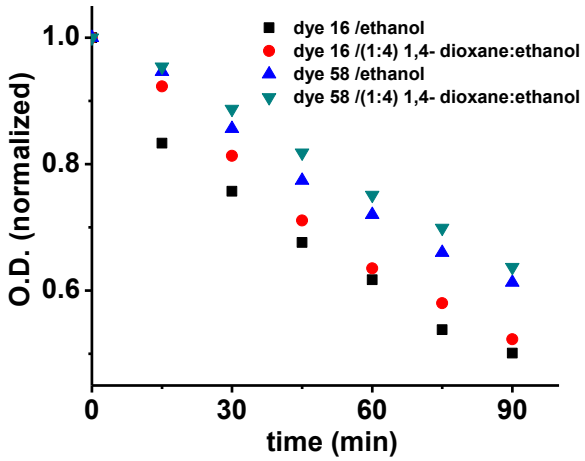

Figure 3.4.8.2: Relative rate of reactivity of $^1O_2$ with dyes **16** and **58** in ethanol and in 1,4-dioxane/ethanol (1:4) determined by measuring time-dependent OD of the dyes at their respective λ_{max} in presence of photo-excited methylene blue (MB).

Similar observations were also found in 1,4-dioxane/ethanol (1:4). The rate of degradation of dye **58** i.e. the reactivity of $^1O_2$ with the **58** is lesser than that of with dye **16** (Figure 3.4.8.2). After 90 min. of illumination, the extent of degradation of dyes **16** and **58** were found to be 47% and 35%, respectively. This degradation study and analysis of dyes **16** and **58** confirmed that the relative reactivity of $^1O_2$ with the dyes would be dye **16** > dye **58** in both ethanol and 1,4-dioxane/ethanol (1:4). It may be mentioned that decrease of solvent polarity may

decrease the rate of reactivity of $^1O_2$ with both the dyes. This is matching with our experimental observations that both the dyes are more photostable in 1,4-dioxane than that in ethanol. To understand the difference in reactivity of $^1O_2$ with dyes **16** and **58** in solvents of different polarity, we have computed ground and excited states of the dyes as well as the $^1O_2$ by DFT based theoretical calculations.

3.4.9 Theoretical interpretations:

The ground-state (S_0) minimum- energy structure **58a** (Figure 3.4.9.1) of the Bodipy dye **58** was optimized by carrying out DFT calculation. Then the reaction course of the dye **58** with $^1O_2$ was investigated by placing the $^1O_2$ in the proximity of the most vulnerable position, the C7'=C8 double bond of the dye (Figure 3.4.9.2). The transition state (TS) structure was identified as **58b**, and the peroxide **58c** was identified as the reaction product (Figures 3.4.9.1 and 3.4.9.2).

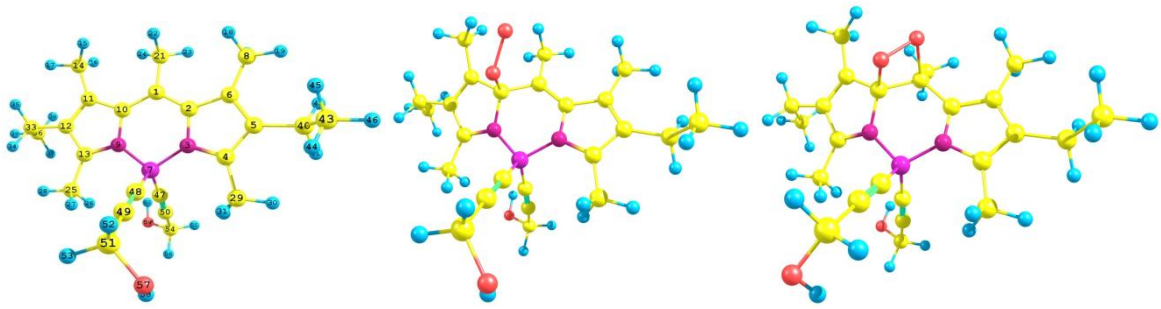

58a **58b** **58c**

Figure 3.4.9.1: Optimised ground state (**58a**), transition state (**58b**) and peroxide compound (**58c**) of the Bodipy dye **58**.

The TS **58b** is formed by partial cleavage of the C7'=C8 π–bond and formation of the C7'─O2 bond as the initial events, as supported by the bond lengths (Table 3.4.9.1). The C7'=C8 (1.41 Å)

and O1=O2 (1.21 Å) bond lengths increase to 1.52 and 1.41 Å, respectively, in the TS. The distance between C7' and O2 (1.50 Å) indicates that a single bond is formed between them. The C8 and O1 atoms are too far apart (2.71 Å) to form a stable bond, but gradually move closer for bond formation (bond length=1.51 Å), furnishing the peroxide compound **58c**. Charge density calculations further established the mechanism. According to the calculations, in the TS, the electron density at O1 is more than that at O2, whereas the electron density at C8 is less than that in **58a** (Table 3.4.9.1). This is consistent with the proposed mechanism (Figure 3.4.9.2). After the formation of the C8─O1 bond, O1 and O2 become electronically similar, as is evident from the charge densities on the two atoms (Table 3.4.9.1).

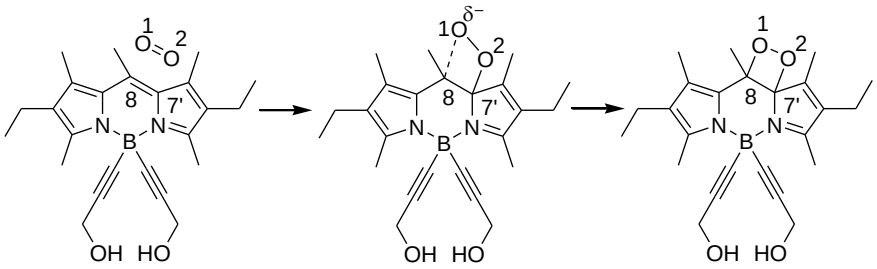

58a **58b** **58c**

Figure 3.4.9.2: Mechanism of the reaction of the Bodipy dye **58** with $^1O_2$.

However, most importantly, the model suggests that charge separation in the TS **58b** is more than that of in the dye **58a** and the peroxide **58c**. This is evident from the calculated dipole moment and charge density values (Table 3.4.9.1). This suggest that energies of the initial and final products will not change much with the change in solvent polarity, but the energy of TS **58b** will be very high in non-polar 1,4-dioxane but it will be stabilized with lower energy in the polar ethanol. This will make the activation energies of the reaction higher in 1,4-dioxane as compared to ethanol. Thus the reaction rate of $^1O_2$ with the dye will be very slower in 1,4-

dioxane than that of in ethanol. This explains the slower reactivity $^1O_2$ with the dyes in non-polar 1,4-dioxane than in polar ethanol i.e. high photostabilities of the dyes in 1,4-dioxane.

Table 3.4.9.1: Changes in the bond lengths, atomic charges and dipole moment during the reaction of dye **58** with $^1O_2$

Dyes	Bond Length (Å)				Atomic charge (a.u.)		Dipole Moment In Debye
	C8-O1	C7'-O2	C8- C7'	O1-O2	O1	O2	
58a	-	-	1.41	1.21	0	0	4.78
58b	2.71	1.50	1.52	1.41	-0.411	-0.254	6.21
58c	1.51	1.45	1.54	1.49	-0.298	-0.289	6.50

3.5 Stability comparison between dyes 16, 17 and 58: Despite the lower oxidation potentials (E_{ox}) of the dye **58** than dye **16 (PM567)**, dye **58** is found to be more photostable than dye **16** in both the solvents. Both optical and pulse radiolysis studies showed that the $^1O_2$ generation capacities of the dyes **16** and **58** are similar but higher than dye **17 (PM597)**. Moreover, the reactivity with $^1O_2$ is less for the dye **58** than dye **16** and higher for dye **17**. This facilitated dye **58** to be more photostable than dye **16** and **17**.

3.6 Stability comparison of dyes in ethanol and 1,4-dioxane and heptane: Both optical and pulse radiolysis studies showed that the $^1O_2$ generation capacities of the dyes **16, 17** and **58** were higher in nonpolar (heptane, 1,4-dioxane) solvents than in ethanol. Also the reactivity with $^1O_2$ was different as indicated by the results of photostability enhancement with DABCO. This was lower in less polar solvents which eventually increases the stability of all three dyes in this order heptane > 1,4-dioxane > ethanol.

3.7 Conclusion:

A new BODIPY dye **58** was judiciously designed and synthesized containing 3-oxa-5-hexynol moieties at the B-centre. The new dye **58** showed comparable lasing efficiency as that of the commercial dye **16** and dye **17** in non-polar (1,4-dioxane, heptane) solvents, which in turn slightly higher than dye **17** in ethanol. Moreover, the excellent photostability of all the three dyes **16**, **17** and **58** in non-polor media such as 1,4-dioxane and heptane in comparision to that of Rhodamine 6G in ethanol makes it a potential photostable BODIPY dyes for further exploration. Hence, these non-polar solvents may be utilized as a practically useful solvent for safe, sustainable, reliable and efficient operation of PM dye lasers; particularly for high average power dye lasers in which a large volume of dye solutions are needed to circulate at high flow speed.

CHAPTER 4

IMPROVED PHOTO-PHYSICS OF COUMARIN USING THE HOST CUCURBIT[7]URIL

Chapter 4: Table of Contents

4.1 Introduction:

In previous chapter we have discussed the improvement of lasing properties of commercial and synthesized BODIPY (PM) dyes using organic solvents (polar and non-polar). It is anticipated that water is the preffered solvent for high average power dye lasers compared to common organic solvents. This is due to the fact that water possesses the highest photothermal figure of marit ($F= \rho sk/(dn/dT)$) among all the solvents for dye lasers, arising primarly from its low gradient of refractive index with temperature (dn/dT), high density (ρ), specific heat (s) and thermal diffusivity (k). However, pure water is generally not used for dye laser due to formation of non-fluorescent aggregates of dye, which could be improved by host-guest complex formation. The phenomenon of host-guest inclusion has been the focus of the recent and growing fields of supra-molecular chemistry, and has found widespread and important applications.[113-116] Living organisms, pharmaceutical solubilization, controlled drug delivery, natural plants etc. utilize properties of host-guest inclusion aggregates,[117,118] which are stabilized by non-covalent bonds with hydrophobic organic molecules. The supra-molecular complex formation is a dynamic phenomenon and leads to a system of equilibrium between the complex and the free host and guest. These complexes are usually formed in aqueous solutions, while utilizing the relative difference in local polarity between the non-polar internal cavity of the organic host and the bulk solvent, thus maximizing the hydrophobic effect as a driving force for inclusion of organic guests. Among various known macrocyclic hosts such as calixarene, cyclodextrins, cucurbit[n]urils (CBn), the molecules of CBn families have shown significantly stronger interaction with neutral or cationic organic guests and recently revealed many interesting and promising results.[81,119] Lately, low toxicity of CBs[120] such as high cell tolerance in living

biological systems at a concentration of up to 1 mM has been demonstrated, indicating their potential use towards the molecular containers as an advanced drug delivery system.

Among CBs, the 7-member analogue cucurbit[7]uril (CB[7]) has been shown to form strong inclusion complexes with water soluble fluorescence dyes due to its appropriate cavity size[42a,45b,121] resulting significant improvement in microscopic photo-physical properties of guest dyes,[33c,60a,122] which also led to other novel applications such as demonstration of efficient and highly photostable aqueous dye lasers.[123] In addition to usual hydrophobic effect in water which favors inclusion of organic dyes inside the CB[7] cavity, it provides another distinct supramolecular interaction, namely ion-dipole interactions at carbonyl-laced portals, which promote binding of cationic sites of organic guests. Recently, CB[7] host has been used to form strong and stable inclusion complexes in water with some organic dyes, mostly belonging to xanthene class of chromophore.[33c,60a,122] We have extended host-guest inclusion study of the relatively recent host CB[7] with UV laser dye coumarin as guest to enhance its photophysical and laser properties.

4.2 Coumarin dyes:

Coumarin is a versatile class of hydrophobic organic fluorophores,[124] found in many plants and medicines, used in fluorescence microscopy as sensitive fluorescent probes for proteins and other biological cells, dye sensitized solar cells, dye lasers as UV dyes, etc. However, preferred use of aqueous solutions of coumarin dyes for these applications have been limited due to low solubility, drastic reduction in fluorescence intensity and photochemical stability in water, which may largely overcome upon addition of host CB[7].[125] For a preliminary study on the interaction of CB[7] with coumarin, 7-diethylamino-4-methylcoumarin or

coumarin1 (abbreviated as C1-N), a widely used fluorescent molecule, was used as guest. Further, the hydrochloride salt of C1-N (abbreviated as C1-NH^+) was prepared (characterized by ^1H NMR and FT-IR) to improve its solubility in water as well as interaction with host CB[7]. In these coumarin1 dyes, 7-diethyl amine moiety can play an important role in modulating their photo-physics in aqueous solutions. Earlier, Nau *et al*[125c] reported the enhancement in fluorescence intensity of aqueous solution of coumarin 102 dye in presence of host CB[7], but only by 1.14 time. A recent report[125a] on the inclusion behavior of parent coumarin dye with CB[7] as biological fluorescence probe in aqueous solutions inspired us to carry out a detail study on the interaction of coumarin1 with CB[7]. To the best of our knowledge, our study was the first report on supramolecular interaction of the host CB[7] with amino substituted coumarin derivatives.

In this chapter, we present our recent results starting with UV dye i.e. effective inclusion of two forms of coumarin1 (cationic vs. neutral) dyes inside the cavity of CB[7] thereby improving its photo-physical properties and photostability in aqueous system. The chemical structures of C1-N (**59**), C1-NH^+ (**60**) and CB[7] (**50**) molecules are displayed in Figure 4.2.1.

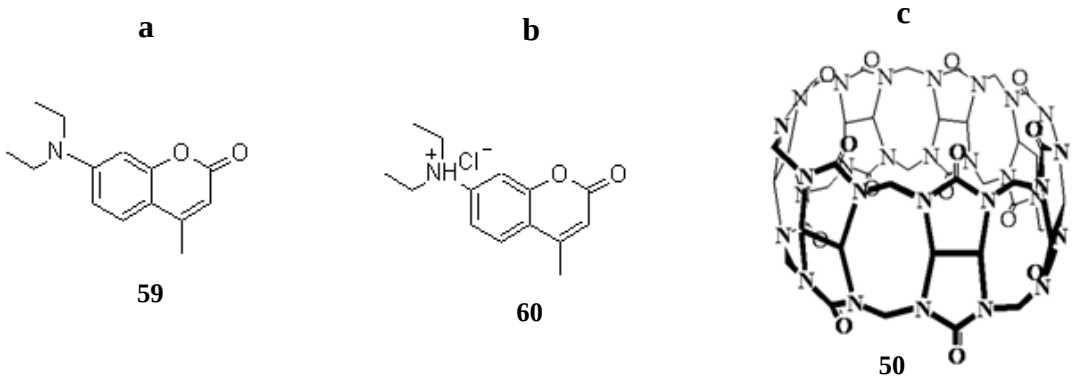

Figure 4.2.1: Molecular structures of (a) C1-N (**59**), (b) C1-NH^+ (**60**), (c) CB[7](**50**)

4.3 Experimental:

4.3.1 Materials:

Laser grade dye **59** (7-diethylamino-4-methylcoumarin) and **4** (4,6-dimethyl-7-ethylaminocoumarin) were obtained from Lambda Physik (Germany); their purity was checked by TLC and ^{1}H NMR in $CDCl_3$ and used without further purification. The macrocyclic host cucurbit[7]uril was synthesized in high purity in our lab by reported procedure.[43,44] The purity of synthesized CB[7] (**50**) sample was verified using ^{1}H NMR, ^{13}C NMR and spectrophotometric titration techniques. Spectroscopy grade ethanol was used to prepare the dye solutions. Nanopure water was obtained by passing distilled water through a Barnstead nanopure water system and was used for all the dye solution preparations.

4.3.2 Methods:

4.3.2.1 Absorption and steady-state fluorescence spectra:

Absorption and steady-state fluorescence spectra of dilute (5-20 $x10^{-6}$ M) solutions of both coumarin (**59** and **60)** dyes, using ethanol, water and water in presence of host CB[7] (**50)**, were measured using commercial UV-vis spectrophotometer (JASCO V-550) and spectrofluorimeter (JASCO FP-6500), respectively. The dye solutions were excited at the isosbestic point, observed in their absorption spectra. All these measurements were performed at ambient temperature (~25^{0} C), the solutions being in equilibrium with the air.

4.3.2.2 Fluorescence quantum yield (Φ_f):

Quantum yield of fluorescence of dyes **59** and **60** in different solvents was determined by comparative method. Ethanol solution of dye **4** and dye **59** was considered as fluorescence

standard and its reported value was verified by this procedure.[126] In order to minimize re-absorption effects, absorbance in the 10 mm path length quartz fluorescence cuvette was kept below 0.1 at the excitation wavelengths of dye solutions. Refractive indices of solvents were taken into account for the calculations of Φ_f values.

4.3.2.3 Time-resolved fluorescence study:

Fluorescence life time decay of dye solutions was measured using a time-correlated single photon counting (TCSPC) set up FluoTime-200 from Pico Quant, Germany. In the present work, a 405 nm pulsed diode laser (~100ps, 10 MHz repetition rate) was used for excitation. The instrument response function for this set up is ~272 ps at FWHM. To eliminate depolarization effect on the fluorescence decays, measurements were carried out with magic angle geometry (54.7^0) for the excitation and emission polarizer. The fluorescence decays I(t) of dyes were analyzed using an exponential function as

$$I(t) = \Sigma B_i \exp(-t/\tau_i)$$

where B_i and τ_i are the pre-exponential factor and the lifetime, respectively, for the i^{th} component of fluorescence decay.

4.3.2.4 Fluorescence anisotropy study:

In order to measure fluorescence anisotropy of dye solutions, samples were excited with vertically polarized output of a pulsed diode laser at 405 nm and the vertically and horizontally polarized fluorescence decays were recorded. The anisotropy decay function, r(t), was calculated from these polarized fluorescence decays as follows:

$$r(t) = [I_V(t) - GI_H(t)] / [I_V(t) + 2GI_H(t)]$$

where $I_V(t)$ and $I_H(t)$ are the vertically and horizontally polarized decays, respectively, and G is the correction factor for the polarization bias of the detection set up. The G factor was determined independently by using a horizontally polarized excitation light and measuring the two mutually perpendicular polarized components of fluorescence decays.

4.3.2.5 ^{1}H NMR study:

^{1}H NMR characterization of aqueous solutions of coumarin dyes (**59** and **60),** in presence and absence of host CB[7] (**50)**, was carried out in D_2O using 500 MHz Bruker spectrometer.

4.3.2.6 Theoretical study:

The minimum energy ground-state molecular structures of dye molecules **59** and **60** and host **50** were determined applying B97D/cc-pVDZ level of theory. Different initial structures were considered keeping two different ends of the guest molecule inside the cavity of the host to locate the minimum energy structure of the host-guest complex. Quasi Newton-Raphson based algorithm was applied to carry out geometry optimization for each of these systems with various possible conformers as the initial structures. All electronic structure calculations were carried out applying the GAMESS suite of *ab initio* program on a LINUX cluster.[78] The binding energy of the host-guest complex of both form of dyes were calculated at the present level of theory. Calculations of various components of the total interaction energy of the host-guest complex were carried out using Kitaura-Morokuma energy decomposition analysis.[127]

4.3.2.7 Laser photostability:

The quantum yield of the photo-degradation (Φ_{pd}) of the dyes is defined as the probability of the decomposition of the dye molecules by the absorbed pump photons. The photostability is

the inverse of the Φ_{pd} value. A known quantity of dye solution (2 ml) in a dye laser cuvette was exposed to pump energy of 6 mJ at 355 nm. The concentration of the coumarin dye solution was chosen such that the pump beam was totally absorbed within the dye solution in the cuvette during the excitation for about 30 min. The solution was constantly stirred with a teflon-coated magnetic stirrer to avoid local heating. The number of photo-degraded dye molecules in the exposed volume of the dye solutions was quantitatively estimated from the absorbance at the corresponding λ_{abs} before and after photo-exposure for a set period of time. The reflection loss of the pump beam on incident surfaces of the dye cell was determined for calculating the absorbed cumulative pump photons.

4.4 Results & Discussion:

4.4.1 Studies on pH dependent equilibrium between coumarin dyes:

Coumarin 1 dye (**59)** was found to be highly soluble in ethanol, but its solubility was very low (< 60 μM) in aqueous media. In order to improve the solubility and binding strength of dye **59**, we converted the N-diethyl amine group at the 6-position of the chromophore into a protonated ammonium salt (**60**). The solubility of the dye **60** was observed to be higher (~1.7mM) and it increased further in presence of the host CB[7] (**50)**. A dynamic equilibrium between dye molecules **59** and **60** is possible in aqueous solution. Therefore, acidity constant (pK_a) value of this system has been determined. The cationic dye **60** was a salt of weak base and strong acid, and thus de-protonation would happen in aqueous media. The measurement of the acidity constant (pK_a) of the aqueous solutions of the dye **59** was carried out by UV-vis spectrophotometric titrations, which gave a value of pK_a = 3.4 (Figure 4.4.1.1). Therefore, a strong acidic condition was required for formation of primarily dye **60** in aqueous solution.

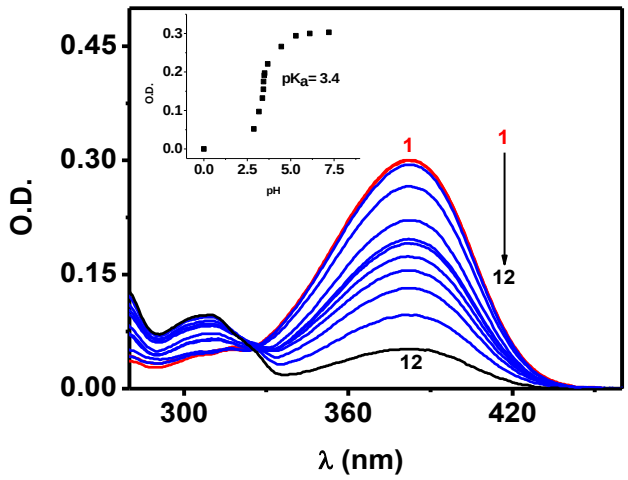

Figure 4.4.1.1: Absorption spectra of aqueous solution of dye **59** by addition of acid (1 to12 increasing). Inset: plot of absorbance at peak maxima vs. pH. The pKa value was 3.4

Hence, we used dye **59** solution in water with addition of HCl acid at pH = 2, so that most of **59** dye molecules exist in form of dye **60.**The formation of quaternary ammonium salt, at nitrogen atom of diethyl amine moiety of dye **59**, was verified in the spectral region 1000-3500 cm^{-1} by recording FT-IR spectra in reflection (ATR) mode of both dyes **59** and **60** in solid-phase. In contrast to dye **59**, dye **60** gave a distinct broad peak[128] at ~2391 cm^{-1}.

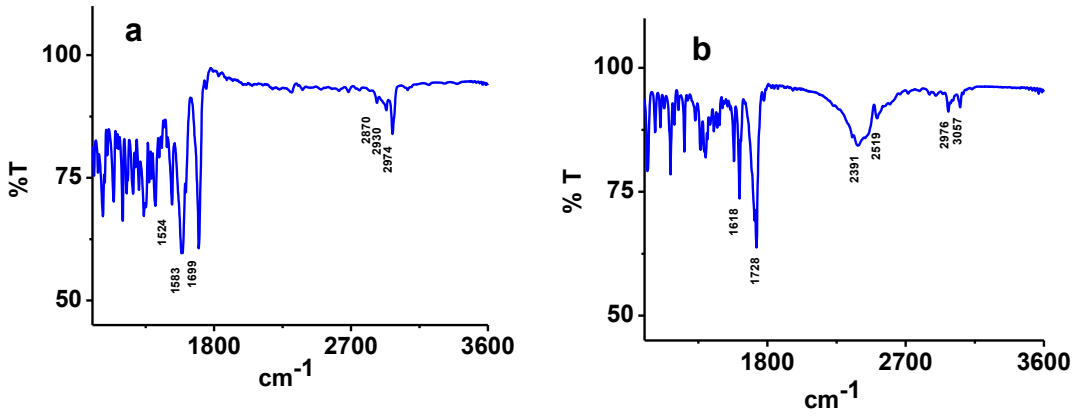

Figure 4.4.1.2: FTIR spectra of (a) dye **59** and (b) dye **60**

FT-IR spectra of both the coumarin 1 dye molecules are shown in Figure 4.4.1.2. Further, the formation of dye **60** was confirmed by recording ^{1}H NMR spectra of dye **59** and **60** in d_4-methanol (CD_3OD), which are illustrated in Figure 4.4.1.3.

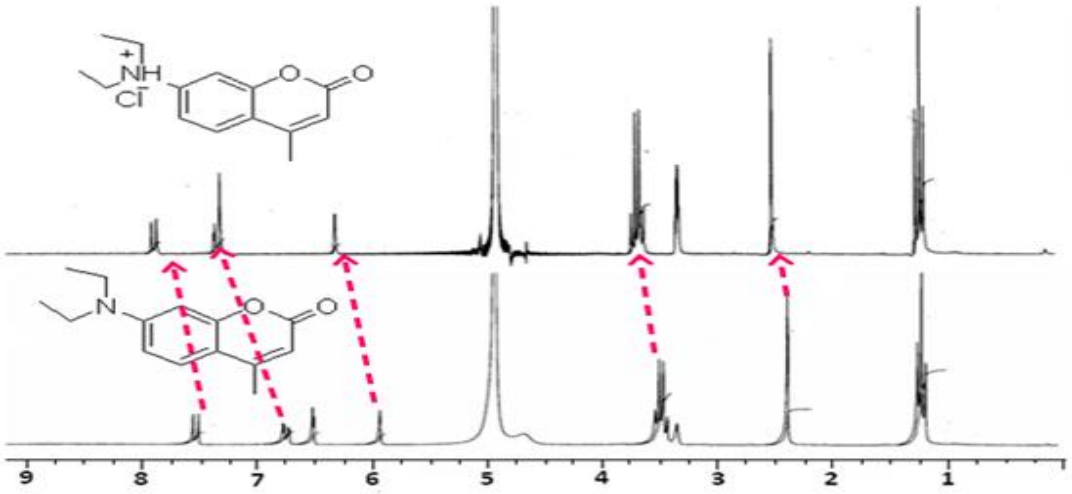

Figure 4.4.1.3: ^{1}H NMR spectra of **59** and **60** in d_4-methanol (CD_3OD)

In case of dye **60**, positively charged nitrogen atom pulls out electron density from the chromophore resulting downfield shift of aromatic protons in comparison to that of dye **59**. Further the photophysical study and interaction study of cationic dye **60** was performed at pH=2.

4.4.2 Absorption studies:

Both dyes **59** and **60** gave similar absorption spectra in ethanol. Absorption maxima of neutral dye **59** were found at 372 nm and 380 nm in ethanol and water, respectively. These values are in agreement with the reported data[126,129] on dye **59.** Addition of host **50** induced progressively red-shifted absorption spectra of dye **59**, which indicated isosbestic point at 385 nm in water, were shown in Figure 4.4.2.1. The shift in longest wavelength absorption maxima (λ_{max}) of dye **59** was observed up to 397 nm in presence of high concentration of CB[7] (**50)**, typically at 20 equivalent concentrations of dye **59**. However, absorption maximum of C1-NH^+

(**60**) molecule showed different behavior than neutral dye in water. There is another absorption peak at 306 nm with addition of peak at 380 nm in water which was not observed in case of dye **59**. Moreover the isosbestic point was observed at 332 nm i.e. between two peak maxima (306 and 380) with addition of CB[7]. With addition of CB[7], decrease in peak maxima at 306 nm with small shift and subsequently large increase in peak absorbance value at 380 nm with progressively red-shift to 397 nm was observed. The modulation in absorption spectra of aqueous solutions of **59** and **60** dyes has indicated different behavior of interaction of cationic form of dye molecule with CB[7].

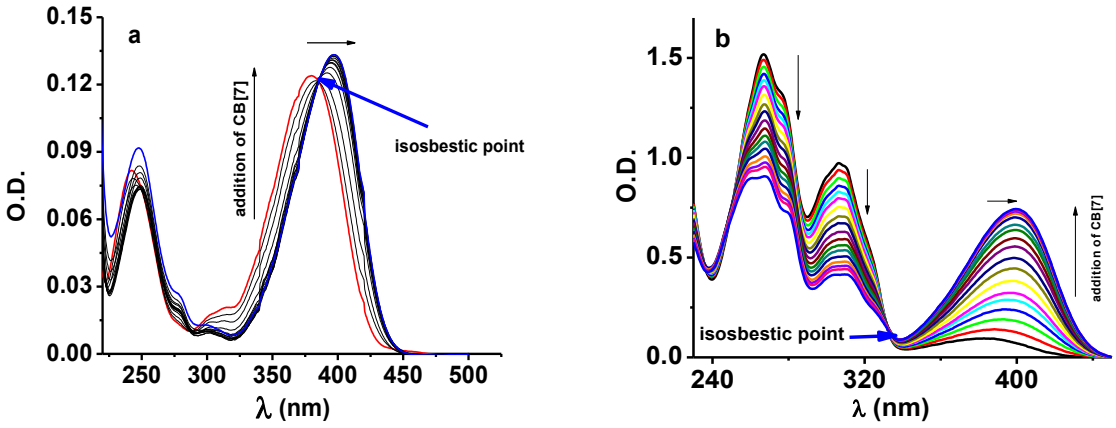

Figure 4.4.2.1: Steady state absorption spectra of (a) dye **59** (9.7µM) and (b) **60** (15.4µM) with increasing concentration of the host **50**

4.4.3 Steady-state fluorescence studies:

Fluorescence spectra of dyes **59** and **60** were also showing different behavior but gave similar red-shifted emission maxima in water (λ_{max} ~ 468 nm) than that in ethanol (λ_{max} ~ 448 nm). The photo-physics of these dyes indicated that their ground and excited electronic states behave quite differently. The larger solvatochromic shift was found in emission (20 nm) in

comparison to absorption (8 nm) spectra of dyes while changing from ethanol to water. This may be associated with the significantly higher dipole moment of the excited state (S_1) in comparison to the ground state (S_0) of dye molecules, which also induced a large Stokes shift of dyes upon electronic excitation. In analogy with its close analogue C311 dye (7-dimethyl amino-4-methylcoumarin), the dipole moment (μ) of dye **59** may increase[130] from 6.0 D (at S_0) to 7.3 D (at S_1). The dye molecule in relatively polar excited state is expected to require higher energy stabilization mediated by a stronger geometrical and solvent relaxation in polar and protic aqueous media than that in ground-state. Emission maxima of dyes in water showed negligible shift upon addition of host CB[7] (**50)**, in contrast to their red-shifted absorption maxima (Figure 4.4.3.1). The cavity of **50** is known[122,131] to have high hydrophobicity, very low polarizability and polarity. The appreciable hydrogen bonding interactions[126,130] between the amine nitrogen, carbonyl oxygen and alkyl groups of the coumarin1 molecules with water would alter upon inclusion of dyes inside the cavity of **50**. Interplay of these interactions might be responsible for observations of bathochromic shift in absorption spectra, but no change in emission transition energy of the dyes in presence of increasing concentration of host **50** in water. Fluorescence intensity of dye **60** in water (at pH 2) was found to possess lower peak intensity than that of the neutral form in water. The dye **60** was excited at two positions, at isosbestic point and near peak maxima 305 nm. With excitation at 305 nm, two fluorescence peaks were observed at 370 nm and 468 nm. However with addition of CB[7] only the fluorescence intensity of peak corresponds to 468 was found to increase (~24 fold) significantly to a similar peak intensity value but with much higher (~20 times) concentration of dye **60**. Whereas, excitation at isosbestic point (at 332 nm) get only single fluorescence peak at 468 nm and found 11 times

enhancement in fluorescence intensity. In both cases of the observed fluorescence spectra of **60** in presence of CB[7] indicated strong binding of the C1-NH^+ (**60**):CB[7] complex.

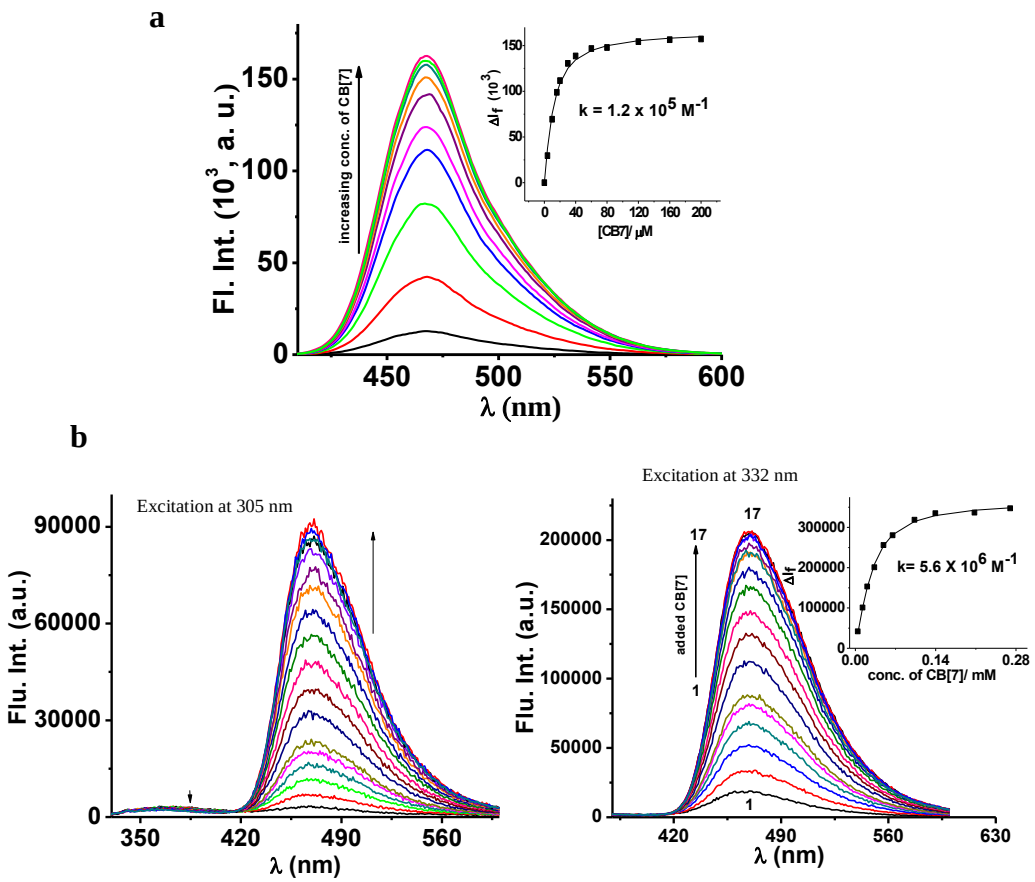

Figure 4.4.3.1: Steady state fluorescence spectra of (a) dye **59** (9.7μM) with increasing concentration of CB[7] (**50)** from 0 to 200 μM and (b) dye **60** (15.4μM) with increasing concentration of CB[7] (**50)** from 0 to 0.3 mM. INSET: The dependence of increase in the fluorescence intensity (ΔI_f) of the dye with addition of **50** in aqueous solution for excitation at isosbestic point. The solid line represents the best fit of the data corresponding to a 1:1 inclusion complex, showing binding constant k = 1.2 x 10^5 $M^{-1}$for dye **59** and k = 5.6 x 10^6 M^{-1} for dye **60**.

Photo-physical properties of dyes **59** and **60** in absence and presence of the host CB[7], are shown in Table 4.4.3.1. The observation of a larger enhancement in maximum fluorescence

intensity (~24 fold) for dye **60** in presence of **50**, which is much higher than that of dye **59** (~ 13 times) with the host **50**, pointed towards a stronger binding of the cationic form (**60**) of the dye with the host **50**. Quantum yields of fluorescence (Φ_f ~ 0.52 for dye **59** and 0.58 for dye **60**) in water, in presence of high concentration of **50**, was calculated and found slightly higher of dye **60** than dye **59** also favor the stronger binding.

Table 4.4.3.1: Photo-physics of dye **59** and **60** in ethanol, water and water with CB[7] (**50)**

Dye (dye:50)	**Solvent**	λ^a_{max} [a] **(nm)**	λ^f_{max} [b] **(nm)**	Φ_f [c]	τ_f [d] **(ns)**	τ_r [e] **(ps)**	k_r [f] **(s^{-1}) 10^8**	k_{nr} [f] **(s^{-1}) 10^8**
59 (1:0)	Ethanol	373	448	0.54	3.09	-	1.75	1.49
59 (1:0)	Water	380	468	0.04	0.4	72	1.17	23.8
59 (1:20)	Water	396.5	468	0.52	5.10	290	1.02	0.94
60 (1:0)	Ethanol	374	447	0.54	3.08	90	1.75	1.49
60 (1:0)	Water	306	468	0.025	0.39	84	0.64	25
60 (1:20)	Water	307.5	468	0.58	5.12	300	1.13	0.82

[a] Error: ± 0.2 nm. [b] Error: ± 0.3 nm. [c] The quantum yield of fluorescence of the dyes **59** and **60** were measured at the excitation wavelength 385 and 332 nm, respectively of **59** in ethanol as standard. [d] Error: ± 0.05 ns. [e] Error: ± 10 ps. [f] The values of k_r and k_{nr} were calculated using the following equations: $k_r = \Phi_f / \tau_f$, $k_{nr} = (1-\Phi_f)/\tau_f$, assuming that the emitting state is produced with unit quantum efficiency

The systematic improvement in fluorescence intensity of dyes in water with addition of **50** may be correlated to confinement of guest dye molecule inside the cavity of **50** and the dominance of hydrophobic effects related to the removal of very high-energy water molecules (eight for **50**)[131] from the cavity. The binding constants of both dyes **59** and **60** with host **50** in

aqueous solutions were determined by nonlinear fitting of increase in fluorescence intensity (ΔI_f) of dye as a function of concentrations of **50** using 1:1 complex formation equation:[81]

$$\Delta I_f = \left(I_{obs} - I^0_{Dye}\right)$$

or

$$\Delta I_f = \left(1 - \frac{[Dye]_{eq}}{[Dye]_0}\right)\left(I^{\infty}_{Dye\bullet 50} - I^0_{Dye}\right)$$

where $[Dye]_0$ and $[\mathbf{50}]_0$ are the initial concentrations of dye and **50**, respectively, $[Dye]_{eq}$ is the concentration of free dye in equilibrium, I^0_{Dye} and $I^{\infty}_{Dye.50}$ are the initial fluorescence intensity of dye in the absence of **50** and at high concentration of **50** (corresponds to complex formation of all the dye molecules), respectively.

Non-linear fitting ($\chi^2 \sim 1$) analysis of the increase in fluorescence intensity of dyes as a function of host concentration yields average equilibrium binding constant (k) to be (1.2 ± 0.2) x 10^5 M^{-1} and (5.6 ± 0.2) x 10^6 M^{-1} for dyes **59** and **60**, respectively (insets of Figures 4.4.3.1a and 4.4.3.1b). These values were measured from two independent experiments for each dye. In the fluorescence titration fitting, the increase in integrated or peak fluorescence intensity was used as experimental data and both gave similar values of binding constant k. The formation of 1:1 Dye:50 complex and values of k for both the dyes were also verified by checking linearity in double reciprocal plot[132] using inverse of changes in observed fluorescence intensity [$1/(I_{obs} - I_f^0)$] with inverse of concentration of host [**50**], 1/[**50**] .

Moreover, to confirm the stoichiometry of the dye-50 complexes, peak fluorescence intensities of aqueous solutions of both dyes were measured by varying mole-fraction concentrations of **50**, while maintaining the total concentrations of dye and **50** constant. The peak emission intensity values of these dye-CB[7] solutions were correlated by the continuous

variation method of Job's plot (Figure 4.4.3.2), which show maxima at a value of 0.5 for [**50**]/ ([**50**] + [dye]), indicating 1:1 binding stoichiometry for both dye:50 complex.

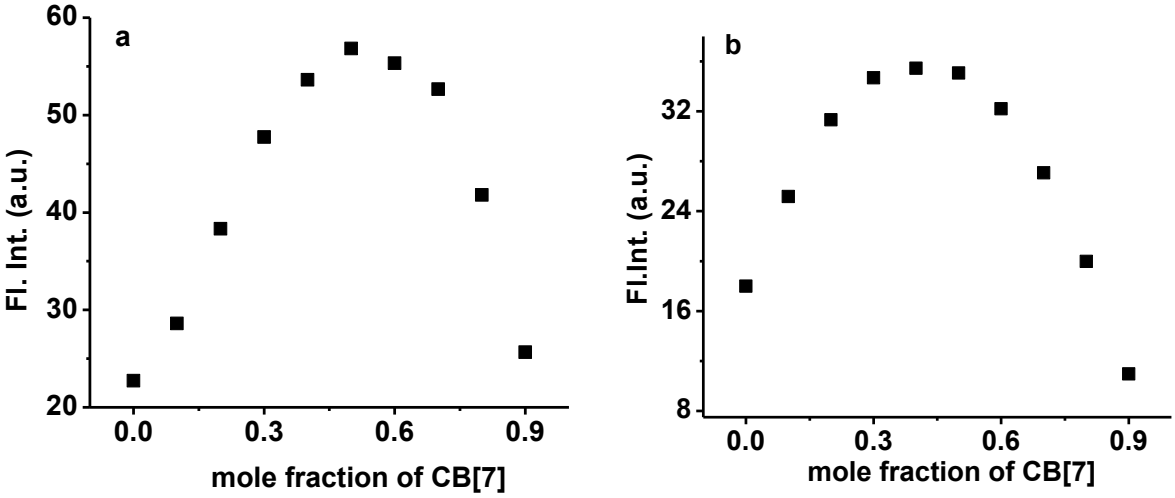

Figure 4.4.3.2: Job's plot of the coumarin1:CB[7] complex (a) dye **59** (b) dye **60**. Symmetric plot with maxima at 0.5 mole fraction indicates the 1:1 inclusion complex formation.

4.4.4 Time-resolved fluorescence studies:

The dynamic equilibrium features of free dye and dye-50 complex formation can be followed by observing the change in fluorescence lifetime (τ_f) of the dye in water with addition of host **50**. The fluorescence decays of both dyes in pure water were found to be mono-exponential in nature, correspond to lifetime 0.4 ns (Table 4.4.3.1). Alternatively, fluorescence decay curves were observed to be mono-exponential and fitted to 100% complex dye with a lifetime τ_f = 5.1 ns at a high concentration of host i.e., at 1:20 molar ratios of dye:50 for both form of dye (Figure 4.4.4.1 for **59**). However, in presence of lower concentrations of host **50**, the dye lifetime decay curves were bi-exponential, consisting of two species, free dye and dye-complex. Thus, for 1:1 molar ratio of dye **59** and host **50**, the life time decay curve was fitted to two components, 19.4% free dye (τ_f = 0.4 ns) and 80.6% dye-50 complex (τ_f = 5.1 ns). Similarly,

on further addition of **50** to this dye at a molar ratio of dye:50=1:5, the decay curve was fitted to 4.2% free dye (τ_f = 0.4 ns) and 95.8% dye-complex (τ_f = 5.1 ns).

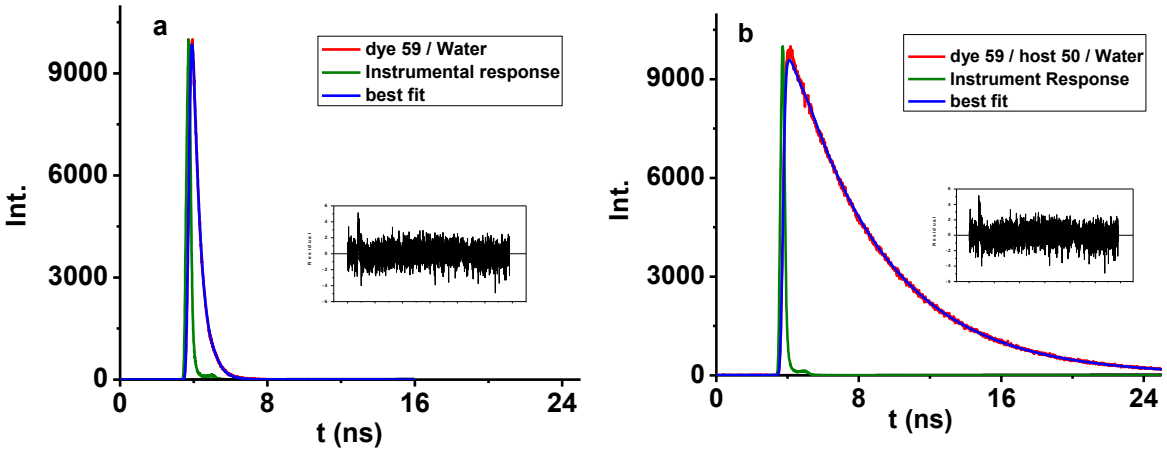

Figure 4.4.4.1: Fluorescence life time decay in aqueous solution of (a) dye **59** is 0.4ns and (b) dye **60** with host **50** (1:20) is 5.12ns. INSET: panels represent the distribution of the weighted residuals for dye **59** and dye **59** with host **50,** respectively.

Increase in fluorescence lifetime (τ_f) of aqueous solutions of dye from 0.4 ns to 5.1 ns upon complexation with host **50** have indicated restricted rotational/vibrational motions of the dye molecule inside the cavity of host **50.** Free rotational/vibrational motions of 7-diethylamine moiety in the excited electronic state of coumarin 1 dye were suggested[124a,129c,133] for dissipation of excitation energy through non-radiative decay process. This is in agreement with our calculated values of radiative rate (k_r) and non-radiative decay rate (k_{nr}) showing a large decrease in k_{nr}, rather than increase in k_r, of both dyes upon complex formation with **50**.

4.4.5 Fluorescence anisotropy studies:

To obtain further insight in the nature of the rotational dynamics of the dye molecules, in absence and presence of the host CB[7] (**50**), fluorescence anisotropy study was carried out for

both the dyes. Time-resolved fluorescence anisotropy measurement was carried out in aqueous solutions of the dyes in absence and presence of high concentration of host **50** (dye:50). These anisotropy decays could be precisely fitted to a single-exponential function indicating existence of either free or complex dye. In contrast, observed anisotropy decay curves for dye solutions with lower concentration of host **50** have supported presence of both species, free and complex dye.

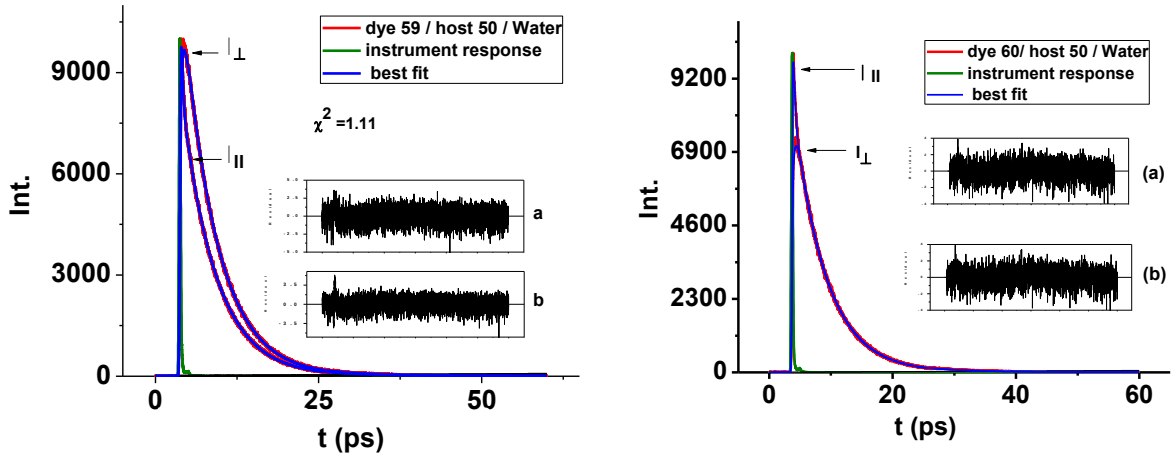

Figure 4.4.5.1: Time resolved anisotropy decay of aqueous solution of dye **59** and **60** (20μM each) containing 20 molar ratio of host **50** at 25^0C. The values of rotational relaxation time (τ_r) were found 290ps for **59** and 300ps for **60**. The (a) and (b) represents the distribution of the weighted residuals for $I_\parallel(t)$ and $I_\perp(t)$, respectively.

The measured value of rotational reorientation time (τ_r) of dye **59** in water was (72±10) ps, which agreed with reported[133] value of (66 ± 6) ps. The τ_r values of dye **60** was measured to be (90±10) ps and (84±10) ps in ethanol and water, respectively. However, the rotational relaxation of dye-complex was found to be considerably slower, and thus reorientation time was evaluated to be much longer for both the dyes, in the presence of host **50**. During formation of 100% dye-complex species, upon addition of high concentration of **50**, the rotational

reorientation times (τ_r) of both the dye-50 complexes were measured to be (290±10) ps and (300±10) ps, for dye **59** (Figure 4.4.5.1a) and **60** (Figure 4.4.5.1b), respectively. The initial anisotropy (r_0) was also estimated to be ~0.33 for both dye-50 complexes. Therefore, evaluation of increased rotational reorientation time of dyes in water (Table 4.4.3.1) from values in the range of 72-84 ps to 290-300 ps with addition of host **50,** endorsed the formation of inclusion complexes of both dye molecules inside the host CB[7] (**50**) cavity.

4.4.6 Temperature dependent fluorescence studies:

The measured fluorescence spectra of dye **59** in ethanol, dye **60** in water and water with host **50** (molar ratio 1:20) in the temperature range 274-302 K were shown in Figures 4.4.6.1 (a), (b) and (c), respectively and the plot of calculated QYF values of dye **60** vs. temperature of dye solutions in all three cases were shown in Figure 4.4.6.2. These results showed sharp reduction in peak fluorescence intensity of the dye in water with increase in temperature.

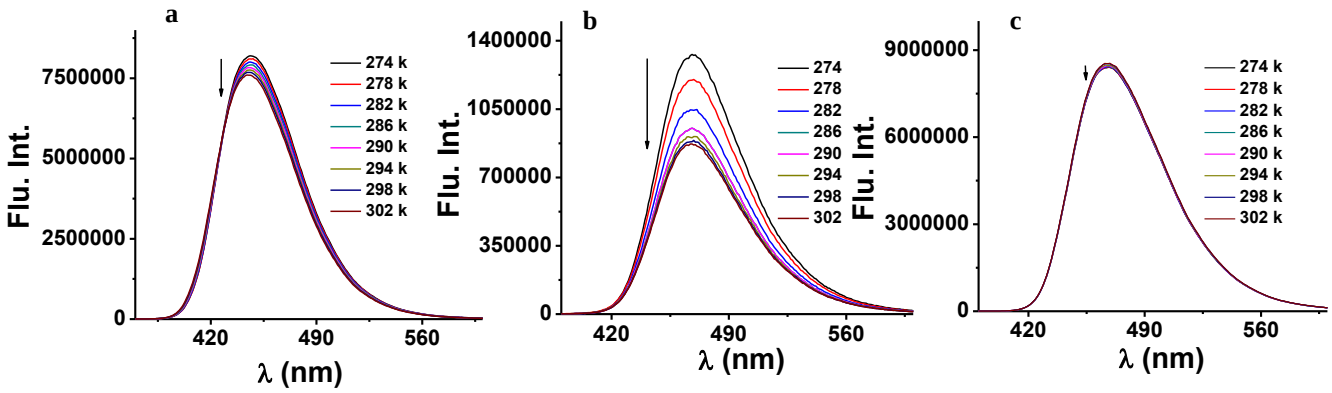

Figure 4.4.6.1: Temperature dependent fluorescence spectra of dye **59** in (a) ethanol, dye **60** in (b) water and (c) water with host **50** at different temperatures in the region 274 K to 302 K

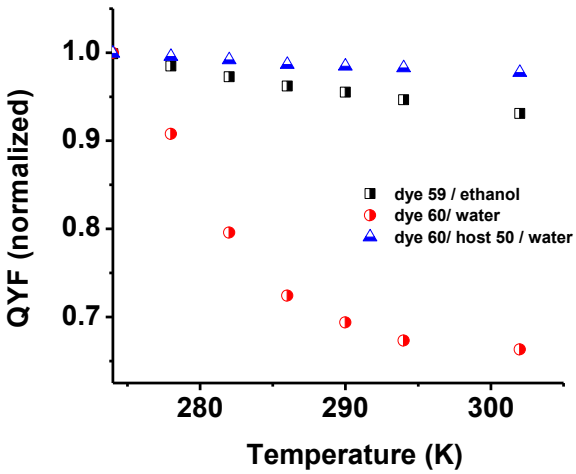

Figures 4.4.6.2: Plots of QYF vs. temperature of dye **59** in ethanol (black), dye **60** in water (red), and dye **60** in water with additive **50** (blue).

However, fluorescence intensity of aqueous solutions of the dye, in presence of the host **50**, was found to be independent of temperature in the region 274 K to 302 K. In the latter case, the fluorescence intensity was found to slightly increase when temperature of dye solution was decreased to 274 K. It has been observed that reduction in fluorescence intensity of dye **60** is more in water ~ 34% than in ethanol (8%) while only 2% reduction in fluorescence intensity was found upon complex formation of dye **60** with **50.** This suggested that the container molecule **50** possess electron rich portals on both sides makes ion dipole interation in addition to hydrophobic interaction with dye **60** molecule through its positively charged diethylamine group ($-N^{+}(C_2H_5)_2$). The formation of supramolecular complex of the dye **60** in presence of the host **50**, may retard the torsional motions of the $-N(C_2H_5)_2$ groups of the dye molecule and hence its rate of non-radiative decay was less at low temperature. Thus, in the latter case, QYF was observed to be almost independent of temperature (Figure 4.4.6.2). Also, similar experiment was performed with dye **59** in water and dye **59** with host **50** (Figures 4.4.6.3 and 4.4.6.4). In

comparison to dye **60**, fluorescence intensity of dye **59** was reduced more, ~ 58% in water and ~6% in water in presence of the host **50** on complex formation from its initial value. This also suggests that both forms of coumarin 1 dyes may have different geometry of binding and that might be the reason for higher binding constant of dye **60** than dye **59** complex with the host **50**. This data also agrees with our observed optical properties and fluorescence binding constant.

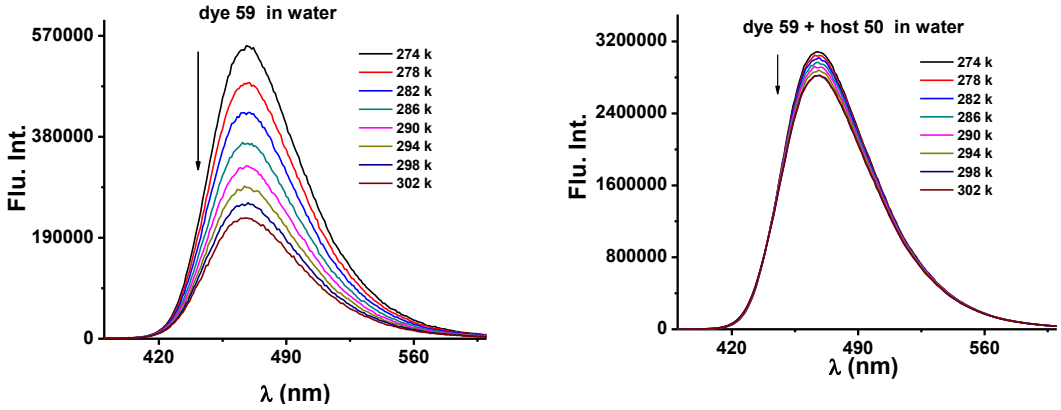

Figure 4.4.6.3: Temperature dependent fluorescence spectra of dye **59** in water in presence and absence of the host **50** at different temperatures in the region 274 K to 302 K

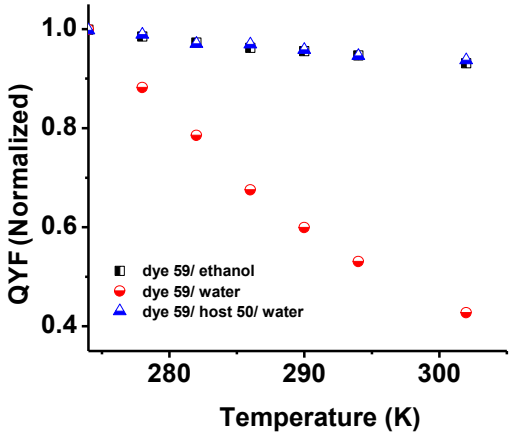

Figures 4.4.6.4: Plots of QYF vs. temperature of dye **59** in ethanol (black), water (red), and water with additive **50** (blue).

4.4.7 Rotational dynamics of dye-complex:

The evolution of rotational relaxation dynamics of the fluorescent dyes **59** and **60** and its supramolecular complexes with host **50** in aqueous solutions can be understood by calculating the frictional forces experienced by the molecules, in concurrence with experimentally measured rotational reorientation time. According to the Stokes-Einstein-Debye (SED) hydrodynamic theory, the molecular orientation is a diffusive process and expresses the dye rotational reorientation time (τ_r) as a function of the hydrodynamic volume (V) of the probe dye molecule and macroscopic solvent characteristics, temperature (T) and viscosity (η), and is expressed for a spherical probe molecule by equation:

$$\tau_r = (V\eta/k_BT) \qquad (1)$$

where k_B is the Boltzmann constant. This equation (1) is modified for axi-symmetrical ellipsoidal probes and also to account for different types of solute-solvent interactions, and is given by[133]

$$\tau_r = (V\eta/k_BT)\, f(\rho)C(\rho) + \tau_r^0 \qquad (2)$$

where $f(\rho)$ is the shape factor of the ellipsoidal shape probe, $C(\rho)$ describes the solute-solvent friction and its value depends on the boundary condition of the probe and solvent system, and τ_r^0, a very small term, is identified with free rotation of the probe molecule at solvent of negligible viscosity. The ellipsoidal shape is defined by the ratio ρ of the longitudinal radii to the average equatorial radii and accordingly the f values are calculated.[134] Depending on the probe-solvent friction, boundary condition can be either of 'stick' or 'slip' type. The stick type hydrodynamic condition is applicable in this case since the size of the probe is much larger than the solvent molecules.

The dye molecules **59** and **60** may be considered as close to an oblate ellipsoid. In order to evaluate the shape factor f(ρ) and the friction coefficient C(ρ) for dye probe, a good estimation of ρ, the ratio of the shorter and the longer semi-axes, is needed. The optimization of ground state geometry of coumarin 1 molecule was carried out recently by T. Gustavsson *et al*,[133] and those reported dimensions are considered for calculation of τ_r. The three radii of molecule were reported as 6.35 Å, 4.55 Å and 1.9 Å. Thus, hydrodynamic volume of coumarin 1 dye molecule is calculated as $V = 23 \times 10^{-29}$ m^3. For the shorter radii we have considered the value 1.9 Å, but for the longer radii we have taken average of the two values (6.35 Å, 4.55 Å) to obtain value 5.45 Å. Thus value of ρ is calculated as 1.9/5.45 = 0.35. For an oblate ellipsoid with ρ = 0.35, we find[134] the two f values 1.42 and 1.63 for the symmetry axis and in-plane axis, respectively. The average of these two f values is f(ρ) = 1.52. The viscosity of water at working temperature (T=298 K) is taken as $\eta = 0.8903 \times 10^{-3}$ Pa-s. Considering 'stick' hydrodynamic boundary condition and the values of C(ρ)=1.0, $\tau_r^0 = 0$ and η (at 298 K) = 0.8903×10^{-3} Pa-s in water, τ_r value of coumarin1 is calculated using equation (2) as τ_r = 75.7 ps. This calculated value of τ_r was found to be in good agreement with our experimentally measured values (72 to 84 ps) for both dye **59** and **60** in water. Similarly, τ_r value of dye in ethanol, which possess higher viscosity (1.04×10^{-3} Pa-s) than water, is calculated to be τ_r = 88.4 ps, close to experimentally measured value 90 ps.

The accuracy in estimation of τ_r value of dye-50 complex depends on evaluation of its hydrodynamic volume (V). The calculated structure of host **50** (Figure 4.4.8.1) is quite symmetric having outer cavity diameter of ~16 Å and height of ~9 Å, which agree closely with the reported[41] values. The cavity diameter of dye-50 complex was estimated by quantum chemical calculation, which gave radii of the complex, r ~ 7.3 Å. Volume of this inclusion

complex of host **50** and dye **60** is also calculated considering the volume inside a contour of 0.001 electrons/Bohr^3 density, which gave volume, V = 1630 x 10^{-30} m^3 assuming it close to spheroid. Thus, the value of rotational reorientation time (τ_r) of dye-50 complex was calculated to be ~353 ps (using equation 1), slightly larger (by ~18%) than our experimentally measured value of τ_r=300 ps (Table 4.4.2.1). It may be noted that hydrogen bonding interactions of the outer cavity of host **50** with bulk water molecules may provide additional frictional force to the complex, which was not taken into account for this calculation of τ_r. This would reduce the gap in calculated and experimentally measured values of τ_r. Hence, a close agreement in experimentally measured value of τ_r with the calculated value for dye-50 complex, while considering inclusion of dyes **59** and **60** inside host **50** cavity, have confirmed the tighter binding and rotation of whole dye-50 complex as a single entity.

4.4.8 ^{1}H NMR study:

^{1}H NMR spectra of free dye **59** and **60** as well as dye-50 complex in presence of host **50** at 1:2 molar ratio provide interesting and useful information on the macroscopic location of the guest inside the inner cavity of host. A large up-field shifts and broadening of aromatic protons 6, 8 and aliphatic protons 9, 10 labeled as in Figure 4.4.8.1, while down field shifts of 3 and 5 labeled protons suggested that amino moiety might be inside the host cavity for dye **59**. However, in case of dye **60,** all aromatic and aliphatic protons show up field shift except proton 10, which shows down field shift, were observed. This suggested that whole aromatic part of the dye **60** was inside the cavity and cationic N-atom make ion-dipole interaction with carbonyl portals of host **50**.

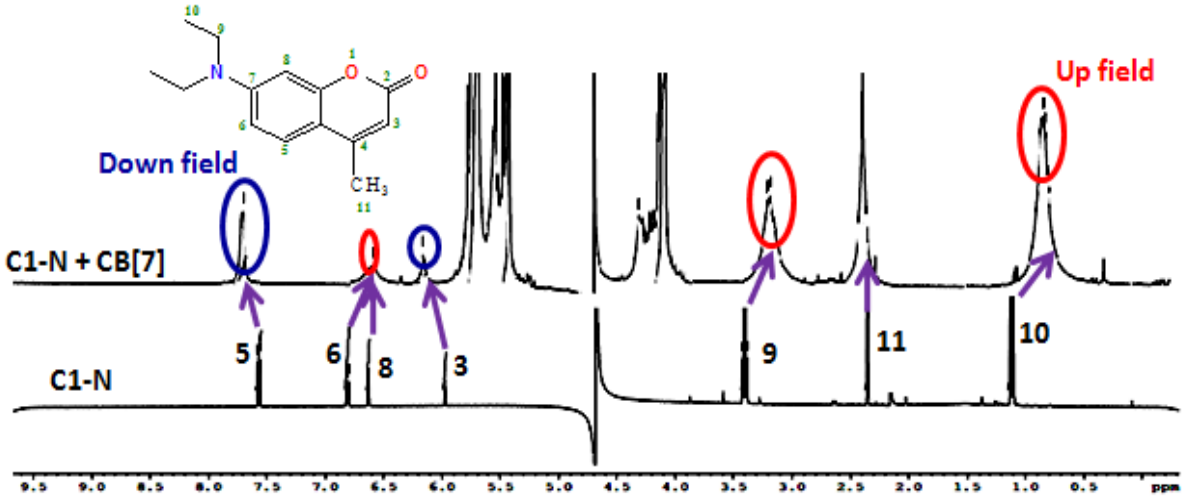

Figure 4.4.8.1: ^{1}H NMR spectra of dye **59 (C1-N)** (taken at a fixed concentration) with 1:2 ratio concentration of host **50** in D_2O

These results clearly indicate that both dye molecules **59** and **60** have different geometry of host-guest complex depending on their location inside the cavity of host **50**. The comparative ^{1}H NMR spectra of both dyes **59** and **60**, in absence and presence of 2 times higher concentrations of host **50**, are shown in Figures 4.4.8.1 and 4.4.8.2. Interestingly, no separate resonances were observed for free and bound dye protons of positively charged N-diethyl amine group, in all the ^{1}H NMR spectra at different concentrations of **50**. This was in contrast to NMR titration spectra of rhodamine B and sulphorhodamine B dyes with the host **50**, in which two separate peaks for each methyl and methylene hydrogens of N-diethyl amine group were observed.[35a, 123]

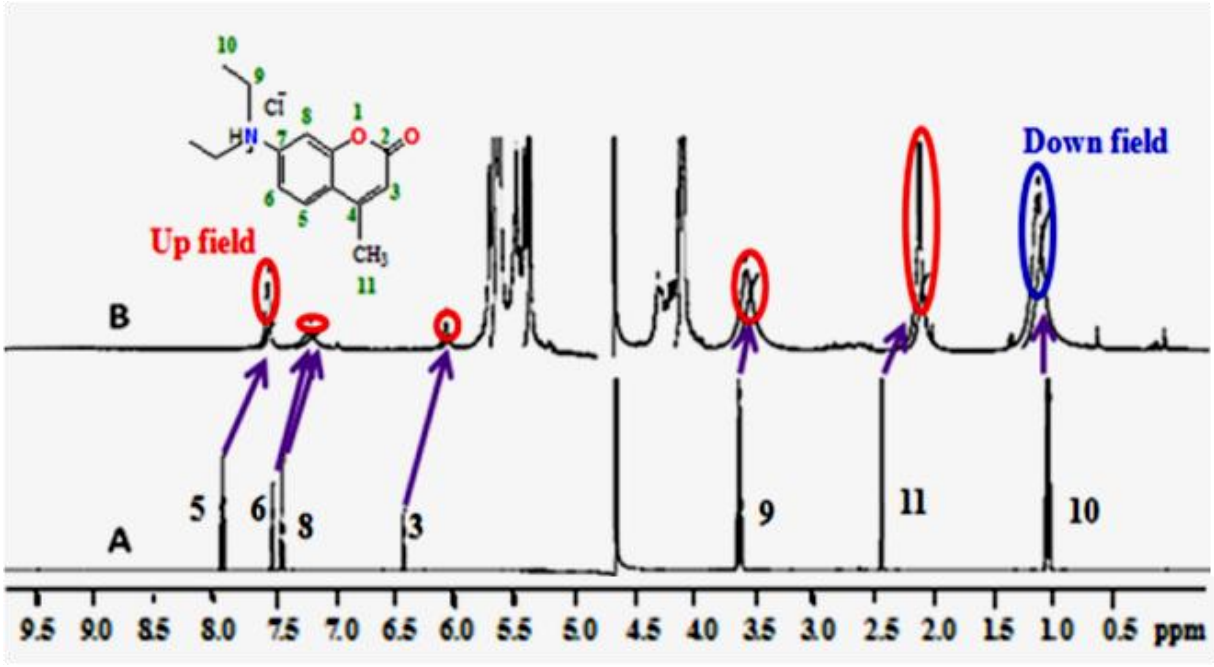

Figure 4.4.8.2: ^{1}H NMR spectra of dye **60** (taken at a fixed concentration) with 1:2 ratio concentration of host **50** in D_2O. (A) dye **60**, and (B) dye **60** with 2 eq. **50**.

However, the structures of rhodamine dyes contain two N-diethyl amine groups, one at each end of the chromophore, but dye **59** and **60** have only one group. The observations of broadening of all dye-proton resonance peaks and absence of separate resonances for free and bound guest protons indicated the association-dissociation process between dye molecule and host **50** took place at intermediate to fast exchange rate on a timescale determined by ^{1}H NMR chemical shift splitting.

4.4.9 Structure and stability of dye complex:

The minimum energy ground-state molecular structures of the dye molecules, complex of neutral (**59**) and cationic (**60**) forms of the dye and host **50** was determined applying B97D/cc-pVDZ level of theory. This particular DFT functional takes care of long range dispersion correction.[135] Dispersion effect is expected to play an important role in shaping the structure of

such host-guest complex producing realistic binding energy. Initially, structures of the **59**, **60** and **50** molecules were calculated (Figure 4.4.9.1).The calculated geometry of **50** was quite symmetric having outer cavity diameter of ~16 Å and height of ~9 Å. The cavity diameter was calculated based on the circle formed by 7 oxygen atoms at one end of the host. The length and width of the dye **59** molecule were calculated as ~ 12 Å and ~9 Å, respectively.

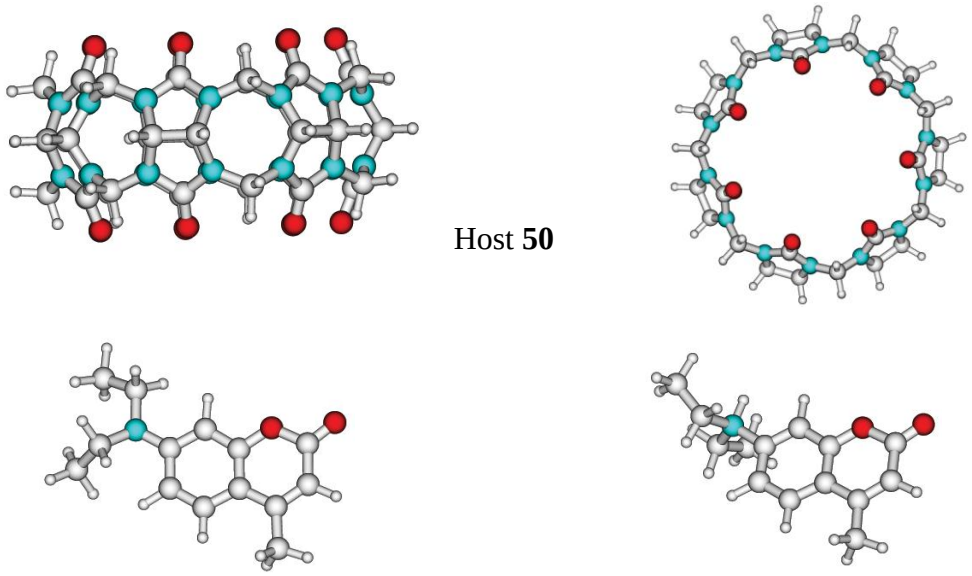

Figure 4.4.9.1: Optimized ground state structures of dyes (**59** and **60**) and host **50** (in two views) calculated applying B97D/cc-pVDZ level of theory. Colour codes: **red** for O atoms, **blue** for N atoms and out of rest, smaller balls are for H atoms and larger balls are for C atoms.

This suggested that the dye molecule can enter host cavity from any one of the longitudinal ends. Different initial structures were considered keeping two different ends of dye molecules inside the cavity of the host to locate the minimum energy structures of host-guest complexes. Three minimum energy host-guest structures were obtained for both neutral and charged guest dye molecule with host **50**. The calculated binding energy for the most stable host-guest complex of dye **60** and host **50** was calculated as -91.1 kcal/mol, which was more than two

times compared to the neutral guest, dye **59** (-44.7 kcal/mol) and host **50** for their most stable structure at the present level of theory. The most stable structure of complex of dye **59** showed that dye molecule makes hydrophobic interaction via diethyl amino moiety which goes inside the cavity and remaining (aromatic part) still outside the cavity. While dye **60** with host **50** showed stronger complex in which whole aromatic part inside the cavity with hydrophobic interaction and amino moiety near to portals having ion-dipole interaction due to charged species is shown in Figure 4.4.9.2 and 4.4.9.3, respectively with two different views.

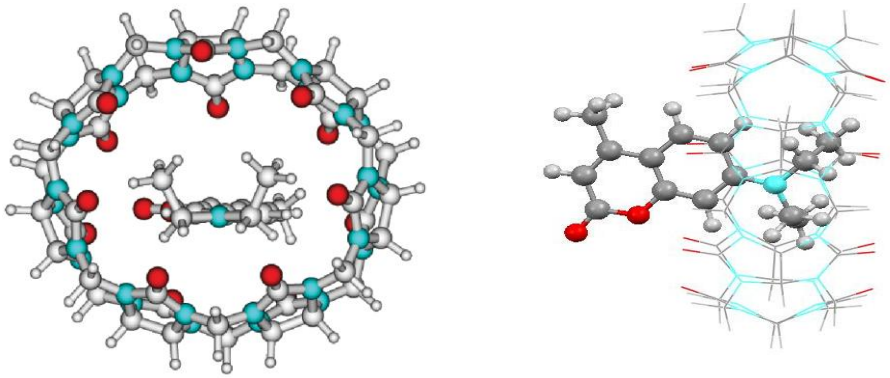

Figure 4.4.9.2: Optimized ground state structures of host-guest complexes of dye **59** with host **50** calculated applying B97D/cc-pVDZ level of theory. Colour codes: **red** for O atoms, **blue** for N atoms and out of rest, smaller balls are for H atoms and larger balls are for C atoms

Calculations of various components of total interaction energy of host-guest complexes for both the neutral and cationic dyes were carried out using Kitaura-Morokuma energy decomposition analysis.[127] The energy decomposition analysis of complexes of dye **59** and **60** with host **50** (Table 4.4.9.1) revealed that electrostatic interaction energy component provided substantially higher stability to dye **60** (-75.71 kcal/mole) than that to dye **59** (-15.36 kcal/mole).

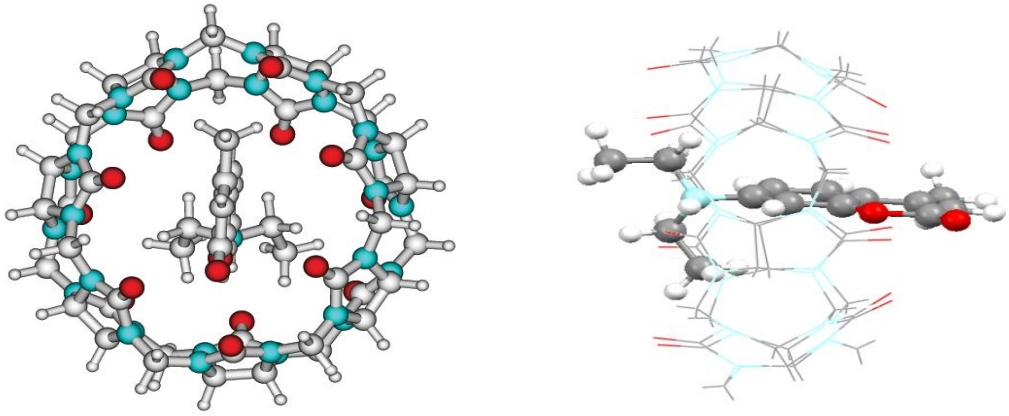

Figure 4.4.9.3: Optimized ground state structures of host-guest complexes of dye **60** with host **50** calculated applying B97D/cc-pVDZ level of theory. Colour codes: **red** for O atoms, **blue** for N atoms and out of rest, smaller balls are for H atoms and larger balls are for C atoms

Other interaction components of smaller energy, viz., polarization and charge transfer energy provided more stability to dye **60**. However, the important instability component toward formation of host-guest complex, exchange repulsion energy was found to be higher with dye **60** (+28.31 kcal/mole) in comparison with dye **59** (+18.89 kcal/mole). The calculation of total interaction energy of dye-50 complexes suggested higher stability with dye **60** (-73.24 kcal/mole) than that with dye **59** (-11.68 kcal/mole). This was supported by our experimentally measured values on binding constants of dye-50 complexes using fluorescence titration analysis, revealing higher binding constant of dye **60** (k= 5.6 x 10^6 M^{-1}) than that of dye **59** (k= 1.2 x 10^5 M^{-1}). The calculated structures of dye-50 complexes agreed broadly with inclusion geometry predicted by analysis of experimentally observed ^{1}H NMR spectra of free and complex dye.

Table 4.4.9.1: Decomposition analysis of interaction energy of complexes of dye **59** and **60** with host **50** applying HF/6-31G (d) level of theory

Interaction Components	**Dye 59** **kcal/mole**	**Dye 60** **kcal/mole**
Electrostatic energy (ES)	-15.36	-75.71
Exchange repulsion energy (EX)	18.89	28.31
Polarization energy (PL)	-2.67 -2.26 -0.78 Total = -5.71	-2.28 -9.40 -0.57 Total = -12.25
Charge transfer energy (CT)	-3.63 -5.82 Total = -9.45	-3.10 -11.04 Total = -14.15
High order coupling energy (MIX)	-0.05	0.55
Total interaction energy	**-11.68**	**-73.24**

4.4.10 Laser Photostability:

Laser photostability (inverse of quantum yield of photo-degradation, $1/\Phi_{pd}$) of dye **60** has been studied in presence and absence of host **50** using the third harmonic of Nd:YAG laser (at 355 nm). Each solution was irradiated for 30 min. Host-guest complex was studied by addition of 2 times higher concentration of host **50** with respect to the dye while keeping similar input power. Since dye **59** has very low solubility (<60μM) in water and thus almost transparent with exposure of pump laser, it could not be used for laser stability study.

Table 4.4.10.1: Photo-degradation rate of free and complexes of dyes **59** and **60** in ethanol and water using third harmonic of Nd:YAG laser (at 355nm)

Dye **dye:50**	**59** (1 : 0)	**60** (1 : 0)	**60** (1 : 0)	**60** (1 : 2)
Solvent	Ethanol	Ethanol	Water	Water
Φ_{pd} **(10^{-3})**	2.9	2.5	3.14	1.58

Pump laser: 10Hz repetition rate and 6ns pulse width.

The photo-degradation rate (Φ_{pd}) was observed to increase for dye **60** in water than that in ethanol. However, in presence of host **50**, photo-degradation rate was 2 times lower. Quantum yield of photo-degradation (Φ_{pd}) was calculated by using equation Φ_{pd} = N/P, where N= no. of dye molecules degraded and P = no. of photon absorbed and these are listed in Table 4.4.10.1.

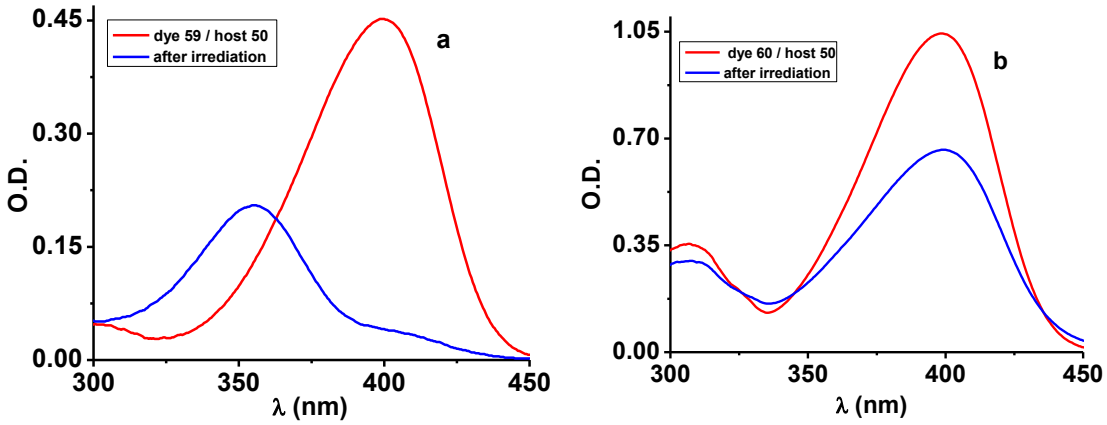

Figure 4.4.10.1: Absorption spectra of complex with host **50** before (red) and after irradiation (blue) of 30 min. (a) dye **59** and (b) dye **60** in water

Interestingly, in case of dye **59** with host **50** complex, the absorption peak maxima was observed to be blue shifted (Figure 4.4.10.1a) while there was no shift in peak maxima of absorption of dye **60** in complexed form (Figure 4.4.10.1b). This indicated fast degradation of

the aqueous solution of neutral coumarin1 dye in presence of the host CB[7] and formation of new fragmented molecule upon exposure to laser. These interesting observations were not analysed further.

4.5 Conclusion:

In comparison to neutral form (**59**) of coumarin 1 dye, its hydrochloride salt (**60**) showed stronger binding with host **50** in water. ^{1}H NMR, fluorescence titration, Job's plot and fluorescence anisotropy studies revealed the formation of 1:1 dye-50 inclusion complex. The poor fluorescence yield of the coumarin 1 dye in aqueous solutions was improved strongly (24 fold), which was higher than dye **59** (13 fold) in presence of the host **50** and yielded binding constant k to be 5.6 x 10^{6} M^{-1}, also one order higher than dye **59** (1.2 x 10^{5} M^{-1}). Laser photostability was also enhanced by ~ 2 times indicating higher photostability and low rate of degradation in water was 1.58 x 10^{-3} of dye **60** with host **50**. The geometry of both dyes was estimated by DFT and ^{1}H NMR study and showed in contrast to dye **59**, the dye **60** remains at the centre of the host **50** cavity keeping almost equal part of it at the both end, outside the cavity of the host. The binding energy of the complexed dye **60** is found to be -91.1 kcal/mol, which is about two times higher than that in case of complex of dye **59**. These results may lead to the promising applications of water based coumarin 1 dyes as a sensitive and efficient fluorescent probe in chemical and biological studies and in aqueous dye laser area.

In this chapter, host-guest study of coumarin 1 i.e. blue emitting UV dye has been performed. The same strategy of host-guest complex formation of new BODIPY dyes in visible region with the host CB[7] has been focused in next chapter.

CHAPTER 5

HOST-GUEST INTERACTION STUDY OF WATER SOLUBLE BODIPY DYES

Chapter 5: Table of Contents

5.1 Introduction:

In continuation of previous chapter there has been a great interest in the development of water soluble laser dyes in green-yellow region because of the superior thermo optical properties and the excellent safety factor associated with water over organic solvent for high power and high repetition rate dye lasers.[136] But the potential drawback with organic dyes in water is their tendency to aggregate,[137] which include multichromophoric interaction that alter the color quality and quench the fluorescence. In principal these problem can be attenuated by supramolecular encapsulation strategy that isolate individual dye molecules and prevent self aggregations or similar interaction with chemical environment. Macro-cyclic host have the potential to increase the solubility of poorly soluble or insoluble guest molecules by forming inclusion complex.[125c,138,139] The possibility to form complexes with chromophoric guest molecules[140] and their by improve their fluorescence properties[141] remains an important application area of supramolecular chemistry.[1b] There are several known dyes in green-yellow spectral region. Among them relatively recent Bodipy dyes are the most attracting dyes for laser study due to its good photostability, low triplet-triplet extinction coefficient and low inter system crossing rate.[13,14,97] However, Bodipy dyes, except PM556, have very low solubility in water. A few water soluble Bodipy dyes have been reported recently, but their host-guest interaction study is rarely reported.

Host-guest supramolecular system is ideal platform to control photo-physical and photochemical properties of organic dyes and their interaction with biomolecules. It is well known that the weak intermolecular forces (electrostatic interaction, hydrophobic interaction, hydrogen binding, vender Waals forces, donor-acceptor interaction) are of primary importance in supramolecular host-guest chemistry.[142] The selected host molecule in the present study are

cucurbit[7]uril. The cucurbit[7]urils are pumpkin shaped, highly symmetrical and rigid molecules with an extremely nonpolarizable cavity.[143] They are capable of forming strong complexes with positively charged molecules by coordination of cationic sites with their portals and /or immersing organic residues in their hydrophobic cavities.[42a,47]

Previously it has been reported that introduction of ionic hydrophilic groups[13c,144] (carboxylic acid, phosphonic acid, sulphonic acid and ammonium salt) on Bodipy core increases solubility of Bodipys in water. But still these new dyes gave a small Stokes shift. Compare to other known Bodipy molecules, dye **17** where 2, and 6 positions have bulky t-butyl group facilitating larger Stokes shift and more photostability.[102d,145] In this context, we report here our attempts to design new congeners of Bodipy dyes with t-butyl nitrogen atom instead of t-butyl carbon atom at 2 or 6 positions via formation of two different ammonium salts (dye **63** and **64**) to improve its important characteristics such as solubility in water as well as larger Stokes shift and fluorescence intensity via host-guest interaction study. Moreover, we have carried out study of dye **64** using calf thymas DNA in phosphate buffer at pH 7.4.

5.2 Experimental:

5.2.1 Synthesis:

4,4-Difluoro-1,3,5,7,8-pentamethyl-2-nitro-4-bora-3*a*,4*a*-diaza-*s*-indecene (61): To cooled (0^oC) HNO_3 (8.5 ml, 42%) was added dye **18** (100 mg, 0.38 mmol), and the resulting orange mixture stirred at 0^oC for 1.5 h. After that the mixture was filtered, washed with H_2O (4 × 10 ml) and dried under vacuo. Then the column chromatography of the residue (silica gel, hexane/EtOAc) furnished **61**. Yield: 95 mg (81.5%); orange needles ($CHCl_3$/hexane); Mp: 250°C; IR (KBr): 1338, 1481, 1531, 1568 cm^{-1}; ^1H NMR (200 MHz, $CDCl_3$, 25^oC, TMS): δ =

2.49 (s, 3H), 2.59 (s, 3H), 2.70 (s, 3H), 2.71 (s, 3H), 2.80 (s, 3H), 6.29 ppm (s, 1H); ^{13}C NMR (50 MHz, $CDCl_3$, 25^{o}C, TMS): δ = 14.1, 14.3, 15.1, 17.6, 18.0, 125.2, 132.0, 136.0, 143.7, 146.8, 147.6, 162.5 ppm; EI-MS *m/z* (%): 307.1 (26) $[M]^+$, 308.1 (100) $[M + 1]^+$; elemental analysis calculated (%) for $C_{14}H_{16}N_3BF_2O_2$: C 54.75, H 5.25, N 13.68; found: C 54.35, H 5.12, N 13.77.

2-Amino-4,4-difluoro-1,3,5,7,8-pentamethyl-4-bora-3*a*,4a-diaza-*s*-indecene (62): To a solution of **61** (0.33 mmol) in methanol (20 ml) were added HCO_2NH_4 (0.33 mmol) and Zn-dust (0.33 mmol), and the mixture stirred for 10 min when the orange solution turned dark pink. The reaction mixture was eluted through cellite, the eluate concentrated in vacuo, and the residue column chromatographed (basic alumina, hexane/ EtOAc) to furnish **62** as brown solids. Yield: 72 mg (80%); Mp: >300°C; IR (KBr): 1492, 1562, 2965, 3368, 3448 cm^{-1}; ^{1}H NMR (200 MHz, CD_3OD, 25^{o}C, TMS): δ = 2.28 (s, 3H), 2.38 (s, 6H), 2.43 (s, 3H), 2.59 (s, 3H), 5.96 ppm (s, 1H); ^{13}C NMR (50 MHz, $CDCl_3$, 25^{o}C, TMS): δ = 12.7, 14.1, 16.4, 17.0, 17.6, 119.6, 125.2, 128.4, 130.8, 138.1, 139.1 ppm; EI-MS: *m/z* (%): 277.2 (100) $[M]^+$, 278.2 (84) $[M+1]^+$. elemental analysis calculated (%) for $C_{14}H_{18}N_3BF_2$: C 60.68, H 6.55, N 15.16; found: C 60.93, H 6.56, N 14.90.

Compound 63: To a solution of **62** (28.7 mmol) in dry DCM (60 ml) were added HCl gas from a mixture of sulfuric acid and HCl solution and stirred for 10 h till the coloured solution turned precipitated. The reaction mixture was washed with DCM and dried in vacuo. The residue furnish **63** as brown solids. Yield: 60 mg (60%); ^{1}H NMR (200 MHz, CD_3OD, 25^{o}C, TMS): δ = 2.45 (s, 3H), 2.50 (s, 9H), 2.70 (s, 3H), 6.30 (s, 1H); Mp: >300°C; ^{13}C NMR could not be possible due to low solubility.

Compound 64: A mixture of **62** (100 mg, 0.36 mmol) and MeI (5 ml) in a sealed tube was heated at 40^{o}C for 3 d. Excess MeI was removed under vacuo and the residue purified by column chromatography (C-18 silica gel, methanol) to obtain **64**. Yield: 42 mg (26%); Mp: >300°C; IR (KBr): 1417, 1431, 2832, 2941 cm^{-1}; ^{1}H NMR (300 MHz, $(CD_3)_2SO$, 25^{o}C, TMS): δ = 2.49 (s, 6H), 2.66 (s, 3H), 2.71 (s, 3H), 2.76 (s, 3H), 3.69 (s, 9H), 6.51 ppm (s, 1H); ^{13}C NMR (125 MHz, $(CD_3)_2SO$, 25^{o}C, TMS): δ = 16.4, 16.7, 17.9, 18.6, 58.5, 125.0, 129.0, 129.4, 134.2, 134.9, 139.3, 145.1, 147.3, 160.8 ppm; EI-MS: *m/z* (%): 447.2 (100) $[M]^{+}$. elemental analysis calculated (%) for $C_{17}H_{25}BF_2IN_3$: C 45.67; H 5.64; N 9.40; found: C 45.35; H 5.87; N 9.23.

5.2.2 Theoretical calculations:

The theoretical calculations were performed using the GAMESS[78] electronic structure program with the standard 6-31G* basis sets for all the atoms. The density functional theory (DFT) with B3LYP[75,76,146] exchange correlation functional has been employed for the optimization of the structures. No symmetry constraint has been imposed to obtain the optimized structures of the molecules, considered in this work. The excited states calculations were carried out using time-dependent variants of DFT (TDDFT).[147] For the structural optimization, polarizable continuum model[148] has been used to include the effect of solvent (methanol).

5.2.3 Gel electrophoresis:

A mixture of 2.4 µl of supercoiled pBR322 DNA in separate as well as with 3 µl and 6 µl of each stock solution of dye **64** (0.2 mM in D_2O and H_2O) and remaining 17.6, 14.6 and 11.6 µl PBS (pH 7.4) solution of D_2O and H_2O was added to make total solution of 20 µl. Out of which half of the solution mixture of each sample were irradiated under an white light intensity of 0.77 mW /cm^{2}of for 1h. After that, 2 µl of gel loading buffer was added to irradiated and dark solution and mixed well. Now 2 µl of each solution of irradiated and kept in dark for 1h was

subjected to agarose gel (1%) electrophoresis (Tris/acetic acid/EDTA buffer, pH 8.0) at 80 V for about 1.5 h. The gel was stained with mg/l EB for 30 min., and then analyzed with a Gel Doc XR system (Bio-Rad).The same experiment was performed of dye **64** with reactive oxygen species (ROS) scavenger NaN_3 in absence and presence of light.

5.3 Results and discussion:

5.3.1 Synthesis:

Both BODIPY dyes were synthesized starting from unsubstituted PM546 (**18**). Reaction started with controlled nitration of starting reactant dye **18** using dilute nitric acid (45%) to obtain 2-nitro Bodipy (**61**). Presence of singlet of one proton instead of two at delta 6.29 in proton NMR and peak at 1388 cm^{-1} in IR spectra corresponds to nitro group confirmed the formation of dye **61** as shown in Figure 5.3.1.1a-b. Followed by catalytic hydrogenation transfer of dye **61** afford amino dye **62** (Scheme 5.3.1.1).

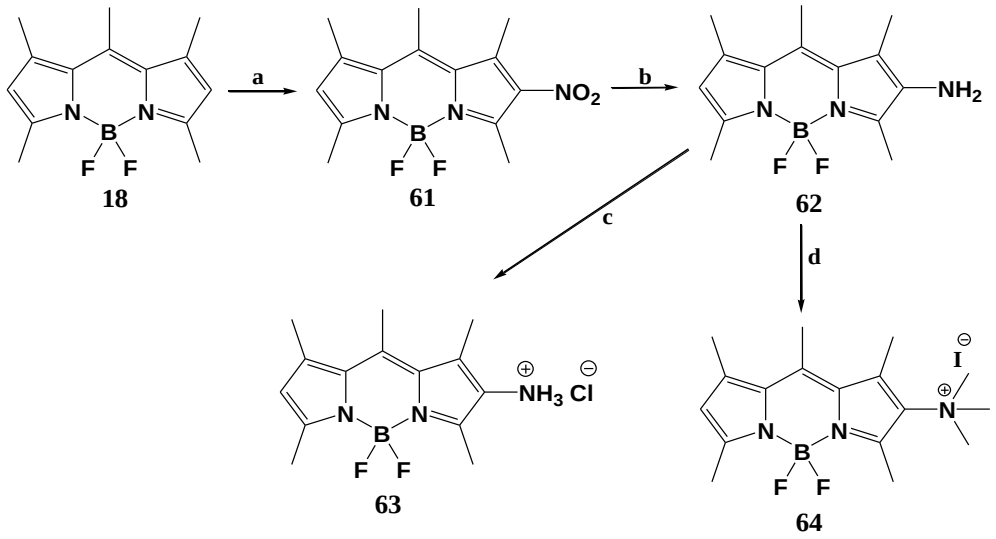

Scheme 5.3.1.1: Synthesis of dyes **63** and **64** (a) HNO_3, 0^oC, 1.5 h; (b) HCO_2NH_4, Zn-dust, MeOH, 25^oC, 10 min; (c) HCl, DCM 10 h; (d) MeI, 40^oC, 3 days

Two bands at 3368, 3448 cm^{-1} corresponds to primary amino functional group due to N-H stretching in IR spectrum gives identification of formation of **62**. From dye **62** two separate reactions were allowed to take place. One by passing HCl gas into solution of amino dye **62** followed by washing with dry DCM to make quaternary ammonium HCl salt (dye **63**). ^{1}H NMR predicted downfield shift (Figure 5.3.1.2) for all protons in comparison to its precursor amine dye **62** after HCl addition reaction indicate the formation of cationic form which leads to electron deficient and more deshielded than dye **62** confirms the formation of dye **63**. In another reaction trimethyl ammonium iodide salt (dye **64**) was synthesized by N-alkylation of dye **62** with methyl iodide. In ^{1}H NMR, formation of new singlet of 9 -CH_3 protons at δ 3.69 in addition of all characteristics peak of **63** (Figure 5.3.1.3a-b) confirmed the formation of dye **64**. However host **50** was synthesized according to reported procedure.[43,44] Purity of the synthesized compounds was checked by ^{1}H/ ^{13}C NMR, mass spectroscopy.

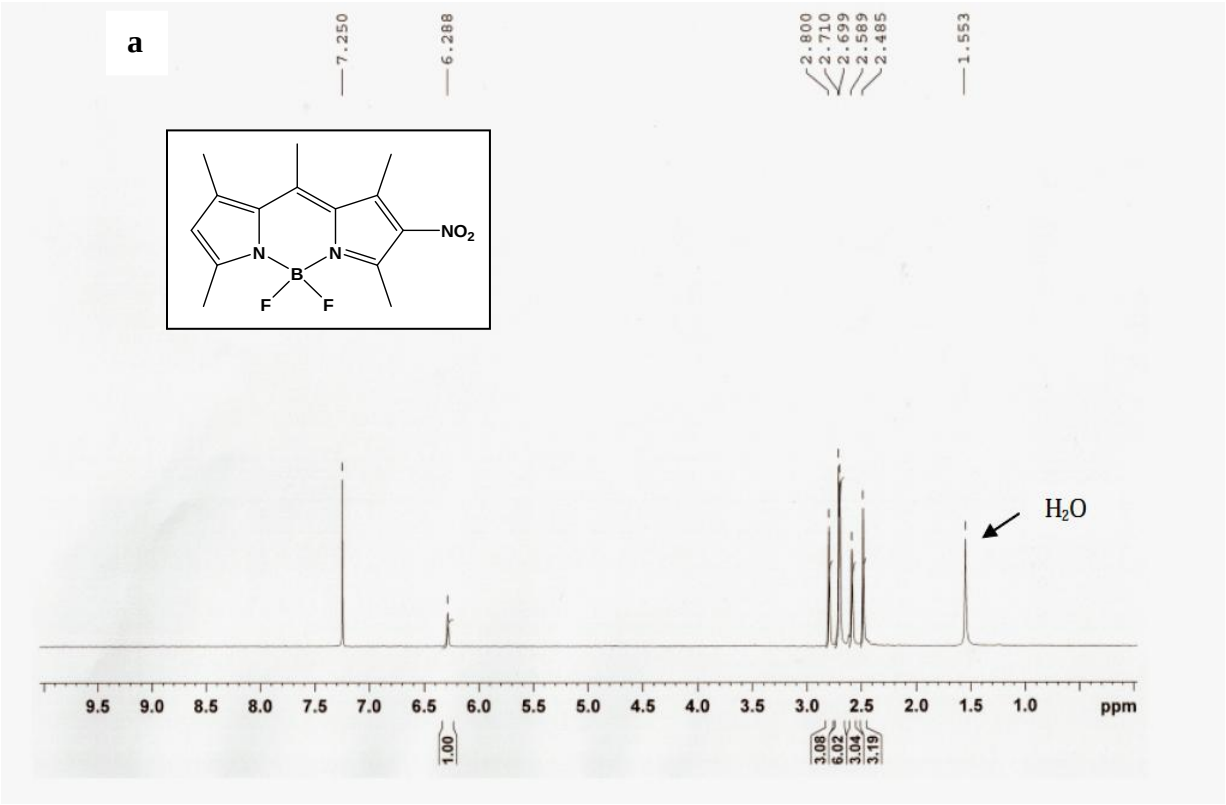

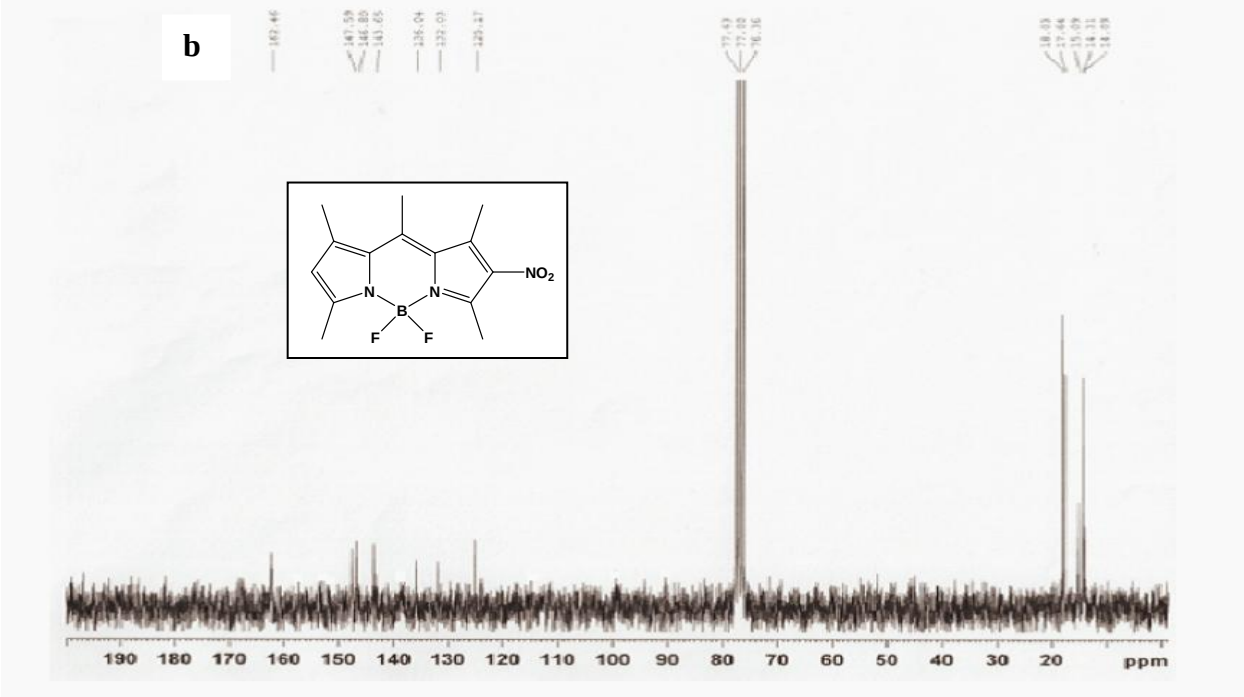

Figure 5.3.1.1: Dye **61** (a) ^{1}H NMR spectrum (b) ^{13}C NMR spectrum

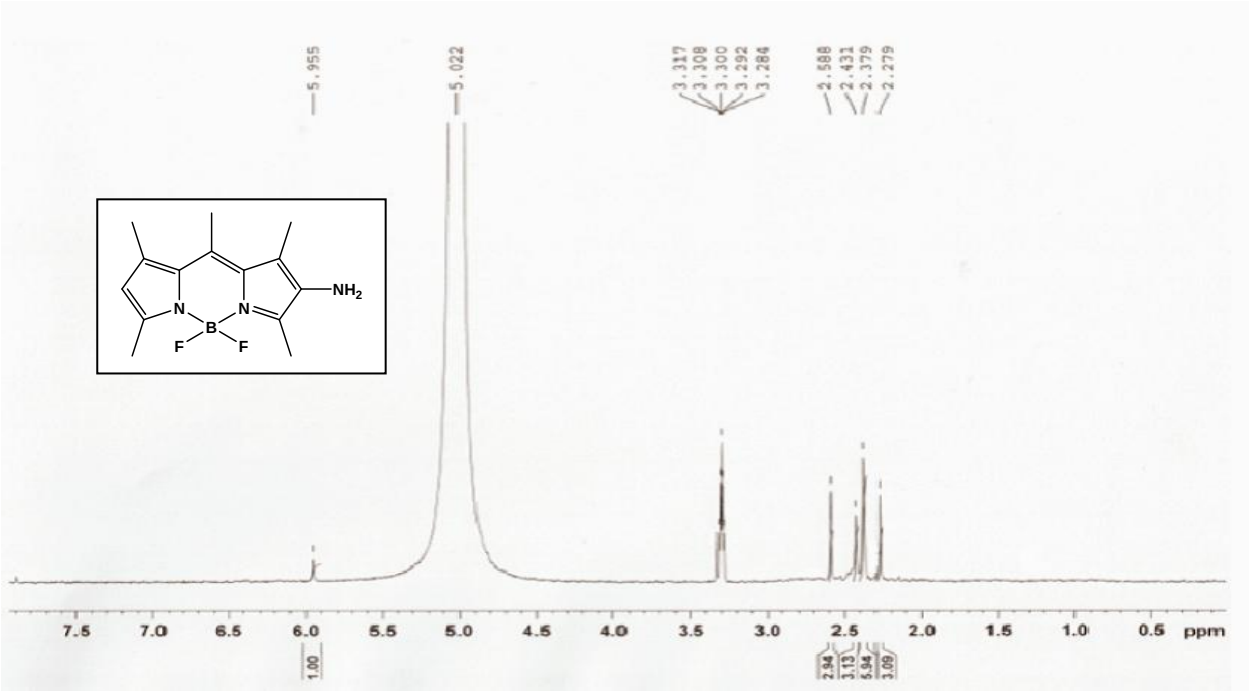

Figure 5.3.1.2: (a) ^{1}H NMR spectrum of **62**

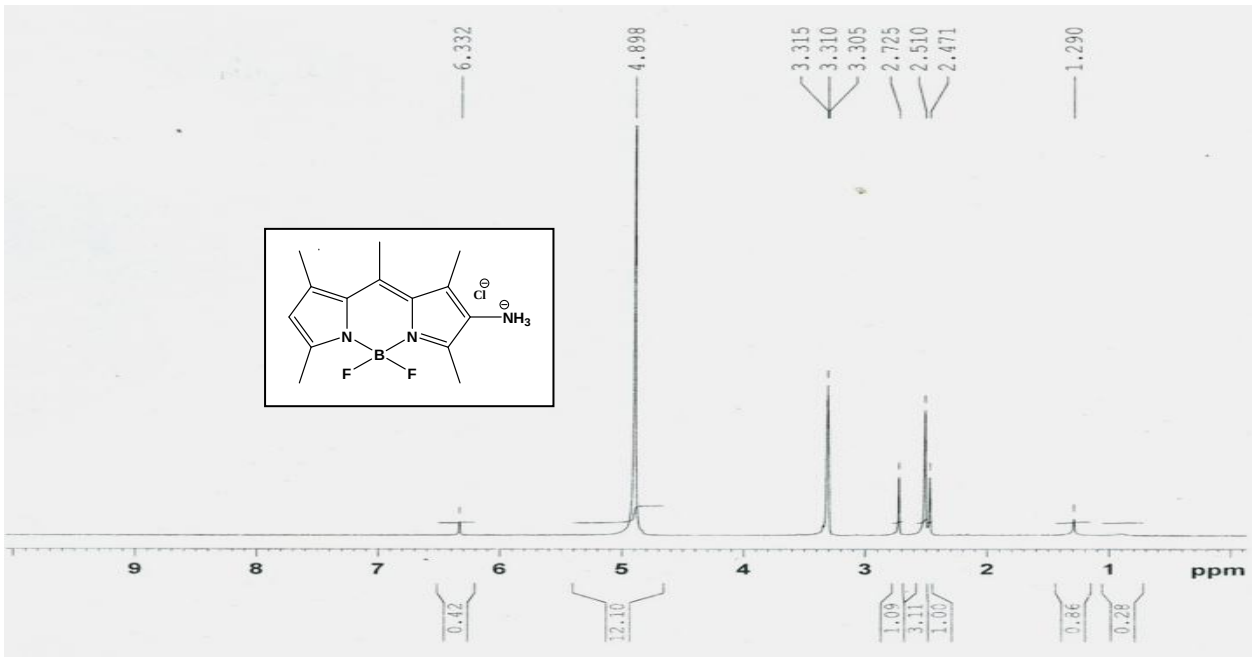

Figure 5.3.1.2: (b) ^{1}H NMR spectrum of **63**

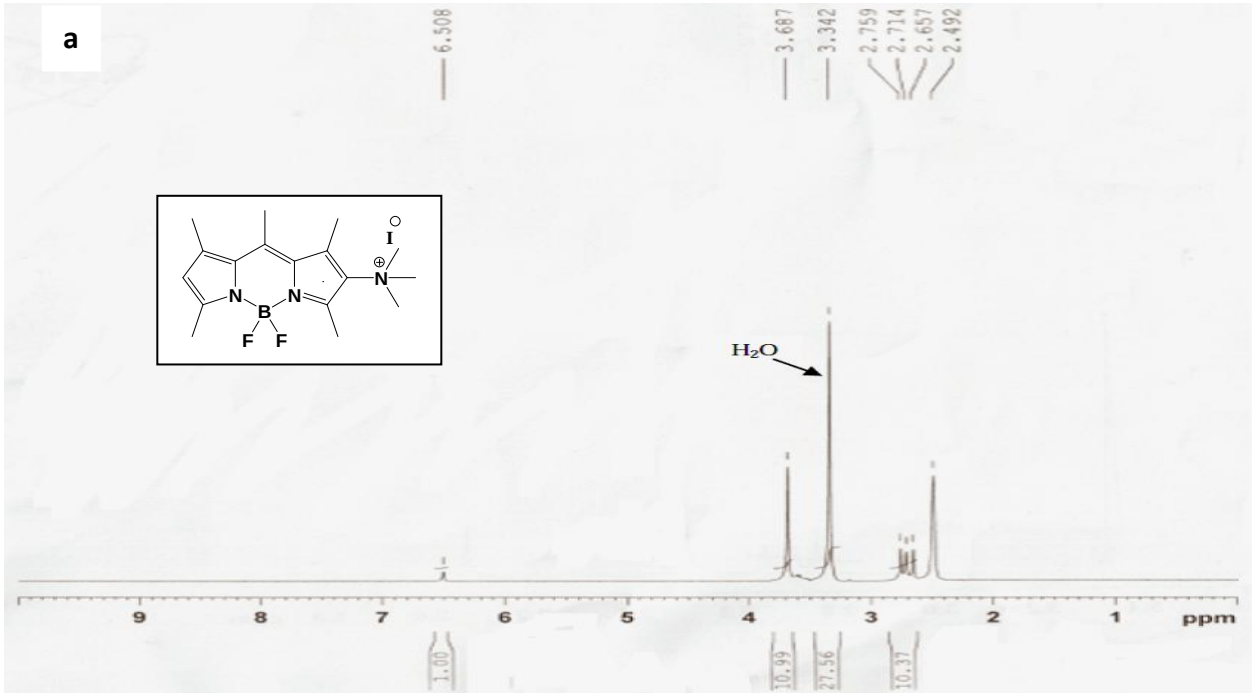

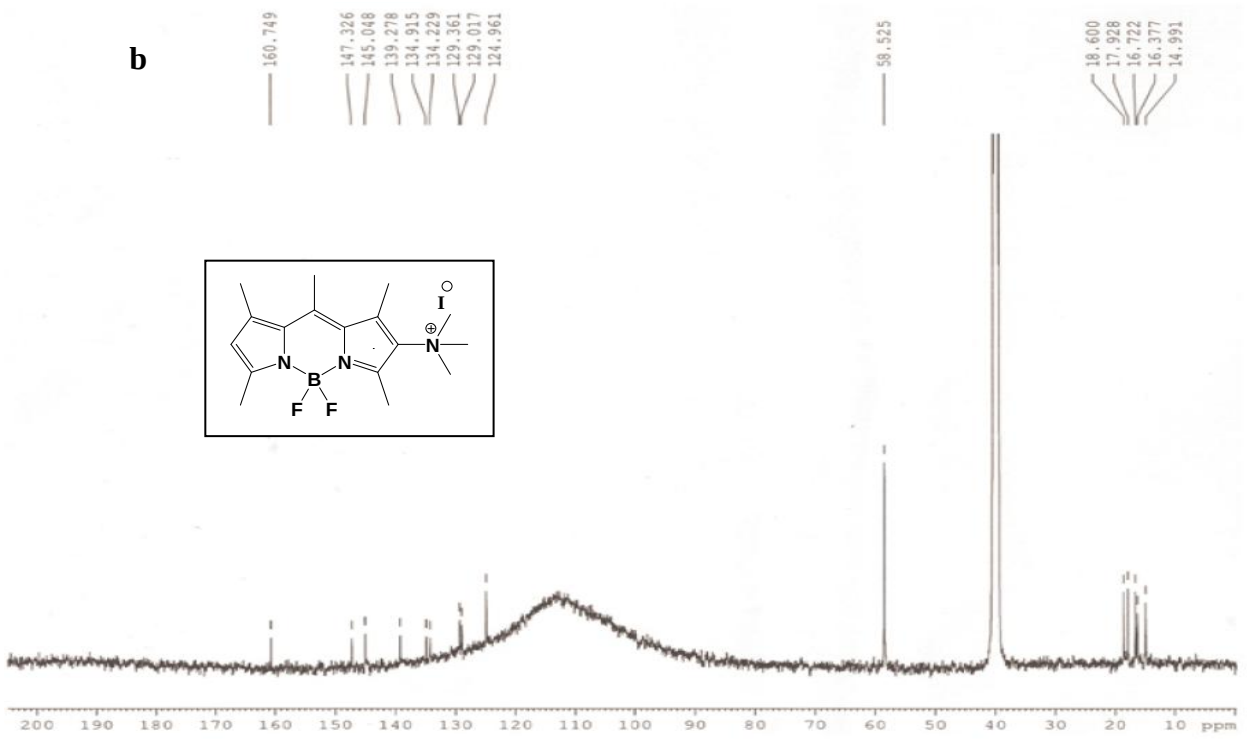

Figure 5.3.1.3: (a) ^{1}H NMR spectrum of **64**, (b) ^{13}C NMR spectrum of **64**

5.3.2 Photo-physical study:

5.3.2.1 Absorption study:

The photo-physical properties of the dyes **18**, **63** and **64** in methanol and water in presence and absence of host **50** were presented in Table 5.3.2.1.1. A strong $S_0 \rightarrow S_1$ transition (λ_{abs}) at 493 nm and a mirror image fluorescence spectrum with λ_{em} at 504 nm were observed with dye **18** in methanol. With dye **63** and **64**, the maxima of λ_{abs} was blue-shifted by 17 and 11 nm, respectively, while the λ_{em} was red-shifted by 16 nm of dye **64** only, increasing the Stokes shift to 29 and 38 nm of dye **63** and **64** in water, respectively *vis-à-vis* that (11 nm) of **18**.

Table 5.3.2.1.1: Photo-physics of the dye **18**, **63** and **64** in methanol and water in presence and absence of the host CB[7] (**50)**

Dye *(dye:50)	**Solvent**	**ν (cm^{-1})**	**λ^{a}_{max} (nm)**	**λ^{f}_{max} (nm)**	**Φ_f**	**τ_f (ns)**	**k_r^c (s^{-1}), (10^8)**	**k_{nr}^c (s^{-1}), (10^8)**
18 (1:0)	Methanol	443	493	504	0.99	6.16	1.6	0.016
63 (1:0)	Water	1206	476	505	0.02[a]	0.30	0.7	32.67
63 (1: 50)	Water	933	485	508	0.1	0.39	2.6	23.07
64 (1:0)	Water	1517	482	520	0.4[b]	2.52	1.6	2.38
64 (1:50)	Water	1517	482	520	0.45	2.96	1.5	1.86

*(Dye:50) in molar ratio

[a] and [b] Determined using Φ_f =0.76 for dye **18** in water as the reference; λ_{exc}=470 nm [c] The values of k_r and k_{nr} were calculated using the following equations: $k_r = \Phi_f / \tau_f$, $k_{nr} = (1-\Phi_f) / \tau_f$, assuming that the emitting state is produced with unit quantum efficiency

Both new dyes **63** and **64** were cationic salt even then show different behavior in absorption peak maxima. This might be because of different substitution at nitrogen atom. Dye **64** has electron donating methyl group which balance the counter ion while in case of dye **63** hydrogen atoms facilitates more electropositive effect on nitrogen atom. For better optical properties, host-guest interaction study of dye **63** and **64** with the host CB[7] **(50)** has been performed in aqueous solution. Absorption maxima of dye **63** initially increases with bathochromic shift till addition of 50% host **50** then slowly decreases with further addition of **50** in continuation of bathochromic shift. The peak maximum was shifted from 476 to 485nm (~ 9 nm) of dye **63** upon addition of **50**. While no shift was observed in absorption peak maximum of dye **64** with addition of **50**. Both the dyes showed no change in absorption spectra after addition

of 50 times higher concentration of the host **50** with respect to dyes. Absorption spectra of dyes **63** and **64** were shown in Figure 5.3.2.1.1.

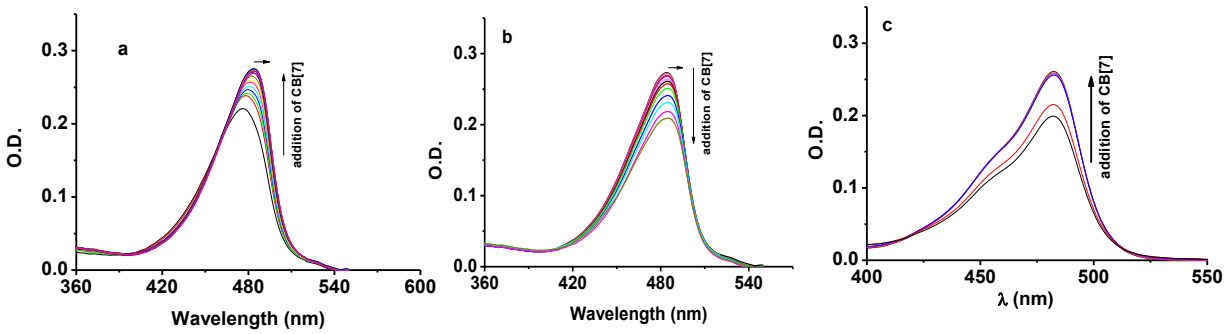

Figure 5.3.2.1.1: Steady state absorption spectra of (a) Dye **63** (30 µM) with increasing concentration of **50** upto 50% addition (0.75mM), (b) Further addition of **50** (1.5mM), (c) Dye **64** (10 µM) with increasing concentration of **50** upto 50 µM.

To know the stiochiometry of the complex of dye with the host **50**, absorption peak maxima of aqueous solutions of the dye were measured by varying mole-fraction concentrations of **50**, while maintaining the total concentrations of dyes and **50** constant. The peak absorption maxima values of dye solutions were correlated by the continuous variation method of Job's plot (Figure 5.3.2.1.2), which showed maxima at a value of 0.5 for [**50**] / ([**50**] + [dye **63**]), indicating 1:1 binding stoichiometry. The same result was observed for dye **64** with the host **50**.

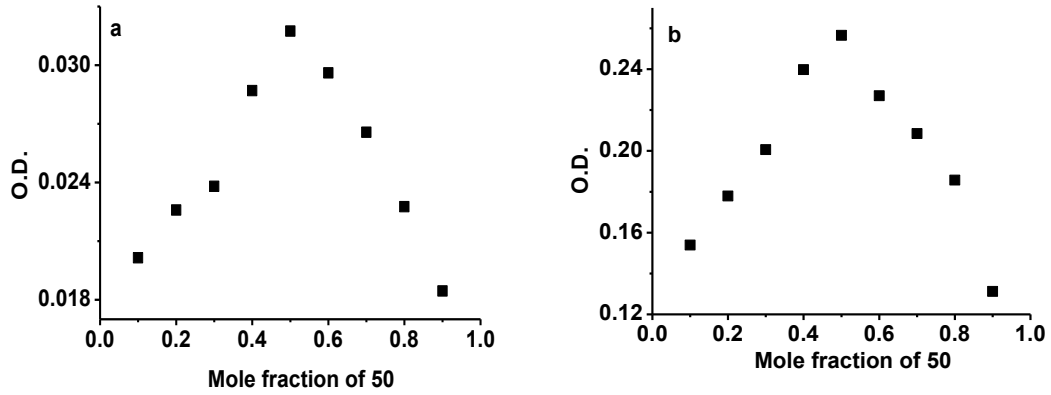

Figure 5.3.2.1.2: Job's plot with complexes of (a) dye **63** and (b) dye **64** with the host **50**. Symmetric plot with maxima at 0.5 mole fraction indicates the 1:1 inclusion complex formation.

Since dye **62** was initially non fluorescent, but become fluorescent after addition of HCl to make quaternary ammonium HCl. It was found that HCl salts have dynamic equilibrium between neutral and cationic forms of the dye **63** in aqueous solution as we explained in case of coumarin 1 dye (previous chapter). Therefore, acidity constant (pK_a) value was calculated. The measurement of the acidity constant (pK_a) of the aqueous solution of the dye **63** was carried out by UV-vis spectrophotometric titrations, which gave a value of pK_a = 3.5 (Figure 5.3.2.1.3). Therefore, we have used dye **63** in water with addition of HCl at pH = 3.0, so that most of dye molecules are in cationic form.

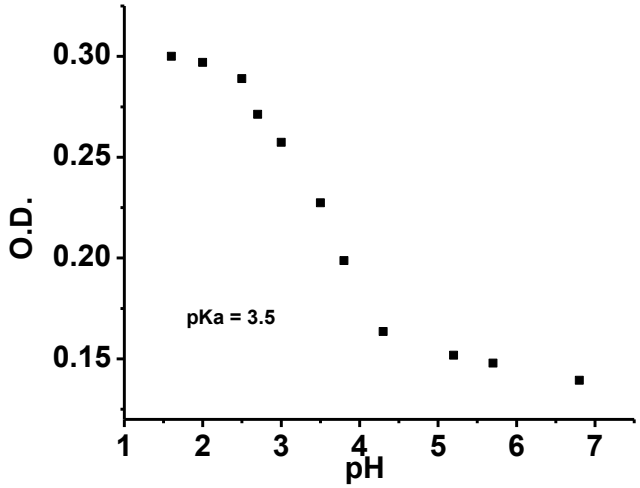

Figure 5.3.2.1.3: Plot of absorbance at peak maxima vs. pH of dye **63** in water with addition of acid. pKa value of dye **63** is 3.5

5.3.2.2 Steady state fluorescence studies:

Fluorescence spectra of dyes **63** and **64** showed negligible shift upon addition of **50**. Dye **63** showed ~7 fold enhancement in its fluorescence intensity with addition of **50 (**Figure 5.3.2.2.1a). While dye **64** gave slight increase in its fluorescence intensity even after addition of fifty times higher concentration of host **50** (Figure 5.3.2.2.1b). It was also observed that the fluorescence quantum yield of dye **63** in water is very poor (0.02) which increased five times upon complexation with **50**. Since dye **64** itself gave good fluorescence quantum yield (0.4) in water and with higher concentration of **50** it showed negligible change in fluoresce intensity which suggested that host **50** did not play an important role in improvement of its fluorescence intensity with complex formation. This might be due to the presence of bulky group at the binding site of the dye (6 position) which make it more distorted in its excited state. The photo-physical data of dyes were given in Table 5.3.2.1.1. Observable changes in the fluorescence

intensity and a large enhancement with addition of the host **50** pointed towards the interaction between dye **63** and host **50**.

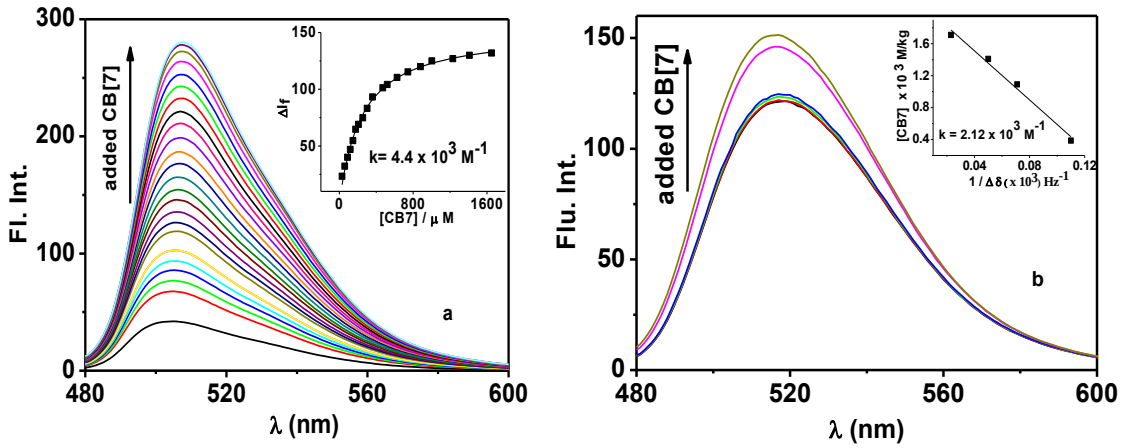

Figure 5.3.2.2.1: Steady state fluorescence spectra of (a) dye **63** (30μM) with increasing concentration of **50** from 0 to 1.5mM and (b) dye **64** (10μM) with increasing concentration of **50** from 0 to 50μM. INSET: Binding constant plot of dyes with addition of **50** in aqueous solution. The solid line represents the best fit of the data corresponding to 1:1 inclusion complex showing binding constant k of 4.4 x 10^3 M^{-1} and k of 2.12 x 10^3 M^{-1} for dyes **63** and **64**, respectively

The binding constant of the dye **63** with **50** was determined by a nonlinear fitting of the observed increases in its fluorescence intensity (ΔI_f) as a function of host **50** concentration using a 1:1 complex formation equation reported earlier which yielded average equilibrium binding constant (k) to be (4.4 ± 0.1) x 10^3 M^{-1} (inset of Figure 5.3.2.2.1a). The formation of a 1:1 Dye:50 complex and its k value was also verified by checking linearity in double reciprocal plot[131] using inverse of changes in observed fluorescence intensity [$1/(I_{obs} - I_f^0)$] with inverse of concentration of the host, 1/[**50**].

However in case of dye **64** due to the negligible enhancement in fluorescence intensity with addition of **50,** the binding constant of dye **64** with the host **50** was performed by NMR

titration method.[149] Where observable changes in its peak intensity with addition of host **50** for a particular methyl proton revealed binding of interaction. The plot of concentration of **50** (in moles/kg) vs. change in chemical shift in Hz for 9th proton of methyl (labeled as 7 in Figure 5.3.4.1) at a fixed concentration of dye **64** in water was plotted. From the intercept we calculated binding constant of dye **64** with **50** to be k = 2.12 ± 0.1 x 10^3 M^{-1} (inset of Figure 5.3.2.2.1b)

5.3.2.3 Time resolved fluorescence studies:

The fluorescence life times of both dyes were calculated from observed mono and bi-exponential decay of free dye and dye with host **50** in water at high concentration of dye:CB[7] (1:50 ratio). The fluorescence decay plots of the dyes **63** and **64** in water were found to be mono-exponential in nature, correspond to a lifetime 0.3 ns and 2.52 ns, respectively. Alternatively, fluorescence decay curves of complexes of dyes **63** and **64** showed lifetime τ_f = 0.39 ns and 2.95 ns, respectively, with an uncertainty value ± 0.02, at a high concentration of the host i.e., at about 1:50 molar ratio of dye:50 (Figure 5.3.2.3.1a and 5.3.2.3.1b).

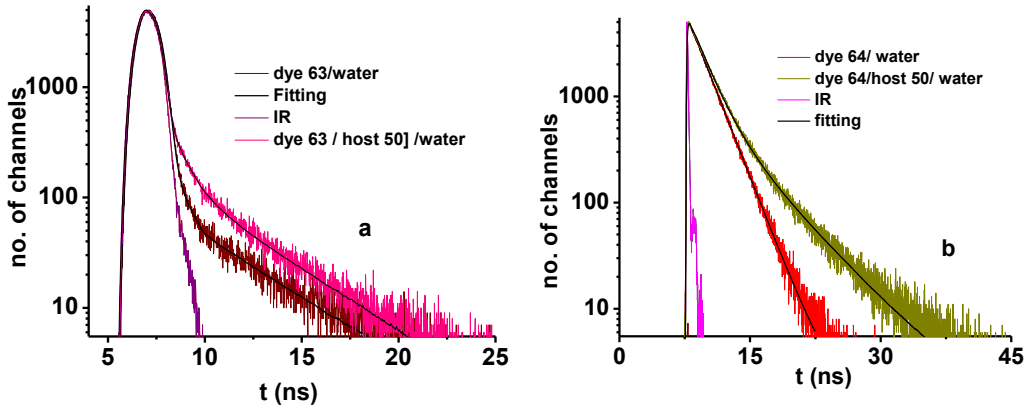

Figure 5.3.2.3.1: Experimentally measured fluorescence lifetime decay of the dye (a) **63** and (b) **64** in water with high concentration of host **50** (dye: 50=1:50)

It was observed that dye **63** gave 1.3 times enhancement in its fluorescence life time upon complexation and dye **64** showed only 1.17 times. This observation indicated that dye **63** formed stronger inclusion complex with the host **50** than dye **64.** This was in agreement with our previous result.

5.3.3 Theoretical Study:

Photophysical studies of dyes **18**, **63** and **64** showed larger Stokes shift of the dye **64** in water than dye **63** and **18** (Table 5.3.2.1.1**)**. In order to rationalize the high Stokes shift of the new dye **64**, the ground state (S_0) geometries (Figure 5.3.3.1a) of the dyes **18** and **64** were optimized by density functional theory (DFT). The calculated dihedral angles of the dyes (Figure 5.3.3.1b) revealed a highly twisted structure of dye **64** as compared to dye **18**. The pyrrole ring, containing the Me_3N group was more twisted than the other parts. The distortion in the ground state geometry of dye **64** may reduce the conjugation leading to the blue shifted absorption. Conversely, the distorted excited state geometry of dye **64** is stabilized by dipolar relaxation with the polar solvents. Hence its emission is red shifted compared to dye **18**. Whereas dye **63** has only NH_3 moiety which is not that much distorted as dye **64** but more than dye **18**.

a

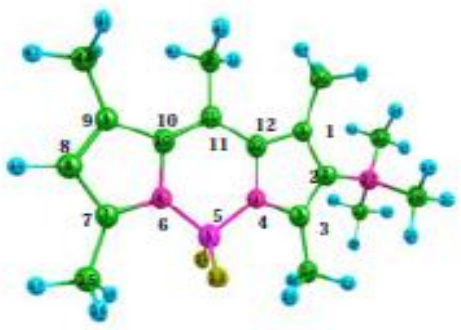

b

Dihedral angle	Dye 18	Dye 64
9-10-11-12	3.49	4.89
7-8-9-10	0.01	0.47
3-2-1-12	0.07	4.38
5-4-12-11	1.06	3.52
5-6-10-11	0.11	1.65
10-11-12-4	1.97	5.72
6-10-11-12	2.53	3.26

Figure 5.3.3.1: (a) DFT-optimized S_0 state geometry of dye **64** (b) Dihedral angles of the DFT-optimized S_0 states of **18** and **64**.

Taken together, the net effect of the steric distortion might be responsible for the high Stokes shift of **63** and **64**. The steric distortion factor can also account for the lower fluorescence yield and higher non-radiative decay rate of **63** and **64** compared to that of dye **18**.

5.3.4 ^{1}H NMR study:

Proton NMR spectra of free dyes **63** and **64** and their complexes with **50,** at 2 times higher concentration with respect to dye, were measured which gave an idea about location of dye molecules interacting with host **50**. Methyl protons (1,2 and 6) of dye **63** showed broadened and upfield shift by 0.214, 0.105, and 0.219ppm with **50** respectively and other methyl protons (3 and 5) showed downfield shift by 0.189 and 0.196ppm, respectively. Further proton 4 remains unshifted. This indicated that dye **63** might be interacting via cationic site with the host **50**. Aromatic part of the dye **63** may be inside the cavity via hydrophobic interaction and cationic nitrogen atom interacting with carbonyl portals of **50**. It may be mantion that proton peak of N-H of dye **63** is absent. However, in case of dye **64** which has three methyl protons in place of hydrogen atom of ammonium salt, it gave distinct peaks in ^{1}HNMR spectra and are more reasonable to throw light on the geometry of the dye-CB[7] complex. Here, methyl protons labeled as 1, 2 and 6 were broadened and upfield shifted by 0.09-0.16 ppm and protons of trimethyl ammonium salt (labeled as 7) showed large (~0.2ppm) upfield shift. This suggested that cationic part has ion dipole interaction with carbonyl portals and these methyl protons are near to the portals. Upfield shift and broadening of protons of the dyes suggested that aromatic part might be inside the cavity and cationic ammonium ion at the portals of both dyes. Further formation of 6 peaks instead of 5 of all aromatic methyl protons of dye **5** suggested that proton 2 splits into two peaks due to the asymmetric orientation with respect to protons at 2/6 position. Therefore, we observed upfield shift and broadening of protons of both dyes upon interaction

with CB[7]This indicates that both dyes have same geometry upon interaction with the host **50**. ^{1}H NMR spectra of dyes **63** and **64,** in absence and presence of **50,** were shown in Figure 5.3.4.1.

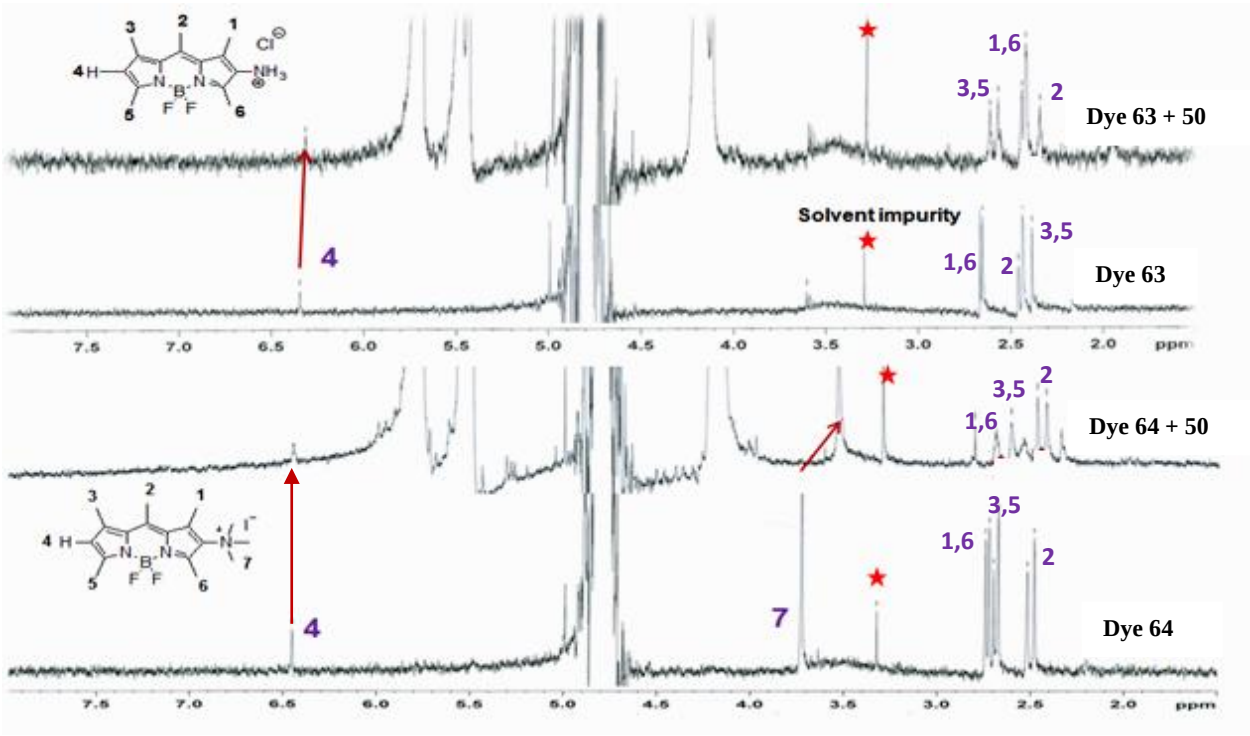

Figure 5.3.4.1: ^{1}H NMR spectra of dye **63** and **64** (taken at a fixed concentration) with 1:2 ratio concentration of the host CB[7] (**50)** in D_2O

5.4 DNA Binding study of Dye 64:

DNA is one of the main target for biological applications such as used to design antitumor drug or to understand toxic mechanism of harmful chemicals etc.[150] which can be justified by study of its photo-physical properties on interaction with DNA. New dye **64** has cationic property as well as good solubility in water even though not suitable for good binding with the host **50**. Though several BODIPYs or aza-BODIPYs bearing either quaternary ammonium groups or protonatable pyridyl groups were investigated as potential PDT agents,[23c,151] there are

very rare reports on the interactions of cationic BODIPYs and DNA up to now, which is believed to be helpful for better understanding of their PDT mechanism by photochemistry. To this end here we present study of electrostatic binding of dye **64** using calf thymas DNA in phosphate buffer at pH 7.4.

5.4.1 Types of binding sites:

There are three types of binding sites of DNA with cationic dye molecules. (i) Intercalation binding i.e. binding between stacked base pairs of DNA. (ii) Non-covalent grove binding and (iii) Electrostatic binding to sugar phosphate skeleton of DNA. Owing to the negatively charged character of DNA, a variety of positively charged dye molecules were scrutinized as DNA photo-cleavers to take advantage of the attractive electrostatic interaction, which may enhance the binding affinity of the dye molecules toward DNA and therefore improve the bioavailability of the reactive oxygen species (ROS).[152]

5.4.2 Photo-physical results:

5.4.2.1 Absorption study:

Dye **64** showed absorption peak maxima at 482 nm initially in phosphate buffer solution with OD in the range of 0.2-0.3, which was sufficient for CT-DNA titration. Absorption spectra of dye **64** (20 μM) with addition of DNA showed decrease in peak intensity (Figure 5.4.2.1.1) but no shift in their peak maxima were observed upto addition of 0.1mM DNA.

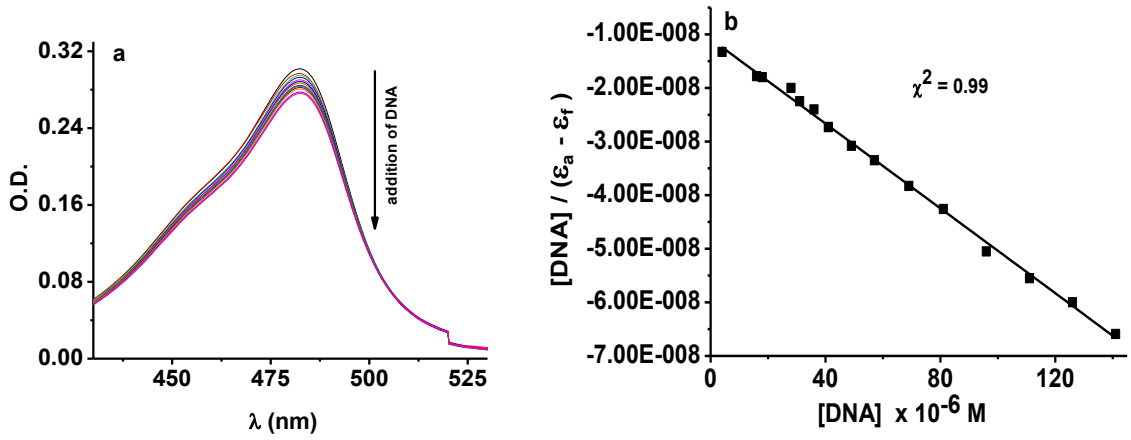

Figure 5.4.2.1.1: Dye **64** (a) absorption spectrum with addition of CT-DNA in phosphate buffer solution at pH=7.4 and (b) Absorption plot for binding with CT-DNA. $K_b = 3.66 \times 10^4\ mol^{-1}$

Gradual decrease in absorbance with CT-DNA revealed that there was no intercalation binding of dye **64** with DNA. These also indicated that dye would have rest types of binding such as groove or electrostatic binding with DNA. From absorption titration, binding constant of the dye with DNA was calculated (Figure 5.4.2.1.1b) by linear plot of [CT-DNA]/ (ε_b- ε_f) vs. DNA concentration and found to be $K_b = (3.66 \pm 0.1) \times 10^4\ M^{-1}$.

5.4.2.2 Steady-state fluorescence study:

Similarly fluorescence titration of Dye **64** (20 µM) with addition of CT-DNA (upto 0.1 mM) in phosphate buffer solution was carried out. Initially fluorescence maxima was at 518 nm and slowly decreased with addition of DNA (Figure 5.4.2.2.1a) which indicated that there is some specific site where dye binds with DNA. Fluorescence quenching of the dye was observed in presence of DNA. Thus, from fluorescence plot, fluorescence quenching constant was determined by using Stern volmer equation and found to be $K_{sv} = (6.86 \pm 0.1) \times 10^3\ M^{-1}$ (Figure 5.4.2.2.1b).

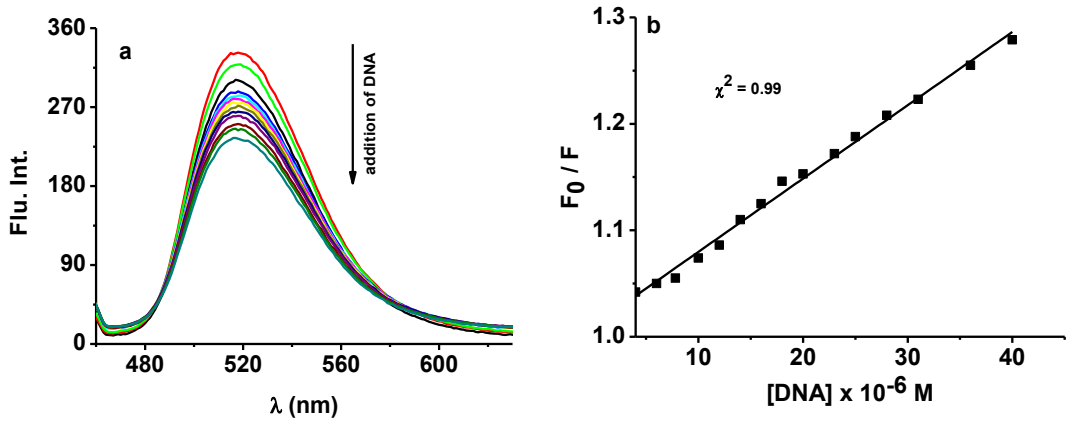

Figure 5.4.2.2.1: (a) Fluorescence spectra of dye **64** with addition of CT-DNA in phosphate buffer solution at pH=7.4 and (b) Stern-Volmer fluorescence plot for quenching constant of dye **64** with CT-DNA. K_{sv}= 6.86×10^3 mol^{-1}

These absorption and fluorescence results indicated that there might be either groove binding or electrostatic binding of dye **64** with DNA. This was further understood by life time study of dye with DNA.

5.4.2.3 Fluorescence life time study:

Fluorescence life time study was performed to confirm the electrostatic binding of dye **64** with DNA. The life time of pure dye (5μM) in phosphate buffer solution was determined to be (τ) 2.22 ns which increased to 3.27 ns in presence of DNA. This suggested that dye **64** definitely have binding with DNA. But this would not explain whether it is groove binding or electrostatic binding. Therefore, binding replacement study using NaCl salt via life time was carried out by further addition of NaCl salt in the dye-DNA solution. Subsequent reduction of its life time from 3.27 ns to 2.69 ns showed electrostatic binding nature of the dye **64** with DNA (Figure 5.4.2.3.1).

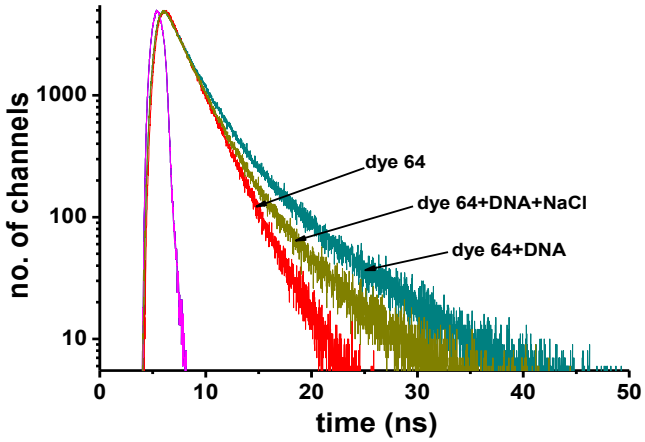

Figure 5.4.2.3.1: Fluorescence life time of Dye **64** (5µM) at pH 7.4 of phosphate buffer solution

5.4.3 DNA-Photo-cleavage activity:

5.4.3.1 Gel electrophoresis (Effect of $^1O_2$):

It has been well established that fluorescent dyes in solution produces singlet oxygen *in situ* during excitation and energy transfer in triplet state via intersystem crossing which would be useful for DNA photo-cleavage. The DNA photo-cleavage activity of dye **64** was characterized by using pBR322 plasmid DNA as a target with two different concentrations (30 and 60µM) of dye in H_2O, in presence of singlet oxygen activator D_2O and scavenger NaN_3 using gel electrophoresis technique. Experiment was performed in presence and absence of light. On irradiation for 1h, dye **64** lead to DNA cleavage from supercoiled circular form to nicked circular form (Figure 5.4.3.1.1a). Control experiment showed that irradiation and presence of dye **64** was necessary for DNA cleavage. However, it was found that presence of light and higher concentration (60 µM) was more prone towards DNA cleavage upto 80% (Figure 5.4.3.1.1b).

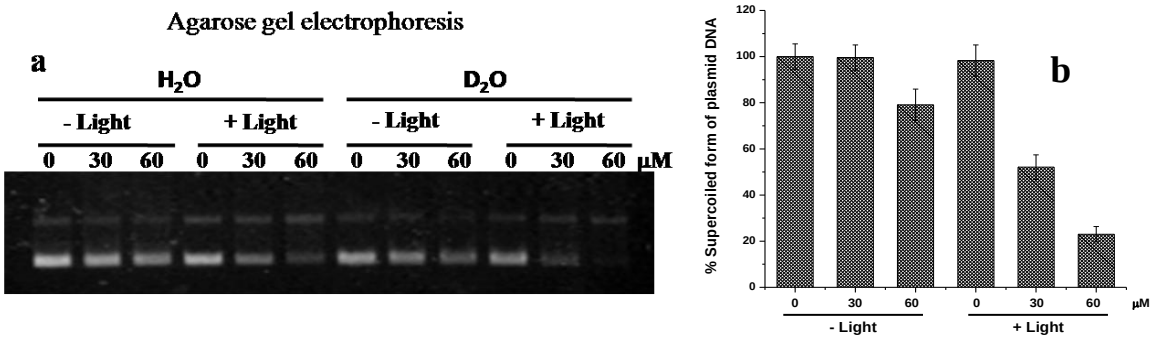

Figure 5.4.3.1.1: (a) Agarose gel electrophoresis showing the nuclease property of dye **64** in H_2O and D_2O; (b) Nuclease property of dye **64**. The pBR322 plasmid DNA and the dye **64** (0-60 µM) in H_2O or D_2O alone, or in conjunction with light (intensity: 0.77 mW /cm^2) was incubated for 1h, and the percentage of supercoiled DNA quantified. The values are mean ± S. E. M. (n = 5).

5.4.3.2 Effect of $^1O_2$ activator and scavenger:

To examine the effect of reactive $^1O_2$ species generated by dye **64** towards DNA photo-cleavage with or without ROS scavengers, such as NaN_3 in H_2O and/or ROS activator D_2O in presence of light, studies were carried out as shown in Figure 5.4.3.2.1. After irradiation for 1h, the percentage of supercoiled DNA was reduced to 2% in absence of dye **64**, while 48 % in presence of 30µM dye and 77% in presence of 60µM dye in H_2O. Whereas in presence of activator (D_2O) it was reduced to 13%, 75% and 95.5% in absence and presence of 30 and 60µM dye, respectively. This observation showed that with increasing the concentration of dye **64** the percentage of reactive oxygen species generated from dye increased which was responsible for DNA photo-cleavage. This was also proved with NaN_3 experiment which inhibited the photo-cleavage activity of dye **64** markedly, and this indicates a $^1O_2$ mechanism for **64**.

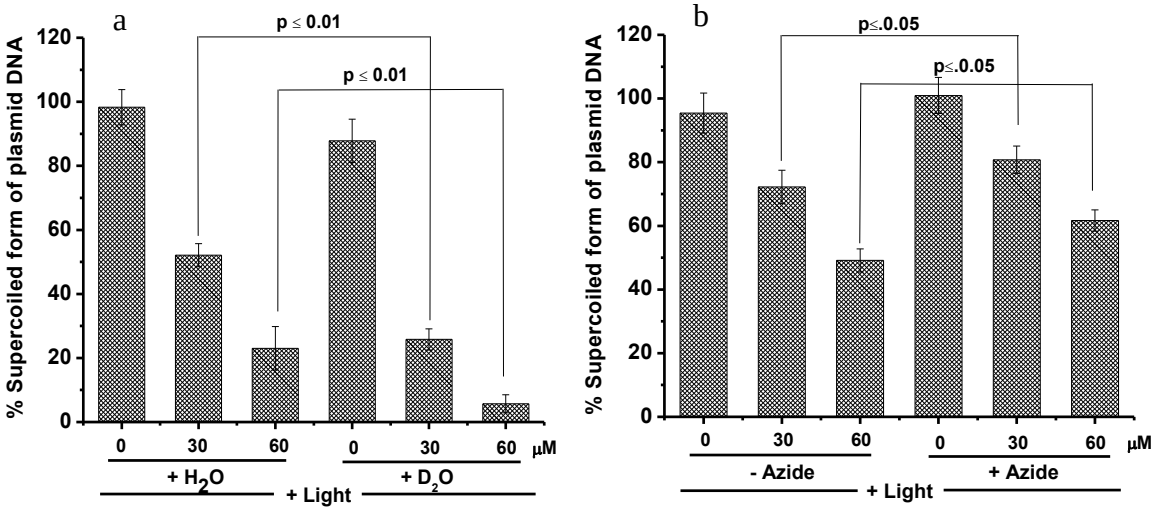

Figure 5.4.3.2.1: Effect of $^1O_2$ (a) activator (D_2O) and (b) scavenger (NaN_3) on the nuclease activity of dye **64**. The pBR322 plasmid DNA and the dye **64** (0-60 μM) in H_2O or D_2O alone or in conjunction with NaN_3 (100 mM) in H_2O was exposed to light (intensity: 0.77 mW /cm^2) for 1h, and the percentage of supercoiled DNA quantified. The values are mean ± S. E. M. (n = 5)

In contrast, NaN_3 can remarkably restrict the photo-cleavage activity of **64** (Figure 5.4.3.2.1b), which suggested that dye **64** exerts photo-dynamic activity through $^1O_2$ mechanisms. To the best of our knowledge, this is an example that BODIPY-type photo-sensitizer participates in the damage of DNA which has not been reported so far. Thus, dye **64** is good photo-sensitizer which produces singlet oxygen upon photo-exposure and responsible for photo-cleavage activity of supercoiled DNA to nicked DNA.

5.4.3.3 Effect on human lung cancer:

Fluorescence microscopy measurement was performed using A549 cells after staining with DAPI, dye **64** separately and also merged with each other. Result of fluorescence microscopy showed a good uptake of dye **64** by the human lung cancer A549 cells (Figure 5.4.3.3.1). However, it was not cytotoxic to the A549 cells even up to 50 μM concentration, both

under dark or photo-irradiation conditions. This may be due to its poor DNA-binding property and accumulation in the cytoplasma, but not in the mitochondria of the A549 cells.

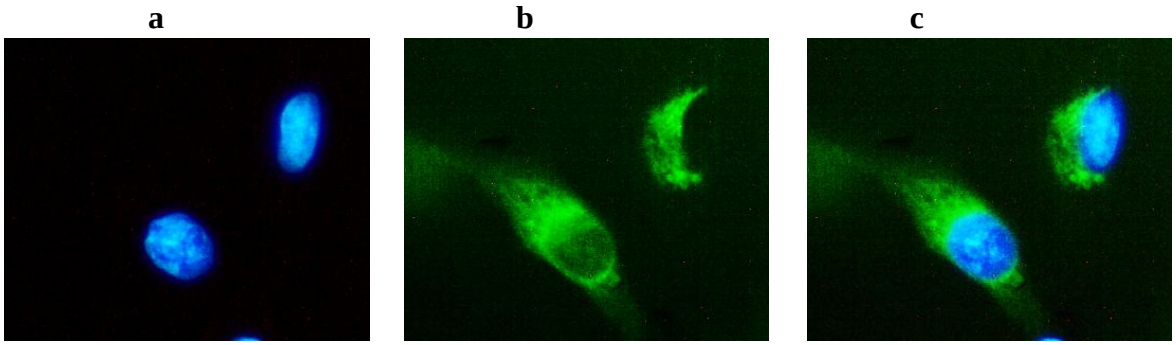

Figure 5.4.3.3.1: Fluorescence images of A549 cells after staining with (a) DAPI; (b) dye **64**; (c) overlay of the images.

5.5 Conclusion:

Taken together, improvement in photo-physical property of dye **63** upon complexation with the host CB[7] (**50)** was observed. Dye **64** showed weaker binding than dye **63** with the host CB[7] (**50**). However, good fluorescence quantum yield (40% in pure water) and large Stokes shift of dye **64** showed promising applications of water based Bodipy dye as a sensitive and efficient fluorescent probe in chemical and biological studies and probably in aqueous dye laser area**.**

CHAPTER 6

RED SHIFTED BODIPY SCHIFF BASES WITH HIGH STOKES SHIFT

Chapter 6: Table of Contents

6.1 Introduction:

This chapter deals with our studies on design, synthesis and characterization of red emitting fluorescent BODIPY dyes with a large Stokes shift. A very few red emitting dyes are so far reported from BODIPY class of fluorophores, but also the small Stokes shift issue is a real problem. This is very often detrimental to its applications, such as in molecular probes or intracellular fluorescence imaging. A small Stokes shift reduces the emission intensity by self-absorption, or the inner filter effect.[153] A few reports are available with large Stokes shifted Bodipy dyes,[154] but rational design is still lacking.

6.2 Bodipy based fluorescent sensor:

BODIPY dyes have several attributes that make them good candidates as fluorescent sensors in biological systems.[155] Their spectroscopic and photo-physical properties can be finely tuned by substitution on the dipyrromethene core. Dehaen and co-workers[26] originally performed systematic work on the reactivity of 3,5-dichlorinated BODIPY with carbon, nitrogen, oxygen, and sulfur directed toward nucleophilic aromatic substitution (SNAr) and palladium-catalyzed cross-coupling. Mono- and disubstituted products were prepared selectively by careful tuning of the reaction conditions. The monochlorinated BODIPY derivatives could be modified further by replacing the chlorine with a nucleophile. Unfortunately, the typical chemical modification of the Bodipy core, i.e., substitutions at pyrrole ring and at the B-centre are not helpful at all in increasing the Stokes shift.[156] The same problem persists with the extended π-conjugated Bodipy frameworks, which leads to red-shifted absorption and emission. The most investigated method for the red-shifted Bodipy dyes is the Knovenegel condensation.[157] The resulted mono-, di- and polystyryl Bodipys also have low Stokes shifts. Thus red shifted Bodipys with high Stokes shift are urgent requirement. Although the large Stokes shift can be observed with the strategy of

fluorescent-resonance-energy-transfer (FRET, Föster energy transfer), but strong self-absorption is still a drawback of this method and the large Stokes shift is actually a pseudo-Stokes shift.[158]

6.3 Types of fluorescent sensor:

Fluorescent sensors are widely used for detection of protons and metals in several applications,[1b,159] especially intracellular imaging.[160] Indicators may be divided into three types: (i) ones that are insignificantly fluorescent in the absence of analyte but are much more emissive when it is present; (ii) the inverse, where fluorescence of the probe is quenched by the analyte; and (iii) sensors which have observable spectroscopic differences when the analyte is present compared to when it is absent.

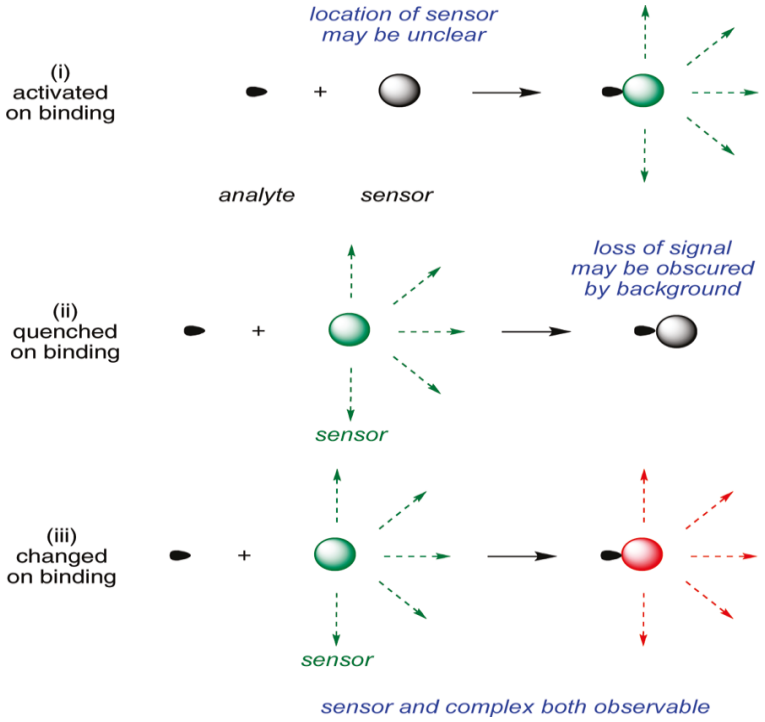

Figure 6.3.1: Fluorescent sensors may be (i) activated, (ii) quenched by analytes and (iii) "always on" but change wavelength of fluorescence emissions on binding

The third type of sensor is "always on"; this is a significant advantage because it is clear that the probe is present even if the analyte is not (Figure 6.3.1). Intracellular pH is a

fundamental property that correlates with many events in cell biology. To measure this, researchers tend to rely on subtle changes in sensors that are "always on"[161-169] for instance, they observe emission intensities as a function of excitation wavelength.[169-172] However, most of such type of sensors do not change emission wavelength maxima as the pH is varied; but if they did, they would be far easier to use. To this end, we rationally designed two different colored *i.e.* orange and red Bodipy schiff bases, dye **67** and **68**, respectively by extending the conjugation via amino group at 2 and / or 6 position of dye **18**.

6.4 Experimental:

6.4.1 Synthesis:

4,4-Difluoro-1,3,5,7,8-pentamethyl-2-nitro-4-bora-3*a*,4*a*-diaza-*s*-indecene (61): Same as discussed in previous chapter 5.2.1 section.

4,4-Difluoro-2,6-dinitro-1,3,5,7,8-pentamethyl-4-bora-3*a*,4*a*-diaza-*s*-indecen (65): Following a similar procedure as for **61**, compound **18** (100 mg, 0.38 mmol) was reacted with HNO_3 (1.7 ml, 70%) at 0^oC, the resultant mixture poured into crushed ice, the precipitate filtered, washed with cold H_2O (4 × 10 ml) and dried under vacuo to get **65** as a orange solid. Yield: 90 mg (67.0%); Mp: 279°C (lit.[96] mp: 279-281°C); IR (KBr): 1338, 1487, 1534, 1568 cm^{-1}; ^1H NMR (200 MHz, $(CD_3)_2SO$, 25^oC, TMS): δ = 2.39 (s, 9H), 2.59 ppm (s, 6H); ^{13}C NMR (50 MHz, $(CD_3)_2SO$, 25^oC, TMS): δ = 12.8, 13.8, 111.2, 111.4, 127.8, 128.8, 134.5, 135.4 ppm; EI-MS *m/z* (%): 351.1 (100) $[M\text{-}1]^+$, 352.1 (14) $[M]^+$. elemental analysis calculated (%) for $C_{14}H_{15}N_4BF_2O_4$: C 47.76, H 4.29, N 15.91; found: C 48.10, H 4.34, N 15.79.

2-Amino-4,4-difluoro-1,3,5,7,8-pentamethyl-4-bora-3*a*,4*a*-diaza-*s*-indecene (62) and 2,6-Diamino-4,4-difluoro-1,3,5,7,8-pentamethyl-4-bora-3*a*,4*a*-diaza-*s*-indecene (66): To a solution of **61** or **65** (0.33 mmol) in methanol (20 ml) were added HCO_2NH_4 (0.33 mmol) and

Zn-dust (0.33 mmol), and the mixture stirred for 10 min when the orange solution turned dark pink. The reaction mixture was eluted through cellite, the eluate concentrated in vacuo, and the residue column chromatographed (basic alumina, hexane/ ethyl acetate) to furnish **62** and **66**, respectively as brown solids.

Compound 66: Yield: 80 mg (84%); Mp: >300°C; IR (KBr): 1485, 1536, 1566, 3410, 3540 cm^{1}; ^{1}H NMR (200 MHz, CD_3OD, 25°C, TMS): δ = 2.25 (s, 6H), 2.38 (s, 6H), 2.55 ppm (s, 3H); ^{13}C NMR could not be done due to very poor solubility. EI-MS: *m/z* (%): 291.1 (96) $[M\text{-}1]^{+}$, 290.1 (100) $[M\text{-}2]^{+}$; elemental analysis calculated (%) for $C_{14}H_{19}N_4BF_2$: C 57.56, H 6.56, N 19.18; found: C 57.86, H 6.44, N 18.99.

Compound 67 or 68: To a solution of **62** or **66** (0.26 mmol) in dry CH_2Cl_2 (20 ml) were added *p*-methoxybenzaldehyde (1 or 2 equiv.) and anhydrous Na_2SO_4 (100 mg), and the mixture were stirred at 25°C for 12 h and 24 h respectively. The reaction mixture was filtered, concentrated in vacuo, and the residue column chromatographed (basic alumina, hexane/EtOAc) to furnish **67** or **68**.

Compound 67: Yield: 25 mg (25%); red-brown solid; Mp: 214°C; IR (KBr): 1558, 1604, 2836 cm^{-1}; ^{1}H NMR (200 MHz, $(CD_3)_2CO$, 25°C, TMS): δ = 2.41-2.46 (m, 9H), 2.51 (s, 3H), 2.67 (s, 3H), 3.88 (s, 3H), 6.15 (s, 1H), 7.04 (d, *J* = 8.6 Hz, 2H), 7.90 (d, *J* = 8.6 Hz, 2H), 8.43 ppm (s, 1H); ^{13}C NMR (50 MHz, $CDCl_3$, 25°C, TMS): δ = 12.5, 13.8, 14.4, 16.6, 17.3, 55.4, 114.1, 120.9, 128.5, 129.3, 130.1, 131.0, 132.0, 140.4, 141.0, 143.0, 147.3, 153.1, 161.2, 162.3 ppm; EI-MS: *m/z* (%): 396.3 (100) $[M]^{+}$; elemental analysis calculated (%) for $C_{22}H_{24}N_3BF_2O$: C 66.85, H 6.12, N 10.63; found: C 66.62, H 6.39, N 10.89.

Compound 68: Yield: 45 mg (31%); brown solid; Mp: >300°C; IR (KBr): 1417, 1448, 2858 cm^{1}; ^{1}H NMR (200 MHz, $CDCl_3$, 25°C, TMS): δ = 2.39 (s, 6H), 2.56 (s, 6H), 2.66 (s, 3H), 3.87

(s, 6H), 7.00 (d, J = 8.6 Hz, 4H), 7.86 (d, J = 8.6 Hz, 4H), 8.25 ppm (s, 2H); ^{13}C NMR (50 MHz, $CDCl_3$, 25^{o}C, TMS): δ = 12.5, 13.8, 55.5, 100.1, 114.2, 128.3, 129.3, 130.1, 131.1, 161.1, 162.2 ppm; EI-MS: *m/z* (%): 509.4 (40) $[M\text{-}19]^+$, 528.4 (37) $[M]^+$, 529.4 (100) $[M+1]^+$; elemental analysis calculated (%) for $C_{30}H_{31}BF_2N_4O_2$: C 68.19, H 5.91, N 10.60; found: C 68.31, H 6.17, N 10.35.

6.4.2 Theoretical calculations:

The methodology of theoretical calculations was similar as discussed in previous chapter (section 5.2.2) and detail in chapter 2.

6.5 Results and discussion:

6.5.1 Synthesis:

The new dyes, **67** and **68**, were synthesized from 2,6-unsubstituted Bodipy dye, PM546 (**18**). At first, the nitration of the dye **18** at the C-2 and C-6 position was studied. This reaction can nicely be controlled using the diluted (45%) and concentrated HNO_3 which furnished exclusively the 2-nitro (**61**) and 2,6-dinitro Bodipy (**65**) respectively (Scheme 6.5.1.1). These dyes, **61** and **65** were successively reduced to amino dyes **62** and **66** respectively *via* catalytic hydrogen transfer same as discuss in previous chapter. The schiff bases **67** and **68** were synthesized by the condensation of **62** and **66** respectively with *p*-methoxybenzaldehyde (Scheme 6.5.1.2).

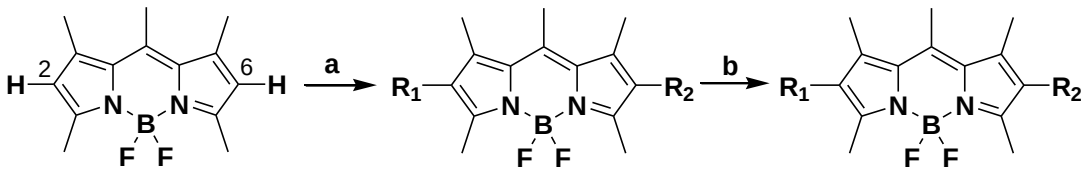

18

61. R_1 = H; R_2 = NO_2
65. R_2= NO_2; R_2= NO_2

62. R_1 = H; R_2 = NH_2
66. R_2= NH_2; R_2= NH_2

Scheme 6.5.1.1: Synthesis of the dyes **65** and **66** (a) HNO_3, 0^oC, 1.5 h; (b) HCO_2NH_4, Zn-dust, methanol, 25^oC, 10 min.

Both the dyes, **67** and **68** were unambiguously characterized by NMR, IR, CHN and mass spectroscopy. For example, the dye **67** was confirmed by the imine proton peak at 8.29 ppm and C-6 proton peak of the BODIPY core at 6.09 ppm in the ^1H NMR spectrum (Figure 6.5.1.3a). The phenyl ring exhibits two doublets of an AA'BB' system at 7.05 and 7.90 ppm. The BODIPY methyls resonate at 2.43, 2.46, 2.56, 2.60 and 2.67 ppm, and the methoxy methyl group resonate at 3.92 ppm. NMR spectrum of dye **65**, **66**, **67** and **68** were shown in Figure 6.5.1.1-6.5.1.4

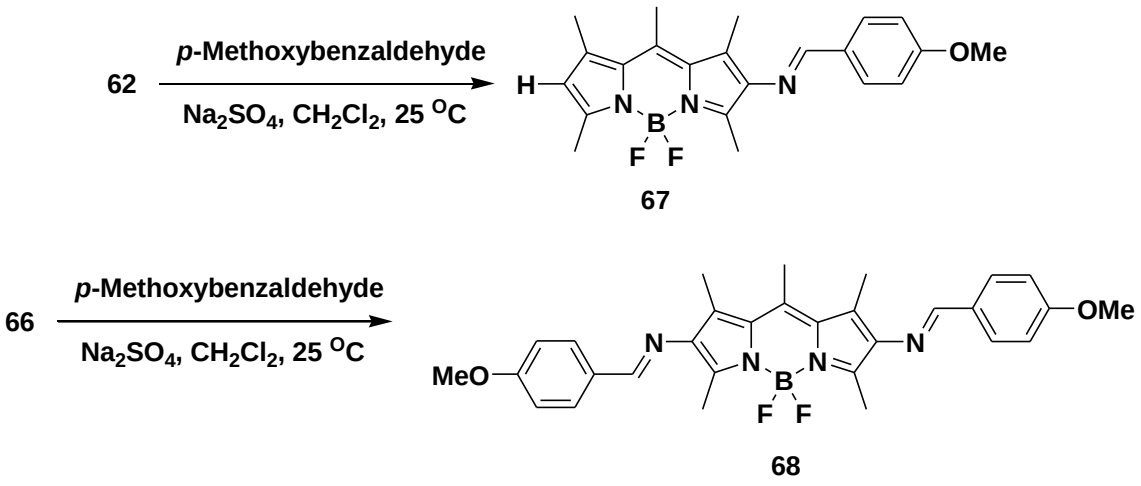

Scheme 6.5.1.2: Synthesis of the dyes **67** and **68**.

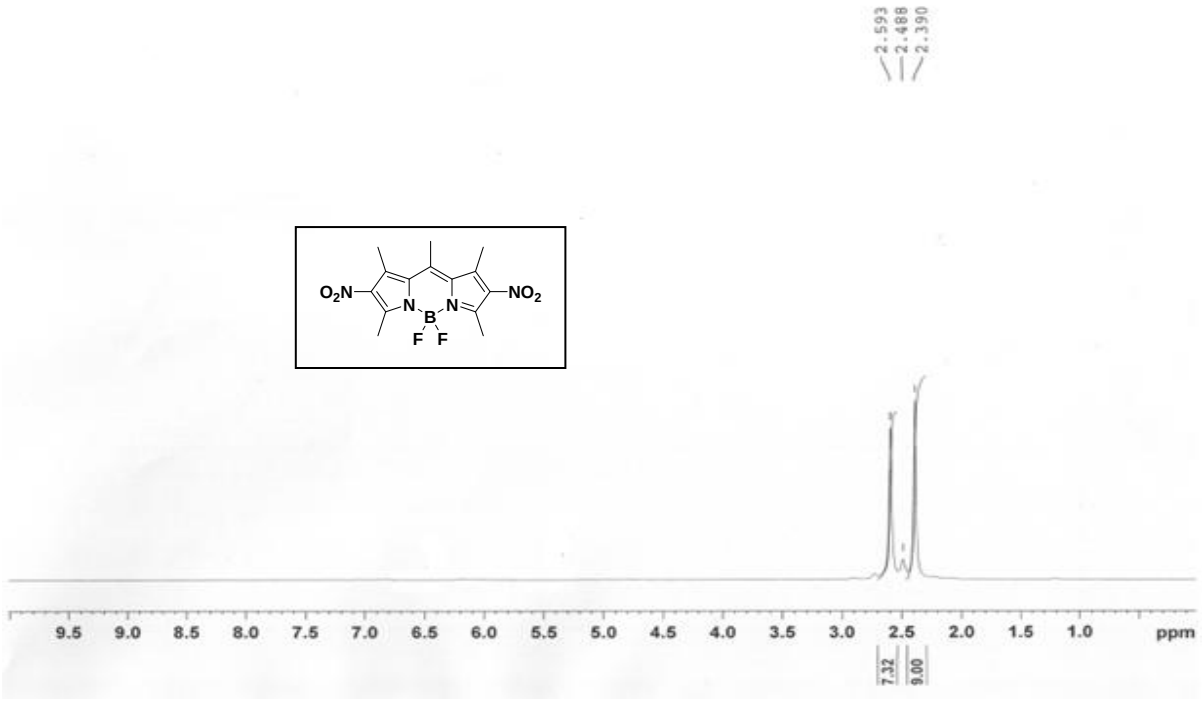

Figure 6.5.1.1a: ^{1}H NMR spectrum of dye **65** in CD_3OD

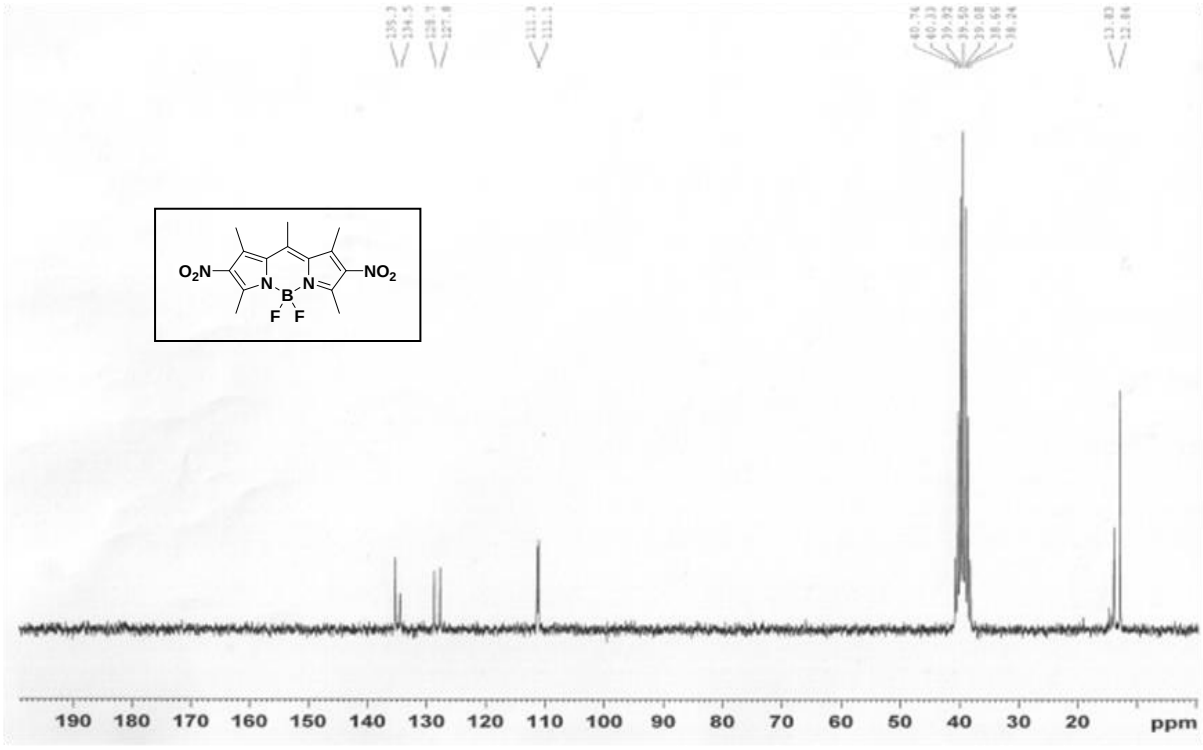

Figure 6.5.1.1b: ^{13}C NMR spectrum of dye **65** in CD_3OD

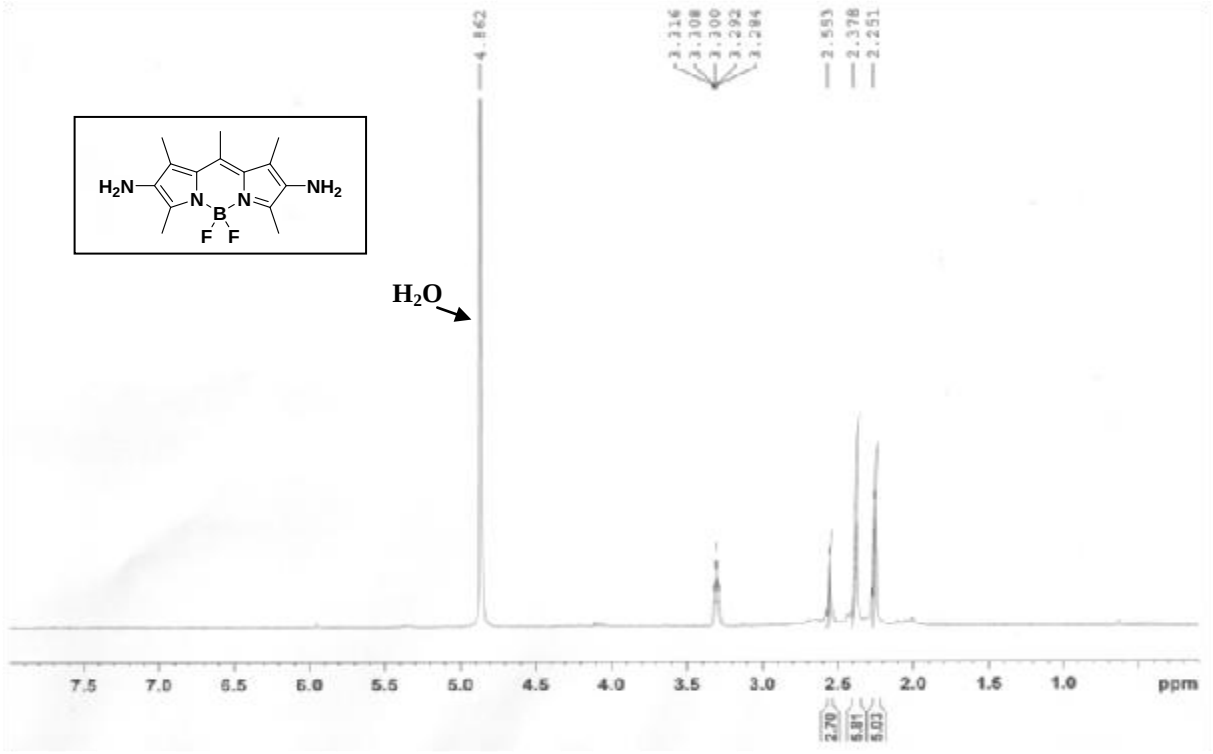

Figure 6.5.1.2: ^{1}H NMR spectrum of dye **66** in CD_3OD

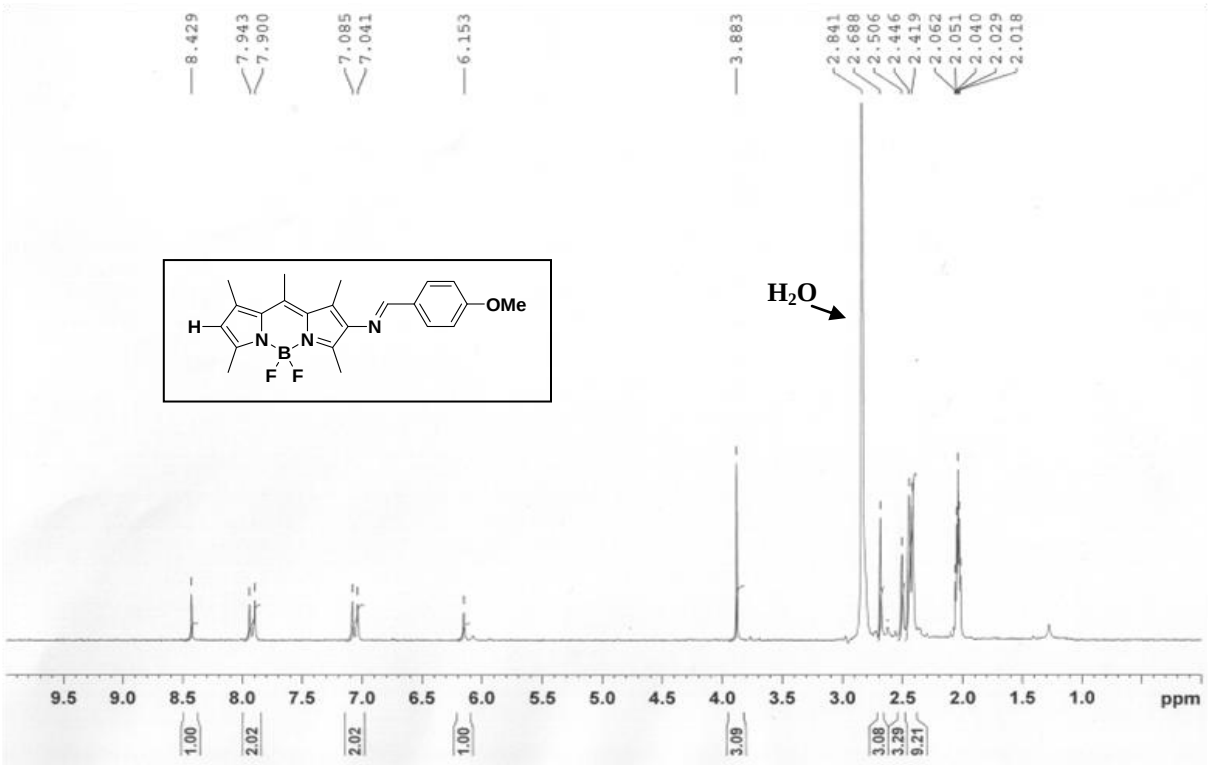

Figure 6.5.1.3a: ^{1}H NMR spectrum of **67** in ($CDCl_3$)

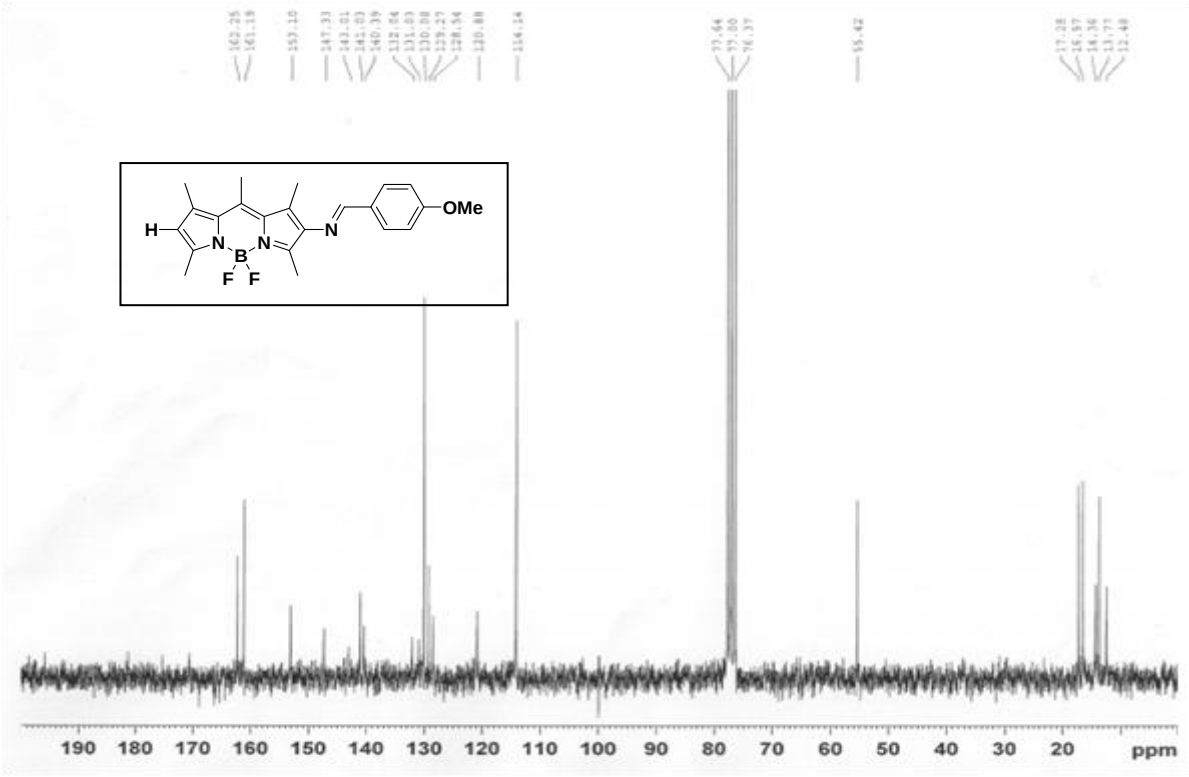

Figure 6.5.1.3b: ^{13}C NMR spectrum of **67** in $CDCl_3$

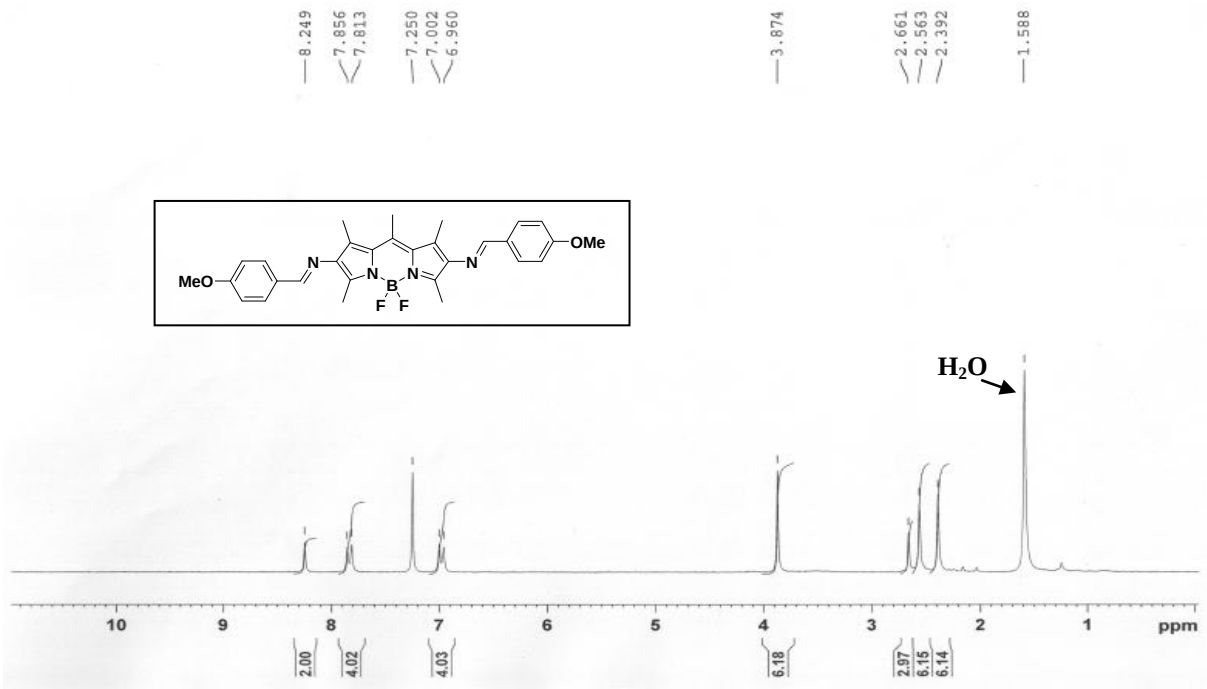

Figure 6.5.1.4a: ^{1}H NMR spectrum of **68** in $CDCl_3$

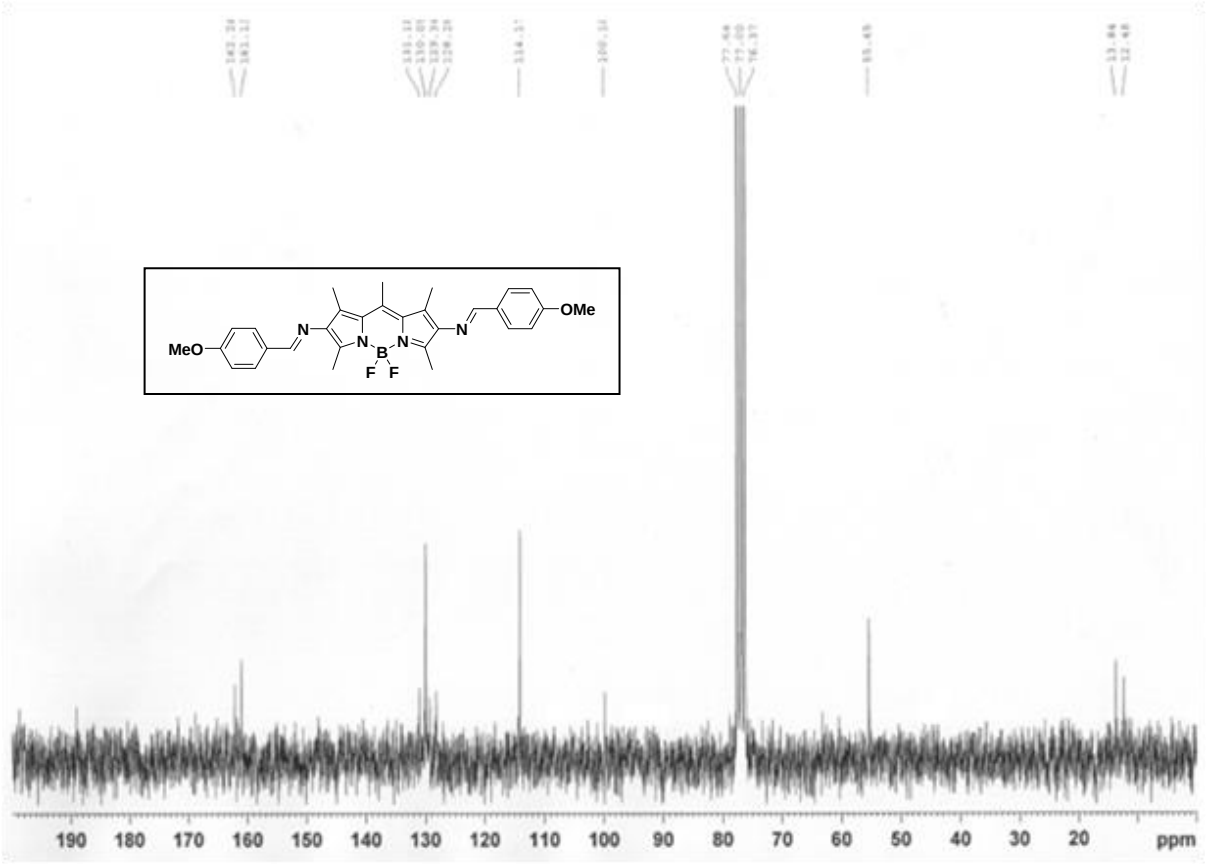

Figure 6.5.1.4b: ^{13}C NMR spectrum of **68** in $CDCl_3$

6.5.2 Photo-physical properties:

The salient photo-physical properties of the dyes **18**, **67** and **68** in methanol are presented in Table 6.5.2.1. The normalized absorption and emission spectra are also shown in Figure 6.5.2.1. A strong $S_0 \rightarrow S_1$ transition (λ_{abs}) at 493 nm and a mirror image fluorescence spectrum with λ_{em} at 504 nm were observed with **18**. With the dye **67**, the λ_{abs} was blue-shifted by 11 nm while the λ_{em} was red-shifted by 16 nm, increasing the Stokes shift to 38 nm *vis-à-vis* that (11 nm) of **18**. Imine functionalities of the dyes **67** and **68** facilitated to shift the absorption and emission band of the dyes towards lower energy than **18** due to the extended conjugation.

Table 6.5.2.1: Selected optical properties of dyes **18**, **67** and **68** in methanol at 25^0C

Dyes	λ_{abs} (nm)	ε x 10^{-4} (M^{-1} cm^{-1})	λ_{em} (nm)	ν (cm^{-1})	τ_f (ns)	Φ_f	k_r^d (10^8 s^{-1})	k_{nr}^d (10^7 s^{-1})
18	493	7.90	504	443	6.16	0.99	1.6	0.16
67	526	1.58	579	1740	2.16	0.04[a]	0.2	44.4
68	562	1.14	610	1400	1.79	0.07[b]	0.4	51.9

[a] Determined using Φ_f = 0.48 for PM 597 in methanol as the reference; λ_{exc}=500 nm.[102d] [b] Determined using Φ_f = 0.913 for RH 101 in ethanol as the reference; λ_{exc}=540 nm.[173] [c] The values of k_r and k_{nr} were calculated using the following equations: $k_r = \Phi_f / \tau_f$, $k_{nr} = (1-\Phi_f) / \tau_f$, assuming that the emitting state is produced with unit quantum efficiency.

The λ_{abs} (526 nm) and λ_{em} (579 nm) of dye **67** are red shifted by 33 nm and 75 nm, respectively than **18**. Thus the Stokes shift (1740cm^{-1}(53 nm)) of dye **67**is ~5 fold than that of **18**. The dye **67** has beautiful orange fluorescence although Φ_f is very low (4%). Similarly the λ_{abs} and λ_{em} of the dye **68** are 562 nm and 610 nm, respectively. The Stokes shift (48 nm) is ~4.5 fold than that of **18**. The dye **68** has very low red fluorescence (Φ_f = 0.07).

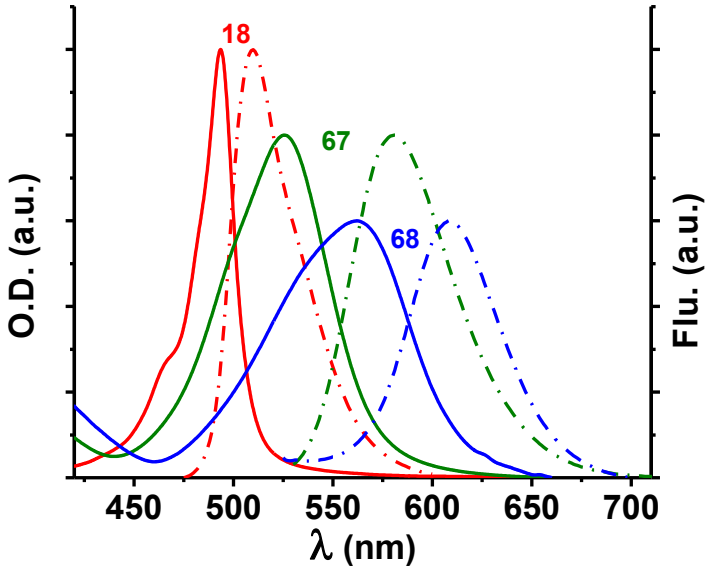

Figure 6.5.2.1: Normalized absorption (—) and fluorescence (- -) spectra of dyes **18**, **67** and **68** in methanol

6.5.3 Effect of solvent polarity:

To see the effect of solvent polarities in the photo-physical properties of dyes **67** and **68**, λ_{abs} and λ_{em} of both the dyes were recorded in different polar and non-polar solvents (Table 6.5.3.1). It is interesting that λ_{abs} of both the dyes showed negative solvatochromism with increasing the solvent polarity. In case of dye **67**, λ_{abs} is 16 nm blue shifted in methanol than that of in toluene. This blue shift is more in case of dye **68** (21 nm). The more stability of the ground state of both the dyes in polar solvents may be the reason for this negative solvatochromism. It is important to note that there is no effect on the λ_{em} of both the dyes on solvent polarities. As a result, Stokes shift of both the dyes are more in polar solvents than that of in non-polar solvents that would be useful in tuning the Stokes shift by merely changing the solvent polarities.

Table 6.5.3.1: λ_{abs}, λ_{em} and ν of **67** and **68** in different solvents at 25°C

Solvent	Dye 67			Dye 68		
	λ_{abs} (nm)	λ_{em} (nm)	ν (cm^{-1})	λ_{abs} (nm)	λ_{em} (nm)	ν (cm^{-1})
Methanol	526	579	1740	562	610	1400
Ethanol	529	583	1751	570	611	1177
Acetonitrile	529	579	1632	571	611	1146
n-Hexane	540	578	1217	581	611	845
Toluene	542	581	1238	583	617	945

6.5.4 Theoratical study:

In order to rationalize the high Stokes shift of the new dyes **67** and **68**, the geometry of the molecules at the ground state (S_0 state) and the S_1 excited state in methanol was optimized by density functional theory (DFT) method. The ground state (S_0) geometry of dye **67** was shown in Figure 6.5.4.1a. The dihedral angle between the imine substituent and the BODIPY moiety (C12-C13-C35-C36) is 42.5°. However, HOMO is spread over both the BODIPY and the imine moiety (Figure 6.5.4.3a), indicating that the π-conjugation between the imine moiety and the BODIPY core is remarkable even when the two moieties are not fully coplanar. This efficient π-conjugation shifts the color of the dye towards red side.

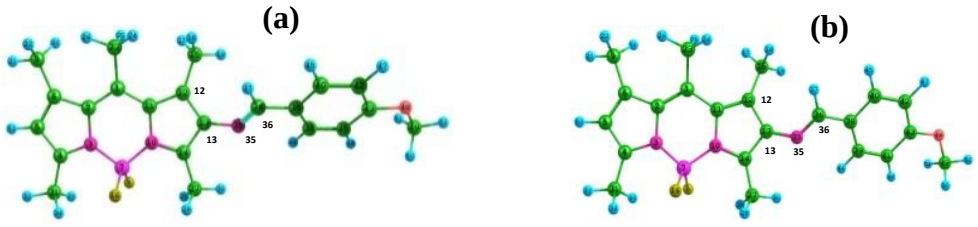

Figure 6.5.4.1: DFT-optimized structures of dye **67** (a) S_0 state and (b) S_1 state

The S_1 state geometry optimized in methanol solvent is shown in Figure 6.5.4.1b. The most prominent difference between the S_0 and S_1 state geometry is the dihedral angle between the BODIPY core and the imine moiety. Compared to the dihedral angle at S_0 state geometry (42.5°), the imine moiety become more coplanar at the optimized S_1 excited state, for which the dihedral angle is 18.9°. This geometry relaxation upon photo-excitation imparts remarkable effect on the energy level of the molecular orbitals which ultimately increases the Stokes shift.

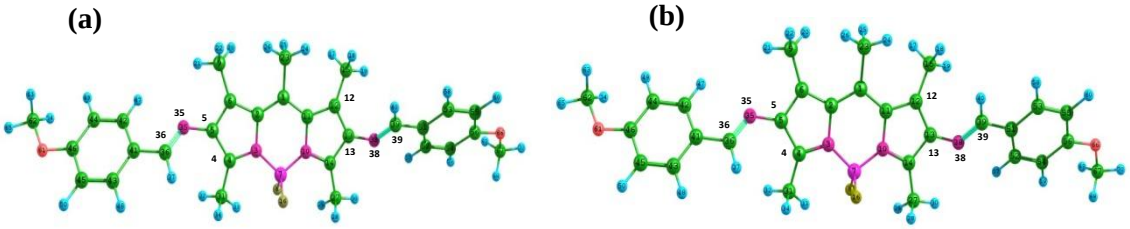

Figure 6.5.4.2: DFT-optimized structures of dye **68** (a) S_0 state and (b) S_1 state

In case of dye **68**, the HOMO is also spread over both the BODIPY (Figure 6.5.4.3b) and the imine moieties in the S_0 state, indicating that the π-conjugation between the imine moieties and the BODIPY core which red shifted the color of the dye. In the ground state (S_0) (Figure 6.5.4.2a) of dye **68**, the dihedral angles between the imine substituents and the Bodipy moiety i.e. C12-C13-C38-C39 and C4-C5-C35-C36 are 42.8° and 37.4° respectively which reduce to 27.2° and 31.6° respectively in S_1 state (Figure 6.5.4.2b). Thus, in this case also the molecular geometry relaxes upon excitation which ultimately increases the Stokes shift.

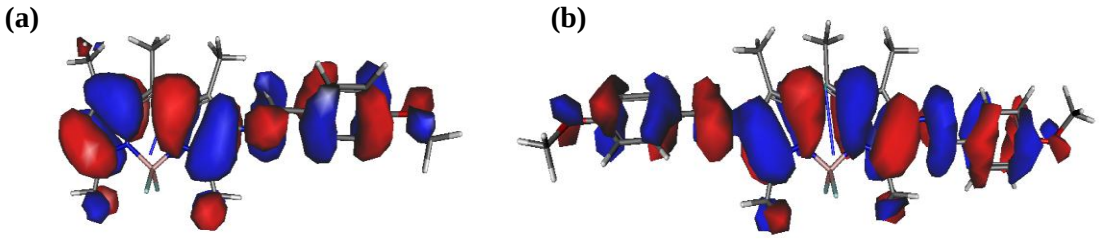

Figure 6.5.4.3: DFT-optimized HOMO of (a) dye **67** and (b) dye **68**

6.6 Use of dyes 67 and 68 as a proton sensor:

Because of the importance of pH measurement in various applications, optical pH sensors have attracted significant attention. Various organic dyes including the BODIPY fluorophore have been used to construct these optodes. The BODIPY-based fluorescent indicators have recently been highlighted in an excellent review.[155a] As the potential application of these dyes, their pH sensing abilities were tested. They were expected to act as colorimetric H^+ sensor as the imine bonds are known to be very sensitive to the acid environment. Thus with increasing addition of H^+, imine bond get cleaved and converted to the corresponding amine and then to the chloride salt. This conversion can nicely be identified by the change in the absorption and fluorescence spectra.

6.6.1 Absorption study:

Absorption titration was performed in ethanol with HCl and shown in Figure 6.6.1.1a. Addition of increasing concentrations of H^+ ion (HCl) to the dye **67** resulted in a dramatic color change from pink to yellow (Figure 6.6.2.1a), associated with a gradual decrease of the λ_{abs} at 529 nm and simultaneous growth of a new strong absorption band centered at 495 nm, which was shifted to 490 nm on addition of more H^+ (Figure 6.6.1.1b).

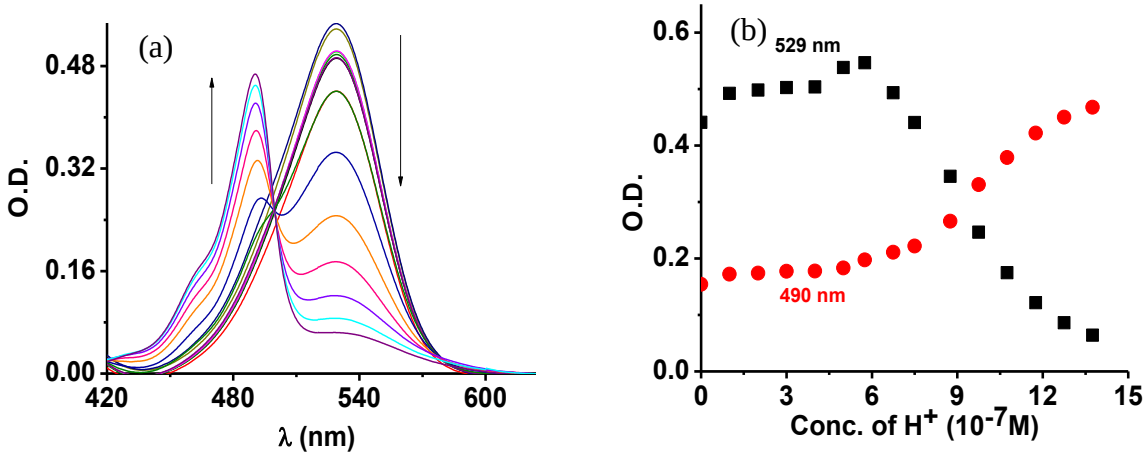

Figure 6.6.1.1: (a) Absorption spectrum of dye **67** (27.8µM) with addition of HCl in ethanol. (b) Change in absorption of dye **67** at 529 nm and 490 nm in the reaction with different conc. of HCl

Evidently, the dye **67** initially gets converted to the precursor amine **62**, and then to the corresponding chloride salt. This reaction was very fast, and the changes in the absorption peak at 490 nm and 529 nm reached their respective plateau values in 80 sec (Figure 6.6.1.2).

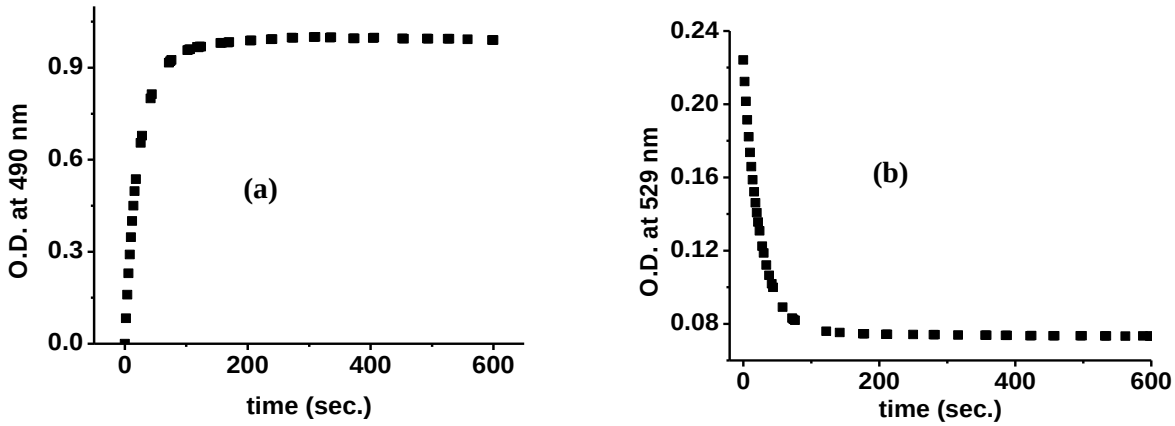

Figure 6.6.1.2: Time-dependent absorption changes of **67** (27.9 µM) in presence of HCl (1.4 µM) in water (a) λ_{max} = 490 nm; (b) λ_{max} = 529 nm

In case of the dye **68**, the two imine bonds got cleaved sequentially with the addition of H^+, resulting in a gradual conversion of the λ_{abs} at 570 nm to 525 nm corresponding to the monoimine dye, and ultimately to 495 nm for the chloride salt of **66** (Figure 6.6.1.3).

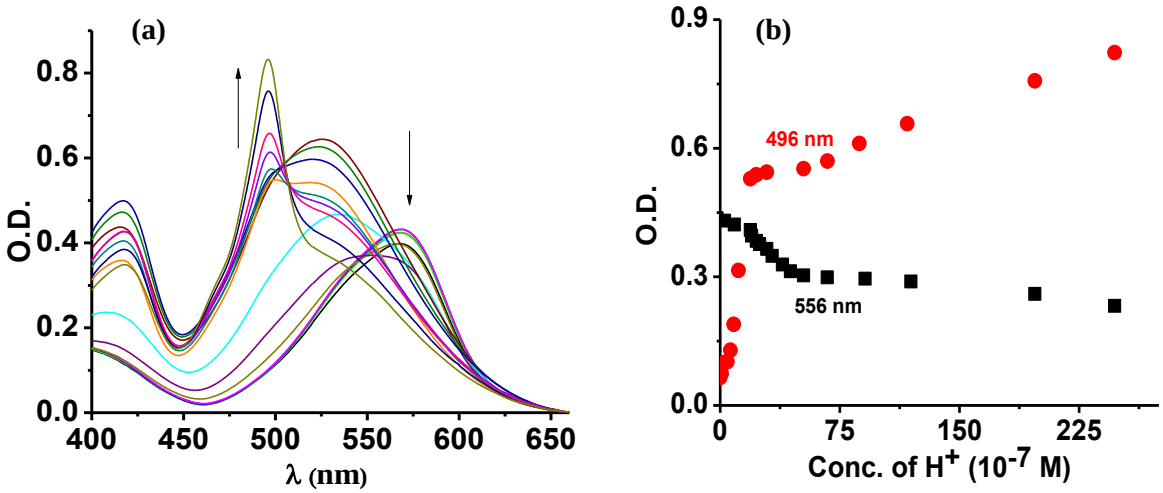

Figure 6.6.1.3: (a) Absorption spectrum of dye **68** (35µM). (b) Change in absorption of dye **68** at 556 nm and 496 nm in the reaction with different conc. of HCl

6.6.2 Steady-state fluorescence study:

In the fluorescence titration, the low orange fluorescence of the dye **67** changes to greenish yellow with increase in intensity. The λ_{em} of dye **67** (579 nm) blue shifted by 70 nm, which makes the quantitative measurements more easy and accurate (Figure 6.6.2.2). The colour and fluorescence changes of the dye **67** solution is distinctly visible (Figure 6.6.2.1b) in the entire test concentration range (pH 1.8-7.4). Further, the exaggerated blue shift (70 nm) of λ_{em} (580 nm) would provide more accurate quantitative measurements of pH (Figure 6.6.2.1a).

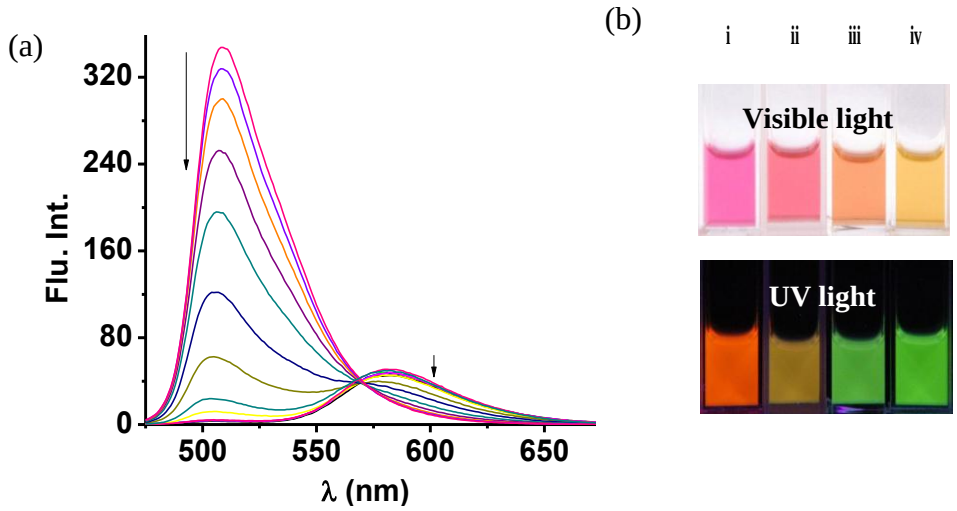

Figure 6.6.2.1: (a) Fluorescence titration plot of dye **67** (b) H^+ sensing by the dye **67** (27.8 μM) solution in ethanol was titrated with 0 μM, 0.2 μM, 0.5 μM, 1.2 μM aqueous HCl (i to iv) under visible and UV light.

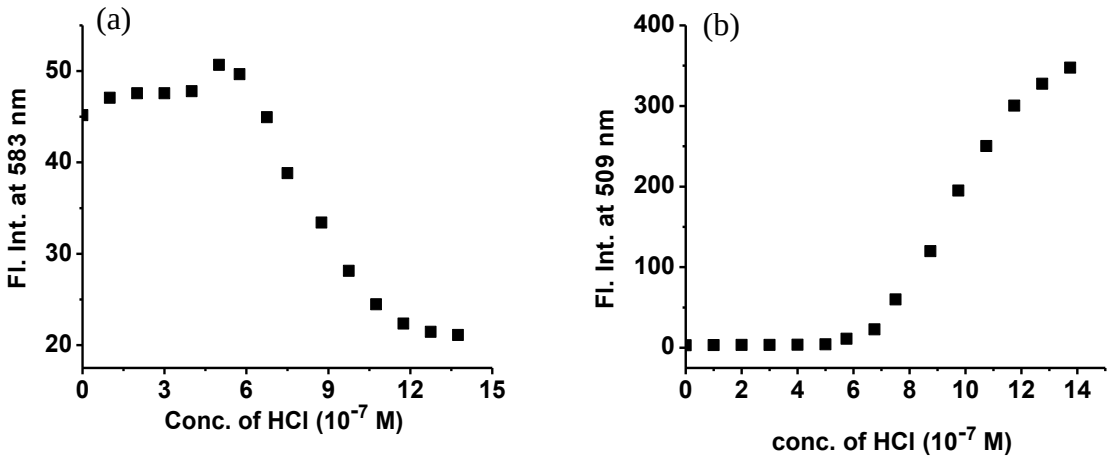

Figure 6.6.2.2: Change in Fluorescence of dye **67** (a) at 583 nm and (b) 509 nm in the reaction with different conc. of HCl

Similarly low red fluorescence of the dye **68** converted to greenish yellow fluorescence (Figure 6.6.2.3b). The λ_{em} peak at 610 nm of dye **68** decreases gradually and the peak at 517 nm increases (Figure 6.6.2.4), this wide difference in colour will be very helpful to measure the H^+ concentration very accurately. The change of fluorescence colour of the dye **68** solution from a week red (pH 8.2) to greenish yellow (pH 0.6) is also distinctly visible. The fluorescence spectra

and change in fluorescence peak intensity with acid were shown in Figure 6.6.2.3a and Figure 6.6.2.4.

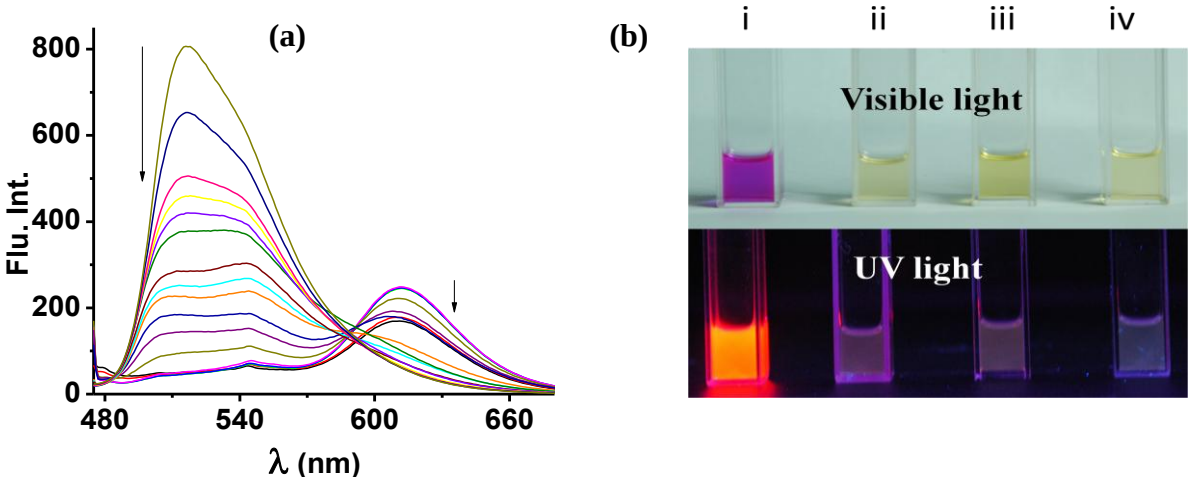

Figure 6.6.2.3: (a) Fluorescence titration plot of dye **68**; (b) H^+ sensing by the dye **68** (35 μM) solution in ethanol was titrated with 0 μM, 3.2 μM, 9.5 μM, 19.2 μM aqueous HCl (i to iv) under visible and UV light

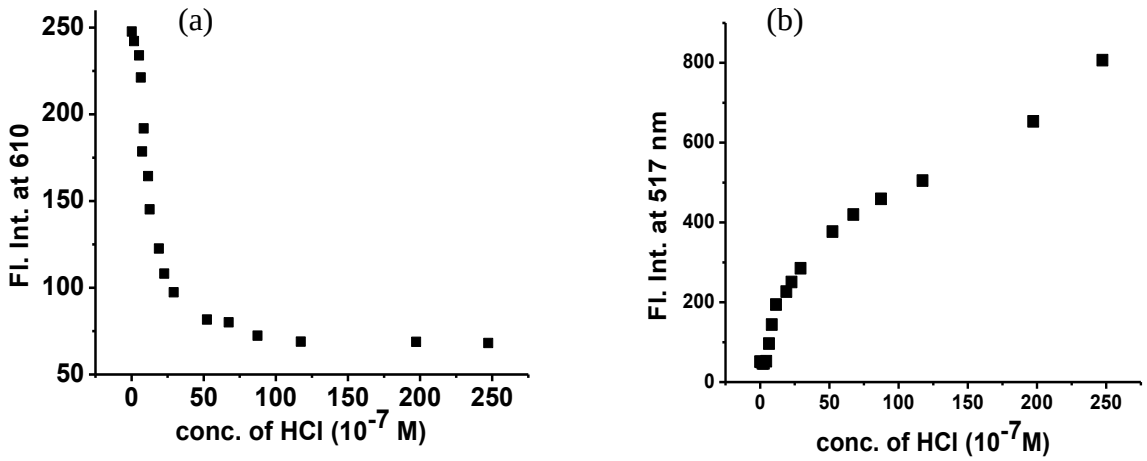

Figure 6.6.2.4: Change in Fluorescence of dye **68** (a) at 610 nm and (b) 517 nm in the reaction with different conc. of HCl

6.7 Conclusion:

The sensing mechanism of most of the optodes is based on changes in the emission intensities in presence of an analyte. The reported BODIPY-based H^+ sensors also relied on the

off-on/on-off fluorescence strategies. The main drawback of such strategy is that both the H^+ and the metal ions act in similar way to increase the fluorescence of the dyes thus can't discriminate between H^+ and other positively charged species.[160c] But with our strategy the H^+ concentration could accurately be estimated in presence of the metal ions also. More recently, several exotic energy transfer BODIPY systems, synthesized via multiple steps were found to detect H^+ as well as metal and quaternary ammonium ions.[174] Moreover, sensors, showing change in the absorption/emission wavelength maxima as a function of pH would be advantageous for practical use. But pH sensors with these attributes are rarely reported. The new imino-dyes **67** and **68** are highly selective in detecting and quantifying H^+ ions. Their H^+-sensing was also associated with changes in colour and fluorescent wavelengths.

Taken together, Both the *Schiff* bases have ~5 times higher Stokes shift than **18** and despite low fluorescence the above results clearly established that the dyes **67** and **68** can be used as efficient colorimetric as well as fluorimetric proton sensors.

SUMMARY

With an aim to design and development of novel fluorescent dyes having good solubility in organic and water (preferred) solvent for laser and sensor applications point of view, different dye molecules were synthesized and characterized. Important optical properties such as quantum yield of fluorescence, Stokes shift, molar extinction coefficient, fluorescence life time were evaluated by photo-physical study. Host-guest complexations using supramolecular strategy with relatively recent host cucurbit[7]uril (CB[7]) were studied for water soluble dyes. The highlights of the research work carried out during this period are given below.

Solvent mediated effect in lasing efficiency and photostability of new Bodipy dyes: For better lasing properties (lasing efficiency and photostability), effect of solvent on the lasing efficiency and photostability of known (**16** and **17**) BODIPY dyes as well as new derivative **58** after substitution at boron centre were studied. Laser study was performed using a second harmonic of a pulsed Nd:YAG laser. A large enhancement in photostability (~50-200 times) and improved lasing efficiency of dyes by changing from polar ethanol to no-npolar solvents like heptane and 1,4-dioxane was observed. The large improvement in photostability was correlated to rate of generation of singlet oxygen and its reactivity with dyes in solvents. These are rationalized by performing several spectroscopy techniques (pulse radiolysis, cyclic voltammetry, dye sensitized photooxidation etc.)

Design and development of new water soluble fluorescent dyes and their host guest study: Different water soluble fluorescent dyes were designed and synthesized via formation of ammonium salt at 7^{th} position of coumarin 1 and 2 or 6 position of BODIPY core, their purity was checked by $^{1}H/^{13}C$ NMR and mass spectroscopy techniques. Their poor solubility and low

quantum yield of fluorescence in water were significantly improved, adopting supramolecular interaction strategy, which was monitored using steady and time resolved absorption/ fluorescence, NMR spectroscopy techniques. Both form of coumarin 1 (cationic and neutral) dyes, upon complex formation with CB[7], showed a large enhancement in fluorescent intensity with improved laser photostability. In case of BODIPY derivatives, ammonium hydrochloride salt (**63**) make strong binding and 7 times enhancement in its fluorescence intensity with CB[7]. On the other hand, synthesized trimethyl substituted BODIPY dye (**64**) showed good electrostatic binding with DNA. Its fluorescence microscopy study revealed good uptake of dye by human lung cancer A549 cells. However it was not cytotoxic to the A 549 cells even up to 50 μM concentrations both under dark or photo irradiation condition.

Rational design and development of new BODIPY dyes with a large Stokes shift: The new red emitting Bodipy dyes containing imine group at 2 and/or 6 position of BODIPY core in place of the C-C bond was synthesized starting from the BODIPY **18** with good Stokes shift (~3.5-5.0 fold) compared to known BODIPY **16** because of the steric crowding and also impart solvatochromism. Large Stokes shift of both dyes was explained by calculating the geometry of dye molecules in ground and excited states via DFT method. Moreover, the presence of C=N bonds of both dyes are very sensitive towards acidic environment and demonstrated to be useful tool for pH sensing at low concentrations.

FUTURE SCOPE

1. Water soluble dye **64** (chapter 5) may be useful for high average power dye laser, excited by green component (at 510 nm) of the high repetition rate (10-20kHz) Cu-vapour lasers. We have not been able to study this aspect due to lack of CVLs in our lab. For dye **4** in which methyl groups are present at 1,3,5,7 and 8 positions, if we design and synthesize similar ammonium salt derivative with unsubstituted methyl bodipy, this is expected to reduce the steric crowding as well as size of dye molecule. This new dyes may become more suitable to make stronger complex with the host CB[7] with better photo-physical property and further would be useful for aqueous dye lasers.

2. Substitution at B-centre of **16** makes it suitable for long term use in high repetition rate dye lasers using non-polar solvents, pumped by DPSSGL (at 532 nm). Similarly, if same substitution is carried out at the B-centre of **17**, it may show excellent photostability as compared to **16** and its derivatives, which would be much more useful for high average power dye laser study.

3. The present theoretical calculations (B3LYP/TDDFT + PCM solvent model) would be extended for further modeling of new dyes in different solvents, with or without host molecule, for predicting photo-physical properties of new dyes, prior to synthesis, for dye laser applications.

REFERENCES

1. (a) Schäfer, F. P. *Dye Lasers* 3rd Ed., Springer-Verlag, Berlin, **1990**; (b) De Silva, A. Prasanna; Gunaratne, H. Q. N.; Gunnlaugsson, T.; Huxley, A. J. M.; McCoy, C. P.; Rademacher, J. T.; Rice, T. E. *Chem. Rev.* **1997**, *97*, 1515-1566.
2. (a) Valeur, B.; Leray, I. *Coord. Chem. Rev.* **2000**, *205*, 3-40; (b) Rurack, K.; Resch-Genger, U. *Chem. Soc. Rev.* **2002**, *31*, 116-127.
3. Zollinger, H. *Color Chemistry* 3rd Ed., Wiley-VCH, Zurich, **2003.**
4. Lakowicz, J. R. *Principles of Fluorescence Spectroscopy* 3rd Ed., Springer, Singapore, **2006**.
5. (a) Vogel, M.; Rettig, W.; Sens, R.; Drexhage, K. H. *Chem. Phys. Lett.* **1988**, *147*, 452 460; (b) Reisfeld, R.; Brusilovsky, D.; Eyal, M.; Miron, E.; Burstein, Z.; Ivri, J. *Chem. Phys. Lett.* **1989**, *160*, 43-56; (c) López Arbeloa, F.; Costela, A.; López Arbeloa, I. *J. Photochem. Photobiol. A* **1990**, *55*, 97-103; (d) López Arbeloa, F.; López Arbeloa, T.; López Arbeloa, I. *Trends Photochem. Photobiol.* **1994**, *3*, 145-155.
6. (a) López Arbeloa, T.; López Arbeloa, F.; López Arbeloa, I.; Costela, A.; García-Moreno, I.; Figuera, J. M.; Amat-Guerri, F.; Sastre, R. *J. Lumin.* **1997**, *75*, 309-317; (b) López Arbeloa, F.; López Arbeloa, T.; López Arbeloa, I.; Costela, A.; García-Moreno, I.; Figuera, J. M.; Amat-Guerri, F.; Sastre, R. *Appl. Phys. B* **1997**, *64*, 651-657; (c) Serova, V. N.; Chirkov, V. V.; Morozov, V. I.; Semashko, V. V.; Arkhireev, V. P. *Chem. Trans*. **1999**, *41*, 1409; (d) Huang, J.; Bekiari, V.; Lianos, P.; Couris, S. *J. Lumin.* **1999**, *81*, 285-291.

7. (a) Pavlopoulos, T. G. *IEEE J. Quantum electron*, **1973**, *9*, 510-516; (b) Schimistschek, E. J.; Trias, J. A.; Hammonod, P. R.; Atkins, R. L. *Optical commn.* **1974**, *11*, 351-355.

8. Pavlopoulos, T. G.; Hammonod, P. R. *J. Amer. Chem. Soc.* **1974**, *96*, 6568-6579.

9. Drexhage, K. H. *J. Res. Nat. Bur. Stand.* **1976**, *80*, 421-428

10. Schäfer, F. P. *Dye laser Topics in Applied Physics* New York: Springer-Verlag, **1973**, 1-8.

11. (a) Drexhage, K. H. *Topics in Applied Physics*, *Dye Lasers*, edited by Schäfer, F. P. (Springer, Barlin) **1973**, *1*, 161; (b) Fletcher, A. N.; Bliss, D. E. *Applied Phys.* **1978**, *16*, 289-295; (c) Atkins, R. L.; Bliss, D. E. *J. Org. Chem.* **1978**, *43*, 1975-1980; (d) Schimitschek, E. J.; Trias, J. A.; Hammond, P. R.; Henry, R. A.; Atkins, R. L. *Opt. Commun.* **1976**, *16*, 313-316.

12. Wang, Y. W.; Descalzo, A. B.; Shen, Z.; You, X. Z.; Rurack, K. *Chemistry* **2010**, *16*, 2887-2903.

13. (a) Pavlopoulos, T.; Boyer, J. H.; Shah, M.; Thangaraj, K.; Soong, M. L. *Appl. Optics* **1990**, *29*, 3885-3886; (b) Pavlopoulos, T.; Boyer, J. H.; Thangaraj, K.; Sathyamoorthi, G.; Shah, M. P.; Soong, M. L. *Appl. Optics* **1992**, *31*, 7089-7094; (c) Boyer, J. H.; Haag, A. M.; Satyamoorthi, G.; Soong, M. L.; Thangaraj, K.; Pavlopoulos, T. *Heteroat. Chem.* **1993**, *4*, 39-49.

14. (a) Ricardo, D.; Lucia, B. S.; Angel, C.; Inmaculada, G. M.; Roberto, S.; Alberto, U. A. *Appl. Opt.* **2003**, *42*, 1029-1035; (b) Pavlopoulos, T. G.; Shah, M.; Boyer, J. H. *Opt. Commun.* **1989**, *70*, 425-427.

15. (a) O'Neil, M. P. *Opt. Lett*. **1993**, *18*, 37-38; (b) Pavlopoulos, T.; Boyer, J. H. *Proc. SPIE- Int. Soc. Opt. Eng.* **1994**, *2115*, 231-239.

16. (a) Haughland, R. P.; Kang, H. C. US Patent US4774339 **1988**; (b) Monsma, F. J.; Barton, A. C.; Kang, H. C.; Brassard, D. L.; Haughland, R. P.; Sibley, D. R. *J. Neurochem.* **1989**, *52*, 1641-1644; (c) Saki, N.; Dine, T.; Akkaya, E. U. *Tetrahedron* **2006**, *62*, 2721-2725; (d) Sathyamoorthi, G.; Wolford, L. T.; Haag, A. M.; Boyer, J. H. *Heteroat. Chem.* **1994**, *5*, 245-249.

17. (a) Qin, W.; Rohand, T.; Baruah, M.; Stefan, A.; Auweraer, M. van der; Dehaen, W.; Boens, N. *Chem. Phys. Lett.* **2006**, *420*, 562-568; (b) Baruah, M.; Qin, W.; Vallce, R. A. L.; Beljonne, D.; Rohand, T.; Dehaen, W.; Boens, N. *Org. Lett*. **2005**, *7*, 4377-4380.

18. Goud, T. V.; Tutar, A.; Biellmann, J. -F. *Tetrahedron* **2006**, *62*, 5084-5091.

19. Jagtap, K. K.; Maity, D. K., Ray, A. K.; Dasgupta, K.; Ghosh, S. K. *Appl. Phys. B* **2011**, *103*, 917-924.

20. (a) Ulrich, G.; Goze, C.; Guardigli, M.; Roda, A.; Ziessel, R. *Angew Chem.* **2005**, *117*, 3760-3764; (b) Goze, C.; Ulrich, G.; Mallon, L. J.; Allen, B. D.; Harriman, A.; Ziessel, R. *J. Am. Chem. Soc.* **2006**, *128*, 10231-10239; (c) Goze, C.; Ulrich, G.; Ziessel, R. *J. Org. Chem.* **2007**, *72*, 313-322; (d) Goze, C.; Ulrich, G.; Ziessel, R. *Org. Lett.* **2006**, *8*, 4445-4448; (e) Ulrich, G.; Goeb, S.; Nicola, A. De; Retaileau, P.; Ziessel, R. *Synlett.* **2007**, 1517-1520; (f) Bonardi, L.; Ulrich, G.; Ziessel, R.; *Org. Lett.* **2008**, *10*, 2183-2186

21. (a) Harriman, A.; Izzet G.; Ziessel, R. *J. Am. Chem. Soc.* **2006**, *128*, 10868-10875; (b) Mula, S.; Ulrich, G.; Ziessel, R. *Tetrahedron Lett.* **2009**, *50*, 6383-6388.

22. (a) Namkung, W.; Padnawar, P.; Mills, A. D.; Verkman, A. S. *J. Am. Chem. Soc.* **2008**, *130*, 7794-7795; (b) Byrne, A. T.; O'Connor, A. E.; Hall, M.; Murtagh, J.; O'Neil, K.; Curran, K. M.; Mograin, K.; Rousseau, J. A.; Lecomte, R.; McGee, S.; Callanan, J. J.; O'Shea, D. F.; Gallagher, W. M. *Br. J. Cancer* **2009**, *101*, 1565-1573; (c) He, H.; Lo, P. -C.; Yeung, S. -L.; Fong, W. -P.; Ng, D. K. P. *J. Med. Chem.* **2011**, *54*, 3097-3102; (d) Gorman, A.; Killoran, J.; O'Shea, C.; Kenna, T.; Gallagher, W. M.; O'Shea, D. F. *J. Am. Chem. Soc.* **2004**, *106*, 10619-10631; (e) Niu, S. L.; Massif, C.; Ulrich, G.; Ziessel, R.; Renard, P. Y.; Romieu, A. *Org. Biomol. Chem.* **2011**, *9*, 66-69.

23. (a) Killoran, J.; Allen, L.; Gallagher, J. F.; Gallagher, W. M.; O'Shea, D. F. *Chem. Commun.* **2002**, *17*, 1862-1863; (b) Gallagher, W. M.; Allen, L. T.; O'Shea, C.; Kenna, T.; Hall, M.; Gorman, A.; Killoran, J.; O'Shea, D. F. *Br. J. Cancer* **2005**, *92*, 1702-1710; (c) Byrne, A.; Gallagher, W. M.; O'Shea, D. F. *J. Am. Chem. Soc.* **2005**, *127*, 16360-16311.

24. Lower, S. K.; Elsayed, M. A. *Chem. Rev.* **1966**, *66*, 199-241.

25. Coskun, A.; Deniz, E.; Akkaya, E. U. *Org. Lett.* **2005**, *7*, 5187-5189.

26. (a) Rohand, T.; Baruah, M.; Qin, W.; Boenes, N.; Dehean, W. *Chem. Commun.* **2006**, 266-268; (b) Rohand, T.; Qin, W.; Boenes, N.; Dehean, W. *Eur. J. Org. Chem.* **2006**, 4658-4663.

27. Valeur, B. *Molecular fluorescence*, Wiley-VCH, Weinheim, **2002**.

28. (a) Kollmannsberger, M.; Gareis, T.; Heinl, S.; Breu, J.; Daub, J. *Angew. Chem.* **1997**, *109*, 1391-1393; (b) Kollmannsberger, M.; Gareis, T.; Heinl, S.; Breu, J.; Daub, J. *Angew. Chem. Int. Ed. Engl.* **1997**, *36*, 1333-1335.

29. Rohatgi-Mukherjee, K. K. *Fundamentals of Photochemistry* Wiley Eastern Ltd. India, **1986**.

30. (a) Browell, E. V. *Opt. Photon News 2* **1991**, *10*, 8-11; (b) Goldman, L.; Duarte, F. J.; Hillman, Eds. L. W. *Laser Principles Academic, New York* **1990**, 419-432.

31. Ghanadzadeh, A.; Ghanadzadeh, H.; Ghasmi, G. *J. Mol. Liq.* **2000**, *88*, 299-308.

32. (a) Dsouza, R. N.; Pischel, U.; Nau, W. M. *Chem. Rev.* **2011**, *111*, 7941-7981; (b) Bhasikuttan, A. C.; Pal, H.; Mohanty, J. *Chem. Commun.* **2011**, *47*, 9959-9971.

33. (a) Wang, R.; Yuan, L.; Ihmels, H.; Macartney, D. H. *Chem.- Eur. J.* **2007**, *13*, 6468-6473; (b) Villalonga, R.; Cao, R.; Fragosa, A. *Chem. Rev.* **2007**, *107*, 3088-3116; (c) Wang, R.; Yuan, L.; Macartney, D. H. *Chem. Commun.* **2005**, 5867-5869; (d) Pluth, M. D.; Bergman, R. G.; Raymond, K. N. *Science* **2007**, *316*, 85-88.

34. (a) Frampton, M. J.; Anderson, H. L. *Angew. Chem. Int. Ed.* **2007**, *46*, 1028-1064; (b) Brewster, M. E.; Loftsson, T. *Adv. Drug Delivery Rev.* **2007**, *59*, 645-666; (c) Szejtli, J. *Cyclodextrins: Applications in Encyclopedia of Supramolecular chemistry* Atwood, J. L.; Steed, J. W.; Eds., Marcel Dekker Inc: New York, **2004**, 398-413; (d) Nau, W. M.; Zhang, X. *J. Am. Chem. Soc.* **1999**, *121*, 8022-8032.

35. (a) Mohanty, J.; Jagtap. K.; Ray, A. K.; Nau, W. M.; Pal, H. *Chem. Phys. Chem.* **2010**, *11*, 3333-3338; (b) Shaikh, M.; Mohanty, J.; Bhasikuttan, A. C.; Uzunov, V. D.; Nau, W. M.; Pal, H. *Chem. Commun.* **2008**, 3681-3683; (c) Shaikh, M.; Dutta Choudhury, S.; Mohanty, J.; Bhasikuttan, A. C.; Pal, H. *Phys. Chem. Chem. Phys.* **2010**, *12*, 7050-7055.

36. (a) Kandoth, N.; Dutta Choudhury, S.; Mohanty, J.; Bhasikuttan, A. C.; Pal, H. *J. Phys. Chem. B* **2010**, *114*, 2617-2626; (b) Burai, T. N.; Bag, N.; Agarwal, S.; Iyer, E. S. S.; Dutta, A. *Chem. Phys. Lett.* **2010**, *495*, 208-211.

37. Szejtli, J. *Chem. Rev.* **1998**, *98*, 1743-1753.

38. Sansone, F.; Baldini, L.; Casnati, A.; Ungaro, R. *New J. Chem.* **2010**, *34*, 2715-2728.

39. Astruc, D.; Boisselier, E.; Ornelas, C. *Chem. Rev.* **2010**, *110*, 1857-1959.

40. Biros, S. M.; Rebek, J. *Jr. Chem. Soc. Rev.* **2007**, *36*, 93-104.

41. Lagona, J.; Mukhophadhyay, S.; Chakrabarti, S.; Isaacs, L. *Angew. Chem. Int. Ed.* **2005**, *44*, 4844-4870

42. (a) Mock, W. L. *Top. Curr. Chem.* **1995**, *175*, 1-24; (b) Mock, W. L.; Atwood, J. L.; Davies, J. E. D.; MacNicol, D. D.; Vogle, F.; Lehn (eds.), J. M. *Chapter-15: Cucurbituril In Comprehensive Supramolecular Chemistry*, Pergamon: New York **1996**, *2*, 477-493

43. Kim, J.; Jung, I. -S.; Kim, S. -Y.; Lee, E.; Kang, J. -K.; Sakamoto, S.; Yamaguchi, K.; Kim, K. *J. Am. Chem. Soc.* **2000**, *122*, 540-541.

44. Day, A.; Arnold, A. P.; Blanch, R. J.; Snushall, B. *J. Org. Chem.* **2001**, *66*, 8094-8100.

45. (a) Isaacs, L. *Chem. Commun.* **2009**, 619-629; (b) Lee, J. W.; Samal, S.; Selvapalam, N.; Kim, H. -J.; Kim, K. *Acc. Chem. Res.* **2003**, *36*, 621-630

46. Márquez, C.; Hung, F.; Nau, W. M. *IEEE Trans. Nano Biosci.* **2004**, *3*, 39-45.

47. Márquez, C.; Hudgins, R. R.; Nau, W. M. *J. Am. Chem. Soc.* **2004**, *126*, 5806-5816.

48. Mohanty, J.; Nau, W. M. *Angew. Chem. Int. Ed.* **2005**, *44*, 3750-3754.

49. (a) Wheate, N. J.; Day, A. I.; Blanch, R. J.; Arnold, A. P.; Cullinane, C.; Colline, J. G. *Chem. Commun.* **2004**, 1424-1425; (b) Bali, M. S.; Buck, D. P.; Coe, A. J.; Day, A. I.;

Collins, J. G. *Dalton Trans.* **2006**, 5337-5344; (c) Kemp, S.; Wheate, N. J.; Wang, S.; Collins, J. G.; Ralph, S. F.; Day, A. I.; Hughs, V. J.; Aldrich-Wright J. R. *J. Biol. Inorg. Chem.* **2007**, *12*, 969-979.

50. Jeon, Y. J.; Kim, S. -Y.; Ko, Y. H.; Sakamoto, S.; Yamaguchi, K.; Kim, K. *Org. Biomol. Chem.* **2005**, *3*, 2122-2125.

51. Buck, D. P.; Abeysinghe, P. M.; Cullinane, C.; Day, A. I.; Collins, J. G.; Harding, M. M. *Dalton Trans.* **2008**, 2328-2334.

52. Zhao, Y.; Buck, D. P.; Morris, D. L.; Pourgholami, M. H.; Day, A. I.; Collins, J. G. *Org. Biomol. Chem.* **2008**, *6*, 4509-4515.

53. Dong, N.; Xue, S. -F.; Zhu, Q. -J.; Tao, Z.; Zhao, Y.; Yang, L. X. *Supramol. Chem.* **2008**, *20*, 659-665.

54. Wheate, N. J.; Buck, D. P.; Day, A. I.; Collins, J. G. *Dalton Trans.* **2006**, 451-458.

55. (a) Park, K. M.; Suh, K.; Jung, H.; Lee, D. -W.; Ahn, Y.; Kim, J.; Baek, K.; Kim, K. *Chem. Commun.* **2009**, *1*, 71-73; (b) Kim, D.; Kim, E.; Kim, J.; Park, K. M.; Baek, K.; Jung, M.; Ko, Y. -H.; Sung, W.; Kim, H. S.; Suh, J. H.; Park, C. G.; Na, O. S.; Li, D.; Lee, K. E.; Han, S. S.; Kim, K. *Angew. Chem. Int. Ed.* **2007**, *46*, 3471-3474.

56. Saleh, N.; Koner, A. L.; Nau, W. M. *Angew. Chem. Int. Ed.* **2008**, *47*, 5398-5401.

57. Wang, R.; Macartney, D. H. *Org. Biomol. Chem.* **2008**, *6*, 1955-1960.

58. Wang, R.; MacGillivray, B. C.; Macartney, D. H. *Dalton Trans.* **2009**, 3584-3589.

59. Rekharsky, M. V.; Yamamura, H.; Ko, Y. H.; Selvapalam, N.; Kim, K.; Inoue, Y. *Chem. Commun.* **2008**, 2236-2238.

60. (a) Hennig, A.; Bakirci, H.; Nau, W. M. *Nat. Methods* **2007**, *4*, 629-632; (b) Bailey, D. M.; Hennig, A.; Uzunova, V. D.; Nau, W. M. *Chem. Eur. J.* **2008**, *14*, 6069-6077.

61. Hwang, I.; Baek, K.; Jung, M.; Kim, Y.; Park, K. M.; Lee, D. -W.; Selvapalam, N.; Kim, K. *J. Am. Chem. Sci.* **2007**, *129*, 4170-4171.

62. (a) Karcher, S.; Kornmuller, A.; Jekel, M. *Water Res.* **2001**, *35*, 3309-3316; (b) Kornmuller, A.; Karcher, S.; Jekel, M. *Water Res.* **2001**, *35*, 3317-3324; (c) Karcher, S.; Kornmuller, A.; Jekel, M. *Water Sci. Tech.* **1999**, *40*, 425-433.

63. Mock, W. L.; Pierpont, J. *J. Chem. Soc., Chem. Commun*. **1990**, 1509-1511.

64. Sindelar, V.; Silvi, S.; Kaifer, A. E. *Chem. Commun.* **2006**, *20*, 2185-2187.

65. Birks, J. B. *Photo Physics of Aromatic Molecules* Wiley-Interscience, New York; **1970**

66. Gilbert, A.; Baggott, J.; Wagner, P. J. *Essential of Molecular Photochemistry* Blackwell Science Inc., Cambridge, USA; **1991**

67. Williams, A. T. R.; Winfield, S. A.; Miller, J. N. *Analyst* **1983**, *108*, 1067-1071

68. Becker, W. *Advanced Time Correlated Single Photon Counting Technique* Springer, New York; **2005**

69. Demas, J. N. *Excited State Lifetime Measurement* Academic press, New York; **1983**

70. O'Connor, D. V.; Phillips, D. *Time Correlated Single Photon Counting* Academic, New York; **1984**

71. Ware, W. R. *Creation and Detection of the Excited State* (Lamola, A. A.; Ed.), Marcel Dekker: New York, Vol. **1**, Part A **1971**

72. Bevington, P. R. *Data Reduction and Error Analysis for the Physical Sciences* McGraw- Hill, New York; **1969**

73. Ito, M.; Kume, H.; Oba, K. *IEEE Trans. Nucl. Sci. NS-31* **1984**, *1*, 408-412

74. Ray, A. K.; Kundu, S.; Sasikumar, S.; Rao, C. S.; Mula, S.; Sinha, S.; Dasgupta, K. *Appl. Phys. B* **2007**, *87*, 483-488

75. Becke, A. D. *J. Chem. Phys.* **1993**, *98*, 5648-5652

76. Lee, C.; Yang, W.; Parr, R. G. *Phys. Rev. B* **1988**, *37*, 785-789

77. Barone, V.; Cossi, M. *J. Phys. Chem. A* **1998**, *102*, 1995-2001

78. Schmidt, M. W.; Baldridge, K. K.; Boatz, J. A.; Elbert, S. T.; Gordon, M. S.; Jensen, J. H.; Koseki, S.; Matsunaga, N.; Nguyen, K. A.; Su, S. J.; Windus, T. L.; Dupuis, M.; Montgomery, J. A. *J. Comput. Chem* **1993**, *14*, 1347-1363

79. Choudhury, S. D.; Mohanty, J.; Pal, H.; Bhasikuttan, A. C. *J. Am. Chem. Soc* **2010**, *132*, 1395-1401

80. Choudhury, S. D.; Mohanty, J.; Upadhyaya, H. P.; Bhasikuttan, A. C.; Pal, H. *J. Phys.Chem. B* **2009**, *113*, 1891-1898

81. Mohanty, J.; Bhasikuttan, A. C.; Nau, W. M.; Pal, H. *J. Phys. Chem. B* **2006**, *110*, 5132-5138

82. Mohanty, J.; Choudhury, S. D.; Upadhyaya, H. P.; Bhasikuttan, A. C.; Pal, H. *Chem. A. Eur. J* **2009**, *15*, 5215-5219

83. Klock, C.; Dsouza, R. N.; Nau, W. M. *Organic Letters* **2009**, *11*, 2595-2598

84. Hu, J.; Cheng, Y.; Wu, Q.; Zhao, L.; Xu, T. *J. Phys. Chem. B* **2009**, *113*, 10650-10659

85. Lodish, H.; Berk, A.; Kaiser, C. A. *Molecular Cell Biology* (W. H. Freeman, & Co) **2008**, 973

86. Santo, M.; Fox, M. *J. Phys. Org. Chem.* **1999**, *12*, 293-307

87. Sun, S.; Zhang, R.; Andersson, S.; Pan, J.; Zou, D. *J. Phys. Chem. B* **2007**, *111*, 13357-13363

88. Keene, P. J. *Quaderni dell'Area di Ricerca dell'Emilia-Romagna* **1972**, *1*, 63

89. Schmidt, K. H.; Buck, W. L. *Science* **1966**, *151*, 70-71

90. Smaller, B.; Remko, J. R.; Avery, E. C. *J. Chem. Phys* **1968**, *48*, 5174-5181

91. Zagorski, Z. P.; Sehested, K. *Pulse Radiolysis* (Eds. Ebert, M.; Keene, J. P.; Swallow, A. J.; Baxendale, J. H.), Academic Press, New York-London; 29, **1965**

92. Buxton, G. V.; Stuart, C. R. *J. Chem. Soc. Faraday Trans* **1995**, *91*, 279-281

93. Randles, J. *Trans. Far. Soc.* **1948**, *44*, 327-338

94. Sorokin, P. P.; Lankard, J. R. *IBMJ J. Res. Dev.* **1966**, *10*, 162-163.

95. (a) Drexhage, *Dye Laser*, 3rd edn., in : Schäfer (Ed.), *Topics Applied Physics*, Vol 1 (Springer, Barlin, **1990**) pp. 187-200; (b) Maeda, M. *Laser Dyes, Properties of Organic Compounds For Dye Lasers* (Academic Press, New York, **1984**)

96. Shah, M.; Thangaraj, K.; Soong, M. -L.; Wolford, L. T.; Boyer, J. H.; Politzer, I. R.; Pavlopoulos, T. G. *Heteroat. Chem.* **1990**, *1*, 389-399.

97. Guggenheimer, S. C.; Boyer, J. H.; Thangaraj, K.; Shah, M. P.; Soong, M. -L.; Povlopoulos, T. *Appl. Opt.* **1993**, *32*, 3942-3943.

98. (a) Mula, S.; Ray, A. K.; Banerjee, M.; Choudhuri, T.; Dasgupta, K.; Chattopadhaya S. *J. Org. Chem.* **2008**, *73*, 2146-2154; (b) Rahn, M. D.; King, T. A. *Appl. Opt.* **1995**, *34*, 8260-8271; (c) Jones, G. H.; Klueve, O.; Kumar, S.; Pacheco, D. *Solid State Lasers SPIE* **2001**, *24*, 4267-4271.

99. Pavlopoulos, T.; Boyer, J. H. *Proc. SPIE Int. Opt. Eng.* **1994**, *2115*, 231-239.

100. Jones II, G.; Kumar, S.; Klueva, O.; Pacheco, D. *J. Phys. Chem. A* **2003**, *107*, 8429-8434.

101. (a) Arbeloa, T. L.; Arbeloa, F. L.; Arbeloa, I. L.; García-Moreno, I.; Costela, A.; Sastre, R.; Amat-Guerri, F. *Chem. Phys. Lett.* **1999**, *299*, 315-321; (b) Costela, A.; García-Moreno, I.; Carraseoso, M. L.; Sastre, R. *Opt. Commun.* **2002**, *201*, 437-445;

(c) Duran-Sampedro, I.; Esnal, I.; Agarrabeitia, A. R.; Prieto, J. B.; Cerdán, L.; García-Moreno, I.; Costela, A.; Arbeloa, I. L.; Ortiz, M. J. *Chem. Eur. J.* **2014**, *20*, 1-19.

102. (a) Rahn, M. D.; King, T. A.; Gorman, A. A.; Hamblett, I. *Appl. Opt.* **1997**, *24*, 5862; (b) Ahmed, M.; King, T. A.; Ko, Do- Keong; Cha, B. H.; Lee, J. *Optics Communication* **2002**, *203*, 327-334; (c) Arbeloa, F. L.; Arbeloa, T. L.; Arbeloa, I. L.; García-Moreno, I.; Costela, A.; Sastre, R.; Amat-Guerri, F. *Chemical Physics* **1998**, *236*, 331-341; (d) Prieto, J. Bañuelos; Arbeloa, F. L.; Martínez, V. M.; López, T. A.; Arbeloa, I. L. *J. Phys. Chem. A* **2004**, *108*, 5503-5508.

103. Guha, S. N.; Moorthy, P. N.; Kishore, K., Naik, D. B.; Rao, K. N. *Proc. Indian Acad. Sci. (Chem. Sci.)* **1987**, *99*, 261-271.

104. (a) Hurst, J. R.; Mc Donald, J. D.; Schuster, G. B. *J. Am. Chem. Soc.* **1982**, *104*, 2065-2067; (b) Battino, R.; Rettich, T. R.; Tominaga, T. *Solubility of Oxygen and Ozone in Liquids J. Phys. Chem*. **1983**, *2*, 164-177.

105. (a) Yogo, T.; Urano, Y.; Ishitsuka, Y.; Maniwa, F.; Nagano, T. *J. Am. Chem. Soc.* **2005**, *127*, 12162-12163; (b) Adarsh, N.; Avirah, R. R.; Ramaiah, D. *Org. Lett.* **2010**, *12*, 5720-5723; (c) Lim, S. H.; Thivierge, C.; Nowak-Sliwinska, P.; Han, J.; Bergh, H. V. D.; Wagniéres, G.; Burgess, K.; Lee, H. B. *J. Med. Chem.* **2010**, *53*, 2865-2874.

106. Markel, P. B.; Kearns, D. R. *J. Am. Chem. Soc.* **1975**, *97*, 462-463.

107. Turro, N. J.; Ramamurthy, Vaidhyanathan; Scaiano, J. C. in *Modern Molecular Photochemistry of Organic Molecules, Chapter 14, Oxygen in Organic Photochemistry*, University Science Books, Sausalito, CA, **2010**.

108. Jagtap, K. K.; Shivran, N.; Mula, S.; Naik, D. B.; Sarkar, S. K.; Mukherjee, T.; Maity, D. K.; Ray, A. K. *Chem. Eur. J.* **2013**, *19*, 702-708.

109. (a) Álvarez, M.; Costela, A.; García-Moreno, I.; Amat-Guerri, F.; Liras, M.; Sastre, R.; Arbeloa, F. L.; Prieto, J. Bañuelos; Arbeloa, J. L. *Photochem. Photobiol. Sci.* **2008**, *7*, 802-813; (b) Orth, K.; Beck, G.; Genze, F.; Ruck, A. *J. Photochemistry & Photobiology B* **2000**, *57*, 186-192.

110. (a) Kee, H. L.; Kirmaier, C.; Yu, L.; Thamyongkit, P.; Youngblood, W. J.; Calder, M. E.; Ramos, L.; Noll, B. C.; Bocian, D. F.; Scheidt, W. R.; Birge, R. R.; Lindsey, J. S.; Holten, D. *J. Phys. Chem. B* **2005**, *109*, 20433-20443; (b) Chaudhuri, T.; Mula, S.; Chattopadhyay, S.; Banerjee, M. *Spectrochim. Acta Part A* **2010**, *75*, 739-744.

111. (a) Susdorf, T.; Álvarez, M.; Holzer, W.; Penzkofer, A.; Amat-Guerri, F.; Liras, M.; Costela, A.; García-Moreno, I.; Sastre, R. *Chem. Phys.* **2005**, *312*, 151-158; (b) Susdorf, T.; Agua, D. Del; Tyagi, A.; Penzkofer, A.; García, O.; Sastre, R.; Costela, A.; García-Moreno, I. *Appl. Phys. B* **2007**, *86*, 537-545; (c) Tyagi, A.; Agua, D. Del; Penzkofer, A.; García, O.; Sastre, R.; Costela, A.; García-Moreno, I. *Chem. Phys.* **2007**, *342*, 201-214.

112. Mula, S.; Elliott, K.; Harriman, A.; Ziessel, R. *J. Phys. Chem. A* **2010**, *114*, 10515-10522.

113. Pattabiraman, M.; Natrajan, A.; Kaliappan, R.; Mague, J. T.; Ramamurthy, V. *Chem. Commun.* **2005**, 4542-4544.

114. Huang, W. H.; Zavalij, P. Y.; Isaacs, L. *Angew Chem. Int. Ed*. **2007**, *46*, 7425-7427.

115. Croma, A.; Gracía, H.; Navajas, P. M.; Primo, A.; Calvino, J. J.; Trasobares, S. *Chem. –Eur. J*. **2007**, *13*, 6359-6364.

116. Sindelar, V.; Silvi, S.; Parker, S. A.; Sobransingh, D.; Kaifer, A. E. *Avd. Funct. Mater*. **2007**, *17*, 694-701.

117. Hedges, A. R. *Chem. Rev*. **1998**, *98*, 2035-2044.

118. Uekama, K.; Hirayama, F.; Irie, T. *Chem Rev*. **1998**, *98*, 2045-2076.

119. Soufi, W. A.; Reija, B.; Felekyan, S.; Seidel, C. A. M.; Novo, M. *ChemPhysChem* **2008**, *9*, 1819-1827.

120. (a) Wyman, I. W.; Macartney, D. H. *Org. Biomol. Chem.* **2010**, *8*, 247-252; (b) Hettiarachchi, G.; Nguyen, D.; Wu, J.; Lucas, D.; Ma, D.; Isaacs, L.; Briken V. *PLoS One* **2010**, *5*, e10514; (c) Uzunova, V. D.; Cullinane, C.; Brix, K.; Nau, W. M.; Day, A. I. *Org. Biomol. Chem*. **2010**, *8*, 2037-2042; (d) Nau, W. M. *Nature Chemistry* **2010**, *2*, 248-250.

121. (a) Kim, K. *Chem. Soc. Rev.* **2002**, *31*, 96-107; (b) Jeon, W. S.; Moon, K.; Park, S. H.; Chun, H.; Ho, Y. K.; Lee, J. Y.; Lee, S. E.; Samal, S.; Selvapalam, N.; Rekharsky, M. V.; Sindelar, V.; Sobransingh, D.; Inoue, Y.; Kaifer, A. E.; Kim, K. *J. Am. Chem. Soc.* **2005**, *127*, 12984-12989.

122. Arunkumar, E.; Forbes, C. C.; Smith, B. D. *Eur. J. Org. Chem*. **2005**, 4051-4059.

123. Halterman, R. L.; Moore, J. L.; Yakshe, K. A.; Halterman, J. A. I.; Woodson, K. A. *J. Incl. Phenom. Macrocycl. Chem.* **2010**, *66*, 231-241

124. (a) Wagner, B. D. *Molecules* **2009**, *14*, 210-237; (b) Seth, D.; Chakroborty, A.; Setua, P.; Sarkar, N. *Langmuir* **2006**, *22*, 7768-7775; (c) Guan, H.; Zhu, L.; Zhou, H.; Tang,

H. *Anal. Chim. Acta* **2008**, *608*, 73-78; (d) Kuznetsova, N. A.; Kalia, O. L. *Russian Chemical Reviews* **1992**, *7*, 683-696.

125. (a) Wang, R.; Bardelang, D.; Waite, M.; Udachin, K. A.; Leek, D. M.; Yu, K.; Ratcliffe, C. I.; Ripmeester, J. A. *Org. Biomol. Chem*. **2009**, *7*, 2435-2439; (b) Barooah, N.; Pemberton, B. C.; Sivaguru, J. *Org. Lett*. **2008**, *10*, 3339-3342; (c) Nau, W. M.; Mohanty, J. *Inter. J. Photoenergy* **2005**, *7*, 133-141.

126. Jones (II), G.; Jacson, W. R.; Choi, C. Y.; Bergmark, W. R. *J. Phys. Chem*. **1985**, *89*, 294-300.

127. Chen, W.; Gordon, M. S. *J. Phys. Chem*. **1996**, *100*, 14316-14328.

128. Son, M. E. Perel; Zvolinskii, V. P.; Sheinker, Yu. N. *Band of quaternary amines group Infrared and Raman Characteristic Group Frequencies*, George Socrates, 3rd Edition Willey **2011.**

129. (a) Kubin, R. F.; Fletcher, A. N. *Chem. Phys. Lett.* **1983**, *99*, 49-52; (b) Yoshizawa, M.; Klosterman, J. K.; Fujita, M. *Angew. Chem. Int. Ed.* **2009**, *48*, 3418-3438; (c) Brackmann, U. *Lambdachrome Laser Dyes*, Lambda Physik Gmbh., Gottingen, D-3400 **1986,** pg-III-66-67**;** (d) Arbeloa, T. L.; Arbeloa, F. L.; Tapia, M. J.; Arbeloa, I. L. *J. Phys. Chem*. **1993**, *97*, 4704-4707.

130. Moog, R. S.; Kim, D. D.; Oberle, J. J.; Ostrowski, S. G. *J. Phys. Chem. A* **2004**, *108*, 9294-9301.

131. Nau, W. M.; Florea, M.; Assaf, K. I. *Israel Journal of Chemistry* **2011**, *51*, 559-577.

132. Singh, M. K.; Pal, H.; Koti, A. S. R.; Sapre, A. V. *J. Phys. Chem. A* **2004**, *108*, 1465-1474.

133. Gustavasson, T.; Cassara, L.; Marguet, S.; Gurzadyan, G.; Meulen, P. V. D.; Pommeret, S.; Mialocq, J. -C. *Photochem. Photobiol. Sci*. **2003**, *2*, 329-341.

134. G. R. Flemming, *Chemical Applications of Ultrafast Spectroscopy, Oxford University Press* **1986**.

135. Grimme, S. Semiempirical GGA-type density functional constructed with a long-range dispersion correction *J. Comp. Chem.* **2006**, *27***,** 1787-1799.

136. Drexhage, K. H.; Erickson, G. R.; Hawks, G. H.; Reynolds, G. A. *Opt. Commun.* **1975**, *15*, 399-403.

137. (a) Schäfer, F. P. ed., Dye laser, 2nd Ed. (Springer, Berlin, **1977**); (b) Chambers, R. W.; Kajiwarn, T.; Keams, D. R. *J. Phys. Chem.* **1974**, *78*, 380-387.

138. (a) Saleh, N.; Al-Rawashdeh, N. A. F. *J. Fluoresc.* **2006**, *16*, 487-493; (b) Rankin, M. A.; Wagner, B. D. *Supramol. Chem.* **2004**, *16*, 513-519; (c) Baglole, K. N.; Boland, P. G.; Wagner, B. D. *J. Photochem. Photobiol., A* **2005**, *173*, 230-237; (d) del Pozo, M.; Hernandez, L.; Quintana, C. *Talanta* **2010**, *81*, 1542-1546; (e) Megyesi, M.; Biczok, L.; Jablonkai, I. *J. Phys. Chem. C* **2008**, *112*, 3410-3416; (f) Yang, J. Y.; Shen, A. Z.; Du, L. M.; Li, C. F.; Wu, H.; Chang, Y. X. Chin. *J. Anal. Chem.* **2010**, *38*, 1813-1816.

139. (a) Li, C. J.; Li, J.; Jia, X. S. *Org. Biomol. Chem.* **2009**, *7*, 2699-2703; (b) Zhou, Y. Y.; Sun, J. Y.; Yu, H. P.; Wu, L.; Wang, L. *Supramol. Chem.* **2009**, *21*, 495-501; (c) Li, C. F.; Du, L. M.; Wu, W. Y.; Sheng, A. Z. *Talanta* **2010**, *80*, 1939-1944; (d) Zhou, Y. Y.; Yang, J.; Liu, M.; Wang, S. F.; Lu, Q. J. *Lumin.* **2010**, *130*, 817-820; (e) Miskolczy, Z.; Megyesi, M.; Tarkanyi, G.; Mizsei, R.; Biczok, L. *Org. Biomol. Chem.* **2011**, *9*, 1061-1070; (f) Li, C. F.; Du, L. M.; Zhang, H. M. *Spectrochim. Acta, Part A* **2010**, *75*, 912-917; (g) Occello, V. N. S.; Veglia, A. V. *Anal. Chim. Acta* **2011**, *689*, 97-102; (h)

Saleh, N.; Meetani, M.; Al-Kaabi, L.; Ghosh, I.; Nau, W. M. *Supramol. Chem.* DOI: 10.1080/ 10610278.2011.593631.

140. Arunkumar, E.; Forbes, C. C.; Smith, B. D. *Eur. J. Org. Chem.* **2005**, *2005*, 4051-4059.

141. Rao, T. V. S.; Huff, J. B.; Bieniarz, C. *Tetrahedron* **1998**, *54*, 10627-10634.

142. Cho, S. J.; Hwang, H. S.; Park, J. M.; Oh, K. S.; Kim, K. S. *J. Am.Chem. Soc.* **1996**, *118*, 485-486.

143. Márquez, C.; Nau, W. M. *Angew. Chem. Int. Ed.* **2001,** *40*, 4387-4390.

144. (a) Thivierge, C.; Bandichhor, R.; Burgess, K. *Org. Lett.* **2007**, *9*, 2135-2138; (b) Li, L.; Han, J.; Nguyen, B.; Burgess, K. *J. Org. Chem.* **2008**, *73*, 1963-1970

145. Lai, R. Y.; Bard, A. J. *J. Phys. Chem. B* **2003**, *107*, 5036-5042

146. (a) Stephens, P. J.; Devlin, F. J.; Chablowski, C. F.; Frisch, M. J. *J. Phys. Chem.* **1994**, *98*, 11623-11627; (b) Hertwig, R. H.; Koch, W. *Chem. Phys. Lett.* **1997**, *268*, 345-351.

147. (a) Wang, Y.; Li, H. *J. Chem. Phys.* **2010**, *133*, 1-11; (b) Yoo, S.; Zahariev, F.; Sok, S.; Gordon, M. S. *J. Chem. Phys.* **2008**, *129*, 1-8.

148. Tomasi, J.; Persico, M. *Chem. Rev.* **1994**, *94*, 2027-2094.

149. (a) Bhattacharya, S.; Nayak, S. K.; Chattopadhyaya, S.; Banerjee, M. *Spectrochimica Acta part A* **2007**, *66*, 243-249; (b) Bhattacharya, S.; Banerjee, S.; Nayak, S. K.; Chattopadhyaya, S.; Mukherjee, A. K. *Spectrochimica Acta part A* **2004**, *60*, 1099-1104

150. (a) Hofman, J. W.; Zeeland, F.; Turker, S.; Talsma, H.; Lambrechts, S. A. G.; Sakharov, D. V.; Hennink, W. E.; Nostrum, C. F. *J. Med. Chem.* **2007**, *50*, 1485-1494; (b) Kawai, K.; Osakada, Y.; Fujitsuka, M.; Majima, T. *J. Phys. Chem. B* **2007**, *111*,

2322-2326; (c) Ikeda, A.; Doi, Y.; Hashizume, M.; Kikuchi, J.; Konishi, T. *J. Am. Chem. Soc.* **2007**, *129*, 4140-4141.

151. (a) Ozlem, S.; Akkaya, E. U. *J. Am. Chem. Soc.* **2009**, *131*, 48-49; (b) He, H.; Lo, P. C.; Yeung, S. L.; Fong, W. P.; Ng, D. K. P. *Chem. Commun.* **2011**, *47*, 4748-4750; (c) Frimannsson, D. O.; Grossi, M.; Murtagh, J.; Paradisi, F.; O'Shea, D. F. *J. Med. Chem.* **2010**, *53*, 7337-7343.

152. (a) Viola, G.; Dallˇ Acqua, F.; Gabellini, N.; Moro, S.; Vedaldi, D.; Ihmels, H. *Chem. Bio. Chem.* **2002**, *3*, 550-558; (b) Wang, P.; Ren, L. G.; He, H. P.; Liang, F.; Zhou, X.; Tan, Z. *Chem. Bio. Chem.* **2006**, *7*, 1155-1159; (c) Zhou, Q. X.; Lei, W. H.; Sun, Y.; Chen, J. R.; Li, C.; Hou, Y. J.; Wang, X. S.; Zhang, B. W. *Inorg. Chem.* **2010**, *49*, 4729-4731; (d) Sun, Y.; Hou, Y. J.; Zhou, Q. X.; Lei, W. H.; Chen, J. R.; Wang, X. S.; Zhang, B. W. *Inorg. Chem.* **2010**, *49*, 10108-10116

153. (a) Lakowicz, J. R. *Principles of Fluorescence Spectroscopy*, 2nd ed.; Kluwer Academic: New York, **1999**; (b) Valeur, B. *Molecular Fluorescence: Principles and Applications* Wiley-VCH Verlag: Weinheim, **2001**.

154. (a) Chen, Y.; Zhao, J.; Guo, H.; Xie, L. *J. Org. Chem.* **2012**, *77*, 2192-2206; (b) Martin, A.; Long, C.; Forsterab, R. J.; Keyes, T. E. *Chem. Commun.*, **2012**, *48*, 5617-5619; (c) Hu, R.; Gómez-Durán, C. F. A.; Lam, J. W. Y.; Belmonte-Vázquez, J. L.; Deng, C.; Chen, S.; Ye, R.; Peňa-Cabrera, E.; Zhong, Y.; Wong, K. S.; Tang, B. Z. *Chem. Commun.* **2012**, *48*, 10099-10101.

155. (a) Boens, N.; Leen, V.; Dehaen, W. *Chem. Soc. Rev.* **2012**, *41*, 1130-1172; (b) Kobayashi, T.; Komatsu, T.; Kamiya, M.; Campos, C.; González-Gaitán, M.; Terai, T.; Hanaoka, K.; Nagano, T.; Urano, Y. *J. Am. Chem. Soc.* **2012**, *134*, 11153-11160;

(c) Guo, H.; Jing, Y.; Yuan, X.; Ji, S.; Zhao, J.; Li, X.; Kan, Y. *Org. Biomol. Chem.* **2011**, *9*, 3844-3853; (d) Domaille, D. W.; Zeng, L.; Chang, C. J. *J. Am. Chem. Soc.* **2010**, *132*, 1194-1195.

156. (a) Loudet, A.; Burgess, K. *Chem. Rev.* **2007**, *107*, 4891-4932; (b) Ziessel, R. *C.R. Chimie* **2007**, *10*, 622-629; (c) Ulrich, G.; Ziessel, R.; Harriman, A. *Angew. Chem. Int. Ed.* **2008**, *47*, 1184-1201; (d) Ziessel, R.; Ulrich, G.; Harriman, A. *New J. Chem.*, **2007**, ***31***, 496-501.

157. Shivran, N.; Mula, S.; Ghanty, T. K.; Chattopadhyay, S. *Org. Lett.* **2011,** *13*, 5870-5873.

158. (a) Ziessel, R.; Harriman, A. *Chem. Commun.* **2011**, *47*, 611-631; (b) Harriman, A.; Mallon, L. J.; Elliot, K. J.; Haefele, A.; Ulrich, G.; Ziessel, R. *J. Am. Chem. Soc.* **2009**, *131*, 13375-13386.

159. Callan, J. F.; de Silva, A. P.; Magri, D. C. *Tetrahedron* **2005**, *61*, 8551-8588.

160. Que, E. L.; Domaille, D. W.; Chang, C. *J. Chem. Rev.* **2008**, *108*, 1517-1549.

161. Thomas, J. A.; Buchsbaum, R. N.; Zimniak, A.; Racker, E. *Biochemistry* **1979**, *18*, 2210-2218.

162. Briggs, M. S.; Burns, D. D.; Cooper, M. E.; Gregory, S. *J. Chem. Commun.* **2000**, 2323-2324.

163. Galindo, F.; Burguete, M. I.; Vigara, L.; Luis, S. V.; Kabir, N.; Gavrilovic, J.; Russell, D. A. *Angew. Chem. Int. Ed.* **2005**, *44*, 6504-6508.

164. Bizzarri, R.; Arcangeli, C.; Arosio, D.; Ricci, F.; Faraci, P.; Cardarelli, F.; Beltram, F. *Biophys. J.* **2006**, *90*, 330-3314.

165. Tang, B.; Liu, X.; Xu, K.; Huang, H.; Yang, G.; An, L. *Chem. Commun.* **2007**, *36*, 3726-3728.

166. Pal, R.; Parker, D. *Chem. Commun.* **2007**, *5*, 474-476.

167. Liu, Y. -S.; Sun, Y.; Vernier, P. T.; Liang, C. -H.; Chong, S. Y. C.; Gundersen, M. A. *J. Phys. Chem. C* **2007**, *111*, 2872-2878.

168. Balut, C.; Ven, M. vande; Despa, S.; Lambrichts, I.; Ameloot, M.; Steels, P.; Smets, I. *Kidney Int.* **2008**, *73*, 226-232.

169. Bradley, M.; Alexander, L.; Duncan, K.; Chennaoui, M.; Jones, A. C.; Sánchez-Martín, R. M. *Bioorg. Med. Chem. Lett.* **2008**, *18*, 313-317.

170. Diehl, H.; Horchak-Morris, N. *Talanta* **1987**, *34*, 739-741.

171. Klonis, N.; Sawyer, W. H. *J. Fluoresc.* **1996**, *6*, 147-157.

172. Koo, M. K.; Oh, C. H.; Holme, A. L.; Pervaiz, S. *Cytometry, Part A* **2007**, *71A*, 87-93.

173. Rurack, K.; Spieles, M. *Anal. Chem.* **2011**, *83*, 1232-1242.

174. (a) Ziessel, R.; Ulrich, G.; Harriman, A.; Alamiry, M. A. H.; Stewart, B.; Retailleau, P. *Chem. Eur. J.* **2009**, *15*, 1359-369; (b) Bura, T.; Retailleau, P.; Ulrich, G.; Ziessel, R. *J. Org. Chem*. **2011**, *76*, 1109-1117; (c) Thivierge, C.; Han, J.; Jenkins, R. M.; Burgess, K. *J. Org. Chem*. **2011**, *76*, 5219-5228.